Ionic basis for variability in repolarisation and its implications in pathological response

Philip Gemmell
Oriel College



Computational Biology Research Group
Department of Computer Science
University of Oxford

Hilary Term 2014

This thesis is submitted to the Department of Computer Science, University of Oxford, for the degree of Doctor of Philosophy. This thesis is entirely my own work, and, except where otherwise indicated, describes my own research.

Philip Gemmell
Oriel College

Doctor of Philosophy
Hilary Term 2014

Ionic basis for variability in repolarisation and its implications in pathological response

Abstract

Sudden cardiac death represents one of the leading causes of death worldwide, with the majority of these deaths caused by arrhythmias derived from ischæmic events. However, the mechanisms leading from ischæmia to re-entry, arrhythmia and eventual death are poorly understood. Furthermore, variability in the action potential of cardiac tissue, while important in determining arrhythmic risk, is only recently being addressed in computational modelling, with little known about the causes and mechanisms underlying it, nor regarding its evolution in response to pathological conditions such as ischæmia.

This dissertation investigates the causes of variability in the repolarisation of the action potential of the rabbit ventricular myocyte, and the response of this variability to ischæmia. The effect of variability in ion channel conductances is investigated by means of a complete search of the parameter space revealed by simultaneous variation in multiple parameters describing ion channel conductances in computational models of the rabbit ventricular action potential. Rabbit data and models are used in this thesis due to the similarities to human data, both in terms of electrophysiology generally, and the response to ischæmia specifically. The response of two different model frameworks is assessed to determine similarities and differences between model frameworks that are designed to reproduce the same system. Those models producing action potential durations that fall within an experimentally derived range at multiple pacing rates are used to define model populations that thus reproduce experimental variability in repolarisation. These model populations are used to investigate the effects of ischæmic conditions on population variability. Variability is measured not only for action potential duration, but also for other biomarkers commonly implicated in the development of re-entry.

The work presented in this dissertation is significant for: (1) presenting a comprehensive study of the effect of simultaneous variation in ion channel conductances, with details regarding the interactions between conductances and how these interactions change depending on the pacing rate; (2) detailed examination of the differences between two models of the same system; (3) production of the largest extant populations reproducing experimentally observed variability in action potential duration; (4) the first time model populations have been used to investigate the effects of ischæmia on variability.

Publications

Below is a list of publications which directly relate to the work described in this thesis:

1. Gemmell, P. M., Burrage, K., Rodríguez, B., and Quinn, T. A. (2010). Exploring the parameter space of a rabbit ventricular action potential model to investigate the effect of variation on action potential and calcium transients. *Annual International Conference of the IEEE Engineering in Medicine and Biology Society*, 2010:2662–5

2. Gemmell, P. M., Burrage, K., Rodríguez, B., and Quinn, T. A. (2012). Quantifying Importance of Repolarization Currents Underlying Physiological Variability in Rabbit Cellular Electrophysiology. *Biophysical Journal*, 102:540a

3. Gemmell, P. M., Burrage, K., Rodríguez, B., and Quinn, T. A. (2014). Population of computational rabbit-specific ventricular action potential models for investigating sources of variability in cellular repolarisation. *PloS ONE*, 9(2):e90112

4. Gemmell, P. M., Burrage, K., Rodríguez, B., and Quinn, T. A. (2015). Effects of ischæmia on variability in model populations of rabbit ventricular myocytes. *In Preparation*

Contents

Contents vii

List of Figures 1

List of Tables 3

List of Code Excerpts 5

1 Introduction 11
1.1 Motivation . . . 11
1.2 Thesis Goal & Aims . . . 13
1.3 Dissertation Outline . . . 15

2 Physiological Background 17
2.1 Structure and Function of the Heart . . . 17
2.2 Structure and Function of the Cardiomyocyte . . . 21
2.2.1 The Action Potential . . . 23
2.2.2 Ion Channel Properties . . . 27
K^+ Currents . . . 28
L-Type Ca^{2+} Current . . . 30
Exchangers . . . 31
2.2.3 Calcium Dynamics . . . 32
2.3 Cardiac Dysfunction . . . 35
2.3.1 Ischæmia . . . 36
Ischæmic Changes in the AP . . . 37
Ischæmic Changes in $[Ca^{2+}]_i$ . . . 43
2.3.2 Arrhythmogenesis . . . 47
Re-entry . . . 49
Delayed & Early After Depolarisations . . . 50
Alternans . . . 52
Spiral Waves & Rotors . . . 54
2.4 Experimental & Physiological Variability . . . 55
2.4.1 Action Potential Variation . . . 57
2.4.2 Ion Channel Variation . . . 57

3 Modelling Background 59
3.1 Development . . . 60
3.2 Key Concepts . . . 64
3.2.1 Nernst Potential . . . 66
3.2.2 Hodgkin-Huxley Current . . . 67
3.2.3 Markov Models . . . 69
3.2.4 Monodomain & Bidomain Equations . . . 72
3.3 Computational Modelling of Variability . . . 74

3.3.1 Stochastic Modelling . . . 76
3.3.2 Parameter Sensitivity . . . 78
3.3.3 Model Populations . . . 82
3.4 Computational Modelling of Ischæmia . . . 83

4 Computational Methods 87
4.1 Computational Models & Simulation Techniques . . . 87
4.1.1 Parameter Space Simulations . . . 90
4.1.2 Ischæmia Simulations . . . 92
4.1.3 Nimrod Distributed Computing Grid . . . 96
4.2 Represention of Multi-Dimensional Data . . . 99
4.3 Biomarker Calculation . . . 102
4.4 Measures of Variability & Correlation . . . 105

5 Reproduction of Experimental Variability with Model Populations & Effect of Multiple Parameter Variation 109
5.1 Reproduction of Experimental Variation . . . 110
5.1.1 Comparison with Alternative Methods . . . 111
5.1.2 Caveats . . . 113
5.2 Construction of the Parameter Space . . . 114
5.3 Accuracy of Biomarkers in Defining Model Fit . . . 116
5.4 Defining a Population of Models to Reproduce Physiological Variation . . . 118
5.4.1 Variation within the Population . . . 118
5.4.2 Connectivity within the Parameter Space . . . 126
5.5 Effects of Parameter Variation . . . 126
5.6 Rate Dependence of Biomarkers . . . 132
5.7 Summary . . . 134

6 Effect of Ischæmia on Model Population Variability 137
6.1 Ischæmic Changes in Cellular Repolarisation and Refractoriness . . . 139
6.1.1 Changes during Phase 1A Ischæmia . . . 139
Mean APD_{90} Response & Comparison with Experimental Data . . . 140
Population Variability . . . 142
6.1.2 Rôle of $f_{K\text{-}ATP}$ . . . 145
6.1.3 Rôle of Changes in $I_{Ca,L}$ & Na^+ Dynamics . . . 150
6.1.4 Rôle of $[K^+]_o$ . . . 151
6.2 APD_{90}/ERP Relationship During Ischæmia . . . 156
6.3 Relations Between Channel Conductances During Ischæmia . . . 162
6.4 Ischæmic Effects on other Biomarkers . . . 165
6.5 Summary . . . 169

7 Conclusions 171
7.1 Summary . . . 171
7.2 Key Contributions & Findings . . . 176
7.3 Future Work . . . 177

A Diffusion 179
A.1 Simple Diffusion . . . 179
A.2 Facilitated Diffusion, Michaelis-Menten Kinetics . . . 180
A.3 Electrodiffusion . . . 182
A.3.1 The Nernst Equation . . . 182

B Changes in APD During Ischæmia 185
B.1 Literature Data for Ischæmic APD_{90} . . . 185

List of Figures

2.1 Structure of a mammalian heart . . . 18
2.2 Structure of myocardial sheets and fibres . . . 19
2.3 Path of electrical activation in the heart . . . 21
2.4 Schematic of a cardiac AP . . . 23
2.5 Example of a restitution curve with alternans predicted . . . 27
2.6 Schematic of a Calcium Release Unit . . . 33
2.7 Hypothetical distribution of ischæmic properties in tissue . . . 42
2.8 Effect of ischæmia on $[Ca^{2+}]_i$ . . . 44
2.9 Schematic of delayed and early after-depolarisations . . . 50
2.10 Spatially cordant and spatially discordant APD alternans in cardiac tissue . . . 53

3.1 Schematic representation of the cell as an electrical circuit . . . 65
3.2 Markov model for $I_{Ca,L}$ in Mahajan *et al.* (2008) . . . 70
3.3 Hypothetical mapping between input and output parameters . . . 79

4.1 Effect of varying $g_{K\text{-}ATP}$ on APD_{90} . . . 94
4.2 Schematic for possible use of the Nimrod/G computing grid . . . 97
4.3 The dimensional stacking process . . . 101
4.4 Illustration of biomarkers used in this dissertation . . . 102
4.5 Demonstration of correlation, relationship and mapping. . . . 106

5.1 Efficacy of biomarkers in determining model goodness-of-fit . . . 117
5.2 Parameter ranges used for 'Expanded Mahajan' search . . . 121
5.3 Model population for the Shannon framework that produces values of both APD_{50} and APD_{90} that fall within the experimentally derived range . . . 122
5.4 Model population for the expanded Mahajan framework that produces values of both APD_{50} and APD_{90} that fall within the experimentally derived range . . . 124
5.5 Connectivity within model populations . . . 127
5.6 Effect of parameter variation on Shannon population . . . 128
5.7 Effect of parameter variation on Mahajan population . . . 129
5.8 Rate dependence of biomarkers in the parameter space . . . 133

6.1 Effect of different degrees of ischæmia on the Shannon and Mahajan model populations 140
6.2 Comparison of APD_{90} response between simulation results and literature reported values 141
6.3 Illustration of models that are classed as either succeeding or failing to produce an AP in response to stimulus during ischæmia . . . 145
6.4 Effect on APD_{90} of changing environmental parameters to ischæmic values . . . 146
6.5 Effect of $f_{K\text{-}ATP}$ variability on the Shannon and Mahajan model populations . . . 148
6.6 Effect of $[K^+]_o$ variability on the Shannon and Mahajan model populations . . . 152
6.7 Evolution of APD_{90} and ERP due to changes in $[K^+]_o$ . . . 154
6.8 Distribution of biomarker values under specified conditions . . . 157
6.9 Relation between APD_{90} and ERP during ischæmia . . . 158
6.10 Relation between V_{rest} and ERP . . . 161
6.11 APD_{90} and ERP distributions during ischæmia . . . 164

6.12 Relation between V_{rest} and $(\mathrm{d}V_m/\mathrm{dt})_{\text{max}}$ 168

List of Tables

2.1 Summary of current density results from Szentandrássy *et al.* (2005) 58

4.1 Model parameter values used to train ischæmia conditions 92
4.2 Ischæmic environment parameters 95

5.1 Physiological Ranges for APD_{50} and APD_{90} 118
5.2 Number of parameter sets producing both APD_{50} and APD_{90} values within the physiological range 119
5.3 Minimum, mean, and maximum values of all computed biomarkers produced by models reproducing experimental values of APD_{50} and APD_{90} 120
5.4 Optimum stack order for APD_{50}, APD_{90}, and CaT for the Shannon and Mahajan frameworks 130

6.1 Rate of model inexcitability & ERP prolongation during ischæmia 144

B.1 APD changes during ischæmia reported in the literature in rabbit 186
B.2 APD changes during ischæmia from Kurz *et al.* (1993) 187
B.3 APD changes during ischæmia reported in the literature in other species 188

List of Code Excerpts

4.1 Nimrod/G code: Example of a plan file 98
4.2 Nimrod/G code: Example of parameter substitution in C++ code 98

Acknowledgements

It is obvious where I have to start with my thanks—without the unfailing support, help and encouragement from my supervisors, this thesis could never have been completed. I am truly and sincerely grateful to Blanca, Kevin and Alex for all their support over the years, and their patience with my progress. They have all devoted significant time towards my development as a research student, and any advances I have made have been entirely due to their efforts. Without them, none of the work presented here would have been possible, and I cannot possibly express my gratitude enough.

I have also been immensely lucky with the assistance I have received from so many places. I especially want to thank Alberto Corrias, Blair Bethwaite and Jeff Tan for their invaluable assistance with understanding, and eventually using, the Nimrod/G distributed computing grid. The Computational Biology group in Oxford have also been invaluable in providing an arena in which I can explore my thesis, as well as simply allowing me a place where I can enjoy my work.

I also wish to acknowledge the (almost literal) debt I owe to both the EPSRC for my funding through my original studentship with the Systems Biology DTC, and Oriel College for helping to fund my studies towards the end of my project.

Finally, I wish to express my grateful thanks to all my friends and colleagues who have tolerated me with good humour while I have navigated through the DPhil process. My friends in the Oriel MCR, URNU, SCBC and the OULRC have made my time more enjoyable than I could have hoped. Special thanks must go to Deb, who has been sympathetic to my plight and a support in my trials, and most significantly to my parents—without their support, encouragement and help, none of this would have been possible.

ADMG

Notation & Nomenclature

Terminology

Within this dissertation, vectors are represented using lower case bold type (*e.g.* $\mathbf{x}$), with matrices represented using upper case bold type (*e.g.* $\mathbf{B}$). All other conventions are applied in the same manner to these two. The mean value of a population is represented by the variable with an overbar (*e.g.* $\overline{x}$), whereas the *expected* value of a value is represented as $\mathbb{E}[x]$. The sample variance is represented using $s^2(x)$. Where an approximated value is used, it is designated using a circumflex (*i.e.* the approximation of $\mathbf{X}$ is represented by $\hat{\mathbf{X}}$).

All the following terms and definitions are defined more fully within the text of the dissertation—where appropriate, page references are given.

The term *framework* is used to refer to the set of equations that are used to simulate a given system. When used with a particular set of parameter values, it is referred to as a *model*—as such, a framework cannot be said to be simulated, but a model can. A *population* of models refers to a group of models that share an underlying framework, differing only in the parameter values used in each model.

The term *correlation* is used in this dissertation to refer to how closely a line of best fit will match the given data for two different metrics; the form of this line of best fit is referred to as the *relation*. Finally, the *mapping* refers to how a given model's output for one metric relates to its output for a given metric.

Abbreviations

Where the abbreviation refers to a concept that is expanded upon in the text more fully, a page reference is given.

ADP	Adenosine Diphosphate.
AP	Action Potential.
$\mathrm{AP}_{\mathrm{NRMSD}}$	Normalised root mean square difference between 'test' and 'training' data for V_m data. See p. 104.
APD_X	Action potential duration to $X\%$ repolarisation. See p. 102.
ATP	Adenosine Triphosphate.
$[\mathrm{Ca}^{2+}]_\mathrm{i}$	Free cytosolic Ca^{2+} concentration.

Ca^{2+}_{NRMSD}	Normalised root mean square difference between 'test' and 'training' data for $[Ca^{2+}]_i$ data. See p. 104.
CaT	Calcium Transient: difference between systolic $[Ca^{2+}]_i$ and diastolic $[Ca^{2+}]_i$.
CICR	Calcium-induced calcium release. See p. 32.
CTD_X	Calcium transient duration to $X\%$ recovery of diastolic value. See p. 102.
DAD	Delayed after-depolarisation. See p. 50.
$(dV_m/dt)_{max}$	Maximum rate of membrane depolarisation, during the AP upstroke.
EAD	Early after-depolarisation. See p. 50.
ECC	Excitation-contraction coupling. See p. 32.
ERP	Effective refractory period. See p. 102.
g_X	Maximum conductance for current X.
$I_{Ca,L}$	L-type Ca^{2+} current.
I_{K1}	Inward rectifying K^+ current.
I_{Kr}	Rapidly delayed rectifier K^+ current.
I_{Ks}	Slowly delayed rectifier K^+ current.
I_{Na}	Na^+ current.
I_{NaCa}	Na^+-Ca^{2+} exchanger current.
I_{NaK}	Na^+-K^+ pump current.
I_{stim}	Stimulus current.
I_{to}	K^+ transient outward current.
$I_{to,f}$	Fast K^+ transient outward current.
$I_{to,s}$	Slow K^+ transient outward current.
LCC	L-type calcium channel. See p. 32.
PRR	Post-repolarisation refractoriness. See p. 102.
SL	Sarcolemma/cell membrane.
SR	Sarcoplasmic Reticulum.
V_m	Membrane potential.
V_{max}	Maximum membrane potential during the AP.
V_{plat}	Membrane potential of Phase 2 of the AP.
V_{rest}	Resting membrane potential during the AP.
x min PO	*x* minutes post-occlusion, *i.e.* the number of minutes since the initiation of ischæmia.
$[X]_i$	Intracellular concentration of X. Where the intracellular environment is separated into multiple compartments, this represents the cytosolic concentration.
$[X]_o$	Extracellular concentration of X.

1 Introduction

The beginning is the most important part of the work.

The Republic, Plato

The motivation driving the thesis shall be given, with some background provided to place the thesis within the current state of knowledge. With this motivation, the resulting thesis shall be stated, which is reflected in the resulting aims and goals. Finally, a detailed outline of how this dissertation is organised is given.

1.1 Motivation

Sudden cardiac death (SCD) is one of the major causes of death not only in Western society, but worldwide. It represents the cessation of proper functioning of the heart, resulting in severely compromised blood flow round the body and to the vital organs, and without rapid treatment, the patient quickly dies. This not only presents a high cost in mortality, with an estimated ∼17 million deaths worldwide due to cardiovascular disease generally in 2008, but also economically, with the cost to the UK economy estimated at £19 billion in 2010 (Alwan *et al.*, 2010; Townsend *et al.*, 2012).

Approximately half of the incidents of SCD can be attributed to ventricular arrhythmia (John *et al.*, 2012). A particularly dangerous form of ventricular arrhythmia is ventricular fibrillation, which represents the break-up of the electrical wave that causes cardiac contraction into small disorganised wavelets that spread through the myocardium. This disorganisation of the electrical propogation leads to disordered, and thus inefficient, contraction of the ventricle, impairing the function of the

heart as a pump. If these fibrillations are sustained rather than self-terminating, the prolonged cessation of blood flow via the heart is invariably fatal.

Due to the significance of the problem, great effort has been expended on elucidating the causes and mechanisms that lead the heart to transition to these conditions. This effort has not been wasted, with mechanisms now detailed for several different means by which the electrical propogation wave can be disrupted and arrhythmias initiated. *Myocardial ischæmia*, which results from cessation of blood flow to cardiac tissue, is of particular importance as the primary cause of the majority of cases of SCD. Ischæmia is a highly dynamic pathological environment, with changes occurring rapidly both spatially and temporally. The initial stages of acute ischæmia, referred to as *Phase 1A ischæmia*, are when the cardiac environment undergoes the most significant changes. With these changes comes the greatest risk of the development of arrhythmia. However, much as with other arrhythmogenic mechanisms and despite great advances, there remain significant unknowns in our understanding as to how pathological tissue can transition to an actual arrhythmic event.

It is known that variability can play a key rôle in determining the outcome of ischæmia. While the significance of variability is by no means limited to determining ischæmic response—for example, variability in drug response is a key area of investigation in computational biology—the heterogeneity in tissue (that increases with ischæmia) is known to be one of the key factors predisposing ischæmic tissue to arrhythmogenesis. Thus, a proper account has to be made of variability to fully understand the mechanisms at work in ischæmia, and in cardiovascular disease in general. Once the rôle played by variability has been elucidated, the potential courses for treatment are vastly increased.

However, a comprehensive account of variability represents a significant challenge. Variability spans a range of 10^9 spatially and 10^{15} temporally. Spatially, different data can be recorded for the electrical activity for two different cardiomyocytes, or from two different regions of the heart, or from two different individuals, or from two different species. Temporally, variability exists from the scale of an entire lifetime, down to the scale of two consecutive action potentials. These wide ranges make comprehensive modelling difficult. To trace the evolution and emergence of variability from one scale to the next presents a significant challenge, and one that is now being faced up to.

To investigate the mechanisms of ischæmia, and indeed the heart in general, experiments must remain at the heart of the process. However, the use of human hearts for experiments is a rarity, and thus a 'proxy' must be used. To that end, it has been shown that rabbit hearts reproduce many of the salient features of human electrophysiology, including their ischæmic response, with many metrics used to judge heart response able to be scaled according to a body-mass relationship. Due to these correlations, much cardiac electrophysiological research makes use of rabbit heart data, and the work presented in this thesis follows in that trend.

Computational modelling offers great benefits for elucidation of the progression of ischæmia and its consequences, and the rôle that variability has to play in this development. Since the seminal work presented in Noble (1960), computational cardiac electrophysiology has advanced at an impressive rate, now allowing computational modelling to be used to address a wide variety of problems. The successful union between experiments and simulations opens the door for examination of hypotheses that would otherwise be insoluble to each technique individually. As such, computational modelling is now a key tool in the analysis of cardiac dysfunction, with models being advanced to help address a wide range of problems (Kohl *et al.*, 2010; Trayanova *et al.*, 2011; Carusi *et al.*, 2012; Britton *et al.*, 2013; Heijman *et al.*, 2013; Quinn and Kohl, 2013).

1.2 Thesis Goal & Aims

This thesis aims to investigate the sources of variability for cellular repolarisation of ventricular myocytes, and the consequences of ischæmia on this variability. More specifically, the thesis being assessed is:

> The variability in cellular repolarisation exhibited in the experimental literature for rabbit ventricle data can be reproduced by use of a population of computational models. The variability reproduced therein will then increase when the population is subjected to conditions simulating acute phase 1A ischæmia.

This thesis uses population modelling as the method to investigate and reproduce variability, and it is the methodological lynch-pin throughout. In using population modelling, it can be considered that the thesis posed will be addressed by pursuing 3 goals:

1. Investigate the effects of variability in ion channel conductances on the action potential repolarisation of computational models of rabbit ventricular cardiomyocytes.

2. Derive model populations that reproduce experimentally observed variation.

3. Determine the effects of ischæmic conditions on the variability exhibited by these populations.

These goals provide a 'road map' for this thesis—each one is key feature of the dissertation, but the thesis (and thus this dissertation) covers a wider range than is expressed in these 3 goals.

A comprehensive parameter sweep will be used to examine the effect of simultaneously varying six parameters representing the peak conductance of ion channels on the output of computational models of a rabbit ventricular cardiomyocyte. This parameter sweep will search a six-dimensional parameter space. Distributed computing methodologies and innovative visualisation techniques shall be employed to permit comprehensive analysis of how the simultaneous variation of multiple input parameters affects the model output. This investigation shall be conducted at multiple pacing rates to gain insight into how the interactions between input parameters changes with pacing rate. By these means, Goal 1 can be achieved.

From the results of this comprehensive parameter sweep, a population of models that reproduces experimental data can be defined (Goal 2). Within these populations, the distribution of ion channel conductance parameters shall be analysed and associated patterns derived. This is more than just an extension of the study of variability of Goal 1, and serves to indicate relations that may exist in real-life physiological systems. Through this analysis, inter-relations that permit the cell to operate a functional 'repolarisation reserve' can be elucidated.

These model populations can then be adapted to permit simulation of ischæmia. Simulations will be conducted to investigate the changes in population properties caused by ischæmia. Ischæmic changes to the AP are reproduced by modelling four underlying conditions simultaneously; these conditions are also simulated separately. This permits elucidation of the effects of ischæmia on population variability, and determination of which underlying condition plays which rôle in the ischæmic response. Thus, Goal 3 is addressed.

1.3 Dissertation Outline

To address the thesis comprehensively, the dissertation is structured as detailed below.

Chapter 2 provides a review of the existing literature of the physiology of the heart. An outline of the structure and function of the heart is provided, including details of the structure and function of cardiomyocytes . The action potential is described, with details given for both the changes in the cellular membrane potential and the calcium dynamics inherent in the action potential. Details are given for currents that play an important rôle in cellular repolarisation.

This chapter will also provide an overview of cardiac dysfunction, with the main focus being on ischæmia and its consequences. A brief review of the state of knowledge of some of the arrhythmic mechanisms relevant to ischæmia will also be provided. Finally, a review of the literature regarding experimental and physiological variability is given.

Chapter 3 will focus on computational modelling. This will start with a brief history of the development of computational models (with the focus being on models describing cardiac electrophysiology), from their somewhat humble origins to the current state-of-the-art. Some of the key concepts developed in this progression will then be described. This chapter will then provide a summary of the different techniques that can be used to study variability in a computational environment. Finally, the advances in computational cardiac electrophysiology in simulating ischæmic phenomena will be reviewed.

In Chapter 4, details will be given for the specific methods and techniques used in this dissertation

in terms of calibration, visualisation and analysis. A discussion of the parameter sweep simulations will be given, and details presented for how the models are adapted to permit simulations of acute ischæmia. With the computational demands made of comprehensive parameter sweeps in mind, details of the use of the Nimrod/G distributed computing grid will be provided.

The results of the initial parameter sweep will be provided in Chapter 5. This starts with the results for assessing the accuracy of common biomarkers in determining goodness-of-fit of model output to training data. Using data derived from the available literature, populations of models that reproduce experimental variability will be defined, and patterns of parameter variation within these populations explored. Details will also be given on how the population-wide distribution of these biomarkers changes depending on the pacing rate used.

Chapter 6 will detail the results of the investigation into the effects of ischæmic variability, in terms of the effects of ischæmia on the population variability, and how this variability is affected by changes in the parameters used to simulate ischæmia. This starts with investigation of variability of cellular repolarisation, the evolution of this as ischæmia progresses, and the causes behind these changes. Discussion will move on to the changes in the rate of recovery of cellular excitability, and how this is linked to cellular repolarisation. The changes in relative importance of ion channel conductances in response to ischæmia will be considered, with details regarding an individual model's place within the population elucidated. Finally, results will be provided for the changes in variability of other common biomarkers that are known for their importance in signifying arrhythmic risk.

This dissertation will be closed in Chapter 7, which will provide concluding remarks. A summary of the results presented in this thesis will be provided, with the key findings identified and placed in context with other work. Future directions will be discussed.

2 Physiological Background

There are more things in heaven and earth, Horatio,
Than are dreamt of in your philosophy.

Hamlet, Act 1, Scene 5

This chapter provides the necessary biological and physiological background for the thesis, and starts by outlining the structure and function of the heart itself. The constituent cell of the heart, the cardiomyocyte, is then described, with some of the ion channels it contains being outlined. The electrical properties of the cell are then discussed, with the form of the action potential being outlined with the underlying mechanisms detailed. The link to the mechanical action of the heart is described. The fourth section of this chapter reviews some elements of cardiac dysfunction, with special focus given to ischæmia, before moving on to review some of the mechanisms leading to arrhythmogenesis. Finally, an outline is provided of the state of knowledge regarding variation in both the action potential, and the underlying ion channels.

2.1 Structure and Function of the Heart

At the most general level, the heart serves as a pump to transport blood around the body to deliver nutrients and remove waste products. It does this by rhythmic, organised contraction—the rate of this contraction varies depending on species, age, condition of the heart and the activity being undertaken by the organism.

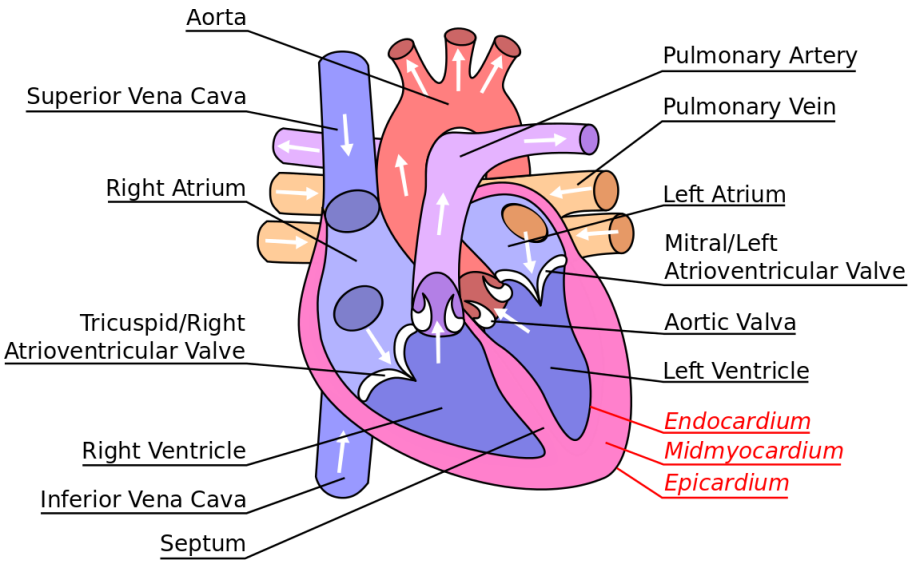
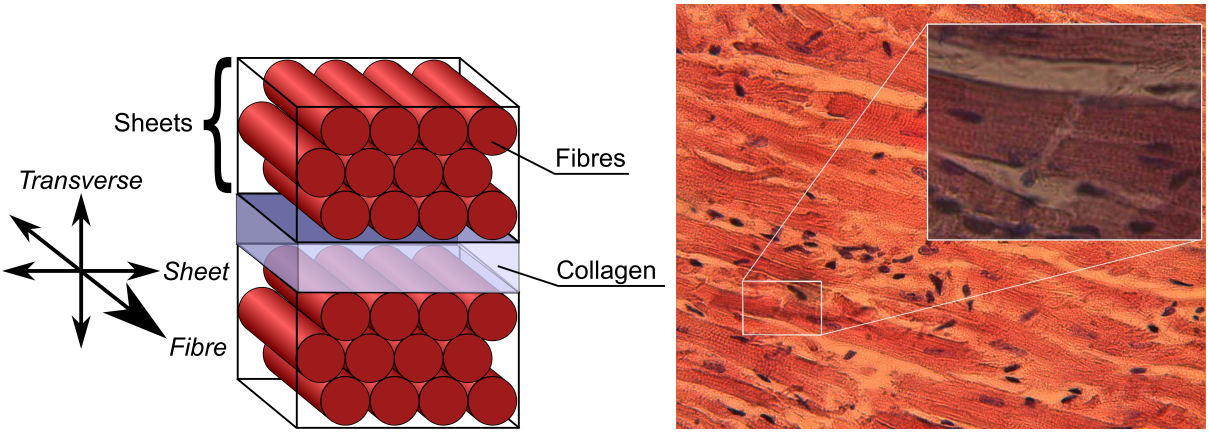


Figure 2.1: *Diagram of a longitudinal cross-section of a mammalian heart. The direction of blood flow is shown by white arrows, and all major structural components are labelled in black. The layers of the myocardium are labelled in red italics.*

Fig. 2.1 shows the anatomical structure of a mammalian heart—while the size varies widely between mammals, the overall architecture remains constant. It is split into two halves, left and right, by a muscular wall called the *septum*, and then further subdivided into two chambers, the larger, lower chamber being a *ventricle*, and the smaller, upper chamber called an *atrium*.

The passage of blood through the heart follows thus: firstly, deoxygenated blood from the body enters the heart via the superior and inferior/posterior *vena cavae*, with superior and inferior representing whether the blood comes from the upper or lower half of the body, respectively. Via these channels, it enters the *right atrium*. Passing through the *tricuspid valve* (also known as the right atrioventricular valve), the blood enters the *right ventricle*, where it is then pumped via the *pulmonary artery* to the lungs, where it is oxygenated. The blood returns to the heart via the *pulmonary vein*, entering the *left atrium*, before moving through the *mitral valve* (also known as the left atrioventricular valve) into the *left ventricle*. The blood is then pumped via the *aorta* to the rest of the body. The valves in the heart serve to ensure the flow of blood is always in the correct direction.

The walls of the heart are mostly composed of muscular tissue known as *myocardium*. The thickness of the myocardium is not constant throughout the heart, being thickest in the left ventricle, which requires the greatest force of contraction to pump the blood from the heart to the rest of the body. The



(A) *Schematic* (B) *Image*

FIGURE 2.2: *(2.2a) Schematic of the structure of myocardial sheets and fibres. The 'directions' within the structure are labelled. (2.2b) Image of cardiomyocytes demonstrating the interconnected nature of the individual myocytes into fibres, with the inset highlighting the junction between 2 cardiomyocytes (Girod and Becker, 2006).*

myocardium can be split into three different layers, as labelled in italics in Fig. 2.1: the *epicardium* is the outermost layer of the myocardium, the *midmyocardium* is the middle layer, and the *endocardium* is the innermost layer. The cells composing these different layers possess different electrophysiological properties—some of these differences will be mentioned in §2.2.1.

The structure within the myocardium is shown in Fig. 2.2a: it is composed of a series of sheets of tissue (usually 4 to 6 cells thick) separated by collagen. These sheets of tissue are composed primarily of muscle cells (*myocytes*, or specifically cardiomyocytes in the heart), which in the ventricles are $\sim$ 120 μm long, and $\sim$ 25 μm wide (Saffitz *et al.*, 1994). These myocytes are connected to one by intercalated discs spanning the $10 - 20$ nm separation between the cells (as opposed to skeletal muscle, which is composed of multinucleated fibres); this structure is seen in Fig. 2.2b. One attribute of these discs is the presence of *gap junctions*, which serve to electrically couple the myocytes by allowing ion flow between neighbouring myocytes. It should be noted that the cells are electrically coupled by more than just gap junctions, *e.g.* ephaptic coupling and K^+ accumulation in the membrane space; for a review of these coupling methods, see Sperelakis and McConnell (2002).

Each ventricular myocyte is electrically coupled to $\sim$ 11 neighbouring myocytes, with preferential coupling in the longitudinal direction (this is not true for all myocytes) (Luke and Saffitz, 1991; Saf-

fitz *et al.*, 1994; Smaill *et al.*, 2013). It is thus entirely due to the cellular and tissue geometry, rather than coupling arrangements, that conduction velocity has a ratio of ∼4:2:1 between fibre, sheet and transverse directions (Caldwell *et al.*, 2009). The arrangement of the myocytes into fibres, and the arrangement of these fibres into sheets, allows for ordered contraction in the fibre direction; the fibrous structure also allows the heart to twist as it contracts, leading to a more efficient pumping mechanism.

It has been shown that calcium ions (Ca^{2+}) can cross the gap junctions in a so-called *calcium wave*, triggering activity in neighbouring cells (Miura *et al.*, 1998). This Ca^{2+}-based 'triggered propogated contraction' moves more slowly than the Na^{+}-dependent action potential (the usual means for conducting the electrical activity through the heart tissue—see §2.2.2) (Clusin, 2003).

The conduction pattern of the heart is key to the effective pumping mechanism—by controlling the sequence of electrical events in the heart, the sequence of contraction is similarly controlled (see §2.2.3 for details of the coupling between the heart's electrical and mechanical activities). An outline of the conduction pattern of the heart is shown in Fig. 2.3. The sequence of activation starts amongst a complex of self-excitatory cells at the top of the right atrium, called the *sinoatrial node*. This node is electrically isolated from the atria, save for specialised conduction pathways; this both prevents depression of the self-excitation of the node by the hyperpolarising influence of the surrounding atrium, and allows several excitation locations, depending on the condition of the heart (Fedorov *et al.*, 2012). Once the node self-excites, a wave of depolaristion spreads from this node; the depolarisation of the atrial cardiac cells causes the atrium to contract. This depolarisation then reaches the *atrioventricular node*—this is the only pathway for electrical excitation to pass from the atria to the ventricles. From the atrioventricular node, the excitation wave passes to the *Bundle of His*, which conducts the electrical stimulus via the left and right bundle branches into the *Purkinje system* near the bottom of the heart, which transmits the stimulus to the ventricular surface; as the stimulus has thus been transmitted directly from the atria to the bottom of the ventricles, the excitation wave thus spreads upwards through the ventricles, allowing the ventricles to contract from the bottom up as required.

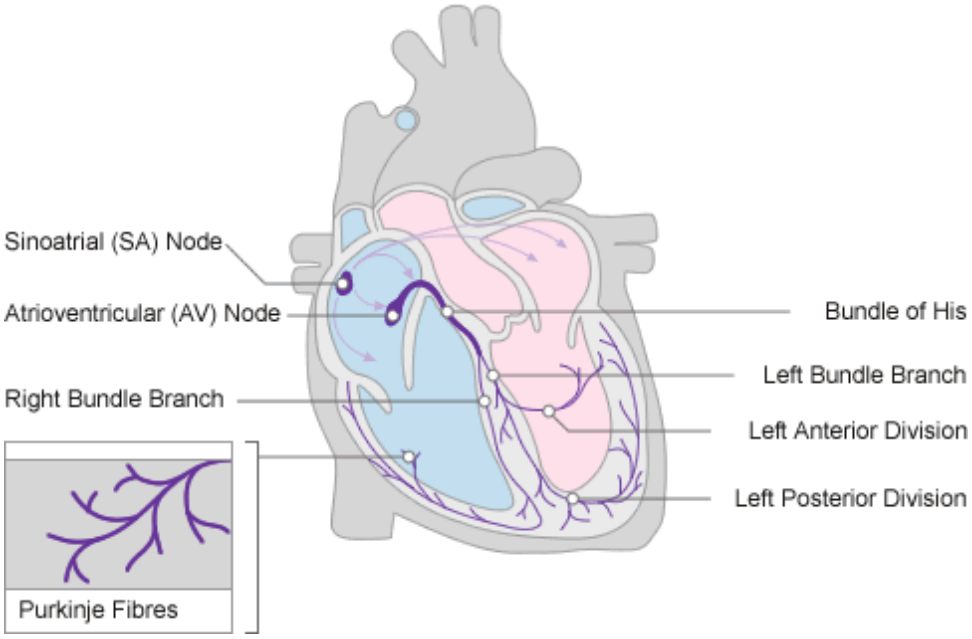


FIGURE 2.3: *Schematic outline of the path of electrical activation in the mammalian heart. Image originally downloaded from www.nottingham.ac.uk on 10th December 2012.*

2.2 Structure and Function of the Cardiomyocyte

Physically, cardiomyocytes are typically 10 – 25 μm in diameter, and 50 – 125 μm in length (Hoyt *et al.*, 1989; Hurst *et al.*, 1990; Bers, 1991; Luke and Saffitz, 1991; Saffitz *et al.*, 1994; Levick, 1995; Adler *et al.*, 1996; Carmeliet and Vereecke, 2002; Klabunde, 2005; Levkau *et al.*, 2008). They are cells bound by a lipid bilayer membrane (referred to as either the cell membrane or the sarcolemma, which in turn can be abbreviated as SL), separating the intracellular space (containing the cytoplasm and nuclei[1]) from the extracellular space. The intracellular space has a very different composition to the extracellular space, with the intracellular space containing a high and low concentration of potassium (K^+) and sodium (Na^+) ions, respectively; the reverse is true for the extracellular space. The concentrations of other ions are also tightly controlled. The ion concentration differences are the main reason behind there being an electric potential difference set up across the cell membrane, referred to as the *membrane potential* (V_m). This potential is defined as negative when the intracellular space contains a greater negative charge than the extracellular space. The resting membrane potential (V_{rest}) is nega-

[1]The *cytoplasm* is the entire contents of the cell save the nucleus, and can be said to itself consist of the *cytosol* and other organelles.

tive, though the exact value varies depending upon the location in the heart; a cardiomyocyte in the ventricles typically has a V_{rest} of about -80 mV, while the sinoatrial node has one of between -50 and -60 mV (Carmeliet and Vereecke, 2002).

Embedded within the bilayer are various membrane-spanning proteins that serve to transport ions across the membrane, allowing it to be selectively permeable to particular ions, and allowing regulation of this permeability as required. These transporters can be classed as either *channels* (allowing ions to move according to their electrochemical gradient), *pumps* (translocating ions in the opposite direction to their electrochemical gradient by the use of energy) or *exchangers* (translocating a number of ions of one type across the membrane in 'exchange' for a number of ions of another type). Most of these transporters are ion-specific, though some are not exclusively selective. Most of these channels are also controlled by, amongst other things, the membrane potential itself (Bezanilla, 2000), with the membrane potential causing a conformational change in the ion channel protein, causing it to 'open' or 'close'; that is, to allow ions to be conducted through it or not. It should be remembered that there are also many other possible regulators of ion channel activity.

These ion channels are discrete molecular entities, and thus the conformational changes that lead to the open/close transition are stochastic; some of the effects of this stochasticity, and some techniques used to model it, are discussed in greater detail in §2.4 and §3.3, respectively. However, each type of ion channel possesses its own range of attributes, such as the time it takes to inactivate, the time it takes to reactivate, its permeability to different types of ions, and its susceptibility to other gating factors. Comprehensive summaries of the properties of ion channels are given in Carmeliet and Vereecke (2002) and Roden *et al.* (2002), with greater details of ion channels pertinent to this thesis given in §2.2.2.

It is a point of nomenclature that an 'inward' current represents the movement of positive ions from the extracellular to the intracellular space, and an 'outward' current is the reverse. This definition is based on the movement on electrical charge, and not on the movement of ion flow. This is subtly different to the definition of an inward or outward rectifier current, where an inward rectifier current passes current more easily inward than outward, and vice versa for an outward rectifier current.

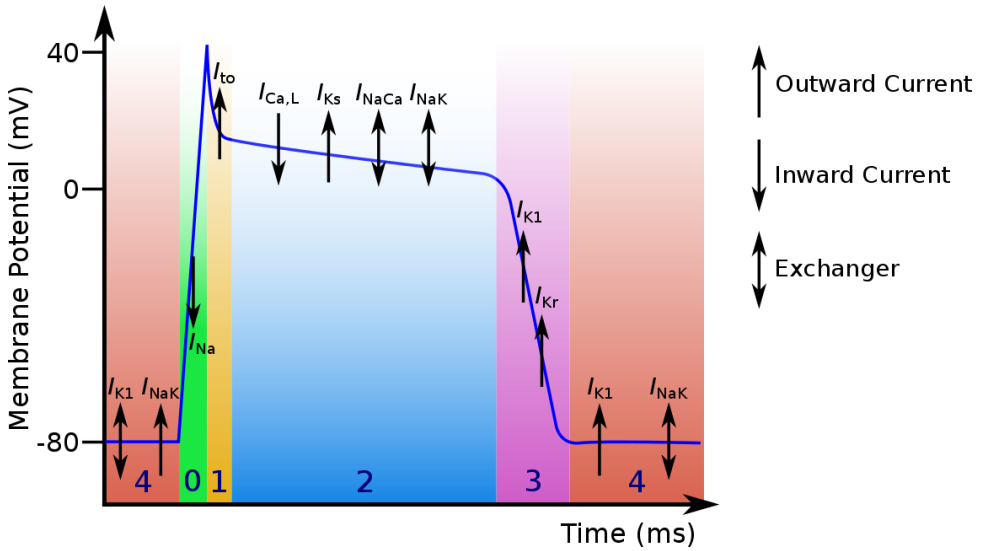


FIGURE 2.4: *Schematic of a ventricular cardiac AP, with the different 'phases' of the AP shown, and which key currents are involved in each phase. Upward arrows represent outward currents, downward arrows represent inward currents, and double arrows represent exchangers. The position of the arrows indicates their importance during a particular phase (their precise location is not important in this schematic) without necessarily implying complete inactivity during any other phase of the AP.*

2.2.1 The Action Potential

The ion flow through these transporters causes changes in the internal/external ion concentrations that manifest as changes in V_m (which in turn influences the action of the channels). The cyclic, periodic change in membrane potential is referred to as the *action potential (AP)*. An example of an action potential, showing the different 'phases', is shown in Fig. 2.4. It should be noted that direct measurement of the AP is not possible for all experimental protocols, as it requires electrodes *in situ* in the intracellular and extracellular spaces; in a clinical setting this is rarely practicable. As such, indirect measurements of the AP are of great use, with one of the key techniques being *electrocardiograms (ECGs)*—by measuring the potential difference between different points on the surface of the body, inferences can be made about the state of depolarisation of the heart, and thus of the progression of the AP.

The AP is separated into 5 different phases, outlined below, with the important currents in each phase mentioned (further details regarding the currents will be provided in §2.2.2).

Phase 0: Period of rapid depolarisation that marks the start of the AP. It is initiated by V_m reaching a threshold value that causes the sodium current (I_{Na}) to activate, causing a rapid influx of sodium (Na^+) into the cell; this threshold potential is reached either by external stimulus within the ventricles and atria, or due to peculiar properties of the cells within the sino-atrial node and atrio-ventricular node. In response to the increase of the intracellular Na^+ concentration ($[Na^+]_i$), the direction of the sodium-calcium exchanger (I_{NaCa}) transiently reverses, and this newly outward current brings in calcium (Ca^{2+}) and removes Na^+.

Phase 1: Transient repolarisation. The Na^+ channels rapidly deactivate (the process leading to their reactivation does not start until the cell repolarises at the end of the AP), and the activation of transient outward potassium (K^+) current (I_{to}) results in a period of rapid, partial repolarisation. There may also be a contribution from a Ca^{2+}-activated Cl^- current (referred to in the literature as either I_{CaCl} or I_{to2}). Depending on the strength of these currents, this repolarisation may be such that there is a 'notch' in the AP, where the cell transiently repolarises beyond the subsequent plateau potential. For example, there is a notch in the AP for ventricular epicardial cells, but no notch for ventricular endocardial cells. The characteristics of this phase are also species-dependent (Carmeliet, 2006).

Phase 2: Plateau phase. The membrane potential is sustained at a relatively constant level by a balance of Ca^{2+} influx via L-type Ca^{2+} current ($I_{\mathrm{Ca,L}}$), and K^+ efflux, through the rectifier K^+ currents (rapid, I_{Kr}, and slow, I_{Ks}). Despite being a rapidly activated current, I_{Kr} does not carry a large current early during this phase, but only peaks at the end. The inward rectifier K^+ current (I_{K1}) shows a dramatic fall in conductance during this phase. While most I_{Na} is inactivated during phase 1, there is a small contribution from I_{Na} when V_m is in the limited range where activation and inactivation both occur. Late during phase 2, due to the increase in intracellular Ca^{2+} concentration ($[Ca^{2+}]_i$) as compared to the extracellular ($[Ca^{2+}]_o$), the reversal potential for I_{NaCa} increases to a value greater than V_m, and thus I_{NaCa} returns to being an inward current (for details of the reversal potential, see §3.2.1).

Phase 3: Repolarisation. The L-type Ca^{2+} current channels close, while the I_{Ks} channels remain

open, allowing continuing K^+ efflux resulting in a repolarisation of the cell to the original resting potential (V_{rest}). I_{K1} opens during this phase.

Phase 4: The resting phase. I_{NaCa} is active during this phase, transporting 3 Na^+ ions into the cell in exchange for a single Ca^{2+} ion, thus working to restore the resting $[Ca^{2+}]_i$ concentration, at the cost of a depolarising electrogenic current. In pacemaker cells, there is no counterbalance to this depolarisation, and thus the cell slowly depolarises until it reaches an activation threshold to initiate a fresh AP. In ventricular and atrial cells, however, I_{K1} counteracts the electrogenic current of I_{NaCa}, leading to Phase 4 being a period of relatively stable membrane potential.

It should be noted that the above description of which currents act during which phase is only an outline. The failure or part failure of any individual component of the cell mechanism does not necessarily lead to the failure of the whole system. This pseudo-redundancy was first termed *repolarisation reserve* in Roden (1998), and was demonstrated experimentally in Varró *et al.* (2000). It is essentially the concept that a loss in repolarisation function caused by a reduction or loss of function in one repolarising current can be recovered by increased action of an alternative repolarising current. Such a loss of function can have many possible causes, such as loss-of-function mutations in the genotype (Rosati and McKinnon, 2004) or the effect of drug block. Most often, the term repolarisation reserve is applied to K^+ channels, and specifically for the interaction between I_{Kr} and I_{Ks} (Xiao *et al.*, 2008) . Several currents are noted for their rôle in maintaining the repolarisation reserve of the cell, (I_{Kr}, I_{Ks}, I_{K1}, I_{to}, $I_{Ca,L}$, I_{Na} (Varró and Baczkó, 2011)). The repolarisation reserve is not constant, but rather is dynamic with pacing rate, and variable between species and tissues within the heart (Carmeliet, 2006).

It is not just the repolarisation reserve that is dynamic, but the entire action potential itself—there can be significant variations in the AP morphology between different regions of the heart, caused in turn by different ion channel concentrations (Giles and Imaizumi, 1988). Beyond such so-called 'developmental regulation', it is also possible for the myocyte to adapt to environmental changes, and to ensure the phenotype of the heart is appropriate for the demands placed upon it ('homeostatic regulation') (Rosati and McKinnon, 2004).

A key example of homeostatic regulation is the variation of action potential duration (defined as the interval between the initial upstroke of the AP and subsequent repolaristion, referred to as APD) according to the heart's pacing rate. The manner in which the APD varies with pacing rate is often described using a restitution curve that shows the relation between APD and the *diastolic interval* (DI, defined as to the quiescent phase of the cell); the sum of APD and DI equals the *cycle length (CL), i.e.* APD + DI = CL. The graphical representation and interpretation of the APD in this manner, with a view to a predicting APD changes after rate changes, was first suggested by Nolasco and Dahlen (1968).

The APD restitution curve describes the duration of the $(i+1)$-th APD as a function f of the time since the preceding AP, *i.e.* the i-th DI. This is typically a monotonically increasing function, and can be expressed as $\mathrm{APD}_{i+1} = f(\mathrm{DI}_i)$. By linearising around the fixed point APD^*, and describing changes in APD as small perturbations round this point ($\mathrm{APD}_i = \mathrm{APD}^* + \delta\mathrm{APD}_i$), the following expression can be derived (also making use of the Taylor expansion of $f(\mathrm{DI}_i)$, and assuming $\mathscr{O}(\delta\mathrm{DI}^2)$ is small and can thus be neglected compared to the other terms):

$$\begin{aligned} \mathrm{APD}^* + \delta\mathrm{APD}_{i+1} &= f(\mathrm{DI}_i) && (2.1)\\ &= f(\mathrm{DI}^*) + f'(\mathrm{DI}^*)\delta\mathrm{DI}_i + \mathscr{O}(\delta\mathrm{DI}_i^2) && (2.2)\\ &\approx f(\mathrm{DI}^*) + f'(\mathrm{DI}^*)\delta\mathrm{DI}_i. && (2.3) \end{aligned}$$

By recalling that CL = APD + DI (and thus, at constant CL, $\delta\mathrm{DI}_i = -\delta\mathrm{APD}_i$) and $\mathrm{APD}^* = f(\mathrm{DI}^*)$, this be further simplified:

$$\delta\mathrm{APD}_{i+1} = -f'(\mathrm{DI}^*)\delta\mathrm{APD}_i. \tag{2.4}$$

Whenever $|f'(\mathrm{DI})| > 1$, small deviations from this fixed point will thus be amplified, *i.e.* if the system is perturbed by a change in DI, this small perturbation will amplify, causing greater and greater changes in both APD and DI; this is represented graphically in Figs. 2.5A and 2.5B. If APD is plotted as a function of CL, this behaviour manifests as a *bifurcation*, where a smooth change leads to a sudden qualitative change in the behaviour of the system (Fig. 2.5C).

It should be noted that this approach has some limitations, as it presents the oversimplification that the APD is dependent entirely on the preceding DI. Thus, while the resitution curve can be a useful indicator of a tissue's susceptibility to fibrillation, wave breakup and other disorders, it is by no means the only such indicator (Riccio *et al.*, 1999). Furthermore, it makes no account of the $[Ca^{2+}]_i$ dynamics and their influence on APD—this is discussed further in §2.3.2.

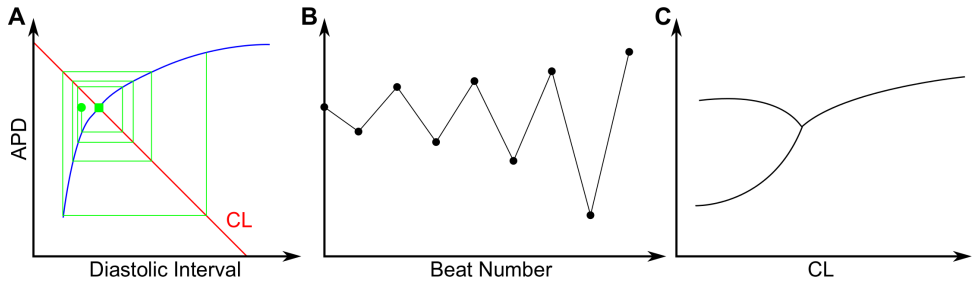


FIGURE 2.5: *Example of a restitution curve with alternans predicted.* (A) *An example restitution curve (shown in blue); pacing at a constant CL can be represented by the red straight line. A small perturbation (represented by the green circle) from the equilibrium point (represented by the green square) can lead to growing perturbations, that eventually settle to alternans* (B) *Resulting variation in APD with beat number resulting from the pattern shown in* (A). (C) *Plot showing variation of APD with CL, with a bifurcation leading to alternans.*

2.2.2 Ion Channel Properties

What follows is a summary of the properties of ion channels of special import for this thesis—it is by no means exhaustive. Focus is given to those currents that are varied in Chapter 5: the rapid delayed rectifier K^+ current (I_{Kr}); the slow delayed rectifier K^+current (I_{Ks}); the inward rectifying K^+current (I_{K1}); the transient outward current (I_{to}); the Na^+/K^+ pump current (I_{NaK}); the L-type Ca^{2+} current ($I_{Ca,L}$). Details are also given for the Na^+/Ca^{2+} exchange current (I_{NaCa}). Where possible, the data relate directly to rabbit, as it is known that differences between species can be significant (Bassani *et al.*, 1994); for example, I_{to} plays an important rôle in repolarisation in rodents, while playing a relatively minor rôle in repolarisation in larger mammels (Rosati and McKinnon, 2004).

Repolarisation, and indeed the entire action potential, is dependent on the operation and interaction of these and other currents. While interactions between currents act to make the process relatively robust with compensatory mechanisms, the vulnerability of repolarisation is evident when depolarising factors (I_{Na}, $I_{Ca,L}$) are augmented or repolarising factors (I_{Ks}, I_{K1}) diminished. The relative importance of any individual current changes depending upon the demands placed upon it by the needs of the action potential, and can thus change during physiological and pathological conditions; the arrhythmogenic properties of some of these currents will be discussed further in §2.3.2.

K^+ Currents

The rapid delayed rectifier K^+ current (I_{Kr}), as the name implies, is the more rapidly activating of the two rectifier K^+ currents ($\tau \approx 40$ ms at $+30$ mV, compared to $\tau \approx 800$ ms for $V_m > 0$ mV for I_{Ks} (Jost *et al.*, 2007; Varró and Baczkó, 2011)), and rapidly activates once V_m increases above -30 mV. However, the channel inactivates even more rapidly in a process that precedes voltage-dependent inactivation (Spector *et al.*, 1996; Carmeliet, 2006; Varró and Baczkó, 2011). Due to this, I_{Kr} channels are largely closed during the plateau phase of the AP, only reopening when the cell repolarises to about 0 mV, and then acts as an outward current to aid repolarisation. The transient nature of the current is due to its rapid recovery from inactivation, and subsequent slow deactivation. At slow rates, the contribution of I_{Kr} diminishes, resulting in a positive feedback loop regarding prolongation of the APD (Virág *et al.*, 2009).

When I_{Kr} is only impaired in a minor way, APD may not necessarily increase due to compensating mechanisms within the AP. However, if the function of I_{Kr} is impaired substantially in some way, APD is measured to be significantly prolonged, both by direct and indirect measurement of the membrane potential, suggesting especial importance in cellular repolarisation (Varró *et al.*, 2000; Lengyel *et al.*, 2001; Jost *et al.*, 2005). It can also be noted that increased extracellular K^+ is known to enhance I_{Kr} (Sanguinetti and Jurkiewicz, 1992; Yang *et al.*, 1997)—this is in opposition to the expected reduction from concentration gradient considerations (see §3.2.1 for further details of the formalism regarding the interaction between ion concentrations and ion channel conductances). Due to its importance for repolarisation, drug block of I_{Kr} is potentially of great concern, and one of the key methods for assessing drug safety is to determine the extent of its block of I_{Kr}. Unfortunately, I_{Kr} passes via a channel encoded by the human ether-á-go-go related gene (HERG), and is known for its susceptibility to the effects of drug block (Haverkamp *et al.*, 2000; Vandenberg *et al.*, 2001). However, recent work indicates the chronic exposure to drugs that were thought to be solely I_{Kr} blockers can increase arrhythmic risk by a mechanism involving an increase of a late Na^+ current (Yang *et al.*, 2014).

The slow delayed rectifier K^+ current (I_{Ks}) takes longer to activate than its partner (500–1,000 ms at plateau phase), and deactivates rapidly at negative V_m (Jost *et al.*, 2005; Varró and Baczkó, 2011). It

carries a slowly increasing current over the duration of the plateau phase. At rapid pacing rates, I_{Ks} increases—this is thought to be due to the kinetics of the channel, with an 'inactivated' state being intermediate between the open and closed states. During rapid pacing, there is less time to transition fully to the closed state, and thus there is a greater proportion of I_{Ks} channels available for immediate opening from the inactivated state (Silva and Rudy, 2005). I_{Ks} is also sensitive to $[Ca^{2+}]_i$, increasing when $[Ca^{2+}]_i$ is increased (Meech and Standen, 1975; Tohse, 1990; Carmeliet, 2006), though this effect is not modelled in the computational models considered in this dissertation.

Drug block of I_{Ks} causes AP prolongation, but not to the same extent as I_{Kr}; while direct measurements show a slight increase in APD during I_{Ks} block, there is very little or no change in indirect measurements of repolarisation, unless the AP is already (artificially) prolonged (Varró *et al.*, 2000; Lengyel *et al.*, 2001; Jost *et al.*, 2005). This implies that its amplitude, compared to that of I_{Kr}, during a typical AP is small—this has been confirmed experimentally under normal conditions (Varró and Baczkó, 2011). Combined with its slow activation, there is thus relatively little I_{Ks} active during the AP (Jost *et al.*, 2005). However, its long activation time also means the effect of I_{Ks} block is more pronounced when APD is prolonged, due to (i) the net outward current at long pacing rates is smaller, so the fractional effect of I_{Ks} is greater, and (ii) more channels are activated during a long AP (Carmeliet, 2006). Due to this action, and the response of I_{Ks} to sympathetic stimulation for 'fight or flight' responses, the current provides a negative feedback for APD prolongation, acting to curtail the increased action of $I_{Ca,L}$ that occurs at longer pacing rates. Thus, while under 'normal' circumstances I_{Ks} has limited effect on the repolarisation reserve of the cell, it acts as an effective buffer when APD is longer than normal (and thus serves as a key supporter of the repolarisation reserve if I_{Kr} is blocked).

The transmural differences in the expression of I_{Ks} are one reason behind the transmural variation of APD, and also explains why I_{Kr} block can have a greater or lesser effect, depending on the abundance of the compensatory effect of I_{Ks}; the scarcity of I_{Ks} can be noted in Purkinje fibres and M-cells, while it is abundant in subepicardial and subendocardial cells (Vandenberg *et al.*, 2001; Carmeliet, 2006). The density of I_{Ks} channels has also been shown to increase in response to sustained I_{Kr} block, as an example of cardiac remodelling (Xiao *et al.*, 2008).

I_{K1} is a strongly inwardly rectifying K^+ current, which means that it passes inward current more easily than outward current, and cannot be described as a simple Ohmic conductor. Thus, when V_m is greater than -30 mV, the channel is inactivated, and it plays a negligible rôle during the plateau phase of the AP. However, it has a self-reinforcing rôle in the repolarisation of the cell once V_m decreases to the extent that I_{K1} can be activated. It should be noted that this is not a voltage-dependent activation, but is based on an unblocking of the channel: when $V_m > -50$ mV, the channel is blocked by Mg^{2+} and other biological molecules that enter the channel from the intracellular side in a voltage-dependent manner (Ishihara *et al.*, 2002; Carmeliet, 2006). Similar to I_{Kr}, I_{K1} has been implicated in a positive feedback loop for the lengthening the APD at slow pacing rates (Virág *et al.*, 2009). As the current is fully open at V_{rest}, it resists depolarisation caused by either increased pacemaker activity, or Ca^{2+} overload-related delayed afterdepolarisations (DADs). Consequently, impairment of its function could lead to proarrhythmic effects by making the cell more susceptible to ectopic APs (extrasystoles).

I_{to} (also occasionally referred to as I_{to1}) is actually composed of two separate currents, a rapidly recovering component ($I_{to,f}$) and a slowly recovering component ($I_{to,s}$). As a combined unit, it both activates and inactivates rapidly for $V_m > -20$ mV, and is of greatest importance during the initial repolarisation phase of the AP (see §2.2.1 for more details). As such, it is believed to have little influence directly on the end repolarisation of the cell, but due to its early rôle, and its consequent effect on the plateau potential, it is believed to have influence on subsequent currents, which lead to great indirect influence. I_{to} is also known for its transmural variation, being greater in epicardial than endocardial tissue, which in turn leads to noticeable changes in the AP morphology in the initial stages of the AP (Liu *et al.*, 1993; Rosati *et al.*, 2001; Roden *et al.*, 2002).

L-Type Ca^{2+} Current

In response to an increase in V_m, L-type Ca^{2+} channels (LCC) open, providing the source for $I_{Ca,L}$, an inward current allowing Ca^{2+} ions into the cell. The slight increase in Ca^{2+} in the subsarcolemmal space (the space immediately within the cell membrane) serves as the trigger for release of further

Ca^{2+} sequestered within the sarcoplasmic reticulum (SR)—see §2.2.3 for further details. This trigger action is arguably its main function, and is often noted in conjunction with $I_{Ca,L}$ channels being highly localised to the SR to facilitate this (Bhargava *et al.*, 2013). It slowly inactivates due to voltage, and thus the main reason for its inactivation is due to the more rapid Ca^{2+}-induced inactivation. This is in response to local subsarcolemmal Ca^{2+} concentration, which can vary dramatically from the bulk cytosolic concentration and dynamically changes during the plateau phase. The Ca^{2+}-induced inactivation is modulated via a protein called calmodulin (Carmeliet and Vereecke, 2002; Restrepo *et al.*, 2008). If the AP is prolonged such that $I_{Ca,L}$ channels are able to be reactivated, the resulting resurgence of the inward current caused by this reactivation of $I_{Ca,L}$ can lead to secondary depolarisations or early after-depolarisations (EADs)—see §2.3.2 for further details of EADs (Carmeliet, 2006). If $I_{Ca,L}$ (or the sodium current, I_{Na}) are augmented and have their activity increased, this serves to make the plateau potential more positive. While at first glance this may indicate that AP may lengthen, it is rather the case that this may serve to enhance activation of outward K^+ currents, thus shortening APD.

Exchangers

I_{NaK} is due to the Na^+/K^+ pump, which moves 3 Na^+ ions out of the cell in exchange for 2 K^+ ions, thus making it an electrogenic exchanger (in that the exchange is not electrically neutral); this outward current acts in support of the repolarisation reserve. The Na^+/K^+ pump acts as the main means by which the cell maintains a Na^+ and K^+ concentration gradient across the cell membrane, and it is thus an *active transport* process—it requires an input of energy to perform its function. This input of energy comes from the hydrolysation of adenosine triphosphate (ATP) to adenosine diphosphate (ADP)—as such, the action of the Na^+/K^+ pump is sensitive to the concentrations of ATP and ADP. It is also sensitive to the gradients of the ions it must work to maintain, and due to this sensitivity to the intracellular Na^+ gradient ($[Na^+]_i$), it is affected by the rate of stimulation.

The Na^+/Ca^{2+} exchange current (I_{NaCa}, also referred to as I_{NCX}) is also an electrogenic exchanger, this time exchanging 3 Na^+ ions for one Ca^{2+} ion. By this process, it is, along with the SERCA pump

(which acts to sequester Ca^{2+} from the cytosol to the SR), largely responsible for restoring the low cytosolic Ca^{2+} concentration during diastole. It is the main means for extruding Ca^{2+} from the cell, and responsible for 70-90% of the Ca^{2+} efflux (Eisner and Sipido, 2004). Despite this, the activity of I_{NaCa} can be inhibited by 80-90% with cardiac function still being maintained (Henderson *et al.*, 2004). I_{NaCa} depends strongly on V_m, $[Ca^{2+}]_i$ and $[Na^+]_i$ (Clusin, 1983), and thus its magnitude during the AP is difficult to estimate (a problem compounded by the lack a specific inhibitor for the current). It is an outward current at the start of the AP, when V_m and $[Ca^{2+}]_i$ are both low, but then changes to an inward current during the late plateau phase. Due to this sensitivity to $[Ca^{2+}]_i$, in times of Ca^{2+}-overload I_{NaCa} can provide a depolarising current, thus increasing the likelihood of DADs and EADs (Clusin, 2003).

2.2.3 Calcium Dynamics

Arguably, the complex electrical activity of the AP just described exists for the sole purpose of ensuring the heart acts as an effective mechanical pump. As such, the linking of the electrical activity of the heart to its mechanical contraction is vital, and is referred to as *excitation-contraction coupling* (ECC). What follows is a brief summary of the Ca^{2+} release and recovery mechanisms used by the cell during the AP, and of the mechanism of ECC (the reverse side of this mechanism, termed mechanoelectric feedback, shall not be discussed here). More details of the mechanical aspect of the cardiac cycle, and of the attempts to model it and integrate it with electrical models, can be found in Trayanova *et al.* (2011). A summary of Ca^{2+} handling in the cell is provided by Eisner *et al.* (2000).

For this discussion, the cell may be decomposed into sections called calcium release units (CRUs), also known as dyads (Cleemann *et al.*, 1998); a schematic is shown in Fig. 2.6. These CRUs, each approximately $2 \times 1 \times 1\,\mu m$ in size (Restrepo *et al.*, 2008), are spread roughly evenly throughout the cell to allow for a uniform Ca^{2+} influx and consequent contractile action throughout—the number of CRUs in the cell has been estimated to be between 10,000 and 100,000 (Cleemann *et al.*, 1998; Greenstein and Winslow, 2002). Anatomically, the CRU may be considered to be a section of the cell containing a section of the cell membrane (including invaginations referred to as T-tubules) with

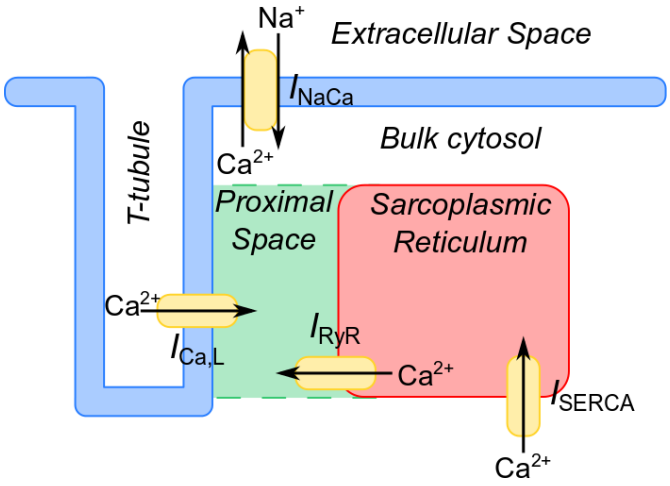


FIGURE 2.6: *Schematic of a Calcium Release Unit. Only currents mentioned in the text are shown—other currents play their own rôle, but are not mentioned here. The proximal space is highlighted in green between the cell membrane (blue) and the sarcoplasmic reticulum (red). Ion channels are shown, with arrows indicating the direction of flow of ions.*

some L-type Ca^{2+} channels (LCCs), and a section of the sarcoplasmic reticulum (SR) (Yu *et al.*, 2008).

When V_m rises at the start of the AP, LCCs open, allowing the flow of extracellular Ca^{2+} into the cell. A key feature of the CRU architecture is the proximity of the T-tubule with its LCCs to the SR, and thus when $I_{Ca,L}$ is activated, the Ca^{2+} concentration in the space between the sarcolemma and the SR, referred to as the *proximal/subsarcolemmal space*, increases at a faster rate than the concentration in the bulk cytosol ($[Ca^{2+}]_i$). In response to the increase in Ca^{2+} concentration in the proximal space, Ca^{2+} is released from the SR to the bulk cytosol, in a process termed *calcium-induced calcium release* (CICR) (Fabiato, 1992). This release is predominately by *ryanodine receptors* (RyR), but at least one other channel (Inositol triphosphate-activated channels, or IP_3) is known to play a part, and others are reported (Pozzan *et al.*, 1994). The RyR-mediated release is modulated by means of a Ca^{2+}-binding protein within the SR called calsequestrin (CSQN)—computational modelling of its effects by Restrepo *et al.* (2008) demonstrate that this modulation results in a steep load-release relationship. This sustained Ca^{2+} release from the SR to the intracellular space occurs during Phase 2 of the AP.

The Ca^{2+} released from the SR is recovered by the sarco/endoplasmic reticulum Ca^{2+}-ATPase pumps (referred to as SERCA) (Franzini-Armstrong *et al.*, 2005), which is inhibited by a protein called phospholamban, among other factors (Xu *et al.*, 1993; Eisner *et al.*, 2000; Talukder *et al.*, 2009). Further Ca^{2+} is extruded from the cell by I_{NaCa} (Laurita and Rosenbaum, 2008). Other mechanisms for removing cytosolic Ca^{2+} are negligible (Bassani *et al.*, 1994). At steady state, the influx from $I_{Ca,L}$ and the efflux from I_{NaCa} are equal. When not in steady state, the value of $[Ca^{2+}]_i$, influenced by SR Ca^{2+}

release (and thus SR Ca^{2+} load), operates to return the system to steady state. This process has been referred to as 'autoregulation' (Eisner *et al.*, 2000).

The 'resting' value of $[Ca^{2+}]_i$, referred to as the diastolic Ca^{2+}($[Ca^{2+}]_i^{dia}$), is heavily dependent on the uptake/extrusion process—if there is an inhibition/upregulation of either process, it can have a significant beat-to-beat effect on $[Ca^{2+}]_i^{dia}$ by leading to conditions for Ca^{2+} alternans (for further details, see §2.3.2). It should be noted that the rate of reduction of $[Ca^{2+}]_i$ is not a linear processes: Bers and Berlin (1995) demonstrated that SERCA can be modelled using Michaelis-Menten kinetics (for details of this mechanism, see §A.2) in the buffering/sequestration process. This is ideal for the requirements of the system, in that it increases the rate of decay of $[Ca^{2+}]_i$ when $[Ca^{2+}]_i$ is increased. That is, if the Ca^{2+} transient (the difference between the minimum and maximum values of $[Ca^{2+}]_i$) is greater, the cell is able to return $[Ca^{2+}]_i$ to a diastolic value within a similar timescale to a small transient.

The reason this Ca^{2+} release is vital for ECC is the interaction between Ca^{2+} and the contractile units of the cell, called the sarcomere, which can be considered to consist of two interlocking proteins, actin and myosin, and is approximately 2 μm in length. Interaction between actin and myosin is prohibited by troponin-I and troponin-T, two of three proteins in the troponin protein complex, binding to the actin filament. When $[Ca^{2+}]_i$ increases, the free Ca^{2+} binds to troponin-C, the third protein in the complex. This binding causes a conformational change in troponin, causing it to unbind from actin. With this inhibition removed, actin and myosin interact in a stepping process that results in the sarcomere, and thus the myocyte, contracting (Kamisago *et al.*, 2000). This peak of this contraction phase is referred to as *systole*, with the following relaxation (when $[Ca^{2+}]_i$ reduces and inhibition of the actin-myosin bonding resumes) referred to as *diastole*. It should be remembered that the Ca^{2+} transients *precede* contraction, and the upstroke velocity of the transient is faster than the rise in force (Lee *et al.*, 1988). Thus, while it is common for the systolic $[Ca^{2+}]_i$ ($[Ca^{2+}]_i^{sys}$) to be synonymous with the maximum value of $[Ca^{2+}]_i$ and $[Ca^{2+}]_i^{dia}$ with the minimum value of $[Ca^{2+}]_i$, a definition of $[Ca^{2+}]_i^{dia}$/$[Ca^{2+}]_i^{sys}$ based on mechanical action of the heart may not correspond to these minimum/maximum values.

2.3 Cardiac Dysfunction

Cardiac dysfunction relates to the situation where the function of the heart is impaired in some way. While this often relates to cardiac disease, it is not always the case that dysfunction equates to disease—disease merely imparts a greater disposition to dysfunction.

Cardiac disease and dysfunction represent significant health problems for Western countries. In the UK, cardiovascular disease (CVD) was the biggest killer in 2010, with almost 180,000 people dying and 46,000 of those deaths being premature (premature death being defined as death before the age of 75); 80,000 of these deaths were from coronary heart disease. This costs the UK health system £8.7 billion, and the economy as a whole £19 billion (Townsend *et al.*, 2012). On a global scale, the World Health Organisation estimates CVD is responsible for ∼17 million deaths worldwide in 2008, which equates to 48% of deaths due to non-communicable disease, or a staggering ∼30% of worldwide deaths that year (Alwan *et al.*, 2010). More recent estimates to assess the economic burden of CVD put the world annual cost at $108 billion in 2012 (Cook *et al.*, 2014).

However, the pathology of CVD can often be complicated. Of the fatalities due to sudden cardiac deaths, approximately half are due to ventricular fibrillation or ventricular tachycardia, but the causes behind these events, and the transition to sudden cardiac death (SCD), are poorly understood (John *et al.*, 2012). In-depth analysis of the mechanisms for disease is vital in determining how to treat diseases at a more fundamental level than symptomatically. As such, research has demonstrated many causal links between the cellular mechanisms, such as ion channels and their links to pacing rate, and pathologies (Kurz *et al.*, 1993; Dumaine *et al.*, 1996; Jurkat-Rott and Lehmann-Horn, 2005; Biagetti and Quinteiro, 2006; Inoue *et al.*, 2006; Rodríguez *et al.*, 2006; Nattel *et al.*, 2010).

What follows is a discussion of the effects of ischæmia, which is a leading cause of sudden cardiac death. Ischæmia represents an imbalance between supply and demand of oxygen and nutrients, and is commonly caused by a cessation of normal coronary bloody flow (itself caused by some form of occlusion). Afterwards, a review of some of the processes leading to arrhythmia, or lack of coordinated contraction of the heart, will be given. These arrhythmic mechanisms do not represent an exhaustive

list, but are those mechanisms whose likelihood is increased due to ischæmia, and thus they serve to place the work presented in this dissertation in greater context regarding potential arrhythmogenesis.

2.3.1 Ischæmia

Eighty percent of those who fall victim to SCD have some form of coronary heart disease, and ischæmia is one of the foremost causes for ventricular tachycardia and fibrillation. Ischæmia represents a cessation of normal blood flow to an area of tissue that leads to waste products not being removed and nutrients not being delivered. This results in a series of changes to the tissue and the surrounding area, which, if left untreated, can lead to irreversible damage to the cells in the tissue and cell death (Carmeliet, 1999). At the tissue/organ level, this process can lead to subsequent fibrillation, arrhythmia and the failure of the pump action of the heart (Harris *et al.*, 1954).

As such, investigation into the effects and possible treatments of ischæmia is of high value. Due to the difficulty of gathering human data, especially during an ischæmic event, animal experiments have moved to fill the gap where possible. To that end, rabbit data has been shown to reproduce many of the salient features of human data (Giles and Imaizumi, 1988; Barrett *et al.*, 1997; Panfilov, 2006), and many metrics can be adapted according to a body mass relation (Noujaim *et al.*, 2007).

As has been discussed previously, ion channels are the key determinant for many of the mechanisms of the cell that relate to its pump action, notably the membrane potential and the concurrent change in $[Ca^{2+}]_i$ that leads to cardiac contraction. Changes to these channels thus have a profound effect on the action of the cardiomyocyte, and thus the heart itself; drug block has already been mentioned as one means for changing the action of these channels. Under conditions of ischæmia, changes in the extracellular and intracellular concentrations of ions and metabolites cause significant alterations in the action of the ion channels. Some of these alterations are obvious due to changes in the electrochemical gradients that drive ion flow through some channels—note that it is not just changes in the ion concentration gradients for the channel that impact it, but also the changes in other ion concentrations leading to changes in V_m (for details of the modelling of this process, see §3.2.1). However, the changes are more involved than this: for example, active transport processes such as the I_{NaK} pump

are sensitive to the ATP/ADP concentrations, which also demonstrate significant changes during ischæmia. The complicated interactions between different changes in the ischæmic environment can make it difficult to predict outcomes: studies have shown that, in some drug trials intended to treat arrhythmic effects, the drug actually had a delitrious effect (Ch'en *et al.*, 1998; Connolly *et al.*, 2011), emphasising the complicated nature of these pathological conditions.

In this thesis, the focus is on the acute inital phase of ischæmia (phase 1A), which is considered as the first $\sim$ 10 minutes following the onset of ischæmic conditions. Much research exists on investigating ischæmia beyond this, in terms of (a) reperfusion, (b) longer infarct times and (c) cardiac remodelling, but these studies are not addressed in detail here as beyond the remit of this work. Phase 1A acute ischæmia is the stage of ischæmia wherein the evolution of changes in the AP is at its most rapid, leading to increased likelihood of wave-breakup due to altered electrophysiological properties (Kaplinsky *et al.*, 1979); it is the period of ischæmia where the arrhythmogenic risk due to reentry is at its greatest (Scherlag *et al.*, 1974; Cascio, 2001; Tice *et al.*, 2007; Trénor *et al.*, 2007). It is for these reasons that it is the focus of this thesis.

The next section details changes to the AP observed during acute ischæmia, with the following section presenting a summary of the changes to the Ca^{2+} handling and dynamics. The results presented here are obtained through a mixture of direct experimentation and insights achieved with the benefit of computational simulation—further details of some of the methods of simulating ischæmia are presented in §3.4.

Ischæmic Changes in the AP

The ischæmic changes in AP are well-documented, and are characterised by an increase in V_{rest}, and a decrease in APD, AP amplitude, and the maximum rate of membrane depolarisation ($(\mathrm{d}V_m/\mathrm{d}t)_{\max}$) (Moréna *et al.*, 1980; Weiss and Shine, 1982; Kléber *et al.*, 1987b; Weiss *et al.*, 1992; Barrett *et al.*, 1997; Carmeliet, 1999; Janse *et al.*, 2001; Rodríguez *et al.*, 2006). These changes are not minor: V_{rest} is increased by $\sim$ 15 mV, APD is reduced by approximately 50%, and AP amplitude is reduced from $\sim$ 120 mV to $\sim$ 90 mV (Carmeliet, 1999; Rodríguez *et al.*, 2002). As a result of these changes, cou-

pled with other underlying changes, ischæmic tissue is known for its arrhythmogenic properties—3 to 9 min after occlusion, APD alternans can be observed in the ventricles, which can then degenerate into spontaneous fibrillation (Downar *et al.*, 1977a).

Another key change in the electrical properties of the cell are changes to the *effective refractory period (ERP)*, which is the time required for the cell to recover its excitability after initiation of the AP. Under normal conditions, in well-oxygenated myocardium, the cell recovers its excitability almost simultaneously with repolarisation. As such, the APD is a good indicator of the ERP (Huang *et al.*, 2004). However, with ischæmic conditions leading to the impaired recovery of I_{Na} (the principal current responsible for the AP upstroke), cellular recovery of excitability is also impaired, and the ERP lengthens beyond the APD; the difference between the two is referred to as *post-repolarisation refractoriness (PRR)*. Some work has shown an initial decrease in ERP during early acute ischæmia (Downar *et al.*, 1977a), while other work has shown a consistent increase (Sutton *et al.*, 2000) during the first three minutes of ischæmia. In both cases, however, the correlation between APD and ERP breaks down, leading to an increase in PRR.

Computer simulations of ischæmia have demonstrated that the changes in the AP can be reproduced by simulating the effects of three key changes induced by ischæmia (Shaw and Rudy, 1994, 1997b,a; Ferrero *et al.*, 1996; Rodríguez *et al.*, 2004): the removal of oxygen from the environment (*anoxia*), the increase in extracellular potassium (*hyperkalæmia*), and the increase in intracellular and extracellular pH (*acidosis*). It should be noted that some simulations and experimental studies of ischæmia use a partial block of the flow of oxygen instead of a complete block: this is referred to as *hypoxia*. Studies have shown that each of these conditions are required for 'successful' ischæmia—individually applied, the conditions present different pathologies (Rodríguez *et al.*, 2006; Ferrero *et al.*, 2014). However, the time course of each of these separate pathologies during ischæmia is poorly defined (Niederer, 2013).

Anoxia's effect is mainly felt not through the lack of oxygen in the ischæmic environment *per se*, but rather through the direct consequence of the lack of oxygen, which is the decline of aerobic respiration and consequent decrease in $[\mathrm{ATP}]_{\mathrm{i}}$ and concomitant increase in $[\mathrm{APD}]_{\mathrm{i}}$. This effects the active trans-

port processes across the cell membrane, which rely on the $[ATP/ADP]_i$ gradient for the energy to perform their function, but the changes also work to activate the ATP-sensitive K^+ current ($I_{K\text{-}ATP}$), which is the single greatest contributor to the shortening of the AP. This outward current was first discovered by Noma (1983), who hypothesised that by shortening the AP, the contraction phase of the myocyte would also be shortened, which would work to conserve the now limited supply of ATP. It also works to hyperpolarise the cell, and by so doing reduce $(V_m - E_K)$—as such, the increased K^+ efflux caused by $I_{K\text{-}ATP}$ is self-limiting (Rodríguez *et al.*, 2002). Experimental data on the channel demonstrated that full activation of the channel in the cell would require a change in ATP/ADP concentrations that are significantly greater than actually observed during ischæmia (Elliott *et al.*, 1989; Furukawa *et al.*, 1991; Ferrero *et al.*, 1996). It is thus currently thought that only minimal activation of the $I_{K\text{-}ATP}$ channels is required to effect the changes in ischæmia. Under this 'spare channel' hypothesis (Cook *et al.*, 1988), activation has been postulated to be as low as $\sim 0.8\%$ (Weiss *et al.*, 1992; Ferrero *et al.*, 1996; Rodríguez *et al.*, 2002; Ferrero *et al.*, 2003b; Trénor *et al.*, 2007). This small degree of activation allows for a very finely balanced activation of the channel to achieve the desired affect. Consequently, it has been noted that the degree of activation of this channel is important for determining the vulnerability of the tissue/organ to reentry in regional ischæmia (Ferrero *et al.*, 2003a; Trénor *et al.*, 2005).

The shortening of the AP (precipitated in large part by the activation of $I_{K\text{-}ATP}$), along with the increase in V_{rest} (minimising the electrochemical gradient for K^+ efflux), works to protect the cell by restricting K^+ loss from the cell as far as possible (Carmeliet, 1999). The anoxic decrease in ATP also works to inhibit I_{NaK}, further reducing K^+ efflux. However, this leads to an increase in $[Na^+]_i$, and coupled with the decrease in $[Na^+]_o$ caused by the lack of perfusion, leads to an increase in $[Na^+]_i$ and an inhibition of the action of I_{NaCa}.

However, the K^+ efflux precipitated by ischæmia does contribute to ischæmic hyperkalæmia. This impact of K^+ efflux via $I_{K\text{-}ATP}$ is negligible on its own—computational simulations have demonstrated that the increase in $[K^+]_o$ requires the coordinated action of $I_{K\text{-}ATP}$ with both inhibition of I_{NaK} and activation of an inward Na^+-pump, I_{NaS} (Rodríguez and Ferrero, 2001b,a; Rodríguez *et al.*, 2002;

Terkildsen *et al.*, 2007). The onset of hyperkalæmia during acute ischæmia is known to follow a biphasic pattern: a rapid rise for the first $\sim$ 10 minutes, followed by a plateau phase (changes later in time are not discussed here) (Wilde *et al.*, 1988). The rate of increase, and final plateau level, of $[K^+]_o$ has been shown to be rate-dependent, with values of $[K^+]_o$ ranging from 12–17 mM reached within 10–15 min (Coetzee and Opie, 1987; Rodríguez *et al.*, 2002). Research indicates that hyperkalæmia (with $[K^+]_o$ greater than 12.5 mM) is vital to the development of reentry, with its absence precluding reentry (Ferrero *et al.*, 2003b). Hyperkalæmia is secondary to $I_{\text{K-ATP}}$ in shortening the APD (Gasser and Vaughan-Jones, 1990)—its main effect is to affect the excitatory properties of the cell/tissue. For the first few minutes of ischæmia, the rise in $[K^+]_o$ and its attendant rise in V_{rest} brings the cell closer to the activation threshold, and thus facilitates an increase in conduction velocity in tissue. However, once $[K^+]_o$ rises beyond 8 mM, the process of reactivation of I_{Na} is inhibited by the increase in V_{rest}. This reduces the number of I_{Na} channels available at the start of the AP, and this reduction in I_{Na} magnitude is reflected in a reduction in the rate of depolarisation of the cell (a reduction in $(\mathrm{d}V_m/\mathrm{d}t)_{\text{max}}$). In severe acute ischæmia (10–12 minutes after onset), this can lead to a biphasic upstroke (Downar *et al.*, 1977a; Russell *et al.*, 1977; Kléber *et al.*, 1978; Janse and Kléber, 1981; Barrett *et al.*, 1997), in which the first phase corresponds to the reduced activation of I_{Na}, and the second phase corresponds to the activation of $I_{\text{Ca,L}}$ that completes the depolarisation. This reduction in availability of I_{Na} channels, and consequent decrease in cellular ability to complete an upstroke for the AP, is thought to be one of the main causative agents behind ischæmic PRR, and changes in myocardial excitability generally (Coronel *et al.*, 2012)—while the APD has shortened, the increase in V_{rest} inhibits the ability of the cell to recover its excitability at the same time.

It should be noted that $(\mathrm{d}V_m/\mathrm{d}t)_{\text{max}}$ is also proportional as the square root to conduction velocity in tissue (Tasaki and Hagiwara, 1957; Walton and Fozzard, 1983; Kléber and Rudy, 2004; Caldwell *et al.*, 2007). However, the reduction in conduction velocity observed in ischæmic tissue may also be at least partly due to the electrical uncoupling of the cells (Kléber *et al.*, 1987a).

The acidosis inherent in ischæmia is due mostly to the accumulation of CO_2 that arises due to the cessation of blood flow, with a lesser rôle being played by the accumulation of lactate (Ichihara *et al.*,

1984). The concentration of hydrogen ions that is represented by the pH is normally a tightly regulated feature of the cell, with small changes being responsible for major cellular dysfunction (Ch'en *et al.*, 1998). During the first 10 minutes of ischæmia, intracellular and extracellular pH drop linearly with time, with a $\sim$ 1 pH unit drop (Neely *et al.*, 1975; Mohabir *et al.*, 1991; Shaw and Rudy, 1997b)[2].

The ischæmic pH drop reduces I_{Na} maximum conductance by 25% (as well as shifting its voltage-current dependence by 3.4 mV) (Kagiyama *et al.*, 1982). For guinea pig ventricular cells, a sigmoidal decrease in maximum conductance of $I_{\mathrm{Ca,L}}$ has been noted (with a 50% reduction at pH 6.6, compared to conductance at a physiological pH of $\sim$ 7.4 (Mohabir *et al.*, 1991; Ferrero *et al.*, 2014)). This contributes further to the decline in of membrane excitability and $(\mathrm{d}V_m/\mathrm{d}t)_{\mathrm{max}}$ already commented upon. In addition to the inhibition caused by anoxia, I_{NaK} has also been shown to be linearly dependent on $\mathrm{pH_i}$, and is thus further inhibited by acidosis (Forbush, 1987; Severi *et al.*, 2002).

It should be noted that the ischæmic conditions described here represent complete ischæmia. In reality, however, it is rarely the case that fully ischæmic tissue occurs without surrounding effects and influences of non-ischæmic tissue, and one must often consider three regions: normal tissue (also referred to as the 'normal zone' (NZ)), the central ischæmic zone (CIZ), and the so-called border zone (BZ), which is the interface between the two. This border zone experiences varying degrees of anoxia, acidosis and hyperkalæmia over different spatial ranges. There are several very important consequences of this spatial heterogeneity, which have been examined in depth in the literature: what follows is a brief outline of the relevant points for this thesis, whose focus is not specifically on the effects of spatial heterogeneity. However, the arrhythmogenic heterogeneities mentioned here may also be found due to underlying variation already present in tissue.

An example model of the spatial distribution of anoxia, acidosis and hyperkalæmia, including transmural variation, is presented in Tice *et al.* (2007) (with another in Romero *et al.* (2009b)). The spatial variation of the different ischæmic parameters used in that study is shown in Fig. 2.7, and demonstrates that the individual components of ischæmia do not vary uniformly across the defined BZ. Niederer (2013) also demonstrated that variation in ion concentrations also varies at different spatial scales across

[2]It should be noted that the value of pH (which is a logarithmic scale of $\mathrm{H^+}$ concentration) falls approximately linearly (see Fig. 10 in Mohabir *et al.* (1991))—it is not the concentration of $\mathrm{H^+}$ that falls linearly.

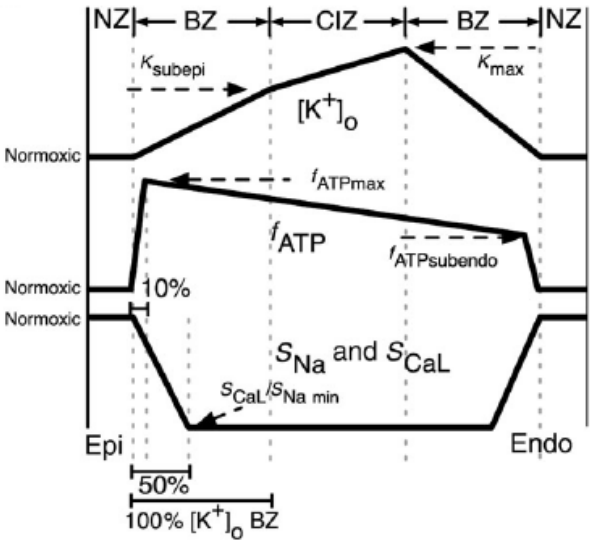


Figure 2.7: *Distribution of hyperkalæmia, anoxia and acidosis in a transmural ischæmic tissue simulation. In non-transmural tissue, there is no gradient of $[K^+]_o$ and f_{ATP} values within their respective ischæmic zones. This figure demonstrates the different ranges of border zones for the different components of ischæmia. Figure originally from Tice* et al. *(2007).*

the BZ. This sets the stage for heterogeneity in tissue responses. One key feature of this is the evolution of APD and ERP: in both the CIZ and BZ, APD decreases due to the action of $I_{K\text{-}ATP}$. However, due to the anoxic conditions with normal $[K^+]_o$ in the border zone, there is no concurrent increase in V_{rest}, and thus no increase in ERP, in the border zone, while the ERP in the CIZ increases as described above (Tice *et al.*, 2007; Coronel *et al.*, 2012; Ferrero *et al.*, 2014). Furthermore, due to the differences in repolarisation states, there can be a current flow from tissue with late repolarisation to tissue with early repolarisation (NZ to CIZ/BZ). This current flow causes depolarisation of the CIZ/BZ. If this depolarisation reaches a threshold value in excitable tissue, a spontaneous, ectopic beat is generated, leading to *phase 2 reentry* (Lukas and Antzelevitch, 1996; Coronel *et al.*, 2009, 2012).

It should be remembered that the BZ is not a simple 'buffer' between the CIZ and the NZ. Experimental data have also shown that a majority of extrasystoles occur in the peri-infarct zone, corresponding here with the BZ. These data imply that the conditions in the BZ, and not just in the CIZ, promote arrhythmogenesis (Chou *et al.*, 2007). This may be due in part to the difference in conditions between the CIZ and the NZ leading to a sharp heterogeneity present in the BZ, which then gives rise to arrhythmogenic conditions (more detail is given in §2.3.2).

Ischæmic Changes in $[Ca^{2+}]_i$

Changes during ischæmia are not limited to changes in the action potential—notable changes also occur in $[Ca^{2+}]_i$ and the contractile mechanisms of the cell. It should be noted that changes in $[Ca^{2+}]_i$ are more important during phase 1B of ischæmia, and not during phase 1A—the following summary of ischæmic changes in the $[Ca^{2+}]_i$ dynamics of the cell serve to provide further context for this thesis, and do not represent the focus therein.

Immediately post-occlusion, there is an increase in $[Ca^{2+}]_i$ until $\sim$ 2 min post-occlusion, followed by a decline (occasionally to pre-occlusion levels), followed by a secondary increase at 5–15 min post-occlusion (see Fig. 2.8) (Lee *et al.*, 1988; Mohabir *et al.*, 1991; Camacho *et al.*, 1993). The increase in $[Ca^{2+}]_i$ could be in small part be responsible for the increase in V_{rest}, due to the action of Ca^{2+}-activated cation channels (Colquhoun *et al.*, 1981). The changes in $[Ca^{2+}]_i$ can be described more fully as

- elevation of $[Ca^{2+}]_i^{sys}$,
- elevation of $[Ca^{2+}]_i^{dia}$,
- broadening of systolic Ca^{2+} peak (indicative of reduced SR uptake function), and
- increase in net amplitude of the Ca^{2+} transient (though this is not always observed (Camacho *et al.*, 1993)).

In addition to the broadening of the systolic Ca^{2+} peak, there is a large body of evidence that the time constant of $[Ca^{2+}]_i^{dia}$ decline increases during ischæmia (Allen and Orchard, 1983; Lee *et al.*, 1988; Camacho *et al.*, 1994) (though not during hypoxia (Silverman *et al.*, 1991)). This may be achieved via reduced Ca^{2+} uptake to the SR, or via reduced extrusion of Ca^{2+} via I_{NaCa}. Evidence indicates that there is minimal change in Ca^{2+}-uptake from the extracellular space during ischæmia (Bourdillon and Poole-Wilson, 1982).

The increase in $[Ca^{2+}]_i$ also occurs for low-flow ischæmia, thus it is also likely to be present in the border zone of ischæmic tissue (Camacho *et al.*, 1993). It should be noted that the time course of

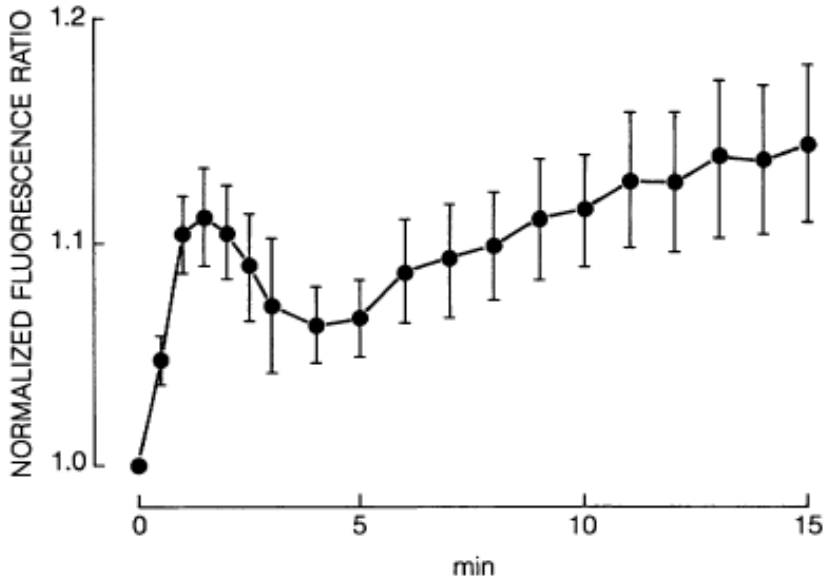


Figure 2.8: *Mean systolic fluoresence ratio for rabbit hearts under ischæmic conditions, normalised to pre-ischæmic values. Data obtained using whole rabbit hearts loaded with indo-1, a cell-permeant fluorescent indicator for* Ca^{2+}*, and demonstrate an initial increase in* $[Ca^{2+}]_i$*, followed by a marginal decrease at 5–10 min post-occlusion, before increasing further. Figure originally from Mohabir* et al. *(1991).*

these changes in $[Ca^{2+}]_i$ is the subject of some debate—different experiments give different results, especially for the time delay associated with the increase in $[Ca^{2+}]_i^{dia}$ (Carmeliet, 1999).

The causes of the initial increase in $[Ca^{2+}]_i$ are not fully defined. It has been hypothesised that it may be due to reduced SR uptake, or due to movement of Ca^{2+} from the mitochondria to the cytoplasm. It has also been suggested that the initial increase is due to competition between H^+ (increasing with decreasing pH) and Ca^{2+}, causing release of Ca^{2+} from binding sites, but the initial increase is not seen under conditions of solely acidosis (Mohabir *et al.*, 1991). The secondary increase, on the other hand, coincides with pH_i increasing to a 'tipping point' at which changes in $[Ca^{2+}]_i$ are noted in purely acidic conditions (Bers and Ellis, 1982; Mohabir *et al.*, 1991). This increase may be augmented due to increased activation of $I_{Ca,L}$ caused by the increase in V_{rest}, though Niederer (2013) concluded that the increase in $[Ca^{2+}]_i^{dia}$ is due primarily to inhibition of I_{NaK}, and the associated changes to the function of I_{NaCa}, rather than by changes in $I_{Ca,L}$.

Changes in the SR uptake/extrusion process are often cited as the prime cause of the increase in

$[Ca^{2+}]_i^{sys}$—for a fuller summary of the changes in SR function during ischæmia, both in terms of uptake (SERCA) and release (RyR), see Mubagwa (1995). Other details of changes in Ca^{2+} handling during ischæmia are given in Talukder *et al.* (2009) and Carmeliet (1999), including changes in the mitochondrial Ca^{2+} handling. However, the consensus is that Ca^{2+} pathophysiology is mainly due to changes in SR uptake/release, and thus no further details shall be given here of the mitochondrial changes (Fauconnier *et al.*, 2013).

There is a large body of evidence for impaired overall SERCA action during ischæmia (Lee *et al.*, 1967; Toba *et al.*, 1978; Dhalla *et al.*, 1988; Kaplan *et al.*, 1992; Temsah *et al.*, 1999). It has been suggested that the decrease in SERCA action is caused by ATP deficiency (Camacho *et al.*, 1993) or by free radicals (Zweier, 1988; Xu *et al.*, 1997; Temsah *et al.*, 1999; Wang *et al.*, 2013). The decrease in function persists after treatment for assays, thus indicating that the causative agent in the change is not $[Ca^{2+}]_i$ itself, while the recovery of SERCA action after reperfusion indicates SERCA is not denatured. It is of note that experiments indicate that during cardiac remodelling post-infarct, expression of SERCA (both in terms of mRNA and protein expression) is down-regulated, and the SERCA inhibitor phospholamban is up-regulated (Sun *et al.*, 2005).

The decrease in SERCA action may come through a decrease in activity of individual SERCA channels, or a decrease in the number of active channels, or both. Kinetic studies appear to show a decrease in action of SERCA with no change in Ca^{2+} sensitivity, with antibody assays also demonstrating a reduction in the number of active SERCA channels (Levitsky *et al.*, 1989). These results indicate that ischæmic conditions reduce the open probability of the SERCA channel.

However, Krause and Hess (1984) presented results indicating that a decrease in pH_i correlates with a shift in the sensitivity of SERCA to higher $[Ca^{2+}]_i$ (which would lead to an increase in the resting levels of $[Ca^{2+}]_i$). This, coupled with the reduction in maximal conductance velocity also observed, would consequently explain the observed depressed Ca^{2+} transient as a consequence of acidosis. However, while a decrease in maximal velocity was also seen in Kaplan *et al.* (1992), there was no observed change in dissociation constant, representing Ca^{2+} sensitivity.

It is unclear if release from, as well as uptake to, the SR is also affected during ischæmia (increased

loss would have a similar effect to reduced gain), with conflicting results. For example, Feher *et al.* (1989) used RyR blockers during ischæmia to achieve a reduction in rate of Ca^{2+} uptake, indicating an influence of RyR in the process, and Fauconnier *et al.* (2011) demonstrated an increase SR leak (though this is likely a reperfusion effect). However, other results do not indicate a change in release (Kaplan *et al.*, 1992), and others indicate RyR action is actually decreased (RyR channels are inhibited by NADH (Wang *et al.*, 2013), which increases during ischæmia (Esumi *et al.*, 1991)).

The rôle of I_{NaCa} during ischæmia is unclear—that it transiently reverses direction is not in doubt, but it is considered unlikely that this is a permanent feature of the ischæmic milieu (Noble, 2002; Rodríguez *et al.*, 2006). The reverse action of I_{NaCa} brings about the exact conditions required to return the exchanger to its normal operation, indicating that, at most, there is a reduction in I_{NaCa} during ischæmia. Inhibition of I_{NaCa} is brought about not just due to the changes in Ca^{2+} concentration, but is also driven by the changing Na^+ gradient, with a decrease in $[Na^+]_o$ caused by lack of perfusion, and an inhibition of I_{NaK} caused by anoxia. Noble (2002) used simulations to demonstrate the requirement of this increase in $[Na^+]_o$ to be modelled to account fully for the increase in $[Ca^{2+}]_i$, driven by the reduction in action of I_{NaCa}. There is a sustained monotonic increase in $[Na^+]_i$ during ischæmia, leading to a two- to five-fold increase (leading to values of 20–25 mM 15–20 min after ischæmia). However, within the realm of acute ischæmia that concerns this thesis, the increase is more often noted as $\sim 50\%$ (Tani and Neely, 1989; Malloy *et al.*, 1990; van Echteld *et al.*, 1991; Pike *et al.*, 1993). Tani and Neely (1989) demonstrated that the decrease in pH led to a rapid initial increase in $[Na^+]_i$ (via the H^+-Na^+ exchanger), which then correlated with an increase in $[Ca^{2+}]_i$. Cross *et al.* (1998) also showed a correlation in male mice between increased I_{NaCa} and declined ischæmic recovery, indicating inhibiton of I_{NaCa} has cardioprotective properties.

Opposing this increase in $[Ca^{2+}]_i$, there is a counter-intuitive decrease in contractile strength of the myocyte (Lee *et al.*, 1988; Kaplan *et al.*, 1992), accompanied by an increase in diastolic tension (Mubagwa, 1995). There are many suggested mechanisms to explain this. Mohabir *et al.* (1991) postulated competitive inhibition by H^+ with Ca^{2+} in the troponin-C complex (Blanchard and Solaro, 1984) in a process that makes this decline in contractile strength independent of changes to the Ca^{2+} transient,

and thus the ischæmic decline in pH_i is responsible. Alternatively, Camacho *et al.* (1993) suggests that the increase in inorganic phosphate (P_i) also attendant to ischæmia (being the product, along with ADP, of the hydrolysation of ATP) is responsible. However, against this is that contractile strength is reported to increase under hypoxic conditions (Kihara *et al.*, 1989).

Another way to explain the decrease in contractile strength is the 'garden hose effect', whereby the contractile strength of the myofilaments are reduced if the preceding relaxation is reduced (Vogel *et al.*, 1982; Kléber *et al.*, 1987a; Kléber, 1987; Camacho *et al.*, 1993) (though some findings dispute such a mechanism *in vivo* (Zhao *et al.*, 1988)). As such, while an increase in $[Ca^{2+}]_i^{sys}$ might indicate an increase in contractile strength, it is the increase in $[Ca^{2+}]_i^{dia}$, preventing relaxation, that is more influential by this hypothesis. Of note for this hypothesis is the increase in the time constant for decline in left ventricular pressure (Serizawa *et al.*, 1981; Applegate *et al.*, 1987; Isoyama *et al.*, 1987; Serizawa *et al.*, 1987).

At 2–3 min post-occlusion, $[Ca^{2+}]_i$ alternans is known to occasionally develop. This is likely due to the change in function of the SR, rather than being caused by APD alternans (see §2.3.2 for further details of this coupling): the smaller transient follows a higher diastolic $[Ca^{2+}]_i$, indicating reduced SR release due to reduced SR sequestration. This is not to say that the SR release itself is impaired; rather it is a consequence of the steep-load relation of the SR previously mentioned (Shiferaw *et al.*, 2003; Restrepo *et al.*, 2008).

2.3.2 Arrhythmogenesis

Ischæmia is known to play a prominent rôle in many instances of sudden cardiac death. As such, it is of key importance to determine how ischæmia can lead to sudden cardiac death, and thus the study of ischæmic arrhythmogenesis is vital. Studies have been conducted to establish the means by which ischæmic conditions can provide the substrate for arrhythmogenesis, and how it can lead to sustained arrhythmias. It should be emphasised at this point that arrhythmogenesis is not the preserve of ischæmia—arrhythmias can develop for any number of reasons, ischæmia being just one of them. Increasing susceptibility to arrhythmias is a consequence of something as harmless as ageing,

due to the increasing heterogeneity presented by certain breakdowns in the heart structure that occur naturally (*e.g.* fibrosis) (Spach *et al.*, 1988). Furthermore, it is not the case that tissue will 'become' arrhythmic, and then, inevitably, arrhythmia will occur. Rather, tissue changes dynamically, and while it may have greater arrhythmogenic properties, this does not necessarily guarantee arrhythmia (Weiss *et al.*, 2006).

Fibrillation in cardiac tissue can be initiated, and subsequently maintained by several different mechanisms, with each mechanism able to play a rôle in either process:

- ectopic beats (Haïssaguerre *et al.*, 1998; Tobón *et al.*, 2010; Zhang *et al.*, 2011);
- unidirectional conduction block (Allessie *et al.*, 1976; Gough *et al.*, 1985; Cabo *et al.*, 1996);
- rotors and spiral/scroll waves(Allessie *et al.*, 1977; Mandapati *et al.*, 2000; Jalife, 2003, 2009; Pandit and Jalife, 2013);
- mechano-electric feedback effects (Ferrero *et al.*, 2014).

Each of these mechanisms does not necessarily exist in isolation. For example, an ectopic beat can work with unidirectional conduction block, resulting in a spiral wave emerging. Ischæmia has been shown to provide the substrate for all of these mechanisms. Furthermore, research has demonstrated that structural heterogeneities, another potential side-effect of ischæmia, can increase incidence of arrhythmia and other atypical electrical activity, such as early after-depolarisations (EADs) (Auerbach *et al.*, 2011).

While ischæmia is well known to increase the vulnerability to ectopic beats (Zhang *et al.*, 2011), the 'width' of the vulnerability window (the range of coupling intervals at which an ectopic beat will lead to sustained arrhythmias) does not increase throughout the onset of ischæmia, *i.e.* arrhythmogenic risk does not increase linearly with duration of ischæmia (Barrett *et al.*, 1997; Tice *et al.*, 2007; Romero *et al.*, 2009b). As has previously been noted, the cardiac system is an inherently dynamic one—multiple different currents interact in a time- and voltage-dependent manner with each other, and other complicating factors such as ion concentration, to produce the complete AP and associated

cardiac contraction. These interactions vary depending on the condition of the heart, and the environment the heart is found in. This dynamic nature is true not only for the normal, 'healthy' conditions, but also for the pathological conditions such as arrhythmia and ischæmia. This dynamic nature means that prediction of arrhythmic events is fraught with difficulties. For example, it is insufficient to have only unidirectional conduction block in tissue for a sustained arrhythmia: an interaction between the coupling interval, the unidirectional block, the restitution properties of the tissue, the scale of the block, and the conduction velocity in the tissue are all required (Coronel *et al.*, 2009; Cherry *et al.*, 2012). Due to these requirements, there is a minimum size of tissue for which arrhythmias can be maintained, though this size can vary depending on the circumstances of the tissue (Adeniran *et al.*, 2011).

This is not to say that increased dispersion of electrophysiological properties, evident on the cellular scale, is meaningless—quite the opposite. Rather, the dispersion can provide the underlying properties that, given the correct interaction, leads to dangerous tissue properties. Thus, increase in dispersion is a key area for investigation for arrhythmogenic properties (Kuo *et al.*, 1983). Coupled with this, an increase in beat-to-beat variability in repolarisation is noted for its proarrhythmic properties (Johnson *et al.*, 2010).

With the consideration that the key thrust of this thesis is concerned with variability in ion channel properties and its correlation with experimentally observed variation, it is necessary to consider the ionic bases that exist for arrhythmias, and how these manifest in arrhythmia. What follows are very brief introductions to some key topics regarding arrhythmogenesis.

Re-entry

Generally speaking, *re-entry* refers to the mechanism by which the electrical activity of the heart does not complete its 'normal' circuit, but instead enters a process whereby it self-excites itself (hence the term)—the process has also been termed 'circus movement'.

Re-entry can occur in many forms, as spiral waves (§2.3.2) or figure-of-eight patterns (Ferrero *et al.*, 2003b) to name but two. Modes of re-entry are often associated with tachycardia, and if the re-entry

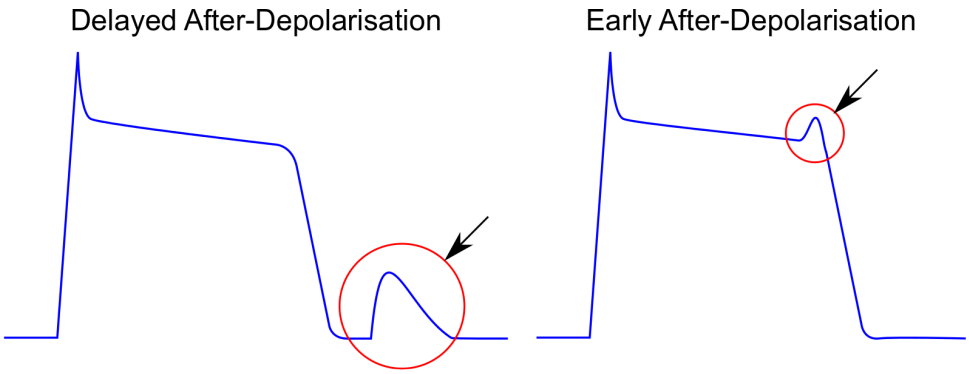


Figure 2.9: *Schematic of delayed* (left) *and early* (right) *after-depolarisations, highlighted by the arrow and red circle.*

is self-sustaining, it can subsequently lead to fibrillation and other forms of arrhythmogenesis.

It must be noted that ectopic beats are not required to initiate reentry—dispersion of electric properties in the tissue leading to 'unidirectional block' are sufficient (Xie *et al.*, 2007). An example is the case where there are two regions with different ERPs, one of which is greater than the CL, the other where it is less. The region with ERP > CL is thus unexcitable when the AP wavefront is incident, and conduction block occurs at this region. However, the region with ERP < CL is excitable, and thus the wavefront progresses through this region, and subsequently may excite the previously blocked region when it is no longer refractory in a figure-of-eight reentry pattern (Weiss *et al.*, 2006).

Delayed & Early After Depolarisations

Delayed after-depolarisations (DADs) refer to a spontaneous depolarisation of the cell after cellular repolarisation with no external stimulus—an example is shown in Fig. 2.9. These can provide an ectopic source of excitation, which if successful in exciting other regions of tissue, can lead to a fully fledged ectopic beat. DAD frequency is sensitive to increases in $[Ca^{2+}]_i$, with the underlying mechanism by which the $[Ca^{2+}]_i$ overload occurs usually being attributed to changes in $I_{Ca,L}$. However, $[Ca^{2+}]_i$ overload can also be due to alterations in CICR (Volders *et al.*, 1997). The increased $[Ca^{2+}]_i$ activates I_{NaCa}, which due to its electrogenic properties, depolarises the cell to a threshold potential, causing a DAD (Clusin, 2003).

The occurrence of DADs is reduced during ischæmia (though not in the border zone or otherwise

partly ischæmic tissue), mostly due to the action of hypoxia, but DAD amplitude increases after reperfusion of the ischæmic tissue (Ferrier *et al.*, 1985; Coetzee and Opie, 1987).

Early after-depolarisations (EADs) are spontaneous, premature depolarisations that occur before the original cellular repolarisation is completed, and usually occur under situations when the AP is prolonged. As with DADs, they may provide the source for ectopic excitation. There are many possible ionic causes for EADs: the most commonly mooted ionic bases for EADs are changes in $I_{\mathrm{Ca,L}}$ and I_{Na}, with changes in I_{Na} (*e.g.* mutations, drug effects) resulting in reduced inactivation working to prolong the action potential, thus allowing $I_{\mathrm{Ca,L}}$ to reactivate and depolarise the cell (Hiraoka *et al.*, 1992; Clancy and Kass, 2005; Hashambhoy *et al.*, 2011). The upstroke of an EAD is often slower than the usual AP upstroke, due to the fact that it is based on $I_{\mathrm{Ca,L}}$, rather than I_{Na} (the lack of repolarisation means the I_{Na} current is still deactivated, with the earlier mentioned effect of 'late' I_{Na} being sufficient only to prolong the AP, and not to initiate an upstroke) (Clusin, 2003).

In addition to defects in the currents regulating repolarisation causing EADs, it is also possible for defects in the Ca^{2+}-handling system, including CICR, to be responsible. If the Ca^{2+} concentration near the sarcolemmal surface remains high during the AP, an EAD may be initiated by I_{NaCa}, though it can be difficult to distinguish the action of I_{NaCa} and $I_{\mathrm{Ca,L}}$, with the two acting in concert (Volders *et al.*, 1997). Moreover, it has been demonstrated that the stochastic effects within each of these systems, and also within the overall repolarisation reserve, can increase the likelihood of the development of EADs (Tanskanen *et al.*, 2005; Sato *et al.*, 2009; Pueyo *et al.*, 2011; Heijman *et al.*, 2013).

By both DADs and EADs providing the potential substrate for ectopic beats, they are regarded as a potential trigger for re-entry, and thus represent a key mechanism for the development of arrhythmia. The mode of transmission from the occurence of DAD/EAD to arrhythmia is complicated, especially in connexion with the effects of cell coupling, but recent research is beginning to unravel the substrate requirements for an after depolarisation event to graduate to an arrhythmogenic event (Tanskanen *et al.*, 2005; Weiss *et al.*, 2010).

Alternans

Alternans is a phenomenon wherein the AP, or $[Ca^{2+}]_i$ transient, alternates properties from beat to beat. Usually (and for the majority of the following discussion), this is defined in terms of the duration of the AP alternating between long/short duration and the $[Ca^{2+}]_i$ transient alternating between large/small magnitude, respectively. However, it should be remembered that alternans of the AP amplitude also exists, and may reflect the inability of I_{Na} to fully recover between beats. Such a process could lead to a reduction in plateau amplitude, which in turn could lead to $[Ca^{2+}]_i$ alternans (Clusin, 2003). AP amplitude and APD alternans are not exclusive of each other.

There is a long-known association between alternans in the Ca^{2+}-handling mechanisms of the cell and arrhythmias, on the basis of the feedback between the Ca^{2+} system and the AP itself. However, the precise mechanism, and the causal links involved, are still the topic of much debate, and work is ongoing to establish the means by which Ca^{2+} alternans and arrhythmias are linked (Restrepo *et al.*, 2008; Chen *et al.*, 2009; Alvarez-Lacalle *et al.*, 2013).

In tissue, alternans can be either spatially concordant or spatially discordant (Fig. 2.10). It is a consequence of spatially discordant alternans that, between the out-of-phase regions there is a region where no alternans is present (referred to as the *nodal line*). Due to the APD/$[Ca^{2+}]_i$ gradients being steepest here, this region is most predisposed to develop unidirectional conduction block. Thus, a region with long APD (and consequently longer ERP) remains inexcitable if and when a region with short APD is re-excited. The resulting AP is blocked initially, and if the line of block is such that it permits the AP to circle round it and allows the AP to travel in a subsequent retrograde motion, a reentrant circuit can be established (Laurita and Rosenbaum, 2008). It has been shown that heterogeneity is not required for spatially discordant alternans to occur—due to the dependence of conduction velocity on diastolic interval (referred to as *conduction velocity restitution*), rapid pacing can induce spatially discordant alternans in homogeneous tissue (Watanabe *et al.*, 2001). Moreover, the ischæmic reduction in I_{Na} availability increases the DI range over which CV varies, and thus increases the risk of this phenomenon. Ectopic beats have also been shown to induce spatially discordant alternans in homogeneous tissue.

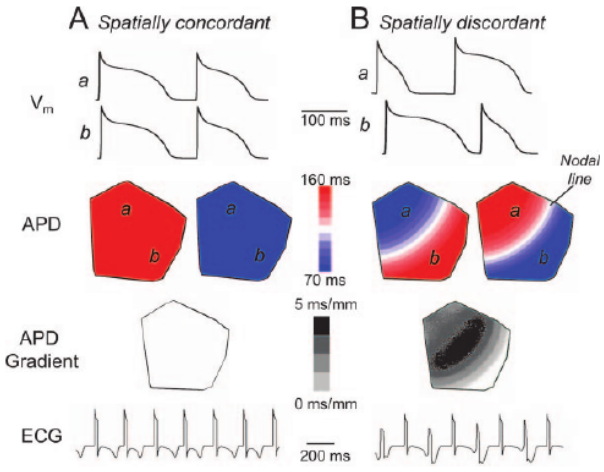


FIGURE 2.10: *Spatially cordant* (left column, A) *and spatially discordant* (right column, B) *APD alternans in 2D simulated cardiac tissue. The top panel shows AP data for the same time for two spatially separate locations in the tissue, demonstrating long/short alternans (labelled accordingly). The second panel shows the spatial APD distribution during the two APs shown in the top panel; the nodal line for spatially discordant alternans is indicated. The third panel showing the APD gradient resulting from such distributions. The bottom panel shows the simulated ECG for each tissue. These simulations were performed using a modified Luo-Rudy model from Qu* et al. *(2000) at a CL of 220 ms. Figure originally from Weiss* et al. *(2006).*

As concordant alternans do not demonstrate the same APD dispersion that has been shown to set the stage for arrhythmia, they are less arrhythmogenic than discordant alternans. Qian *et al.* (2001) demonstrated that Ca^{2+} alternans 'self-organises' into regions of tissue with the same phase, and hypothesised that this was due to movement of Ca^{2+} across gap junctions to neighbouring cells, allowing some degree of synchronisation.

While the restitution curve can provide a useful indication of when tissue is at risk of developing alternans (see §2.2.1), it must be remembered that this assumes that the APD depends entirely on the preceding DI, which is not the case. It has been observed that alternans can occur when the restitution curve is flat, and no alternans when it is steep (Shiferaw *et al.*, 2005). Part of the reason for these anomalies is the influence of $[Ca^{2+}]_i$. It is of note that ischæmia has been observed to flatten the restitution curve (Taggart *et al.*, 1996) while the occurence of alternans is increased (Qian *et al.*, 2001).

There is no firm evidence as to whether APD alternans drives Ca^{2+} alternans or vice versa, but mounting experimental evidence indicates that the onset of APD alternans is caused by instability in the cellular $[Ca^{2+}]_i$ dynamics, rather than by a steep APD restitution curve which then leads to Ca^{2+} alternans (Pruvot *et al.*, 2004; Goldhaber *et al.*, 2005; Wilson *et al.*, 2006); there are also expected spatial differences in the nodal line distributions depending on whether the alternans are AP or Ca^{2+} driven (Weiss *et al.*, 2006). Lee *et al.* (1988) demonstrated that, when APD alternans and Ca^{2+} alter-

nans were both present (and recorded simultaneously), there was no variation in the APD until after the Ca^{2+} transient had reached its peak—it was only after this that the APD alternans manifested. Chudin *et al.* (1999) were able to induce Ca^{2+} alternans without APD alternans at rapid pacing rates in cell (demonstrating an instability in the Ca^{2+} system independent of the AP). Similar results have been achieved *in vivo* (Aistrup *et al.*, 2006) and *in silico* (Sato *et al.*, 2006).

Research is ongoing to determine the mechanisms behind Ca^{2+} alternans (Shiferaw *et al.*, 2003; Weiss *et al.*, 2006). A simple hypothesis is that, at rapid pacing rates, there is simply not enough time for the SR to resequester the Ca^{2+} it has previously expended. Thus, the subsequent Ca^{2+} release from the SR is smaller, leaving more time for a complete resequestration of the Ca^{2+} by the SR. Mechanistically, Shiferaw *et al.* (2003) were able to reproduce Ca^{2+} alternans at rapid pacing rate without APD alternans by including a steep release-load relation for the Ca^{2+} sequestered in the SR. On a molecular level, evidence indicates that alternans prone regions express significantly less SERCA and RyR—this indicates responsibility lies with both SR uptake and release (Wilson *et al.*, 2006). Research is ongoing to find methods to protect these functions in ischæmia/reperfusion therapy (Wang *et al.*, 2013).

The coupling between APD and Ca^{2+} alternans can be either positive or negative, *i.e.* a long APD corresponds to a large $[Ca^{2+}]_i$ transient, or to a small $[Ca^{2+}]_i$ transient. Which of these relations predominates depends on the dominant current—a large $[Ca^{2+}]_i$ transient enhances both I_{Ks} and inactivation of $I_{Ca,L}$ (which would shorten the APD, *i.e.* negative coupling), but this process also enhances the activity of the exchanger I_{NaCa} (which would prolong the APD, *i.e.* positive coupling) (Shiferaw *et al.*, 2005). Positive coupling is the more common of the two (Laurita and Rosenbaum, 2008), but negative coupling has been noted in ischæmia (Lee *et al.*, 1988).

Spiral Waves & Rotors

Spiral/scroll waves represent an ectopic source for excitement that exists within tissue, wherein a curved wavefront and curved wavetail meet each other at a 'phase singularity', referred to as a rotor (Fitzhugh, 1960, 1961; Gray *et al.*, 1998; Jalife, 2009). This singularity processes around an excitable

core, with this core able to be either stationary or mobile. Not only do spiral waves represent a local source of activation within ventricular tissue, they are also liable to break-up, leading to fibrillation (Riccio *et al.*, 1999).

Spiral waves and rotors have proved amenable to analysis, with conclusions regarding their ionic bases being gained. Of the previously discussed ion channels, three are known to have an effect on rotor dynamics: I_{Na}, I_{K1} and I_{Ks}. I_{Na} is of note due to its impact on the conduction velocity of the AP, and thus affects the speed (and thus dominant frequency) of the spiral wave. Reducing I_{Na} also increases the meander of the core of the rotor (Pandit and Jalife, 2013). I_{K1} mediates the electrotonic interactions between the unexcited core and the immediate surroundings, and stabilises reentry due to its ability to shorten APD and reduce conduction velocity near the core, thus preventing wavefront-wavetail interactions that could destabilise and break up the rotor. Furthermore, by decreasing the resting membrane potential, it facilitates the reactivation of I_{Na} (Pandit and Jalife, 2013). I_{Kr} has been shown to accelerate the rotor, but not to a degree comparable to the effect of I_{K1}. While I_{Ks} does not in itself change the rotor dynamics, it is important in determining post-repolarisation refractoriness and wave break formation, and thus important for the transition from tachycardia to fibrillation. It is also interesting to note that regional cooling of a rotor decreases its frequency and increases the rotor's meander, causing it to collide with a boundary and extinguish (Yamazaki *et al.*, 2012). Block of $I_{Ca,L}$ has been shown to stabilise reentry and thus prevent fibrillation in some studies, while other studies have shown that this block increases the arrhythmic properties of the rotor—its exact rôle is thus unclear (Jalife, 2003, 2009; Pandit and Jalife, 2013).

2.4 Experimental & Physiological Variability

Variability represents a key current area of research in computational biology. This is due to the realisation that variability can have a significant impact on many processes, from variability within the population relating to differing drug response, through to development of arrhythmias due to increased heterogeneity in tissue. As such, increased effort is being devoted to understanding the mechanisms and consequences of variability, and it is one of the key aspects of this thesis that it aims to

model variability and examine its effects during ischæmia.

Variability exists at all scales, both temporally and spatially: from individual ion channels, to the level of the cell, to tissue, to organ, and to organism. At the scale of ion channels, variability has been noted in the mRNA concentrations that are translated to functional ion channels (Gaborit *et al.*, 2007) (while it has been noted that mRNA levels do not translate directly to ion channel density for numerous reasons (Edelman and Gally, 2001; Nattel *et al.*, 2010), a link has still been demonstrated between mRNA levels and observable effects on the AP (Walmsley *et al.*, 2013)). There is also a substantial body of evidence for notable variability in cellular processes—in neuronal studies, maximal conductance of ion channels has been shown to vary substantially (Schulz *et al.*, 2006; Goaillard *et al.*, 2009; Marder and Taylor, 2011), both in theoretical and experimental studies.

There are notable differences in cellular APs, depending on the spatial location of the cell—this is evident from variability between ventricular and atrial (and other) cardiac cells (Carmeliet and Vereecke, 2002), to transmural variability (Antzelevitch *et al.*, 1991). Furthermore, temporal variability is also a common phenomenon (Walmsley *et al.*, 2010). At the organ level, numerous factors have been cited as having notable effects on the AP (Taylor and Lipsitz, 1997). At the organismal level, different individuals react differently to different therapies (Kannankeril *et al.*, 2010). Many experiments, aware of the added variation associated with differences in gender and age, pick the experimental test subjects to be as homogeneous as possible to reduce the effect of variation as much as possible (Kurokawa *et al.*, 2012; Yang and Clancy, 2012).

A complete and comprehensive discussion of experimental variability is beyond the scope of this dissertation. However, mention shall be made for the experimentally observed variability that is of note for the models and experiments contained within this thesis. It should be noted that the variability reported in the literature often falls short of a complete account of variability, if simply by virtue of the fact that such an account requires the totality of the data, which is almost impossible to give in the literature. However, an estimate of the variability that exists within the literature can be made by (i) details given by studies directly investigating variability, (ii) figures given in the literature often given a limited measure of variability by reporting mean $\pm$ standard deviation, (iii) comparison of values

reported in different studies.

What follows is a very brief mention of some of the variation mentioned in the literature for APD and ion channel properties, these two topics being of especial concern for this thesis.

2.4.1 Action Potential Variation

Collaborators led by Prof. Andras Varró from the University of Szeged have been able to obtain AP traces for ventricular tissue at cycle lengths of 600 ms and 1, 000 ms. These preparations were internally consistent—the trace for each preparation came from a single sample (although the electrode recording the potential occasionally lost contact, and thus had to be reapplied, thus leading to the recording not necessarily coming for the same individual myocyte). These data allowed assessment of the intra-preparation variation in AP, and inter-preparation variation. Using data for APD_{90} (arguably the most common AP metric, and defined as the time interval between initial cellular depolarisation and 90% repolarisation), these data suggest an intra-preparation variability of $\sim 3.5\%$, and an inter-preparation variability of $\sim 10\%$.

However, these data come from a single laboratory—a full literature review provides a much greater range of values, encompassing as it does a wide gamut of variation from many sources that it would be impossible for a single laboratory to capture. A literature search to determine the extent of APD variation is performed in §5.4.1—further details will be given there.

2.4.2 Ion Channel Variation

Determining the properties of ion channels is an experimental task fraught with difficulties, and achieving usable data is testament to the skill and techniques employed—a summary of some of the difficulties in deriving values for ion channel parameters is presented in Carusi *et al.* (2012). From these data, it is possible to glean some measure of the variability encountered within these ion channels.

Fülöp *et al.* (2004) used experimental data to determine properties of $I_{\mathrm{Ca,L}}$, and found (amongst other details) that the density of peak $I_{\mathrm{Ca,L}}$ in human ventricular myocytes was $-5.5 \pm 0.4\,\mathrm{AF}^{-1}$ ($\pm 7.27\%$).

Current	Location	Value (AF^{-1})	Percentage Variation
I_{to}	Apex	29.6±5.7	±19.3%
	Base	16.5±4.4	±26.6%
$I_{Ks,peak}$	Apex	5.61±0.43	±7.7%
	Base	2.14±0.18	±8.4%
$I_{Ks,tail}$	Apex	1.65±0.21	±12.7%
	Base	0.85±0.19	±22.4%
$I_{Ca,L}$	Apex	−5.85±0.76	±13.0%
	Base	−7.17±0.63	±8.8%

Table 2.1: *A summary of the results for the current densities of basal and apical ventricular tissue in human and canine myocytes and tissue, obtained from Szentandrássy* et al. *(2005). The 'percentage variation' is calculated as standard deviation divided by mean value.*

Similar values were obtained by Li *et al.* (1999), with even greater variability reported for plateau $I_{Ca,L}$ (up to 18.2%). In the work of Fink *et al.* (2008), by fitting to experimental data, g_{K1} was determined to be $0.5871 \pm 0.0503\ AF^{-1}mV^{-1}$.

Notable work has also been carried out in Szentandrássy *et al.* (2005), who examined the amplitude (and time constants) of several ion channel currents in human and canine tissue to study the inhomogeneities between basal and apical ventricular tissue—a summary of these results is given in Table 2.1. It can be seen that the individual results demonstrate significant variability, and variation between apical and basal values is often noteworthy.

The effect of gender is addressed in humans in Verkerk *et al.* (2005), and in rabbits in Sims *et al.* (2008), which also examines the effect of age. The data for humans are not statistically significant, but still shows consistent bias. For example, $I_{Ca,L}$ density in female ventricular myocytes is consistently greater than in male at all voltages (*e.g.* 129% at 0 mV), and female I_{to} density at 50 mV is 84% of the male. The individual measurements in Sims *et al.* (2008) show up to 9.4% variation in individual measurements, but the gender difference can be far greater—from 22% in prepubertal rabbit ventricular myocytes, to 32% in adult myocytes extracted from the base of the ventricle.

3 Modelling Background

I can't be as confident about computer science as I can about biology. Biology easily has 500 years of exciting problems to work on. It's at that level.

Donald Knuth, *Computer Literacy Bookshops Interview*

The development of computational modelling of cardiac environments from its humble origins to its current situation is outlined. Key concepts for cardiac simulations are explained, explaining the underlying assumptions required for the prevalent modelling techniques. The Nernst potential, required for determining ion flow through channels, is explained, and two key methods for calculating ion channel current are detailed: the Hodgkin-Huxley formulation, and Markov models. The monodomain and bidomain equations for tissue simulation are then given. The next part of the chapter focuses on methods available for computational modelling of variability—this includes summaries of stochastic modelling, parameter sensitivity analysis and the use of model populations. Finally, a brief review is given of computational methods to simulate ischæmia.

It is often not practical to test hypotheses in real-life experiments. Under such circumstances, computational/mathematical models have become increasingly important in recent years, as they have developed from their original humble origins to tools exploring complicated processes; this is true not only for the heart, but for many other regimes, *e.g.* neurology, cancer. Computational modelling permits not only investigation of regimes that are insoluble to experimental analysis, but also effective integration of the different scales involved in some processes—a series of articles demonstrating the just some of the modern utility of computational modelling is introduced by Jalife (2013).

It should be noted from the outset, and always kept in the back of one's mind, that computational models are a *tool*, and their effectiveness is in their appropriate use. The virtue of models is that they permit examination of regimes of interest, and can be used to answer a specific posed question. This specificity allows their construction to not only test a given hypothesis directly (*e.g.* Restrepo *et al.* (2008) looked to determine whether the load-release relation of the SR could be explained using CSQN), but can indirectly test other assumptions by what it is considered appropriate to neglect in model construction (Restrepo *et al.* (2008) neglected to model the effects of mitochondrial Ca^{2+} handling, assuming that any effects would be negligible). These approximations are not just useful to test model assumptions, but rather they are a necessity—the sheer range of scales that can be said to exist in the heart require such approximations, with the full range of questions that can be posed for the heart ranging across 10^9 orders of magnitude spatially, and 10^{15} temporally (Abramson *et al.*, 2010).

While a 'good' model will be able to address a wide range of questions, even a model failure can be useful, in that it can direct investigation to the source of the mistake (Noble and Rudy, 2001; Carusi *et al.*, 2012; Quinn and Kohl, 2013; Glynn *et al.*, 2014). By considering models in this way, one can see that computational models are a natural extension of the scientific process: a hypothesis is conceived, a method or model designed to test the hypothesis, and thus the hypothesis is either validated, and further questions may be asked, or falsified.[1]

3.1 Development

A summary of the progression and development of computational cardiac models is now outlined. For further details of the models themselves, the reader is referred to the original papers, and for more in depth summaries of the development of computational modelling, the reader is referred to the reviews given in: Noble and Rudy (2001); Puglisi *et al.* (2004); Rudy and Silva (2006); Niederer *et al.* (2009); Noble (2011); Noble *et al.* (2012).

[1] How one may think of models, and what precise rôle they play in the scientific process, is a topic that is receiving increasing attention in recent years—an example of such a discussion is given in Keller (2000) and Carusi *et al.* (2012).

The precursor to all computational models of cardiac cells was the model developed in Hodgkin and Huxley (1952). This model described the electrical acitivity of a giant squid axon by comparison to an electrical circuit (details of this approximation, and other details of subsequent models, are given in §3.2). It described the ionic currents using a model of a series of activation and inactivation gating variables—the degree of the activation/inactivation determined the amount of current carried by a given channel at any given point in time. This model was able to sufficiently model the AP of the neuron using only three ionic currents: a K^+ current, a Na^+ current, and a 'leak' current of other ions. It was further developed by Fitzhugh (1960) to demonstrate that, with the correct adaptations of the model equations, the output could be altered to reproduce the longer APs of cardiac cells. Both models were keen to point out that, while the 'truth' of the model was not universally accepted, the model nonetheless was successful in reproducing experimental results.

The Hodgkin-Huxley model was hugely successful, and paved the way for the extension of the computational modelling approach to cardiac cells. Preliminary work was shown in Noble (1960) (using data presented concurrently in Hutter and Noble (1960)), which presented an adaptation of the Hodgkin-Huxley model for the AP of cardiac pacemaker cells. The same three currents were used, with adaptations in I_K to reproduce the longer AP of cardiac cells. The model was subsequently refined and expanded to reproduce the AP specific to Purkinje fibre cells (Noble, 1962), taking into account experimental data demonstrating the existence of at least two K^+ currents (labelled I_K and I_{K1}) with the resulting change in K^+ permeabilities of the cell membrane (Hutter and Noble, 1960; Carmeliet, 1961; Hall *et al.*, 1963).

The Noble model was followed by a model designed to reproduce the AP specific to a ventricular myocyte (Krause *et al.*, 1966). The Noble and Krause models were both based on the Hodgkin-Huxley model, with the Noble model being used as the seed for future developments in the computational cardiac modelling field. The next major refinement of the model came with that proposed by McAllister *et al.* (1975). In response to experimental data, this model greatly expanded the number of ion channels that were being modelled—the previous four ODEs of the Noble model were now replaced with ten. This included modelling the components of I_K separately as I_{Kr} and I_{Ks}, as well as incorpo-

rating a Ca^{2+} current based on experimental recordings from patch clamp experiments. This model, despite its success in reproducing experimental data, also contained a seductive flaw, in that it posited the slow conductance changes near the resting potential were due to an outward current, activated by depolarisation. In fact, the change was due to an inward current activated by hyperpolarisation (the so-called 'pacemaker current', I_F). Despite this flaw, the overall model remained sound, and iterations of the current continued through to DiFrancesco and Noble (1985), which was the first model to incorporate a formulation for the Na^+/K^+ exchanger, as well as making most intracellular ion concentrations dynamic. It also including modelling for SR Ca^{2+} release, and demonstrated the stoichiometry of the Na^+/Ca^{2+} exchanger had to be 3:1, not 2:1 as had previously been supposed—consequently, the resulting current from this exchange (I_{NaCa}) was incorporated into future models.

While this progress was still being made in the modelling of Purkinje fibre APs, a new focus was found in modelling the AP of ventricular myocytes. While this had already been achieved to some extent in Krause *et al.* (1966), the first widely used ventricular model was that proposed in the work of Beeler and Reuter (1977). This model was also the first to make more explicit mention of the internal calcium dynamics of the cell, by simulating the SR Ca^{2+} release. Of particular note in the further development of the field is the so-called Luo-Rudy model, first published in Luo and Rudy (1991). This model was originally designed to study arrhythmias in guinea pig ventricular cells, but has been subsequently developed for a wide variety of different tasks, and key components have been adapted into other models for other species (Shaw and Rudy, 1997a,c; Wagner *et al.*, 1999; Viswanathan and Rudy, 1999; Garfinkel *et al.*, 2000; Shannon *et al.*, 2004; Mahajan *et al.*, 2008). Specifically, the model was further adapted in two papers (Luo and Rudy, 1994b,a) to include dynamic intracellular ion concentrations, and $I_{Ca,L}$ was reformulated. It is testament to the significance of this model that it is still common to find new models having their basis in this so-called dynamic Luo-Rudy model. Improvements have nonetheless been made, such as the separation of I_K into the two constituent currents of I_{Kr} and I_{Ks} in Zeng *et al.* (1995), based on experimental evidence for this separation (Sanguinetti and Jurkiewicz, 1990). The Luo-Rudy model was also adapted to be able to model ischæmia by the incorporation of $I_{K\text{-}ATP}$ (Shaw and Rudy, 1997b) (further details of the modelling of ischæmia can be found in §3.4 and §4.1.2). A further significant advance came with Clancy and Rudy (1999), which for the first time

incorporated Markov modelling into a cell model (Markov modelling is described in §3.2.3).

Stern (1992) noted a short-coming of the Luo-Rudy model by its inability to reproduce the graded relationship between $I_{Ca,L}$ and the SR Ca^{2+} release—the Ca^{2+} release during the AP was nearly 'all-or-nothing', in contrast to what was observed experimentally. This was due to what was termed the 'common pool' model for Ca^{2+}, wherein the trigger Ca^{2+} and release Ca^{2+} pass through a common cytosolic pool. This can be overcome by introducing a compartmentalised system to model Ca^{2+} dynamics. This allowed for modelling of not only graded Ca^{2+} release (local $I_{Ca,L}$ influx causes local SR Ca^{2+} release, which spreads across the cell in a Ca^{2+} wave), but also predicted the phenomenon of Ca^{2+} sparks, which were observed experimentally in Cleemann *et al.* (1998). The model was subsequently revised and expanded by Shiferaw *et al.* (2003) to include SR load-release dependence, although on a purely phenomenological basis. This model has been used as the basis for more elaborate models, incorporating greater biophysical details, including 3D cellular architecture (Restrepo *et al.*, 2008; Chen *et al.*, 2009).

Almost all of the currents in the models described above still use the same basic model form as that given in Hodgkin and Huxley (1952)—details and nuances have been added to some equations, and other equations have been formulated using more complicated and precise methods (such as Markov modelling), but the underlying modelling philosophy has remained rather steady, and been found sufficient to the present day.

It is through this evolution of models from relatively humble beginnings that we have reached the point where we are today—computational models of remarkable complexity and insight that can be used to model from the subcellular upwards, with specialisations depending on species, location and situation. The range of models continues to increase, from molecular simulations of ion channels (Nekouzadeh and Rudy, 2011), through the cellular models that have been mentioned and that are the focus of this thesis, to 3D simulation to investigate the source of arrhythmia in tissue (Arevalo *et al.*, 2007). Parallel to this increase in breadth comes further investigation into pathological conditions, such as ischæmia (see later) and mutations (Viswanathan and Rudy, 1999, 2000). Novel insights continue to be made with regards simulation techniques, both in terms of efficient and accurate computa-

tion of stochasticity (Dangerfield *et al.*, 2012) and the modelling of ion flow in tissue during ischæmia (Niederer, 2013). With the increasing wealth of information and techniques available, increasing efforts are being made to curate the data and ensure consistent and reliable simulation methods are used (Hunter *et al.*, 2002; Pitt-Francis *et al.*, 2009; Mirams *et al.*, 2013), coupled with an increasing degree of standardisation of reporting standards for experiments (Quinn *et al.*, 2011).

In this thesis, focus is mainly devoted to the models presented in Shannon *et al.* (2004) and Mahajan *et al.* (2008). These are both models for rabbit ventricular myocytes, with the latter model being itself based on the former—they are both in turn based in large part on the Luo-Rudy model. However, it should not be thought that it is a direct step from the Luo-Rudy model to the Shannon model to the Mahajan model—there are numerous intervening steps, with advances being made both computationally and experimentally (Zeng *et al.*, 1995; Puglisi and Bers, 2001; Bassani *et al.*, 2004).

3.2 Key Concepts

Electrically, the heart has been modelled with great success as an analogue to an electrical circuit (Carmeliet and Vereecke, 2002), where the lipid bilayer is represented as a capacitor, and the various ion channels and transporters that span the membrane are represented as resistors, which change their 'resistance' depending on their state, coupled with electric cells to represent the influence of concentration gradients (Fig. 3.1). By altering the resistance of these channels or the driving potential of the electrochemical gradient, ion flow across the membrane is permitted via an ionic current. It should be noted that knowledge of ion channel dynamics is not solely appropriate for simulating at cellular scales: ion channel dynamics influence and affect cellular AP dynamics, which in turn leads to changes of the tissue dynamics, and so on (Spach *et al.*, 1988).

Within this framework, the model's purpose dictates which variables are considered important, and thus how much effort must be expended to determine their values. Some models (such as Mahajan *et al.* (2008)) have their purpose as investigation of the Ca^{2+} dynamics of the cell and the implications for alternans. Consequently, greater computational effort is given in the form of a Markov model to calculating the state and thus conductance of $I_{Ca,L}$ more precisely. Other models (such as Restrepo

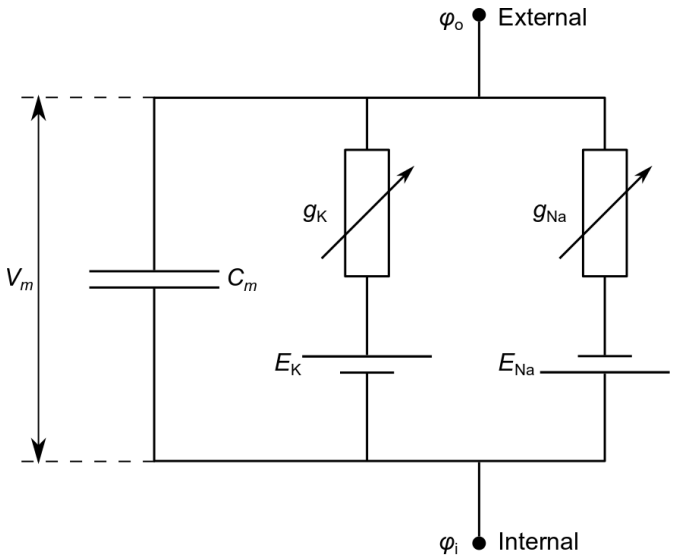


FIGURE 3.1: *Schematic representation of the cell as an electrical circuit. The cell membrane serves to electrically isolate the extracellular space (where an electric potential ϕ_o exists) from the intracellular space (with a corresponding potential ϕ_i), and is thus regarded as a capacitor with capacitance C_m; the potential difference across this membrane (*i.e. *the difference $\phi_i - \phi_o$) is V_m. Ion channels across the membrane are represented as variable resistors, with conductance g_X. Coupled with these variable resistors are cells (in the electric circuit sense of the word) representing the reversal potential (E_X) of the ion channel, and thus accounting for the electrochemical diffusion gradient across the membrane. In this figure, only generalised ion channels for K^+ and Na^+ are shown, with their 'cells' being reversed to demonstrate their opposing electrochemical gradients. Note that this model neglects any leak current directly through the membrane—this can be added by addition of a resistor in parallel. Based on a figure from Carmeliet and Vereecke (2002).*

et al. (2008)) define a certain section of the cellular mechanism as of interest, and thus the model is designed to reflect the spatial distribution of the cell. Equally, the primary output of a model changes depending on the question being posed—for example, Chen *et al.* (2009) is primarily interested in Ca^{2+} sparks, and thus the Ca^{2+} output is the primary output of that model. The approach used in one model does not necessarily lead to that approach being beneficial in all models.

Most models are trained according to the membrane potential, with this being considered the primary output. In modelling the cell as an electrical circuit with the membrane considered as a capacitor, the instantaneous change in membrane potential is calculated according to

$$\frac{\mathrm{d}V_m}{\mathrm{d}t} = -\frac{1}{C_m}(I_{\text{ion}} + I_{\text{stim}}), \tag{3.1}$$

where C_m is the membrane capacitance, I_{ion} is the sum of all ionic currents in and out of the cell, and

I_{stim} is the stimulus current, if applied, to initiate an AP. In experiments and simulation, the value of I_{stim} can vary, but it is usually at least 1.5 times the minimum value required to initiate activation (the 'activation threshold'), though its precise value will also depend on the duration of application (Riccio *et al.*, 1999; Sutton *et al.*, 2000; Ferrero *et al.*, 2003b).

It should be noted that the membrane potential can also be calculated according to an 'algebraic method', based on the charge conservation principle and the charge-voltage relation of a capacitor; identical results are produced by both methods (Hund *et al.*, 2001; Rudy and Silva, 2006).

Most ionic currents are modelled according to:

$$I_X = g_X(\mathbf{x})(V_m - E_X), \tag{3.2}$$

where I_X represents the ionic current being modelled, $g_X(\mathbf{x})$ represents the conductance of the channel, with $\mathbf{x}$ being a vector representing all possible influences on the channel conductance, and E_X represents the Nernst potential; the general form and interpretation of E_X is explained in §3.2.1. $g_X(\mathbf{x})$ is a current-dependent variable, and is commonly modelled as varying with time, voltage and/or extra-/intracellular ion concentration, though it is possible for the model to be constructed in such a way that $\mathbf{x}$ accounts for any number of inputs. It should be noted that this current formulation is not restricted to describing physical currents, but can equally be used to model phenomenological currents, *i.e.* those currents that do not pretend to represent any physical reality, but instead are based entirely on their ability to contribute to the reproduction of an accurate model output (Bueno-Orovio *et al.*, 2008).

3.2.1 Nernst Potential

Of key importance in mathematical modelling of electrically active cells is the *Nernst equation*, which provides a method for calculating the Nernst potential (also referred to as the reversal potential). The Nernst potential represents the potential difference at which there is no *net* ion flow through a given ion channel. This is not just an electrical property, but also considers the concentration gradient, and thus defines when the electrochemical gradient for a particular channel is zero. A full derivation

is given in the appendix (§A.3.1), along with details for situations when a given channel is not fully selective of a particular ion, but the key result is thus:

$$E_X = \frac{RT}{z_X F} \ln \frac{[X]_o}{[X]_i}. \tag{3.3}$$

In the above equation, R represents the gas constant, T represents the absolute temperature of the system, z_X represents the valence of ion X, F represents the Faraday constant, and $[X]_o$ and $[X]_i$ represent the extracellular and intracellular concentrations of X, respectively.

3.2.2 Hodgkin-Huxley Current

As previously stated, the seminal work presented in Hodgkin and Huxley (1952) modelled currents as being composed of one or more activation/inactivation gates. It should be noted that the original paper was at pains to emphasise that this was not intended as a description of the physical reality of the cell, but was to be used as is: as a mathematical equation that provides fidelity to the experimental data. It is of note, however, that it is the case that the four gating variables in the Hodgkin-Huxley formulation of the K^+ current does correspond with the structure of the K^+ channel, consisting of four identical subunits, with a similar correlation of the Na^+ channel and its Hodgkin-Huxley formulation.

Within the Hodgkin-Huxley framework, the channel conductance is modelled as

$$g_X = \overline{g}_X m^a h^b, \tag{3.4}$$

where $\overline{g}_X$ represents the maximum conductance through the channel, a and b are constants, and m and h are dimensionless quantities that vary between 0 and 1. m and h are commonly given a physical basis as activation and inactivation gates, respectively, though Hodgkin and Huxley (1952) described them as proportions of 'activating molecules' and 'inactivating molecules', respectively. If the former metaphor is used, the conductance through the channel is thus proportional to the proportion of the gates that are 'open', while the latter metaphor states proportionality to the activation/inactivation molecules interacting with the channel within and outwith the cell. The values for a and b represent either the number of molecules that must interact with the channel, or the number of gates the channel possesses.

Using this formulation, Hodgkin and Huxley (1952) thus described I_{Na} and I_{K} as

$$I_{\text{Na}} = \overline{g}_{\text{Na}} m(V_m)^3 h(V_m)(V_m - E_{\text{Na}}) \tag{3.5}$$
$$I_{\text{K}} = \overline{g}_{\text{K}} n(V_m)^4 (V_m - E_{\text{K}}), \tag{3.6}$$

where m and h may be considered the activation and inactivation 'gates' for I_{Na}, and n represents the activation 'gate' for I_{K}—these are thus specific examples of the generalisations provided in Equations (3.2) and (3.4).

The changes in m, h and n can all be described according to

$$\frac{\mathrm{d}p}{\mathrm{d}t} = \alpha_p(1-p) - \beta_p p, \tag{3.7}$$

where $p = \{m, h, n\}$, and α_p and β_p are functions of V_m (but not of time). It can be noted that this is often expressed equivalently as

$$\frac{\mathrm{d}p}{\mathrm{d}t} = \frac{p_\infty - p}{\tau_p} \tag{3.8}$$

where $p_\infty = \frac{\alpha_p}{\alpha_p+\beta_p}$ and $\tau_p = \frac{1}{\alpha_p+\beta_p}$, and are the steady state value of p and the time constant, respectively. Solving Eq. (3.7) for a constant value of V_m provides the solution

$$p(t) = p_\infty - (p_\infty - p_0)e^{-t/\tau_p} \tag{3.9}$$

where p_0 is the value for $p(t)$ at $t = 0$.

In the original Hodgkin-Huxley paper, where the modelling metaphor was that of activating and inactivating particles, p represents the proportion of particles in a particular position (inside the membrane), and $(1 - p)$ consequently represents the proportion of particles in the opposing position (outside the membrane). α_p thus represents the rate of transition between the intracellular and extracellular environment, and β_p represents the transition in the opposite direction. In the terminology of gates, Eq. (3.7) may be considered as the rate equation between open and closed gate states: p is the proportion of gates that are open, α_p represents the rate constant for transitioning from closed to open, and β_p represents rate constant for the reverse transition. Regardless of the metaphor, α_p and β_p change in response to changes in V_m—for the particle metaphor, this can be considered a response to the increasing driving force moving the charged particle p across the membrane. Sudden changes

in V_m cause α_p and β_p to assume values newly appropriate to the new potential difference—the values for a given value of V_m can be estimated by use of p_∞ and τ_p, and this was the method used in Hodgkin and Huxley (1952). By empirical means it is thus possible to calculate how α_p and β_p change according to V_m.

3.2.3 Markov Models

One of the implicit assumptions in the Hodgkin-Huxley formulation is that it assumes (to continue the use of the gating metaphor) that the gating properties of all the gates are identical and independent, *e.g.* the transition from the channel being $\frac{1}{4}$ to $\frac{1}{2}$ 'open' occurs with the same rate and same likelihood as the transition from $\frac{1}{2}$ to $\frac{3}{4}$. This assumption makes for a computationally efficient means of simulation, but limits the model's utility for investigation of stochastic effects or state-specific changes in the rate transitions. For example, inactivation of I_{Na} has a greater probability of occurring when the channel is open (Armstrong and Bezanilla, 1977; Bezanilla and Armstrong, 1977), and the Hodgkin-Huxley model fails to capture some characteristics of I_{Ks}(Adeniran *et al.*, 2011).

As an alternative to avoid this assumption and its pitfalls, one may use *Markov modelling*, which calculates the channel's occupancy of a given state explicitly, thus allowing for consideration of changes in transition rate between states. In its most general form, Markov modelling is a method of stochastic modelling that assumes the Markov property, which is that the probability distribution for transitions from the current state depend only on that state, and not on any prior states. A distinction must be borne in mind when discussing Markov models—Markov *processes* are defined as simple stochastic processes, wherein each transition from one state to the next is considered as a single event, and the occurrence of each event occurs at a discrete, random time. With the Markov models presented in this work, the transitions between states is represented by probabilistic distributions, which are modelled according to ordinary differential equations. As such, the Markov models are deterministic (unless a stochastic term is included explicitly).

While other forms of Markov models exist (such as hidden Markov models), this thesis considers only Markov chains, where all possible states of the system and the transitions possible between states are

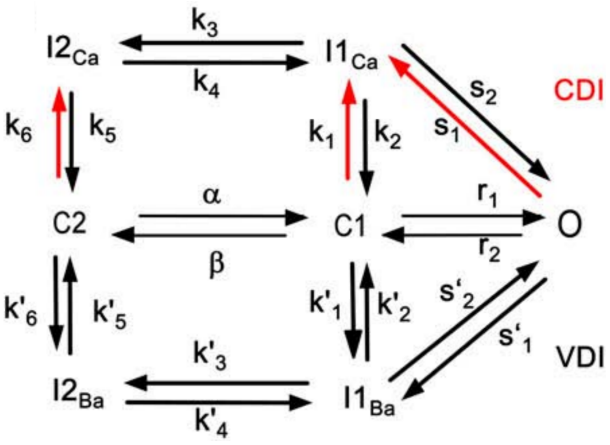


FIGURE 3.2: *Markov model for $I_{\text{Ca,L}}$ in Mahajan* et al. *(2008). The top half of the figure represents Ca^{2+}-dependent inactivation (CDI), with the bottom half representing voltage-dependent inactivation (VDI). The states can be closed (C1 and C2), open (O) or inactivated (all other states).*

known, and the transitions are autonomous. For this, it is assumed that the channel can exist in any one of n discrete states. These states are commonly considered to be either open, closed or inactivated, and there can be multiple types of each state. The simplest form is a two state system transitioning between an open and a closed state, which can be represented as

$$\mathrm{C} \underset{k_{\text{off}}}{\overset{k_{\text{on}}}{\rightleftharpoons}} \mathrm{O} \tag{3.10}$$

where k_{on} and k_{off} represent the transition rates between these two states. A more complicated example, taken from the formulation for $I_{\text{Ca,L}}$ in Mahajan *et al.* (2008), is shown in Fig. 3.2. The transition between states is dependent only on the state itself, and the rate constants, with the rate constants between different states being independent of each other. This example further demonstrates two different modes of activation/inactivation. The lower section of the Markov model represents voltage-dependent inactivation (VDI), whereby the transitions between states are based on V_m. The top section shows Ca^{2+}-dependent inactivation (CDI), and represents changes to the system that are independent of V_m—such a process is rarely captured by an equivalent Hodgkin-Huxley formulation.[2]

If $x_i(t)$ represents the proportion of channels in state i at time t, and k_{ij} represents the transition rate from state i to state j, the transition rates for a system containing m different states may be modelled

[2]It can be noted that the dependencies of α_p and β_p can be modified to include dependencies on parameters other than V_m, but this process would thus combine VDI and CDI in one process. As such, it would be extremely unlikely that a Hodgkin-Huxley model could fully capture the dynamics presented in Fig. 3.2.

according to

$$\frac{\mathrm{d}x_i}{\mathrm{d}t} = \sum_{j=1}^{m}(k_{ji}x_j - k_{ij}x_i). \tag{3.11}$$

The conductance of the channels for a particular current is thus calculated by multiplying the maximum conductance by the proportion of the channels that currently exist in an open state.

It should be further noted that the Markov model used in simulation may be simpler than the model is actually known to be, with simplifications being applied according to the needs of the model at the time. Mahajan *et al.* (2008) mentions, for example, that there are actually thought to be 4 different closed states for $I_{\mathrm{Ca,L}}$, but the 2 closed states used in their model is sufficient to reproduce the voltage dependence of the channel.

If the transitions between states are independent and identical, the orignal assumption held by the Hodgkin-Huxley formulation is thus accurate and the Markov model devolves to an equivalent Hodgkin-Huxley formulation (Rudy and Silva, 2006; Pakdaman *et al.*, 2010). In the two-state example given at the start of this section, the assumption is automatically true, and the open probability for the channel ($P(O)$) can be represented in a Hodgkin-Huxley formulation by the single value m. The Hodgkin-Huxley formulation for I_{K} can be derived by extending the two-state model while retaining the requirement for independent state transitions. In such a model, with 4 independent sub-units, the channel would only be 'open' when all four subunits are open. Thus, there would be 5 possible states for the model, ranging from all sub-units being closed to all sub-units being open. Representing the state with all four sub-units closed as C_4, this could transition to a state where only 3 sub-units are closed (C_3). If the probability for a single sub-unit to transition from a closed to an open state is given by α, and the opposite transition by β, the rate of transition from C_4 to C_3 is 4α, and the reverse rate is β, based on the number of channels available to make the transition. The resulting Markov model can be represented by

$$\mathrm{C}_1 \underset{\beta}{\overset{4\alpha}{\rightleftharpoons}} \mathrm{C}_2 \underset{2\beta}{\overset{3\alpha}{\rightleftharpoons}} \mathrm{C}_3 \underset{3\beta}{\overset{2\alpha}{\rightleftharpoons}} \mathrm{C}_4 \underset{4\beta}{\overset{\alpha}{\rightleftharpoons}} \mathrm{O}\,. \tag{3.12}$$

With each subunit behaving identically, each sub-unit can be represented by a gate with the gating variable n, which represents the probability of the gate being open. Consequently, the probability of the channel being open is equal to all the gates being open, and is n^4. This example illustrates the

computational efficiency of the Hodgkin-Huxley formulation, as a single calculation is made in place of calculating the transitions between the five possible Markov states.

3.2.4 Monodomain & Bidomain Equations

The focus of computational models can be broken down to three areas of scale: the cellular, the tissue, and the organ. It should be noted that there is considerable overlap between each of these scales, and it would be a mistake to think of models as existing solely within one spatial domain. Indeed, the simulation of higher scales often make use of key results from the simulation of lower scales, and *vice versa*.

Of key importance for the simulation of tissue (and higher order) are the bidomain and monodomain equations, which allow the calculation of the spread of electrical potential. A brief derivation is given here—for fuller details, see Keener and Sneyd (2009).

The bidomain equations represent the intracellular and extracellular environments as being continuous and intertwined at all points throughout the tissue where the equations are being applied. The assertion about the continuous nature is not simply an assumption—the extracellular environment is, by its nature, continuous through the tissue, and the intracellular environment is assumed to be continuous enough by the connections between cells via gaps junctions. To make the membrane potential more explicitly a relation between the two environments, it may be expressed as

$$V_m = \phi_\mathrm{i} - \phi_\mathrm{o}, \tag{3.13}$$

where ϕ_i and ϕ_o represent the intracellular and extracellular potentials, respectively (it should thus be noted that the membrane potential is more properly a potential difference across the membrane, rather than a potential in its own right).

The bidomain equations are coupled differential equations, based on a reaction-diffusion model of ion flux, with the application of conservation of ions and charge throughout the domain. The resulting equations, covering the domain Ω, are

$$\beta\left(C_m\frac{\partial V_m}{\partial t} + I_\mathrm{ion}(\boldsymbol{\eta}, V_m)\right) - \nabla\cdot(\sigma_\mathrm{i}\nabla\phi_\mathrm{i}) = I_\mathrm{stim,i} \qquad \text{in } \Omega, \tag{3.14}$$

$$\nabla\cdot(\sigma_\mathrm{o}\nabla\phi_\mathrm{o} + \sigma_\mathrm{i}\nabla\phi_\mathrm{i}) = I_\mathrm{stim,o} \qquad \text{in } \Omega, \tag{3.15}$$

where β is the membrane surface to volume ratio, C_m is the specific membrane capacitance, and $I_{\text{stim,i}}$ and $I_{\text{stim,o}}$ are stimulus currents applied to the intracellular and extracellular space, respectively. I_{ion} is the sum of the ionic currents from the extracellular to the intracellular domain, and depends on the cell model being used. The variable $\boldsymbol{\eta}$ also depends on the cell model choice, being a vector containing the state variables for the cell electrophysiology model. It varies according to

$$\frac{\partial \boldsymbol{\eta}}{\partial t} = \mathbf{f}(\boldsymbol{\eta}, V_m), \tag{3.16}$$

where $\mathbf{f}$ is a vector-valued function, and encapsulates the cell level electrophysiology.The variables σ_{i} and σ_{o} represent intracellular and extracellular conductivity tensors. It can be recalled at this stage that the conductivity of cardiac tissue is anisotropic—it is not equally conductive in all directions, with higher conductivity along the fibre direction of the tissue.

Generally, no flux conditions are applied to the domain, *i.e.* there is no leakage of ions or current across the domain boundary. Mathematically, this is represented as

$$\mathbf{n} \cdot (\sigma_{\text{i}} \nabla (V_m + \phi_{\text{o}})) = 0 \qquad \text{on } \partial\Omega, \tag{3.17}$$

$$\mathbf{n} \cdot (\sigma_{\text{o}} \phi_{\text{o}}) = 0 \qquad \text{on } \partial\Omega, \tag{3.18}$$

where $\mathbf{n}$ is the outward pointing normal vector to the domain. Based on these boundary conditions, equations (3.14) and (3.15) are degenerate, in that they do not have a unique solution, specifying the value ϕ_{o} only up to an additative constant. However, as the quantity of interest is not ϕ_{o} but rather V_m, this does not affect the physiological utility of the bidomain equations.

If it is further assumed that the intracellular and extracellular environments are equally anisotropic and their conductivities can be represented by a scaling relation (*i.e.* $\sigma_{\text{o}} = k\sigma_{\text{i}}$), then the bidomain equations can be simplified further still to

$$\beta \left(C_m \frac{\partial V_m}{\partial t} + I_{\text{ion}}(\boldsymbol{\eta}, V_m) \right) - \nabla \cdot (\sigma_m \nabla V_m) = I_m \qquad \text{in } \Omega, \tag{3.19}$$

where $\sigma_m = \sigma_{\text{i}} \sigma_{\text{o}} (\sigma_{\text{i}} + \sigma_{\text{o}})^{-1}$ and represents the monodomain conductivity tensor, and I_m is the monodomain stimulus current.

It should be noted that the subsequent reduced complexity of computationally solving this equation compared to solving the coupled bidomain equations comes with a cost in terms of physiological accuracy. Generally, it may be considered that the monodomain is appropriate in cases where there is no

significant anisotropy in the tissue *e.g.* interstitial spaces. Work has also recently been conducted to investigate a more physiologically rigorous form, referred to as the *tridomain equation*, which accounts for the interface effects of a volume conductor (such as a perfusing bath) (Ainseba *et al.*, 2012).

3.3 Computational Modelling of Variability

It is generally felt that a 'good' model should be able to reproduce a wide range of data. If a biophysically detailed model can reproduce a wide range of data, it gives us greater confidence that the underlying details of the model can be said to represent reality. However, it is a handicap that is only recently being overcome that, in constructing cell models, the focus has been on fitting the model output to one particular value of a metric (such as APD_{90}), whether this is the mean or some other measure. The choice of what 'data' to fit was therefore important, and yet fraught with difficulties. For example, should one fit to the maximum measured value on the basis that voltage-clamp experiments tend to make the currents appear smaller and slower than they are, or should one fit to the mean value in order to use a greater range of data? Both approaches have problems, not least that a model with mean parameters can fail to have properties exhibited by all of the test subjects (Golowasch *et al.*, 2002; Marder and Taylor, 2011). Furthermore, the associated variability, expressed often in experimental work as a standard deviation, is often ignored in model construction (Carusi *et al.*, 2012): a model would be designed to reproduce only the training data, without reproducing any measure of variability. Such models are often poorly equipped to reproduce the variability that is seen in the original experimental data (Marder and Taylor, 2011).

When modelling variability, it must be remembered once again that models are only useful up to the point of answering the question posed to them—taking a model further than its original purpose is useful only when this new purpose does not stray irrevocably from the original, and the original models assumptions and approximations remain valid. Of great concern for this, and with the process of linking variability in computational models to variability in real-life systems, is the problem of unknown parameters. Even in well-studied systems, there are parameters that, for whatever reason, do not have a well-defined value. There are two possible methods to deal with this: (i) adopt

a parameter derived from a similar system, such as the peak conductance used in a model for a different species, or (ii) adjust the parameter on the basis of producing the expected output (so-called *phenomenological fitting*). Even when one can use a value particular to the species at hand, the parameter can remain weakly defined. This problem is especially prevalent for fitting parameters that describe peak/maximum conductance of ion channels; in voltage clamp experiments, it is often the most poorly defined parameter, due to both the possible detrimental effects of the initial cell isolation procedure on ion channels (Yue *et al.*, 1996), and due to the drug block used to try and isolate particular ion channels for measurement being either incomplete or non-specific, and thus complicating the interpretation of the experimental data.

Furthermore, it has been shown that, under particular conditions, a computational model can produce identical AP traces while using two vastly different input parameter sets. However, these models can then differ in other important regards: Sarkar and Sobie (2010) used two parameter sets for the same model to produce near identical AP traces, but very different data for $[Ca^{2+}]_i$. Obviously, if the model is required only to reproduce the AP, both models are entirely adequate. However, the problem is demonstrated further in Cherry and Fenton (2007) in a comparison between two different canine ventricular models: while both produce APs of similar morphologies, there are significant underlying differences, and these are reflected in different responses to certain conditions. Similar conclusions have been reached in Romero *et al.* (2011), and work has been made in finding some way of curating models according to their differences in response (Terkildsen *et al.*, 2008; Cooper *et al.*, 2011). It is of note that a typographical error, confusing the conductances of $I_{to,s}$ and $I_{to,f}$, was present in Shannon *et al.* (2004), leading to a subsequent correction in Shannon *et al.* (2012). However, this correction pointed out 'that the updated model leads to similar quantitative results obtained with the original model' with regard to key observations.

Even with all due caution being applied, results suggest that so-called 'sloppiness' in parameters (*i.e.* parameters that the model output demonstrates little sensitivity to variation in) within a model is not a result of lack of training data (Brown and Sethna, 2003; Gutenkunst *et al.*, 2007), and Song *et al.* (2010) even go so far as to question whether a 'unique' parameter set can exist in biology.

Even if one has managed to select parameters that produce a given output that is judged reasonable, there are problems with changing this parameter value to reproduce variability. For example, Davies *et al.* (2012) showed that by allowing parameters describing peak ion channel conductance to vary, a wide range of possible values could be made to fit experimental AP, with peak conductance varying by factors of 0.1 to 7.43 of the original model's peak conductance value. However, this demonstrates one possible problem in simply fitting parameters: numerically, it may well be entirely accurate, but it may not represent physiological reality (experimental data for conductance variability implies a variation of as much as threefold (Schulz *et al.*, 2006)). Further difficulties can arise when fitting data phenomenologically to AP output due to the experimentally verified repolarisation reserve. The repolarisation reserve works such that the 'real' value of a parameter, such as I_{Ks} conductance, can vary to a large degree with other parameters compensating for these variations. Consequently, it is difficult to pick out the 'real' value.

Methods of determining the sources of variability in computational models can be divided into two arenas: stochastic variability, by which it is meant that stochastic, random properties are introduced into the model, and deterministic variability, by which it is meant that known variation is applied to the model to observe the resulting effect, *e.g.* introducing 30% variation to a particular parameter and observing the resulting output variation. These arenas are not mutually exclusive, and it is perhaps more useful to consider both methods as tools: the former is adapted for recreation of the actual physical environment, and the latter is adapted for mapping the input/output parameter space. For the purposes of this thesis, they will be discussed seperately below.

3.3.1 Stochastic Modelling

Increasing effort has been focussed of late on incorporating stochasticity into computational models, and using this to reproduce experimentally observed variation. Previously, the requirement for multiple simulations to determine the statistical properties of a stochastic model prohibited large scale use of such methods, but this restriction has diminished both with increasing computational power, and advances in stochastic simulation techniques (Dangerfield *et al.*, 2012). It should be noted that

stochasticity may be introduced to a model in many ways. One of the most common methods is to introduce stochastic differential equations to the model—if a Markov model is being used, stochasticity can be applied to the transition rates. Dangerfield *et al.* (2012) and Heijman *et al.* (2013) were able to demonstrate that applying stochasticity directly to a Markov model, rather than its equivalent stochastic differential equation, produces results that more closely correlate with experimentally observed short and long term variability. However, Dangerfield *et al.* (2012) demonstrated that these differences can be regarded as negligible for simple derivation of the probability distributions, especially if a reflected stochastic method is used.

Significant work has been undertaken in recent years to investigate the importance of stochasticity in cardiac events. Several studies have demonstrated that the introduction of stochasticity at some level within the cardiac system can have significant effects on the observable output. Work has shown the possible import of stochasticity for Ca^{2+} handling (Tanskanen *et al.*, 2005), I_{Ks} (Pueyo *et al.*, 2011), or in ion channel currents and distributions generally (Lemay *et al.*, 2011; Heijman *et al.*, 2013) on numerous important arrhythmogenic biomarkers (*e.g.* APD variability, EADs). Xie *et al.* (2007) presented results indicating that dynamical chaos itself can lead to reentry in tissue simulations. Furthermore, Sato *et al.* (2010) indicated that dynamical chaos (*i.e.* chaos inherent in the system, independent of stochastic interactions), as opposed to stochasticity *per se* is likely responsible for APD variation, though stochasticity in ion channels is likely a potentiating factor. Similarly, Ponard *et al.* (2007) demonstrated both experimentally and computationally that while stochasticity in ion channels and Ca^{2+} release channels does result in increased heart rate variability, it does not match experimentally observed patterns of variability.

Simulations have indicated the importance of electrotonic interactions in tissue, in that they 'smooth out' the stochastic heterogeneities in the cellular substrate, resulting in a more homogeneous tissue environment. Zaniboni *et al.* (2000) demonstrated experimentally that coupling two myocytes reduced the coefficient of variability of APD by 35%, and eliminated EADs induced by one of the two myocytes. Other reports have demonstrated a 'critical length' beyond which the stochastic effects are either reduced (Lemay *et al.*, 2011; Pueyo *et al.*, 2011), or lead to partial synchronisation (Sato *et al.*,

2009).

The *extent* of these electrotonic interactions is important—in situations where the coupling between cells is reduced, the effects of stochasticity are enhanced (Lemay *et al.*, 2011; Pueyo *et al.*, 2011). As such, it must be remembered that cell-level variability is potentiated by pathological conditions which reduce cell-to-cell coupling, and thus any underlying variation is likely to increase in arrhythmogenic significance.

3.3.2 Parameter Sensitivity

The interplay between input parameters and output parameters is decidely non-linear, and the effects of changes in one, or many parameters, cannot easily be predicted (Sarkar *et al.*, 2012); a demonstration of this problem is shown in Fig. 3.3. The previous modelling paradigm has been to consider the model as occupying a single point in the input/output parameter space—this can be represented by the blue point in the figure. However, it is becoming increasingly prevalent to consider variation in both input and output parameter space, represented by the cloud of red points in the figure. However, the *mapping* between the input and output spaces is non-linear, and there is no guarantee that a point in the middle of the input cloud translates to a point in the middle of the output cloud, or even if the clouds are the same shape (as shown in the figure). This point is worth restating: due to the complicated interactions between input components, the effect of a specified change in one input parameter may produce an entirely different effect if other input parameters are altered. The problem increases in complexity as one considers more input parameters and output metrics. To further complicate matters, it is not certain that any mapping relation (if it can be discovered) can be applied across different environments—it is possible that something as simple as changing the pacing rate of the system may alter the input/output parameter mapping. This shall be addressed in Chapter 5.

There are many different ways to try and elucidate the input/output mapping. One method is *parameter sensitivity analysis*, which varies one individual input parameter at a time to elucidate the effect this parameter has on a given set of output metrics, and expressing this effect in a quantitative manner (*e.g.* $\Delta_{\text{output}}/\Delta_{\text{parameter}}$).

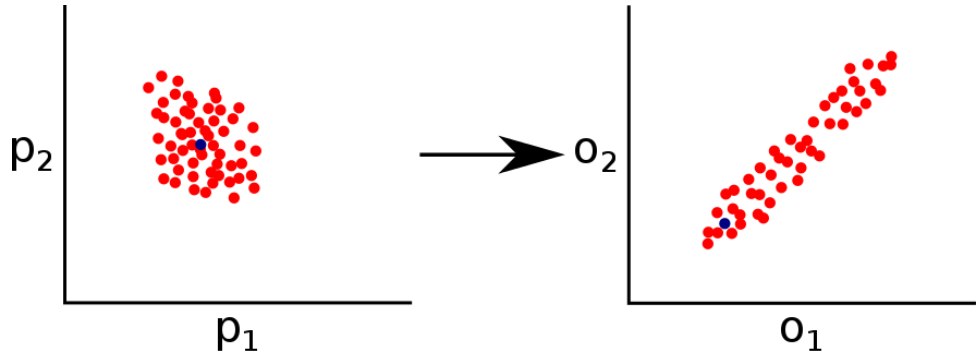


FIGURE 3.3: *Illustration of the effect of possible parameter variation on model output. In this example, changes in two given input parameters (p_1 and p_2) and the resulting effect on two measured outputs of the model (o_1 and o_2) are mapped; one specific data point is highlighted in blue. The mapping between the input parameter space and the output space is impossible to determine* a priori. *Based on a figure from Sarkar* et al. *(2012).*

The initial step in this process (and with all following processes) is to define the range over which the sensitivity of a parameter is to be assessed. There are numerous ways to define this range. In some cases, where sufficient data are available, a range based on available values from the literature is appropriate. When such an approach is not appropriate, an arbitrary range can be defined that is a reasonable representation of reality, often in terms of a percentage range. Alternatively, a log-normal distribution can be used (the range will equally represent halving and doubling the parameter). These three options represent the most common methods, but other methods are possible.

Parameter sensitivity analysis successfully indicates those parameters that are most directly responsible for a given output metric (Nygren *et al.*, 1998; Romero *et al.*, 2009a, 2010; Corrias *et al.*, 2011; Romero *et al.*, 2011). This method (and many of the following methods) has obvious extensions to computational predictions for pharmocological ion channel block.

However, biophysically detailed cell models are highly inter-connected, through membrane channel currents' dependence on V_m and ion concentrations, and the resulting non-linear interactions are often missed by a single dimensional parameter sensitivity analysis. Thus, with increasing computational power available, more work is being conducted to examine the multi-dimensional parameter effects within a model.

As the number of parameters being varied increases, the size of the space increases exponentially. As

such, to minimise the computational cost, it is common to survey a sample of the complete parameter space. There are many ways to extract such a sample, the simplest being a simple random sampling technique. Alternative methods include stratified sampling and Latin hypercube sampling, which attempt to ensure that the parameter space is evenly tested (McKay *et al.*, 1979).

An elegant method to extract the required data from this multi-demonsional sample was demonstrated in Sobie (2009). For a parameter space surveying the effects of p parameters (*e.g.* peak conductance, time to half-maximal activation, *etc.*), a sample of size n parameter sets is selected, where the complete size of the space can be represented by N parameter sets. Models using these parameter sets are simulated, and the results are recorded according to m different output metrics (*e.g.* APD_{90}, $[Ca^{2+}]_i^{sys}$, *etc.*). Before further analysis, the data are mean-centred and normalised by the standard deviation, *i.e.* $x_{new} = (x_{orig} - \mu_x)/\sigma_x$, where x_{new} and x_{orig} are the new and original data values, and μ_x and σ_x are the population mean and standard deviation for the data, respectively.

The data are now organised into matrices: the input parameter data are organised into an input matrix $\mathbf{X}$ of size $n \times p$, and the output metric data are organised into an output matrix $\mathbf{Y}$ of size $n \times m$. Each column thus represents one of the input parameters in $\mathbf{X}$ or output metrics in $\mathbf{Y}$, and each row represents one of the parameter sets simulated. Multivariable regression analysis is then used to derive the effect matrix $\mathbf{B}$ such that

$$\mathbf{XB} = \hat{\mathbf{Y}} \approx \mathbf{Y}, \tag{3.20}$$

where $\hat{\mathbf{Y}}$ is a close approximation of $\mathbf{Y}$. $\mathbf{B}$ is thus a $p \times m$ matrix of regression coefficients, and has been utilised as each row representing the effect of a given input parameter on the numerous output metrics, and each column representing the effect of various input parameters on a particular output metric. This has been shown to be successful in predicting the output of a new parameter set (Sobie, 2009), implying the underlying assumption that the relations remain linear is relatively well-founded while ion concentrations are not varied too much (Sobie, 2009; Sarkar and Sobie, 2010). The method has been used to replicate the results of the original parameter sensitivity analysis, *i.e.* to demonstrate the effect of a series of input parameters on a given output metric, and has also been used to investigate the effect of such variability on the repolarisation reserve (Sarkar and Sobie, 2011). Sarkar and Sobie

(2010) investigated the possible range of variation in a given set of parameters given the experimentally observed variation in certain output metrics by reversing the regression analysis (*i.e.* calculating $\mathbf{B}$ such that $\mathbf{X} \approx \hat{\mathbf{X}} = \mathbf{Y}\mathbf{B}^{-1}$) (Sarkar and Sobie, 2010).

This is an elegant method of investigating the effect of multiple parameter variation on multiple model outputs. However, it should be noted that this method still, to some degree, reduces the multi-dimensional parameter variation to a single-dimensional result. The interactions are still tested, and are thus present in an intrinsic sense in the resulting matrix $\mathbf{B}$. However,the approximation process ($\mathbf{X}\mathbf{B} = \hat{\mathbf{Y}}$) remains fundementally linear, and extracting the non-linear interaction data from $\mathbf{B}$ is a non-trivial matter. Consequently, the results of the multi-dimensional parameter variation are effectively reduced to the result of a single-dimensional parameter variation—while analysis of $\mathbf{B}$ can indicate those parameters most significant in influencing given output metrics, and those output metrics most altered by given parameters, it is less useful in indicating how the *interaction* of two parameters influences a single output metric.

Despite this apparent limitation, the conclusions reached by this method are often robust. Furthermore, the methodology has been shown to be adaptable to stochastic simulations—Heijman *et al.* (2013) used it to examine variation in maximal conductance in ion channels when stochasticity was also included.

An alternative method is to take advantage of so-called genetic algorithms to tune models to given experimental data. This has been used to provide single parameter sets, and adapt models to new data (Kherlopian *et al.*, 2011). Syed *et al.* (2005) and Achard and de Schutter (2006) used genetic algorithms to find multiple parameter sets that reproduce experimental data, where the parameter sets are not considered part of a continuum of models, but are rather loosely connected by a series of hyperplanes. While these studies were trained to reproduce a single set of experimental data, it is not unreasonable to expect this method to be easily adapted to reproduce a range of experimentally observed values.

3.3.3 Model Populations

The effects of multiple parameter variation can also be addressed via a comprehensive parameter sweep (this approach has also been referred to as a database method). It should be noted that this approach is not an alternative to the previously discussed parameter sensitivity methods, but rather can be viewed as a natural rigorous extension of it.

The guiding principle of such a method is to examine comprehensively a given parameter space—for example, if the effect of variation in p different parameters is being investigated, the model is simulated for every single possible combination of these parameters. If there are q different possible values for each parameter, this leads to p^q different simulations that would be run, unless measures are taken to limit this by some means (such as by taking advantage of experimentally demonstrated correlations between parameters (Schulz *et al.*, 2006)). More fully, with p parameters being varied, where each parameter can take n_p values, there are $\prod_{i=1}^{p} n_i$ different parameter sets. While this method can be computationally expensive, such a parameter search is also often embarrassingly parallelisable, and thus can be performed rapidly in real-time using such distributed computing methodologies as Nimrod (Abramson *et al.*, 1997, 2000, 2009, 2010).

The parameter sweep method has been used several times in neuronal studies. Bhalla and Bower (1993) utilised a parameter search method to calculate the values required for neuronal modelling where values were previously unknown; this work was itself an extension of similar, earlier work from Wilson and Bower (1992). Subsequently, a similar approach was used in Goldman *et al.* (2001), and was expanded upon further in Prinz *et al.* (2003), which applied variation to eight maximal conductances in a model of a lobster stomatogastric neuron to generate a database of about 1.7 million different models, and then classified these models according to their activity pattern. This database could then be searched for different models that satisfied a prescribed set of criteria. Similar work has been carried out to investigate cardiac issues, such as CICR (Sobie and Ramay, 2009). Indeed, there is increasing traction for replacing the previous paradigm of a single parameter set with a single model 'framework' with a parameter 'space' for a model, leading to a population of models (Prinz *et al.*, 2003; Taylor *et al.*, 2009; Marder and Taylor, 2011; Davies *et al.*, 2012). Song *et al.* (2010) demonstrated the validity of re-

producing the heterogeneities of population-level results using deterministic models. Indeed, one of the most notable works in relation to this thesis is the work of (Britton *et al.*, 2013), where a possible population was defined for study. To reduce the computational load, Latin hypercube sampling was used to sample from this parameter space, producing a population of $\sim 10,000$ models, which was then compared to experimental data to refine this to a population of 213 models that matched experimental data. This population was then able to successfully reproduce the effects of I_{Kr} drug block.

It is of note, and one of the topics addressed in this thesis, that the progress in investigating parameter variability is in its comparative infancy, and thus it is not surprising that some aspects are not readily addressed. Specifically, while model populations have been used to recreate experimental variation, little investigation has been done on the population itself, in terms of the relations between the parameters involved in these individual models. Indeed, this infancy can present a risk for confusing population-level effects, derived from population studies, with individual effects—the so-called 'ecological fallacy' (Moyé, 2014). However, due to the nature of the work presented here, this risk is avoided in this thesis. Furthermore, while work has shown how the effects of disease and other pathological conditions can be recreated by simultaneous variation of input parameters, this has not yet been linked to the variability already in evidence under physiological conditions. This may be considered the main thurst of this DPhil thesis: to bridge the gap between recreation of physiological evidence, and the investigation of the changes inherent in disease states.

3.4 Computational Modelling of Ischæmia

As was noted in §2.3.1, the dynamics and changes inherent in ischæmia are complicated and subject to great variability. Due to the rapid evolution of acute ischæmia, coupled with the difficulty of getting complete transmural experimental data, computational models present the opportunity to investigate questions that would be almost impossible to address otherwise. Insights into ischæmia granted by computational simulations were included in that prior section—this section deals more specifically with the methods of simulating ischæmia.

A more complete summary of the pathologies involved in successful simulation of ischæmia is presented in Rodríguez *et al.* (2006) and Ferrero *et al.* (2014). As mentioned in those reviews, it was establised through computational simulation (Ferrero *et al.*, 1996; Shaw and Rudy, 1997b,a) that the ischæmic milieu can be adequately represented by reproducing the effects of hyperkalæmia, acidosis and anoxia simultaneously. According to the experimental evidence of each of these actions, they are often simulated thus:

Hyperkalæmia: increase in extracellular K^+ concentration ($[K^+]_o$),

Acidosis: decrease in peak conductance of I_{Na} and $I_{Ca,L}$ by 25%,

Anoxia: activation of $I_{K\text{-}ATP}$ channels.

Most simulation models take the time for $[K^+]_o$ to reach its 'plateau level' to be 10 min, and the plateau concentration to be $\sim$ 12 mM, though higher values have also been used in simulation (Ferrero *et al.*, 2003a; Trénor *et al.*, 2007). Acidosis is often modelled as a linear reduction in maximum conductance of I_{Na} and $I_{Ca,L}$ from $\sim$ 5 minutes after the onset of ischæmia, until a 25% reduction is reached after 10 minutes (Trénor *et al.*, 2007), corresponding to the effect of a pH of $\sim$ 6.4 (Ferrero *et al.*, 2003b). It is also of note that it has been shown that the recovery of $(dV_m/dt)_{max}$ and the $h.j$ inactivation gates of I_{Na} are similar (Shaw and Rudy, 1997b).

While the first two changes are relatively straightforward to model computationally, anoxic conditions require the formulation and inclusion of a new current, $I_{K\text{-}ATP}$, that is rarely included in non-ischæmic models. Two important different formulations of this channel have been developed: the first was originally by Ferrero *et al.* (1996), and has been subsequently used by Trénor *et al.* (2007), while the second was originally shown in Michailova *et al.* (2005), and has been implemented in Terkildsen *et al.* (2007) and Michailova *et al.* (2007). Both are dependent on the ATP and ADP concentrations, and $[K^+]_o$. The Ferrero implementation was used in a Luo-Rudy model, which can be considered as a general mammalian model, but most of its components are derived from guinea pig data. It includes dependency on the intracellular concentrations of Na^+ and Mg^{2+}. The Michailova model was originally implemented in a canine model, and utilises updated data for the effect of Mg^{2+} via its

interactions with ADP, and was subsequently adapted for a rabbit ventricular model, while including modulation of the current by Ca^{2+}.

It can be noted that these models differ only in their efforts to determine $f_{\text{K-ATP}}$ and the details of what affects this value—if the degree of activation of the current is the same, there is no other difference between the models. As such, $I_{\text{K-ATP}}$ can be generally modelled as $I_{\text{K-ATP}} \propto f_{\text{K-ATP}} g_{\text{K-ATP}}(V - E_{\text{K-ATP}})$, with the form of $f_{\text{K-ATP}}$ being model dependent (due to the channel's selectivity, $E_{\text{K-ATP}}$ is the same as E_{K}). It is not uncommon to model $f_{\text{K-ATP}}$ directly, without recourse to ATP/ADP concentrations (Tice *et al.*, 2007; Trénor *et al.*, 2007). If this is done, it is similarly common to model the increase of $f_{\text{K-ATP}}$ as proceeding linearly over the first 10 min of ischæmia.

Computer models of ischæmia have also demonstrated the importance of increased heterogeneity within ischæmic tissue (Avitall, 1979; Behrens *et al.*, 1997), including the important arrhythmogenic risks posed by spatial heterogeneity introduced by the border zone separating ischæmic tissue from normally perfused tissue (Tice *et al.*, 2007; Trénor *et al.*, 2007; Ferrero *et al.*, 2014).

It is of key note that the work presented in this thesis represents the first time (to the author's knowledge) that there has been an explicit investigation into the effects of ischæmia on variability, thus representing a marriage of these two research topics. As such, this counts as the first steps to a more comprehensive understanding of what is already known to be a very variable and dynamic environment.

4 Computational Methods

Though this be madness, yet there is method in 't.

Hamlet, Act 2, Scene 2

This chapter presents the computational methods that are used throughout this dissertation—it provides both a summary of those techniques that are used generally, and also those techniques that are specific to particular chapters. Firstly, details of the computational models used throughout the dissertation will be given, detailing how these models were varied to examine the effect of parameter variability, details of how these models are adapted to simulate ischæmia, and specifics regarding the simulation methods used. Subsequently, the methods used to represent the data in a tractable manner will be presented. Finally, the manner by which the biomarkers/metrics used in this thesis are calculated are given.

4.1 Computational Models & Simulation Techniques

Two models were used in this thesis: both are designed to utilise biophysically detailed formulations of key currents to reproduce the action potential of rabbit epicardial ventricular myocytes. The first is presented in Shannon *et al.* (2004) (henceforth referred to as the Shannon model/framework), and the second is that presented in Mahajan *et al.* (2008) (or the Mahajan model/framework). While the original papers presented these as individual models, it is one of the main driving forces of this thesis to replace a single model with a population of models, differing not in the equations involved but

in the parameters used. As such, in the terminology that will be used in this thesis, the collection of equations that are presented in these papers shall be referred to *frameworks*, while as particular *model* refers to not just the equations, but also to the parameters used, with a collection of models being referred to as a population (it can be noted that a single population thus shares a single framework).

The Shannon framework was constructed on the basis of developing a mathematical model of the rabbit ventricular myocyte with the stated objectives of (i) taking advantage of advances in knowledge of the Ca^{2+}-handling system, and in particular modelling CICR in a manner to allow reproduction of SR Ca^{2+} release; (ii) tracking the ion flow across the cell membrane such that the model moved to steady state; (iii) incorporating realistic parameters for the ion channel equations derived from laboratory experiments; (iv) combining these equations to form a model that reproduces physiological phenomena; (v) producing a final product that is capable of being simulated on a desktop computer. It should be noted that extracellular ion concentrations are assumed to be constant, and only intracellular concentrations for calcium and sodium are tracked, with intracellular potassium concentration ($[K^+]_i$) set to a constant value. The changes in total internal ion concentration ($[X]_T$) are calculated as the difference between the ion flow into the cell ($d[X]_{in}/dt$) and the ion flow out of the cell ($d[X]_{out}/dt$). These ion flows in and out of the cell are calculated according to the current flow through ion channels, and are thus related to (i) the magnitude of the current, and (ii) the stoichiometry to the channel (which is often unitary). In the Shannon framework, the total Ca^{2+} concentration in the cell is thus calculated according to

$$\frac{d[Ca^{2+}]_T}{dt} = (I_{Ca,L} + I_{CaBk}) - (I_{NaCa} + I_{SLCaP}), \tag{4.1}$$

where I_{CaBk} represents the SL leak current, I_{NaCa} represents the Na^+/Ca^{2+} exchange current, and I_{SLCaP} represents the SL Ca^{2+} pump transport. Na^+ concentration changes are similarly calculated according to

$$\frac{d[Na^+]_T}{dt} = (I_{Na} + 3I_{NaCa} + I_{NaBk}) - I_{NaK}, \tag{4.2}$$

where I_{Na} is fast Na^+ current, I_{NaBk} represents the Na^+ leak current and I_{NaK} is the Na^+/K^+ pump current. I_{NaCa} has a coefficient of 3 due to the stoichiometry of the Na^+/Ca^{2+} exchanger, moving one Ca^{2+} ion in exchange for 3 Na^+ ions.

The starting point for the Shannon model was the Luo-Rudy model (Luo and Rudy, 1994a,b), with modifications and additions made according to subsequent work (Tohse, 1990; Negretti *et al.*, 1993; Zeng *et al.*, 1995; Stern *et al.*, 1999; Shannon *et al.*, 2000; Puglisi and Bers, 2001; Weber *et al.*, 2001; Bassani *et al.*, 2004), and further adapted to match the experimental training data used in the paper. The model is a compartmentalised model, accounting for the SR, the junctional cleft (the region directly between the cell membrane and the SR, also known as the dyadic junction—see Fig. 2.6), the subsarcolemmal/submembrane space and the bulk cytosolic space; fractional volumes for these compartments are estimated based on the literature (Page *et al.*, 1971) and previous computational work (Soeller and Cannell, 1997). Compartmentalisation is important in this model both for the subdivision of ion concentrations (the concentration can vary dramatically between spaces, especially between the junctional cleft and the bulk cytosolic space) and for the concentration of ion channels within those spaces, *e.g.* 89% of the $I_{Ca,L}$ channels are within the junctional cleft. The SR Ca^{2+} release channel (RyR channel) is modelled as a Markov model with 4 states: closed, open, inactivated and resting inactivated. Modifications in this paper, such as lumenal $[Ca^{2+}]_{SR}$ dependence to enforce SR Ca^{2+} dependence on the activation/inactivation rate constant, make further states unnecessary.

The Mahajan framework is itself based on the Shannon framework, adapted to reproduce the Ca^{2+} dynamics at rapid pacing rates. This was achieved with alterations made to the L-type Ca^{2+} current, intracellular Ca^{2+} cycling, Na^{+}/Ca^{2+} exchanger and channel distributions. $I_{Ca,L}$ was replaced with a seven-state pseudo-Markov model that reproduces both voltage and Ca^{2+} inactivation, and the Ca^{2+} cycling model originally used in Shiferaw *et al.* (2003) was incorporated, adapted to match available data for Ca^{2+} alternans measured from rabbit ventricular myocytes (Chudin *et al.*, 1999). Other cell parameters were also altered to ensure the model output matched the results of myocyte experiments conducted for the paper.

The frameworks for both models were downloaded from the CellML repository[1] (Lloyd *et al.*, 2008), with the Shannon framework corrected according to Shannon *et al.* (2012). These CellML files were then converted to C++ using the Cellular Open Resource software[2] (Garny *et al.*, 2003, 2009), and

[1] http://models.cellml.org/cellml
[2] http://cor.physiol.ox.ac.uk

these were then adapted to use the Sundials CVODE solver for ordinary differential equations[3], which provides adaptive time-stepping to reduce simulation time (Hindmarsh *et al.*, 2005). Relative and absolute tolerances for error-checking in the solution were set to 10^{-7} and 10^{-9}, respectively.

Both frameworks, in describing the AP of ventricular epicardial myocytes, require stimulation by an external source for the initiation of an AP. This is provided by a stimulus current (I_{stim}), applied appropriately to pace the cell at a given cycle length (CL). This takes the form of a 3 ms step function current, and is initially the same as provided with the CellML file.

4.1.1 Parameter Space Simulations

The first stage in this thesis is to (a) examine the effects of simultaneous variation in multiple parameters on model output, and (b) determine which of those models amongst those simulated produce output that matches the experimental literature, thus producing a population of models to reproduce the experimental variation.

Intracellular K^+ concentration ($[K^+]_i$) was unclamped, and variables introduced to alter the peak conductances of six different ion channels: the transient outward current (I_{to}), the rapid delayed rectifier K^+ current (I_{Kr}), the slow delayed rectifier K^+ current (I_{Ks}), the inward rectifying K^+ current (I_{K1}), the L-type Ca^{2+} current ($I_{\text{Ca,L}}$), and the Na^+/K^+ pump current (I_{NaK}). The reasons for varying these currents will be given in Chapter 5, while here the methodology used to vary these parameters will be described.

For details of equations describing these currents, the reader is referred to the respective papers. For all currents, scaling is achieved by applying a scaling factor to the *peak conductance/flux* of the channel—no changes to the internal dynamics are made. To that end, this can be considered to reflect one of two realities: either a reduction in the peak ion flow through a given ion channel, or a reduction in the number of ion channels expressed in the cell membrane. Mathematically speaking, there is no difference between the two (or of a combination of the two). Where an ion channel is compartmentalised (*e.g.* $I_{\text{Ca,L}}$), the form of the equation is $I_X \propto F_X g_X (V - E_X)$, where F_X represents the fraction of

[3] http://computation.llnl.gov/casc/sundials/main.html

ion channels in a given compartment, and other terms are as previously defined. As such, by scaling the value of g_X, the scaling is performed equally to all compartments.

In the case of I_{to}, both the Shannon and Mahajan frameworks model a fast and slow component of the current ($I_{\text{to,f}}$ and $I_{\text{to,s}}$, respectively). To vary the peak conductance of I_{to} as a whole, a scaling factor (referred to as g_{to}) is introduced, and applied to the sum of the two currents; no change is made to the formulation of either current, or to the values of their individual conductances ($g_{\text{to,f}}$ and $g_{\text{to,s}}$).

In the parameter sweep, each of the six conductances is varied independently, resulting in the exploration of a six-dimensional parameter space. The range of this parameter space initially covers $\pm 30\%$ variation from the value originally provided with the model (the 'control' value) in each conductance, at a resolution of 15%, with the parameter space thus covering $5^6 = 15,625$ different possible combinations of values. The aim in conducting the parameter sweep was not to determine the effect of sudden change in parameter values, but rather to elucidate the model's 'steady state' behaviour to long-term use of a given set of parameters. As such, an extended simulation time was used, to allow the model to fully 'relax' to the behaviour that would characterise the framework's response to a given parameter set, with all changes in response to the 'new' parameter set being completed and new steady-state values being reached. Initial simulations conducted using COR and the original CellML file of the Mahajan framework , using a parameter set chosen at random from within the initial parameter space, indicated that changes to the AP would be complete within 750 s of simulation. On this basis, initial simulation time was set to $1,000$ s, with data recorded for the last two stimulated APs. Each model output was checked for steady state by comparing corresponding data points for these two APs: the cell was considered to be in steady state if the difference for each data point in the AP was less than 5% of the difference between the maximum and minimum AP values for the last AP. Steady state was often reached within the initial simulation time. For those models where steady state was not reached, and yet cell excitation was present (determined as $V_m > 0$ mV), the simulation was repeated with a longer simulation time.

Based on the results of this parameter sweep, two populations were derived, one for each framework, with all APDs within these populations falling within an experimentally observed range—for further

	g_{to}	$g_{Ca,L}$	g_{Kr}	g_{Ks}	g_{K1}	g_{NaK}
Shannon	+30%	+0%	+0%	−15%	−30%	+15%
Mahajan	+0%	+75%	+30%	+75%	+15%	−30%

Table 4.1: *Details of the variations in peak ion channel conductances from originally provided values for the Shannon and Mahajan frameworks that define the models used to train the alterations to prepare the framework for ischæmic simulations. These models produce APs with APD_{90} values closest to the population mean for CLs of* 400 *ms,* 600 *ms, and* 1, 000 *ms.*

details, see §5.4.

4.1.2 Ischæmia Simulations

Both the Shannon and Mahajan model frameworks were designed to reproduce the AP of a normal, healthy ventricular cardiomyocyte. As detailed in §3.4, the distinguishing changes in the AP caused by ischæmia can be reproduced by slight alterations to this 'normal' framework, with no significant changes to the underlying framework.

The first stage in preparing the framework for ischæmic simulations was to define a new 'control' model with which to train the alterations (the original models were not in the defined populations—for further details, see the results presented in §5.4.1). To this end, the model within the populations that produced the value for APD_{90} closest to the population mean for all CLs used to define the population (400 ms, 600 ms and 1, 000 ms) was selected; the resulting model parameters are shown in Table 4.1. It should be noted that these two models do not necessarily produce the APD_{90} closest to $\overline{APD_{90}}$ at all CLs, but rather is the model that produces the values that are all closest simultaneously.

Using these new models, the value of I_{stim} is then retrained (Sutton *et al.* (2000) demonstrated the possible important implications for I_{stim} on calculated ERP). The new value of I_{stim} is designed to be 1.5 times greater than the minimum value that causes cell excitation, with I_{stim} being applied as a 3 ms duration step function. Finally, the cell is simulated for an extended time, with the resulting model parameters (for such details as ion concentrations) then being fixed. This was done to try and ensure that the population, prior to ischæmic conditions, would have conditions that would be most appropriate for the defined population, rather than for a model that is no longer included in the

population.

Alterations were then implemented to adapt the frameworks to be capable of simulating different degrees of severity of phase 1A acute ischæmia. Further details of the changes can be found in §3.4, with the following being details of the implementation rather than the background. The changes made were mostly in common with those from Rodríguez *et al.* (2006), with the addition of alterations in the Na^+-handling system of the cell. Consequently, four separate parameters can be varied individually or in unison, with their combined effect bringing about what can be regarded in this dissertation as phase 1A acute ischæmia:

$[K^+]_o$: Increase in extracellular K^+ concentration, *i.e.* hyperkalæmia.

$f_{\text{K-ATP}}$: Parameter to describe degree of activation of $I_{\text{K-ATP}}$ channels in response to changes in ATP/ADP concentrations.

f_{inhib}: Parameter to describe degree of inhibition of I_{Na} and $I_{\text{Ca,L}}$.

f_{NaK}: Parameter to describe changes in Na^+-handling system of cell, reflecting a percentage increase in $[Na^+]_i$ and a similar decrease in the conductivity of I_{NaK}.

These parameter values are varied both to simulate the progression of acute ischæmia from the moment of occlusion to 10 min hence (referred to as 10 min post-occlusion, or 10 min PO), and also independently to allow investigation of the effects of variability in the ischæmic parameter space and analysis of relative effects of parameters.

The model of $I_{\text{K-ATP}}$ used here is derived from the version presented in Michailova *et al.* (2007), itself inherited from Michailova *et al.* (2005), and is expressed according to

$$I_{\text{K-ATP}} = f_{\text{K-ATP}} g_{\text{K-ATP}} \left(\frac{[\text{K}^+]_o}{[\text{K}^+]_{o,\text{normal}}} \right)^{0.24} (V_m - E_{\text{K}}), \tag{4.3}$$

where $f_{\text{K-ATP}}$ represents the fraction of $I_{\text{K-ATP}}$ channels activated, $g_{\text{K-ATP}}$ represents the peak ion channel conductance and $[\text{K}^+]_{o,\text{normal}}$ represents the pre-ischæmic value of $[\text{K}^+]_o$ (which is considered to be 5.4 mM); the other values in the equation are as defined previously. This is also equivalent to a

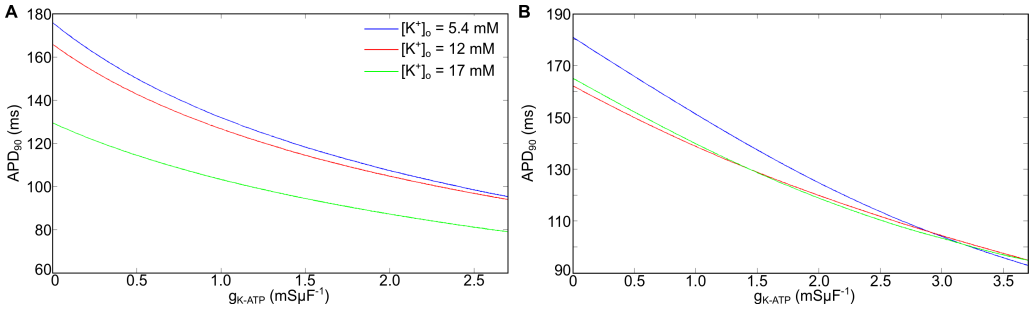


Figure 4.1: *The effect of varying the value of* $g_{\text{K-ATP}}$ *(with* $f_{\text{K-ATP}} = 0.8\%$*) on* APD_{90} *for Shannon* (A) *and Mahajan* (B) *models. The effect is charted against normal conditions, and two possible ischæmic concentrations of* $[K^+]_o$*.*

simplified version of the model from Ferrero *et al.* (1996). As mentioned in §2.3.1, the 'spare channel hypothesis' suggests that full activation of $I_{\text{K-ATP}}$ (*i.e.* $f_{\text{K-ATP}} = 100\%$) is not necessary, and does not occur, during ischæmia, with $f_{\text{K-ATP}} = 0.8\%$ being suggested as a reasonable approximation of the actual degree of activation experienced at 10 min PO.

The $I_{\text{K-ATP}}$ conductance is thus the product of $f_{\text{K-ATP}}$ with the channel's peak conductance ($g_{\text{K-ATP}}$). Preliminary analysis was performed to examine the effects of varying values of $g_{\text{K-ATP}}$ on both models, with $f_{\text{K-ATP}}$ set to 0.8%, corresponding to the activation at 10 min PO. The results are shown in Fig. 4.1, and show that the models respond differently to the value of $g_{\text{K-ATP}}$ used.

From these results, it was decided to use a value of $g_{\text{K-ATP}} = 2.61$ mSμF^{-1}, with the resulting total channel conductance at 10 min PO (*i.e.* the product of $f_{\text{K-ATP}}$ and $g_{\text{K-ATP}}$) being 0.02088 mSμF^{-1}. This can be contrasted with the total channel conductance used in Michailova *et al.* (2007) ($f_{\text{K-ATP}} g_{\text{K-ATP}} =$ 0.02616 mSμF^{-1}), which was implemented in the cell model originally outlined in Puglisi and Bers (2001) (on which the Shannon framework and, in its turn, the Mahajan framework were both based). Similarly, Dutta *et al.* (2011) used a total channel conductance of 0.02716 mSμF^{-1} in a model based on the Mahajan framework.

The extent of increase in $[K^+]_o$ due to ischæmic hyperkalæmia is subject to debate—prior work tends to put the increase to a value of $\sim$ 12 mM. However, $[K^+]_o$ is a remarkably variable quantity, not only with regards its 'ischæmic' value, but also with regards its 'normal' value. As such, while $[K^+]_{o,\text{normal}}$ is set to 5.4 mM and $[K^+]_{o,\text{isch}}$ is set to 17 mM, the parameter space for $[K^+]_o$ is comprehensively

Time (min PO)	0	2	4	6	8	10
$f_{\text{K-ATP}}$ (%)	0.00	0.16	0.32	0.48	0.64	0.80
f_{inhib} (%)	0	5	10	15	20	25
f_{NaK} (%)	0	6	12	18	24	30
$[K^+]_o$ (mM)	5.40	7.72	10.04	12.36	14.68	17.00
$[K^+]_o$ (mM)	5.40	7.32	9.24	11.16	13.08	15.00
$[K^+]_o$ (mM)	5.40	6.72	8.04	9.36	10.68	12.00

TABLE 4.2: *Table showing the parameters used in the simulation to approximate a given time post-occlusion, assuming linear increase in parameters. Here, $f_{\text{K-ATP}}$ represents the degree of activation of $I_{\text{K-ATP}}$, f_{inhib} represents the degree of inhibition applied to I_{Na} and $I_{\text{Ca,L}}$, and f_{NaK} represents the percentage increase/decrease in $[Na^+]_i$ and I_{NaK}, respectively. Multiple different values of $[K^+]_{o,\text{isch}}$ are used—their respective values are also shown, though unless otherwise indicated in the text, $[K^+]_{o,\text{isch}}$ is set to 17 mM.*

explored, with 6 different values tested in the parameter sweep, and 3 different potential values of $[K^+]_{o,\text{isch}}$ investigated (12 mM, 15 mM and 17 mM).

To allow simple and effective simulation of the increase in $[Na^+]_i$, it is clamped, with the change being simulated (applied using f_{NaK}) imposed at the start of the simulation. Inhibition of ion currents (I_{Na}, $I_{\text{Ca,L}}$ and I_{NaK}) is achieved in the same manner as in the earlier parameter space search, by reduction of the peak channel conductance g_X by the required factor (f_{inhib} or f_{NaK}).

In this work and in common with previous work (Rodríguez *et al.*, 2004; Tice *et al.*, 2007), ischæmia is simulated as a linear change in relevant environmental parameters from their 'normal' value to their 'ischæmic' value—the resulting values are shown in Table 4.2. However, due to the dynamic nature of ischæmia, it would be mis-leading to think that the specified parameter values thus uniquely define 'x minutes PO'—it is more accurate to make all judgements in relation to the parameters directly. The notation used in this chapter as 'x min PO' is used purely for brevity. For similar reasons of economy, a parameter shall be described as having a 'normal' value when no changes have been applied ($[K^+]_o$ = 5.4 mM, f_{inhib} = 0%, $f_{\text{K-ATP}}$ = 0.0%, f_{NaK} = 0%), and as an 'ischæmic' value when representing conditions corresponding to 10 min PO ($[K^+]_o$ = 17 mM, f_{inhib} = 25%, $f_{\text{K-ATP}}$ = 0.8%, f_{NaK} = 30%).

The simulation protocol is: (i) impose the relevant conditions directly to the model; (ii) stimulate the

cell at a CL of 600 ms for 10 APs; (iii) record the data for the last AP for subsequent analysis. The model was assessed to be viable if the difference between V_{max} and V_{rest} was greater than 44.0 mV; this value was used based on tests conducting using the Shannon population.

Preliminary simulations using the Shannon model indicated that this simulation protocol is sufficient to enable models to reproduce the expected ischæmic changes to AP. While these preliminary simulations did indicate that a minority of models (especially within the Mahajan population) would demonstrate further AP alterations during a longer simulation time, further simulation time would be misleading: these models, and the changes imposed upon them to reproduce ischæmia, are approximations, and the models are most suited to short-term simulations. Neither model framework is designed to reproduce the complicated effects of the medium to long-term effects of ischæmia. As such, the simulation duration is designed to reproduce most faithfully the short-term impacts of ischæmia.

4.1.3 Nimrod Distributed Computing Grid

While the CVODE solver (with adaptive time-stepping) dramatically reduces simulation time when compared to a forward Euler ODE solver (with fixed time steps), the sheer number of simulations that have to be run can quickly escalate dramatically when investigating parameter spaces—as stated earlier, only 6 different parameters, each taking 5 different values, leads to 15,625 different combinations. However, parameter space investigation is an embarrassingly parallelisable problem, *i.e.* there is no communication between each individual simulation used to investigate the parameter space, and thus, given the correct tools, it is a relatively simple matter to parallelise the search. To this end, the Nimrod/G distributed computing grid (Abramson *et al.*, 2000, 2010) is used. Developed by the Monash eScience and Grid Engineering Laboratory, this system permits a correctly written program to be run in parallel across multiple computing resources. While the use of this tool will be expanded upon only insofar as it furthers the goal of this thesis, it must be remembered that this presents a powerful option for many possible problems (Abramson *et al.*, 2009, 2011).

A schematic for a possible function of Nimrod is shown in Fig. 4.2. Initially, an executable program

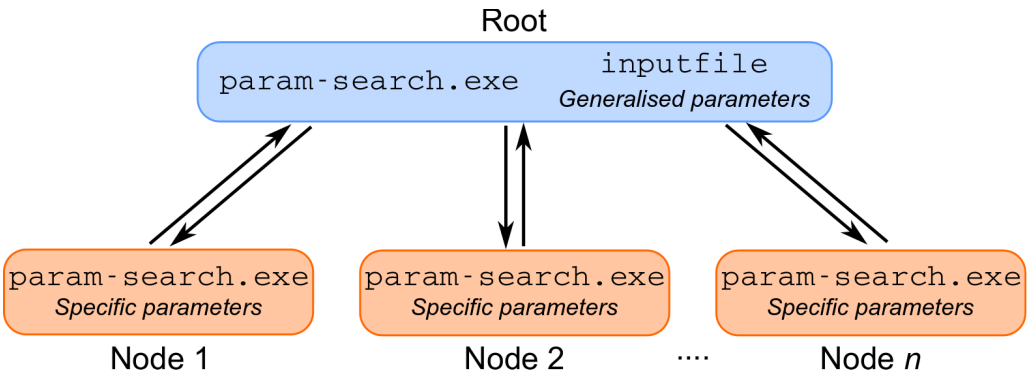


FIGURE 4.2: *Schematic for possible use of the Nimrod/G computing grid, suitable for a parameter sweep for one variable* `x`. *An executable program* `param-search.exe` *is loaded onto the root, along with an* `inputfile` *that describes the substitution process to the Nimrod/G grid. The executable is copied to a number of nodes for execution, with Nimrod delegating the correct parameters as specified by the plan file. Upon completion, the results of execution are copied back to the root.*

is loaded to a central location (referred to as the 'root'), along with a *plan file*, which provides Nimrod with the instructions for the task; an example appropriate to conducting a parameter sweep is shown in Code Excerpt 4.1. According to the instructions given in this plan file, the executable is copied to one of several computational 'nodes', along with a *substitution file*, which lists the name of the parameters being varied. In the example given, only one parameter is being varied, and thus the substitution file will just list the parameter `x`; it is relatively straight-forward to increase the number of parameters being varied.

Implicitly included is a specific value for the parameter `x`. The `node:substitute` command instructs Nimrod to substitute the parameter found in the substitution file with the node-specific value. The number of nodes available, and thus how many instantiations of the executable (referred to as 'jobs') that can be run simultaneously, is arbitrary—if the required number of jobs is greater than the number of available nodes, Nimrod will queue the jobs, distributing them as best it can to achieve the greatest degree of parallelisation, and thus the greatest degree of efficiency, possible.

The executable is then executed at the node. It should be noted that the executable must be designed to accept the input from the substitution file, with an example of C++ code suitable for this given in Code Excerpt 4.2. This code is not specific to Nimrod—it acts to open a file, and input the data found in that file into the code as a parameter value. The key aspect of Nimrod is that it alters the substitution

Code Excerpt 4.1 Example of plan file used to determine Nimrod execution appropriate to the schematic in Fig. 4.2. The executable `param-search.exe` and the substitution file `inputfile.sub` are copied from the root to the node, where the Nimrod/G platform performs the substitution and the exection, before copying the resulting output file `output.dat` from the node back to the root. The output file is renamed to incorporate the value given for `x` when being copied to the root to avoid identically named files being present on the root on completion.

```
parameter x float range from 1 to 10 step 1;
task main
  copy param-search.exe node:./
  copy param_var.sub node:./
  node:substitute inputfile.sub inputfile
  node:execute param-search.exe
  copy node:output.dat output_${x}.dat
endtask
```

Code Excerpt 4.2 Excerpt of C++ code required for resulting executable program to be able to perform substitution as per the plan file shown in Code Excerpt 4.1.

```
/* Declare the file parameter to read the data */
std::ifstream params;
/* Open the file */
params.open("inputfile");
/* Check the file is open */
assert(params.is_open());
/* Push the value that it reads from file into the variables */
params >> x;
```

file to permit each node to run a different value, according to the range specified in the plan file. After execution is completed, the plan file specifies that the output from the executable (again, it should be noted that the executable would produce the output file regardless of the involvement of Nimrod) are copied back to the root, where the results from all nodes are collated. As the root collates the results from all the nodes, it is thus prudent to rename the output file to distinguish it from the other outputs—in the plan file example given, it is renamed to include the value of the parameter `x` that was used in the execution.

It should be noted that there are several different ways of achieving the end result. For example, the plan file can be constructed to omit the substitution file and `node:substitute` command, and in-

stead execute the command `node:execute param-search.exe $x`, which passes the parameter x (with Nimrod again providing a node-specific value) to the C++ program (which must then be designed to accept arguments of this type).

4.2 Represention of Multi-Dimensional Data

Comprehensive investigation of the effect of variability on multiple different parameters in a model can be thought of as an investigation into a multi-dimensional parameter space: each parameter corresponds to a single dimension. A key problem to be overcome when examining multi-dimensional parameter spaces is how to represent the associated data in a manner that is both meaningful and comprehensible. It is only possible to visually represent data in up to three dimensions, with two dimensions being a more common limit. As such, the challenge for higher dimensional spaces is to find a way to represent these spaces in only two dimensions, without losing any of the data in the space—with the parameter space represented in two dimensions, it is possible to use a contour plot to demonstrate the effect of changes in this space on any given metric. The method used here is called *clutter-based dimension reordering (CBDR)*, and has been employed in studying the effect of variation on the electrophysiology of neurons (LeBlanc *et al.*, 1990; Peng *et al.*, 2004; Peng, 2005; Taylor *et al.*, 2006).

This method renders higher dimensional spaces in two dimensions, and can be considered a linear projection from n dimensions to one or two dimensions. For finite data sets (as is the case in this dissertation), this is a relatively simple affair, and can be thought of as rearranging the data, giving each point in the n dimensional a unique point in a 2-dimensional space that has the same number of points contained within it. Moving from 3 dimensions to 2 dimensions can be represented as slicing a cube, and placing the resulting squares sequentially next to each other, and moving from 2-dimensions to 1-dimension would be to divide the square into lines, and placing the lines sequentially.

The general form of projection, to give each entry in an n dimensional space (represented by $(x_1, \ldots, x_n)$)

a unique point (represented by x'_i) in 1D space, is given by

$$x'_i = \sum_{i=1}^{n} \left((x_i - 1) \prod_{j=1}^{i-1} N_j \right) + 1, \tag{4.4}$$

which returns a value between 1 and N, where N is the total number of data points; the number of data points in each dimension is given by N_i. A two dimensional representation can be constructed by splitting the total number of dimensions in two, and treating each separately as above.

A visual representation of this projection process appropriate for this dissertation (that is, reducing a 6-D parameter space to a 2-D space) is given in Fig. 4.3A—the process thus illustrated is referred to as *dimensional stacking*. In it, two of the conductances being varied are chosen at random (g_1 and g_2), and with all other parameters set to their minimum value, the effect of the variation of g_1 and g_2 on a particular output metric is represented using a contour plot; this is referred to as Level 1 of the dimensional stack image, and is the 'lowest' level. Next, two other conductances are chosen (g_3 and g_4), and the original Level 1 plot is repeated for each combination of these two parameters. Each of these plots is arranged in a manner reflecting the variation in g_3 and g_4 to form Level 2 of the stack. Thus, the Level 1 plot that has g_3 and g_4 at their minimum values is at the bottom left of the Level 2 grid, and the Level 1 plot that has g_3 and g_4 at their maximum values is at the top right of the Level 2 grid. This process is then repeated for the last two conductances for the 'highest' level (Level 3).

The choice of the so-called 'stack order' (determining those conductances to be plotted as low order and those conductances to be plotted as high order) has a profound effect on the resulting stack image, and its resulting utility as an analysis tool—see Fig. 4.3B for a demonstration of the difference the choice of stack order makes. To try and maximise the utility of the dimensional stack image, the stack order is optimised in an attempt to 'smooth' the image, on the assumption that a dimensional stack image with minimised contour gradients will provide the most effective representation of the data. This is done by minimising the sum of the absolute differences between the metric value for each point in a given dimensional stack image and its four neighbours in the x and y planes; in more general terms, it is those points that are separated by one step in one dimension. An alternative definition of 'neighbour' is those that are separated by one step in multiple dimensions—in two dimensions, this would thus include the diagonally connected points. However, Taylor *et al.* (2006) demonstrated

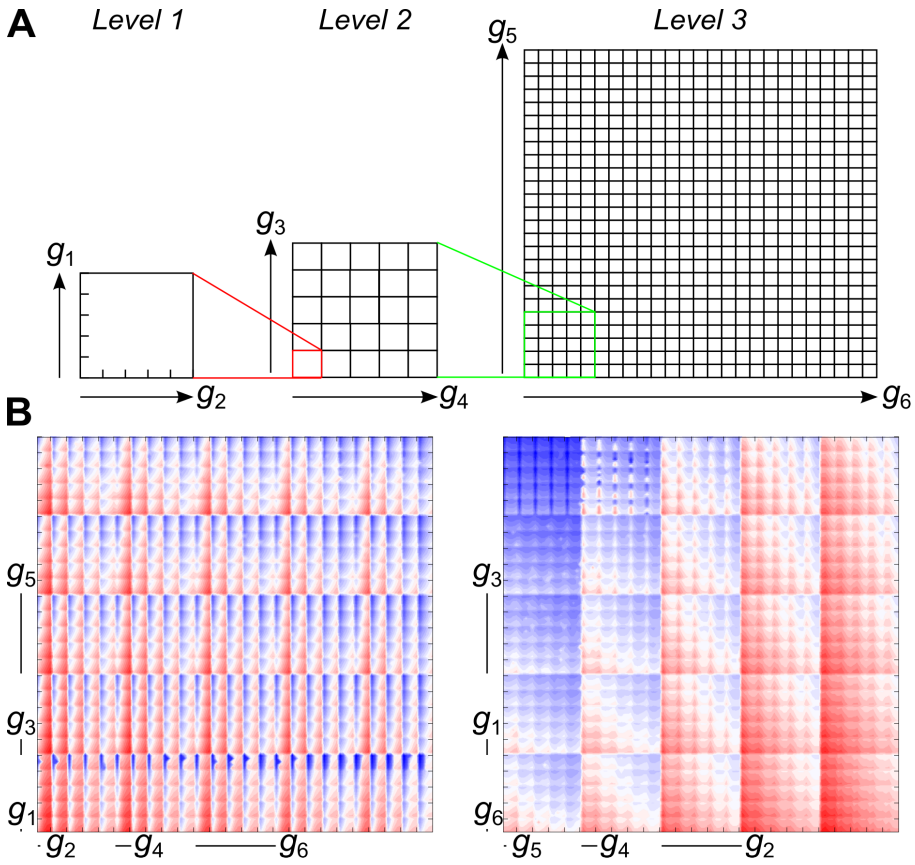


FIGURE 4.3: (A) *The effect of two 'low order' conductances (g_1 and g_2) is represented in a contour plot, with all other conductances set to their minimum values. This plot is then repeated in a larger grid spanning two 'medium order' conductances (g_3 and g_4). For each value of $g_{3,4}$, the $g_{1,2}$ plot is repeated for the respective values. This process is repeated to represent the two 'high order' conductances (g_5 and g_6).* (B) *Example showing a random stack order* (left)*, versus an optimised stack order* (right) *for the same variable. The labelled bars show the scale at which the conductance varies,* e.g. *in the left plot, g_2 varies at the smallest scale (Level 1) on the x-axis.*

that the connectivity of the space is not adversely affected by using the more restrictive definition. The implications of connectivity will be expanded upon further in §5.4.2.

Initially, a random stack order is chosen, and the 'score' of the sum of its absolute differences is calculated. This score is then compared with the score of the neighbouring stack orders, where a neighbouring stack order is identical save for the swapping of two conductances. If one of the neighbouring stack orders has a lower score than the current stack order, the neighbour's order is adopted, and the process is repeated until no neighbouring stack orders have a lower score. While this would technically lead only to a local minimum in the stack order space, in practice it is rare for the global minimum to

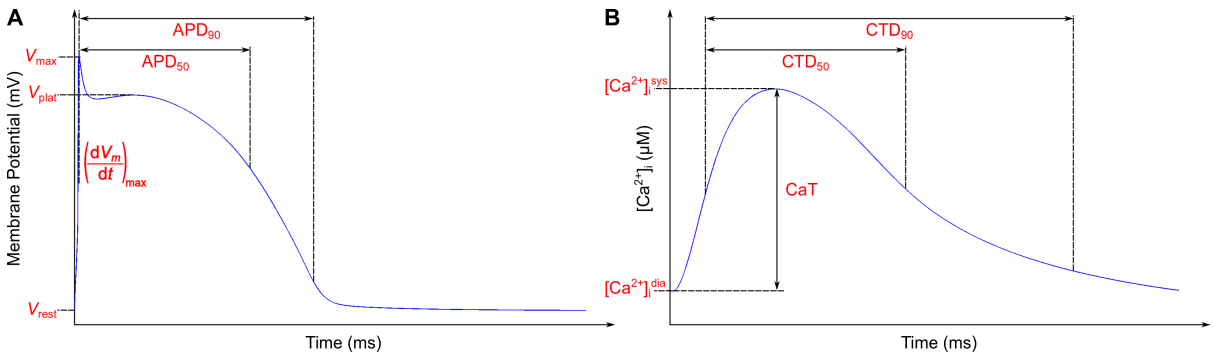


Figure 4.4: *Illustration of some biomarkers used in this dissertation, for the AP* (A) *and* $[Ca^{2+}]_i$ (B). *Precise details of the calculations are given in the text.*

not be found (this is confirmed by performing multiple searches, each for a different start order).

The results of an optimisation process are shown in Fig. 4.3B. The optimum stack order accurately reflects the *interactions* between conductances, making it easier to discern patterns within the data, both in terms of those parameters that have the greatest effect, and also (by virtue of the complete representation of the parameter space) details of the interactions between the parameters. While the stack order reflects the interactions between conductances, it is often the case that the optimised stack order has those parameters with a lesser effect on the measured biomarker assigned as 'lower order' conductances (Level 1), while those that have a greater effect are 'higher order' (Level 3).

4.3 Biomarker Calculation

Biomarkers represent a means of quantitatively comparing different APs, and with the large volumes of data generated by parameter searches and model populations, a means of automating the analysis of model response is vital. Biomarkers also present a valuable tool to compare data with previous experimental data from the literature, where complete AP data are often unavailable. While many biomarkers are common throughout the literature, some are poorly defined. As such, the following defines the terms as used in this dissertation, with Fig. 4.4 illustrating them in relation to typical cell model data.

The resting membrane potential (V_{rest}) is defined as the value of V_m immediately prior to application of I_{stim}—due to the lack of any leak current in these models (due to their being ventricular myocyte

models), this is synonymous with the minimum/diastolic value of V_m during the AP. Similarly, V_{max} is defined as the maximum value of V_m during the AP, and often corresponds to the value of V_m reached during the AP upstroke. $(\text{d}V_m/\text{dt})_{\text{max}}$ is the maximum rate of membrane depolarisation, and corresponds to a measure of the rapidity of the upstroke of the AP. It should be noted that $(\text{d}V_m/\text{dt})_{\text{max}}$ can often be shown to be directly proportional to the square of the conduction velocity of the AP in a cable model, and thus it is often used as a proxy for conduction velocity in tissue (Hodgkin, 1954; Tasaki and Hagiwara, 1957; Walton and Fozzard, 1983; Kléber and Rudy, 2004).

The plateau membrane potential (V_{plat}) is defined as the value of V_m reached when $(\text{d}V_m/\text{dt})$ reaches its maximum value (while still remaining greater than 0 Vs^{-1}) after the initial upstroke. Thus, in an AP with a spike and dome morphology, it corresponds to the maximum value of V_m after the initial upstroke (*i.e.* during phase 2 of the AP). AP duration (APD) is one of the more common AP biomarkers, but suffers from being relatively poorly defined, at least to the extent that there can be confusion about the specific definition while the broad strokes of the definition are agreed upon. Here, APD_X is defined as the time interval between the point of $(\text{d}V_m/\text{dt})_{\text{max}}$ and the point at which V_m is repolarised by $X\%$ (*i.e.* where V_m is less than or equal to $V_{\text{rest}} + X(V_{\text{max}} - V_{\text{rest}})$).

The effective refractory period (ERP) is defined, in tissue, as the length of time required for the tissue to become excitable after excitation; however, ventricular cell models, with a stimulus current applied, are unable to accurately reproduce inexcitability. As such, the method used to calculate ERP here is the same used used in previous literature (Tice *et al.*, 2007; Trénor *et al.*, 2007; Romero *et al.*, 2009b; Pandit and Jalife, 2013), where the time interval between activation and the product of the h and j inactivation gates of I_{Na} equalling 0.012 ($(h.j)_{\text{crit}}$) is used as a proxy for the actual value of ERP. This method is used due to the importance of I_{Na} during the upstroke of the AP, with the rationale that while I_{Na} is still inactivated, the cell can still be regarded as refractory. Under normal conditions, ERP$\approx$APD$_{90}$, and thus $(h.j)_{\text{crit}}$ is corroborated as being valid by confirming that $t((h.j)_{\text{crit}} = 0.012) \approx t(\text{APD}_{90})$ under normal conditions. However, by calculating ERP based on $h.j$, and only recording the data for the duration of the AP, an upper limit on the values of ERP that can be determined is given by the CL.[4]

[4]It is a point of nomenclature that this limit can be described as both an upper and a lower limit: as an upper limit,

The post-repolarisation refractoriness (PRR) is also measured, where PRR is defined as ERP$-$APD$_{90}$. The upper limit on the value for the ERP thus also provides an upper limit on the PRR, but this upper limit is variable depending on the model's APD$_{90}$ value.

Biomarkers for $[Ca^{2+}]_i$ were also calculated. $[Ca^{2+}]_i^{sys}$ and $[Ca^{2+}]_i^{dia}$ are the systolic and diastolic values of $[Ca^{2+}]_i$, respectively, and the difference between these two values is referred to as the calcium transient (CaT). Finally, the calcium transient duration (CTD$_X$) is defined in an analagous manner to APD$_X$.

Which biomarker, or combination of biomarkers, provides the best measure of goodness-of-fit between model output and training data is still a contented point in the literature. In an effort to address this, a novel biomarker, specific to this thesis, is constructed to use the entirity of the available data for a given output from the cell model, which can be said to provide a 'gold standard' for determining goodness-of-fit, against which other biomarkers can be compared. This biomarker, termed a normalised root mean square deviation measure (M_{NRMSD}), is defined for M, where $M = \{V_m, [Ca^{2+}]_i\}$, according to

$$M_{\text{NRMSD}} = \frac{1}{M_{\text{max}} - M_{\text{min}}} \sqrt{\frac{\sum_{j=1}^{N} (M_{\text{test}}(j) - M_{\text{train}}(j))^2}{N}}, \tag{4.5}$$

where M_{max} and M_{min} are the maximum and minimum values for M the training data, $M_{\text{combination}}(j)$ and $M_{\text{original}}(j)$ are the data points for V_m or $[Ca^{2+}]_i$ for a given parameter set and the original model, and N is the number of data points. Importantly, the normalisation step in this equation allowed AP$_{\text{NRMSD}}$ and Ca^{2+}_{NRMSD} to be directly compared. By using data from the entire AP or Ca^{2+} transient, this method is a robust measure of goodness-of-fit; however, it is computationally expensive and poorly suited for comparison of model output with noisy experimental data. Furthermore, a comparison using such a metric requires the raw data for the AP to be available for NRMSD metric calculation—due to the volume of data, this is rarely easily available for published papers.

the CL represents the maximum knowable value of ERP, while as a lower limit, the CL represents the minimum value that ERP at the point takes. In this dissertation, the term 'upper limit' shall be used.

4.4 Measures of Variability & Correlation

One of the key features of this thesis is its explicit focus on reproduction and examination of variability. To do this, it is thus necessary to clarify exactly how this will be measured. The first measure used to quantify the variability of a population is the *variance*, defined for a given metric x as

$$s^2(x) = \frac{1}{n-1}\sum_{i=1}^{n}(x_i - \overline{x})^2, \tag{4.6}$$

where n is the number of measurements, x_i represents an individual measurement, and $\overline{x}$ represents the population mean. Eq. (4.6) technically calculates the sample variance, which differs from the population variance by replacing $\frac{1}{n-1}$ with $\frac{1}{n}$—thus, for large values of n the difference is negligible. The sample mean and the population mean are identical.

The *range* (Δ) is also used as a measure of variability, and is calculated as the difference between the maximum and minimum values within the population. In this thesis, the focus is often placed on the *change* in variability, and when variance and range demonstrate the same change, the overall term *variation* will be used.

It is also necessary to clarify the use of terms relating to how two different metrics may be related to each other. For that purpose, three terms are used: *correlation*, *relationship* and *mapping*. These are illustrated in Fig. 4.5.

Correlation (Fig. 4.5A) refers to how closely a line of best fit will match the data (note that this does not necessarily require the line of best fit to be linear). This is measured using the *correlation coefficient*. Generally speaking, the correlation coefficient determines the correlation between two variables x and y, and is the normalised covariance, which is calculated according to

$$\sigma(x,y) = \mathbb{E}[(x - \mathbb{E}[x])(y - \mathbb{E}[y])] \tag{4.7}$$

$$= \mathbb{E}[xy] - \mathbb{E}[x]\mathbb{E}[y], \tag{4.8}$$

where $\mathbb{E}[x]$ is the expected value of x. It can be noted that the covariance of a variable with itself is the variance, *i.e.* $\sigma(x,x) = \sigma^2(x)$. The closer the correlation coefficient is to 1, the greater the correlation between the two variables.

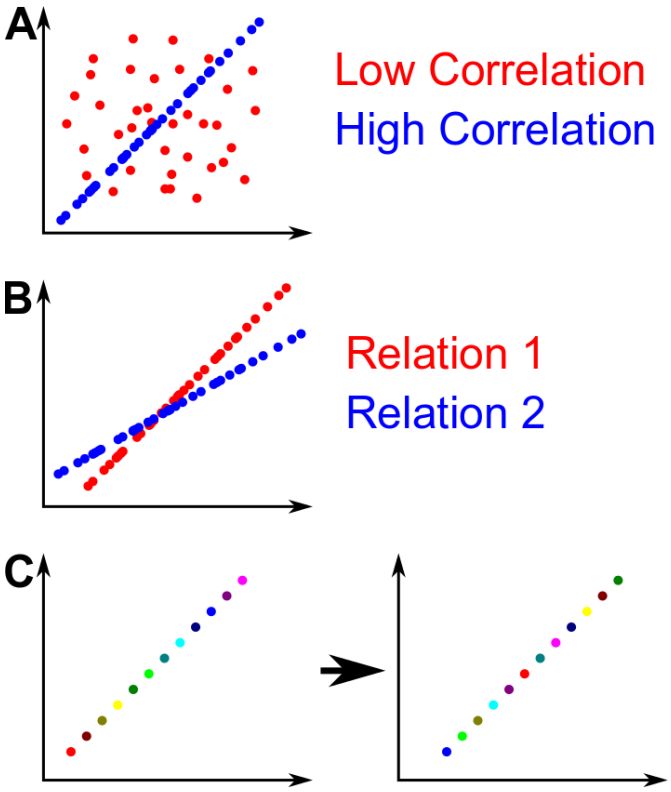


Figure 4.5: *Demonstration of correlation, relationship and mapping.* (A) *Example of high and low correlation between two variables.* (B) *Example of two different relationships between two variables, both with high degrees of correlation.* (C) *Changes in mapping between variables with changing conditions. Each model in the hypothetical population is colour-coded, with the population to the right demonstrating a different mapping, yet with an identical correlation and relationship.*

The relation (Fig. 4.5B) refers to the exact form of the line of best fit used to model the data, *i.e.* for two related variables, x and y, the line of best fit between them may be described according to $y = mx+c$. Note that it is possible, when comparing two populations, that they can share a relation with differing correlations, or that they could both have high correlations but with very different relations.

It should be noted several 'sub-relations' can exist simultaneously. For example, consider two sub-relations, one described according to $y = m_1x + c_1$ and the other according to $y = m_2x + c_2$, with the population's models adhering with high correlation to one of these two populations. Unless the population is divided and the correlation coefficient for each sub-relation calculated separately, the *overall* population correlation coefficient would be misleading.

Finally, mapping (Fig. 4.5C) represents how a particular model translates from variable x to variable y under specified conditions. The population as a whole may demonstrate a high degree of correlation between two output metrics, with a relationship that is nearly identical, but this does not necessarily mean that the same model will produce a consistent value within the population, *e.g.* the model that produces the shortest metric value under one set of conditions may not produce the shortest value

under a different set of conditions.

5 Reproduction of Experimental Variability with Model Populations & Effect of Multiple Parameter Variation

I sometimes ponder on variation form and it seems to me it ought to be more restrained, purer.

Johannes Brahms

The rationale for using parameter space variation as a means to model physiological variation is presented, with caveats appropriate for this thesis given. Details of the parameters that are varied are given, with reasons for their choice. An examination of the efficacy of various different commonly used biomakers as a measure of goodness-of-fit is presented, with a view to determining the biomarkers that are most suited under conditions that may include experimental noise. The results of parameter variation for two separate computational model frameworks are explored, and models that reproduce experimentally observed variation are isolated, with patterns amongst the parameters that contribute to these populations being discussed.

5.1 Reproduction of Experimental Variation

As was elaborated on in §2.4, variation is a constant companion in the experimentalist's world. As computational models of biological processes become more complex, with advancing technology allowing us to discard earlier assumptions made for the sake of computational tractability, and further advances in experimental results allow greater understanding of the system being modelled, variation is now increasingly becoming the computational modeller's companion as well. It is to be noted that this variability includes the so-called experimental variation, the 'noise' that can get in the way of the 'true' data, but also includes the variation that is a normal, and perhaps essential, component of physiological systems.

However, exactly *how* this variation is to be modelled is a question left to the modeller—there are many possible alternatives, some of which were mentioned earlier. Which of these alternatives is to be used depends on the questions being asked: what system is being modelled, how its output is being assessed, and so forth. It depends further on the available resources, and the demands being made of those resources. Perhaps the most important consideration, however, is the research question being posed. If the research question involves the operation of ion channels, modelling of variability may well require stochastic differential equations to model the stochastic transitions between open and closed states of the channel (Mino *et al.*, 2002). However, if the research question requires simulation of tissue, the stochasticity at the level of ion channels is 'washed out', and simulating ion channel stochasticity would be a relative waste of computational resources. Sensitivity must be used when judging what computational methods are to be used—the simulation technique must be as complex as required to reproduce the system behaviour appropriate to the research question, but it need not be any more so.

It is the main drive of this thesis to demonstrate a method for reproducing the observed experimental variation that is

- biophysically detailed,
- computationally tractable, and

- easily scalable.

To this end, we utilise the model population approach used previously in neuron modelling (Marder and Taylor, 2011). As compared to stochastic simulations, such a methodology is computationally simpler—due to their complexity and the requirement for multiple simulations for their statistical properties to be refined, stochastic models are often limited to phenomenological, small scale models. This thus ties in to the other advantage of the model population approach: the biophysical detail that can be applied via such a process. In prescribing variation to certain biophysically specific properties, and observing the consequences, specific output variation effects can be attributed to specific input variation effects. It should be noted, however, that Heijman *et al.* (2013) recently demonstrated the feasibility of using a biophysically-detailed stochastic model, although it is still restricted to small-scale simulations.

Using parallelisation methods available by means of the Nimrod/G distributed computing grid and its various alternatives, a population model approach is also computationally tractable—each individual simulation can be computationally simple, and appropriate distribution to the computing nodes can ensure that non-specialised computing resources are sufficient to the task. Finally, it is also easily scalable. By this, it is meant that not only is it a simple process to introduce variation to further parameters of interest, but also that the methodology is trivially applicable to multiple models (indeed, this thesis is based on investigations using two different models).

5.1.1 Comparison with Alternative Methods

It should be noted that the complete, multi-dimensional parameter sweep method used here provides significant benefits compared to other possible methods, insofar as the goals of this thesis are concerned. By this, it is meant that alternative methods for examining the effect of multiple parameter variation are not appropriate for this thesis. For the purposes of comparison, we may consider three alternative methods:

1. stochastic Models (Heijman *et al.*, 2013),

2. multi-variable regression analysis (Sarkar and Sobie, 2010; Sobie, 2009; Sarkar and Sobie, 2011; Sobie and Sarkar, 2011), and

3. sampling from the multi-dimensional parameter space (Britton *et al.*, 2013).

Further details of these methods can be found in §3.3. It should be noted that significant work has been achieved using single parameter variation, both in deterministic studies (Romero *et al.*, 2009a, 2011) and in stochastic studies (Tanskanen *et al.*, 2005; Sato *et al.*, 2009; Hashambhoy *et al.*, 2011; Pueyo *et al.*, 2011), but this thesis is explicitly multi-dimensional in scope.

Stochastic approaches to variability and variation, due to their computationally intensive nature, are limited in terms of the spatial and/or temporal scale over which they can be applied (Heijman *et al.*, 2013), or in the biophysical detail that can be examined (Walmsley *et al.*, 2010). It is also implicitly the goal of stochastic modelling approaches that their focus is on *intrinsic* noise in the system, whereas the goal of the thesis proposed here is implicitly focussed on *extrinsic* noise, *i.e.* cell-to-cell variability rather than beat-to-beat variability. Whereas these are not necessarily mutually exclusive, and can be (and have been) studied in unison, the computational limitations imposed by stochastic methods make their use here unsuitable.

Multi-variable regression analysis samples from a given parameter space, and uses this to return the effect matrix $\mathbf{B}$ that approximates the effect each parameter has on a given biomarker (Sobie, 2009; Sarkar and Sobie, 2010, 2011; Sobie and Sarkar, 2011). This methodology is limited by not only sampling from a limited number of models from the total parameter space, but also reduces the analysis to a pseudo-single dimensional one—the entries in $\mathbf{B}$ provide insight to the effect of a single parameter on a single output, and it has been demonstrated that the overall effect is relatively accurately approximated by the linear summation of the effects. However, it provides little insight into the interactions between parameters, and especially how these interactions can vary given changes in other parameters (*i.e.* parameters X and Y are correlated in a particular manner when parameters $\{A, B, C\}$ have one set of values, but are correlated in a different manner when $\{A, B, C\}$ have different values).

Methodologically, the most similar method to the parameter sweep method used here is to sample from the multi-dimensional space to generate a population, rather than exhaustively examining the entire space. This was done by Davies *et al.* (2012), but only generated a population of 19 models for a canine ventricular AP. The work previously mentioned by Britton *et al.* (2013) presents the most comprehensive study in cardiac studies. However, sampling from the multi-dimensional space likely gives an incomplete picture, and is thus less suited to analyse the effects of multiple parameter variation. While it does present a computationally efficient means of population production, it should be noted that (a) it may be unable to give a comprehensive account of the parameter variation within the space and (b) Gemmell *et al.* (2010) suggests that there may be 'islands' within the population, and insufficient sampling will either miss these islands, or falsely connect them with nearby groups in the parameter space; further consideration of these problems is given in §5.4.2.

5.1.2 Caveats

It should be noted that constructing a population of models based on a single framework (replacing the initial parameter set with a parameter space) allows for a biophysically realistic method of reproducing physiological variation that remains computationally tractable. However, there are several key points that must be remembered that represent the limitations of this approach, and many related approaches.

1. The underlying assumptions regarding the original model still apply. As such, any inaccurate assumptions remain present in derived populations (Noble and Rudy, 2001; Quinn and Kohl, 2013).

2. The populations derived using experimental data rely on these data remaining appropriate for the considered task. The populations used in this dissertation are derived using 'healthy' data. As such, without further adaptation, the populations are unsuitable for assessing some experimental situations without appropriate alterations made to the framework, *e.g.* where cardiac remodelling has occurred (Walmsley *et al.*, 2013).

3. Related to the point above is the fact that the model populations are united by the data used to create them. As such, if the training data used include differences such as gender, the models cannot then be used to address specific questions regarding gender—these differences are now implicitly encoded within the population.

For this dissertation, cell models are being used, but tissue data are being used for training the population. Moving from cell to tissue represents a large computational task, for two reasons. Firstly, the simple matter of simulating tissue is more computationally intensive, though preliminary simulations using the original Mahajan model indicated little difference between the AP generated using cell simulations and those from tissue simulations (performed for 2-D tissue using the Chaste software (Mirams *et al.*, 2013)). Furthermore, results from Giles and Imaizumi (1988) indicate that tissue and cell APs are often comparable. Secondly, and more pertinent for this thesis, is the problem of cell coupling (that itself is a likely candidate for variation). Heijman *et al.* (2013) predict that cell coupling works to reduce variation between two different cells—by this token, it is likely that any cell model population trained using tissue data is likely to represent an underestimate of the actual variation possible within a cell population. However, to exhaustively test this is computationally challenging. Consider the following: suppose it is wished to test just 20 different cell models. To exhaustively examine every possible combination of this population in a 2 cell chain, it would be required to perform 20^2 simulations. It is simple to abstract this—for a possible cell population of n, in a tissue sample consisting of m cells, the number of simulations that would have to be run to exhaustively examine every possible combination would be n^m. While there are many possible ways to reduce the search space (for example, assuming only gradual variation of parameters between cells), it is beyond the scope of this thesis to consider them.

5.2 Construction of the Parameter Space

The computational tools involved in investigating the effects of multiple parameter variation were described in the previous chapter—the specific methods used to that end and biological reasons for these methods are described here.

Parameters describing the peak conductance for six different ion channels were varied in this study. The currents considered (with their conductance given in parentheses) were: the transient outward current (g_{to}), the rapid delayed rectifier K^+ current (g_{Kr}), the slow delayed rectifier K^+ current (g_{Ks}), the inward rectifying K^+ current (g_{K1}), the L-type Ca^{2+} current ($g_{Ca,L}$), and the Na^+/K^+ pump current (g_{NaK}). These currents were picked in preference to other possible choices based on their perceived impact on the repolarisation of the AP, which has been noted as an indicator of beat-to-beat variability of repolarisation duration (BVR)—a longer plateau implies greater BVR (Heijman *et al.*, 2013). Furthermore, the dynamics of these currents were not changed on the basis that (a) it was expected that AP variability is primarily a result of differences in the relative magnitude of the currents rather than the dynamics, and (b) conductance is often the most poorly defined variable within the equations defining these currents in the models. This difficulty in parameter estimation comes from both the inherent experimental difficulties in measuring peak conductance, and the variation in the experimental techniques used to define these values (with methods sometimes being poorly defined) (Quinn *et al.*, 2011).

The conductances were varied by 0%, ±15%, and 30%, resulting in 15,625 different models for each framework.[1] This variation is in line with the extent of variation used in previous studies (Romero *et al.*, 2009a, 2011; Walmsley *et al.*, 2013), and is also consistent with the range of experimentally observed variation (Iost *et al.*, 1998; Li *et al.*, 1999; Fülöp *et al.*, 2004; Sims *et al.*, 2008; Szentandrássy *et al.*, 2005; Verkerk *et al.*, 2005)—for further detail, see §2.4. While some computational studies have used greater degrees of variation, it was decided the variation applied here provided the best compromise between scale and resolution of the parameter space. Furthermore, variation of such scale is not often seen in experimental literature.

Simulations were conducted at three different cycle lengths (CLs) of 400 ms, 600 ms and 1,000 ms to constrain the population of models further—Syed *et al.* (2005) has demonstrated the importance of considering multiple CLs in order to accurately fit restitution curves. Furthermore, this methodology allows examination of rate-dependent effects, such as changing parameter importance, changing degrees of output variation.

[1] See §4.1 for details of how the conductances were varied.

5.3 Accuracy of Biomarkers in Defining Model Fit

One of the goals of this dissertation is to measure the efficacy of commonly used biomarkers in assessing goodness-of-fit of model output to training data. With a parameter sweep providing a population of models, and thus a population of data, that is free from experimental noise, this provides an opportunity for an assessment of such a question. Without having to consider the problems of experimental noise, the entire range of recorded data can be used to compare a given model output to given training data. The goodness-of-fit by this comprehensive measure can then be compared to the goodness-of-fit given by other biomarkers.

In this specific case, the NRMSD metrics defined in §4.3 were used to compare the output of any given model to the output of the original, unaltered model (*i.e.* the model with 0% variation for all parameters). As previously stated, M_{NRMSD} is unsuited to situations with experimental noise (unless an appropriate, unbiased filter is applied), but in situations where there is no such noise (as in this parameter search), it provides a comprehensive measure of goodness-of-fit. On the assumption that, due to its involving the totality of available data, it provides the 'best' measure of goodness-of-fit, it it is then possible to assess how closely other biomarkers come to agreeing with this new gold standard; those biomarkers that come closest to defining the same models as the NRMSD metrics as 'matching' training data will then be considered accurate measures of goodness-of-fit in their own right.[2] This process uses multiple biomarkers in unison, *e.g.* APD_{50} and APD_{90}, rather than individual biomarkers in isolation.

The ~ 250 models most closely matching the original model output were determined, based on the minimum values of M_{NRMSD}. Similarly, the $\sim$ 250 models that match original model output was determined based on minimum percentage difference according to groups of biomarkers. The degree of overlap between these two groups (those determined by NRMSD metrics and those determined by biomarkers) was then calculated. This comparison was performed both for situations where V_m

[2] It can be noted that, for cells with a long diastolic interval, small differences in V_{rest} would increase AP_{NRMSD} to a great degree, while the rest of the AP may provide an excellent fit to data. Fortunately, both Shannon and Mahajan populations show little variation in V_{rest}, so this problem is not realised.

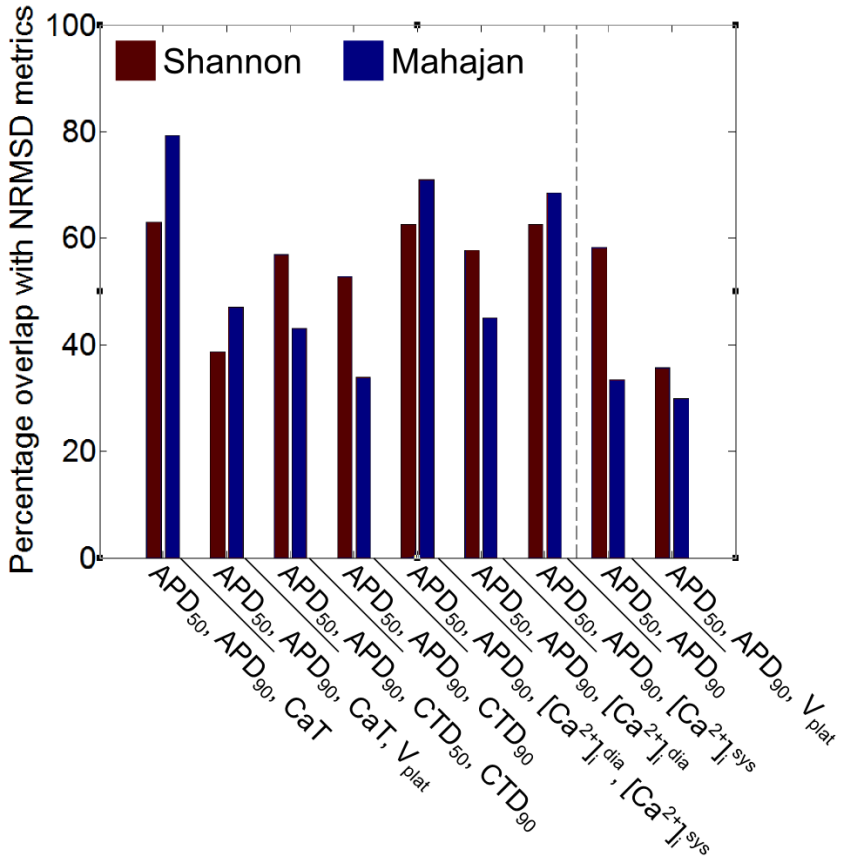


FIGURE 5.1: *Percentage overlap of matches between original model output and model output generated using the* $\sim$ 250 *parameter sets determined by the NRMSD metrics ([*AP_{NRMSD} *and* Ca^{2+}_{NRMSD}*]) and by combinations of biomarkers. While all combinations of biomarkers were tested, those shown represent the combinations with the highest percentage overlap. Combinations to the left of the dashed line include information about both* V_m *and* $[Ca^{2+}]_i$*, while those to the right include only* V_m *data (and thus represent the overlap with only* AP_{NRMSD}*).*

and $[Ca^{2+}]_i$ data are available, and for when V_m data only are available.

The results of the comparison for some biomarker groups is shown in Fig. 5.1. When $[Ca^{2+}]_i$ data is available, and thus Ca^{2+} biomarkers can be used in assessing the goodness-of-fit, the accuracy (judged by percentage overlap) is increased overall. The degree of overlap for groups of metrics is not identical between the Shannon and Mahajan populations. However, overall, a combination of APD_{50}, APD_{90} and CaT (or APD_{50} and APD_{90} where $[Ca^{2+}]_i$ data are not available), is the most accurate measure of goodness-of-fit compared to NRMSD metrics. Consequently, these biomarker combinations were used for the remainder of this thesis.

Biomarker	CL (ms)		
	400	600	1,000
APD_{50} (ms)	104 – 135	116 – 159	137 – 188
APD_{90} (ms)	142 – 185	160 – 220	167 – 230

Table 5.1: *Range of rabbit epicardial APD_{50} and APD_{90} used to define physiological parameter sets. Values are derived from previously reported studies, as described in the text.*

5.4 Defining a Population of Models to Reproduce Physiological Variation

5.4.1 Variation within the Population

In order to constrain the populations of models to those representing physiological variability, only parameter sets that produced APD_{50} and APD_{90} values that fell within the normal range for rabbit epicardium were included. APD_{90} for rabbit epicardium has been well documented and a physiological range was readily established for all CLs (Kurz *et al.*, 1993; Szigligeti *et al.*, 1996; Eckardt *et al.*, 1998; McIntosh *et al.*, 2000; Yan *et al.*, 2001; Kirchhof *et al.*, 2003; Goldhaber *et al.*, 2005; Biagetti and Quinteiro, 2006; Chen *et al.*, 2006; Jung *et al.*, 2011; Wu *et al.*, 2011). Comparison with literature data not included in these training data indicate that the range captures experimental variability (Wu *et al.*, 2006). While many of these values come from tissue preparations, preparatory computer simulations using the Mahajan model (Mahajan *et al.*, 2008) suggest that there is little difference between cellular and tissue results for APD_{90}.

Reports of APD_{50} values sufficient to derive a normal range, however, were not available at all CLs. Thus, values from the literature were used to establish a mean value for APD50 (Eckardt *et al.*, 1998; Kirchhof *et al.*, 2003). It was then assumed that the percentage variation from mean for APD_{50} is the same as the percentage variation from mean for APD_{90}. By this assumption, an assumed range for APD_{50} that is similar to the range for APD_{90} is calculated, and used in subsequent analysis. The resulting values are shown in Table 5.1.

By using these values, it was possible to constrain the tested parameter space to a population of models that reproduces experimentally measured variability at each CL. The number of models in each

Model	CL (ms)		
	400	600	1,000
Shannon	1,691	2,631	5,352
Mahajan	3,946	1,031	0
Expanded Mahajan	9,447	11,229	5,650

Model	CL (ms)			
	400 ∩ 600	400 ∩ 1,000	600 ∩ 1,000	400 ∩ 600 ∩ 1,000
Shannon	1,384	1,511	2,526	1,352
Mahajan	577	0	0	0
Expanded Mahajan	6,797	779	4,331	779

TABLE 5.2: *Number of parameter sets producing both APD_{50} and APD_{90} values within the physiological range. Parameter values were varied by $\pm 30\%$ from the original parameter set, and then further for the Mahajan model ('Expanded Mahajan') as explained in the text. $x \cap y$ and $x \cap y \cap z$ represent parameter sets that produce physiological values at a CL of x and y, or a CL of x, y, and z, respectively.*

population at each CL is given in Table 5.2. Those models that produce output within the physiological range at all CLs are defined to be in the model population that can reproduce given variation at all CLs; the minimum, mean and maximum values of all computed biomarkers for the Shannon and Mahajan populations thus defined are shown in Table 5.3.

With the Shannon framework, there existed at least one parameter set that produced a physiological output at each CL, with some of these generating a physiological output at all CLs. On the other hand, while a relatively large number of models produced a physiological output at a CL of 400 ms with the Mahajan framework (the CL for which the original Mahajan model was designed), fewer parameter sets matched at a CL of 600 ms, and none at a CL of 1,000 ms (the increase in APD with increasing CL was disproportionately large).

In order to address the failure of the Mahajan framework in finding parameter sets that generated a physiological output with increased CL, the range of conductance variation was expanded. To determine the direction of this expansion, the first step was to increase the ranges of APD_{50} and APD_{90} by $\pm 10\%$, and the parameter space was compared to this new range. This expanded range of APD resulted in 'matches' being found at all CLs. Based on the trends in the conductances evident amongst

Biomarker	CL (ms)	Model	Minimum	Mean	Maximum
$(dV_m/dt)_{max}$ (Vs^{-1})	400	Shannon	233	302	329
		Mahajan	200	230	252
	1,000	Shannon	278	327	352
		Mahajan	248	279	311
V_{rest} (mV)	400	Shannon	−92	−88	−82
		Mahajan	−88	−86	−85
	1,000	Shannon	−88	−86	−81
		Mahajan	−89	−88	−87
APD_{50} (ms)	400	Shannon	112	126	135
		Mahajan	104	108	117
	1,000	Shannon	137	155	181
		Mahajan	165	182	188
APD_{90} (ms)	400	Shannon	143	154	169
		Mahajan	142	155	185
	1,000	Shannon	167	186	217
		Mahajan	207	223	230
$[Ca^{2+}]_i^{dia}$ (μM)	400	Shannon	1.24	1.29	1.32
		Mahajan	0.29	0.37	0.47
	1,000	Shannon	0.82	0.84	0.86
		Mahajan	0.15	0.16	0.18
$[Ca^{2+}]_i^{sys}$ (μM)	400	Shannon	4.49	4.92	5.22
		Mahajan	1.43	2.78	4.46
	1,000	Shannon	3.13	3.33	3.68
		Mahajan	0.41	0.59	0.76
CaT (μM)	400	Shannon	3.25	3.63	3.91
		Mahajan	1.14	2.41	4.00
	1,000	Shannon	2.30	2.49	2.82
		Mahajan	0.26	0.42	0.58
CTD_{50} (ms)	400	Shannon	123	130	134
		Mahajan	133	139	147
	1,000	Shannon	139	150	157
		Mahajan	208	231	268
CTD_{90} (ms)	400	Shannon	263	267	271
		Mahajan	245	249	260
	1,000	Shannon	382	394	404
		Mahajan	460	510	585

Table 5.3: *Minimum, mean, and maximum values of all computed biomarkers produced by models reproducing experimental values of APD_{50} and APD_{90}.*

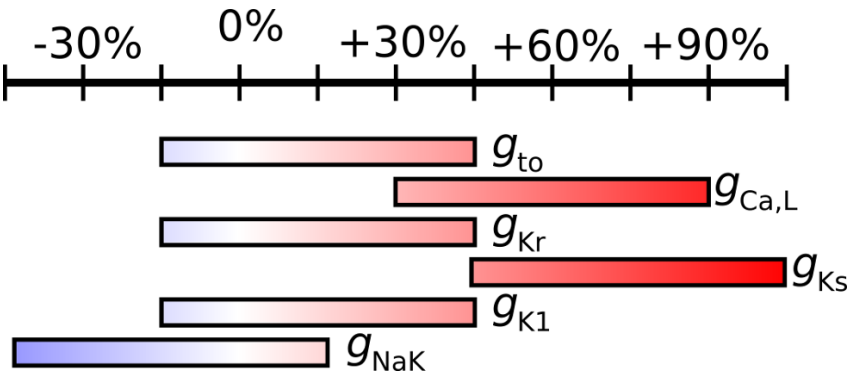


FIGURE 5.2: *Parameter ranges used for 'Expanded Mahajan' search; blue indicates a reduction in the value, whereas red indicates an increase.*

these matches, the parameter ranges were altered and a new parameter space was explored. The new ranges are shown in Fig. 5.2, and resulted in an additional 15,625 models being simulated due to g_{Ks} now exploring an entirely new regime. However, even with this expanded search, the number of parameter sets that matched at all CLs was approximately half of that with the Shannon model.

The parameter sets producing a physiological output with the Shannon framework are shown using a dimensional stack in Fig. 5.3, along with the generated V_m and $[Ca^{2+}]_i$ profiles at a CL of 400 and 1,000 ms, and the associated distribution of conductance values. The most obvious trend is that parameter sets producing a physiological output generally had a simultaneous reduction in both $g_{Ca,L}$ and g_{K1}. This is evident in both Fig. 5.3A, demonstated by a clustering of the valid models at the bottom left of the dimensional stack, and from the associated distribution of conductances, shown in Fig. 5.3D. It also appears that the distribution of the other conductances was fairly even; however, a closer examination of the dimensional stack in Fig. 5.3A reveals trends between the parameters (demonstrating the power of the clutter-based dimension reordering technique for visualisation of multi-dimensional parameter spaces). For instance, within the g_{NaK}/g_{Kr} surfaces (Level 2 of the stack), the matching parameter sets are spread in an approximately diagonal line from top left to bottom right, indicating that when g_{NaK} was increased, this was offset by a decrease in g_{Kr}, and *vice versa*. As $g_{Ca,L}$ and g_{K1} decrease, this diagonal line moves further to the bottom left corner, indicating that a further reduction of g_{NaK} and g_{Kr} was required to continue to produce a physiological output.

The effect of g_{to} is more complicated. When $g_{Ca,L}$ and g_{K1} were reduced by 30%, and g_{NaK} was also

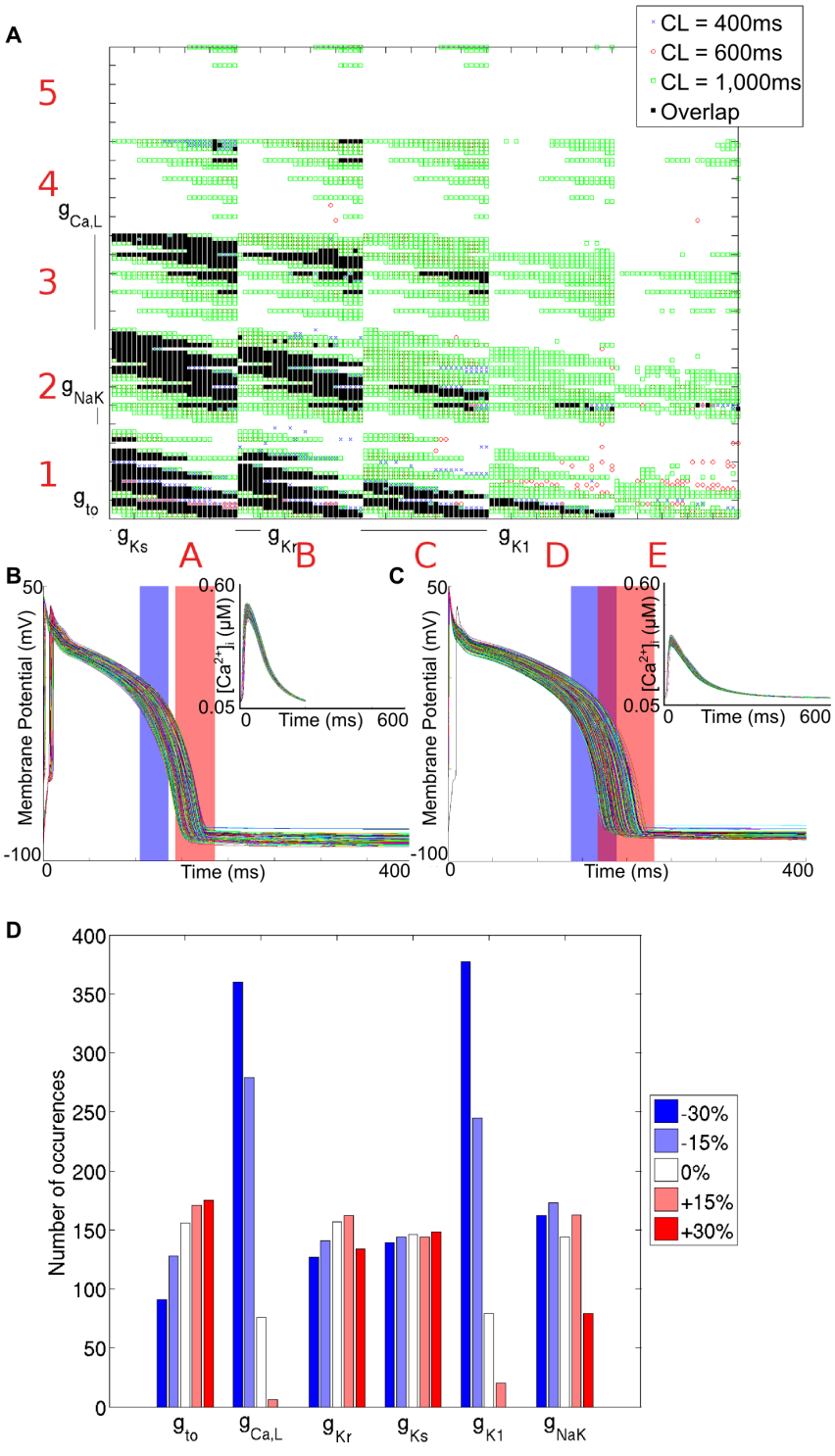


FIGURE 5.3: *Model population for the Shannon framework that produces values of both APD_{50} and APD_{90} that fall within the experimentally derived range. (A) Dimensional stack image showing the location of matching parameter sets for each CL and their overlap. (B) V_m and $[Ca^{2+}]_i$ (inset) profiles for the matching parameter sets at a CL of 400 ms. (C) V_m and $[Ca^{2+}]_i$ (inset) profiles for the matching parameter sets at a CL of 1,000 ms. (D) Distribution of conductance values for the valid parameter sets. For both (B) and (C), the physiological ranges of APD_{50} and APD_{90} are represented by the blue and red rectangles, respectively.*

reduced, matching parameter sets then included those with an increased g_{to}. The opposite was true when g_{NaK} was increased, as in these cases a decrease in g_{to} was necessary (square A1 in Fig. 5.3A). As g_{K1} was increased, fewer parameter sets with an increased g_{NaK} were valid, such that a corresponding decline in g_{to} was not observed (squares B1, C1, and D1 in Fig. 5.3). However, in all cases where $g_{Ca,L}$ was not reduced by 30%, the opposite was true: parameter sets including reduced g_{NaK} and increased g_{to} were no longer valid (squares A2 and A3 in Fig. 5.3A). Finally, in all valid parameter sets, as g_{K1} was increased, g_{to} decreased. On the other hand, there appeared to be no pattern to the values of g_{Ks} within the model population.

For the expanded Mahajan search, the parameter sets producing a physiological output, the generated cellular profiles, and the distribution of valid conductance values are shown in Fig. 5.4. There are some differences compared to the Shannon framework. For instance, with the Shannon framework, g_{Ks} appeared to have no effect in determining the validity of parameter sets, while with the Mahajan framework it had a strong influence, as most matching parameter sets included the largest conductance variation (+105%). The opposite was true for g_{K1}: while it had a large influence with the Shannon framework, it was relatively unimportant with the Mahajan framework. Similarly, with the Shannon framework, g_{to} and g_{NaK} generally varied in the opposite direction, while with the Mahajan framework they changed in the same direction.

With the Mahajan model, there was also a strong correlation between g_{NaK} and g_{Ks}, such that when g_{NaK} was increased, g_{Ks} also increased (demonstrated by a shift of matching parameter sets from the predominantly lower left corner to the upper right corner of the level two plots in Fig. 5.4A; for instance, compare the distribution within E1 and E3). On the other hand, there appeared to be no limitations on the values of g_{Kr}.

It is of note that the original model for both frameworks is not included in the final model populations. This does not in any way remove the validity of these models—they are entirely valid for the CLs for which they were designed. It can also be compared to Sato *et al.* (2009), in which different parameters had to be used within the Mahajan framework to permit examination of the posed question. However, this does demonstrate the limitations of any given model, and the requirement to be

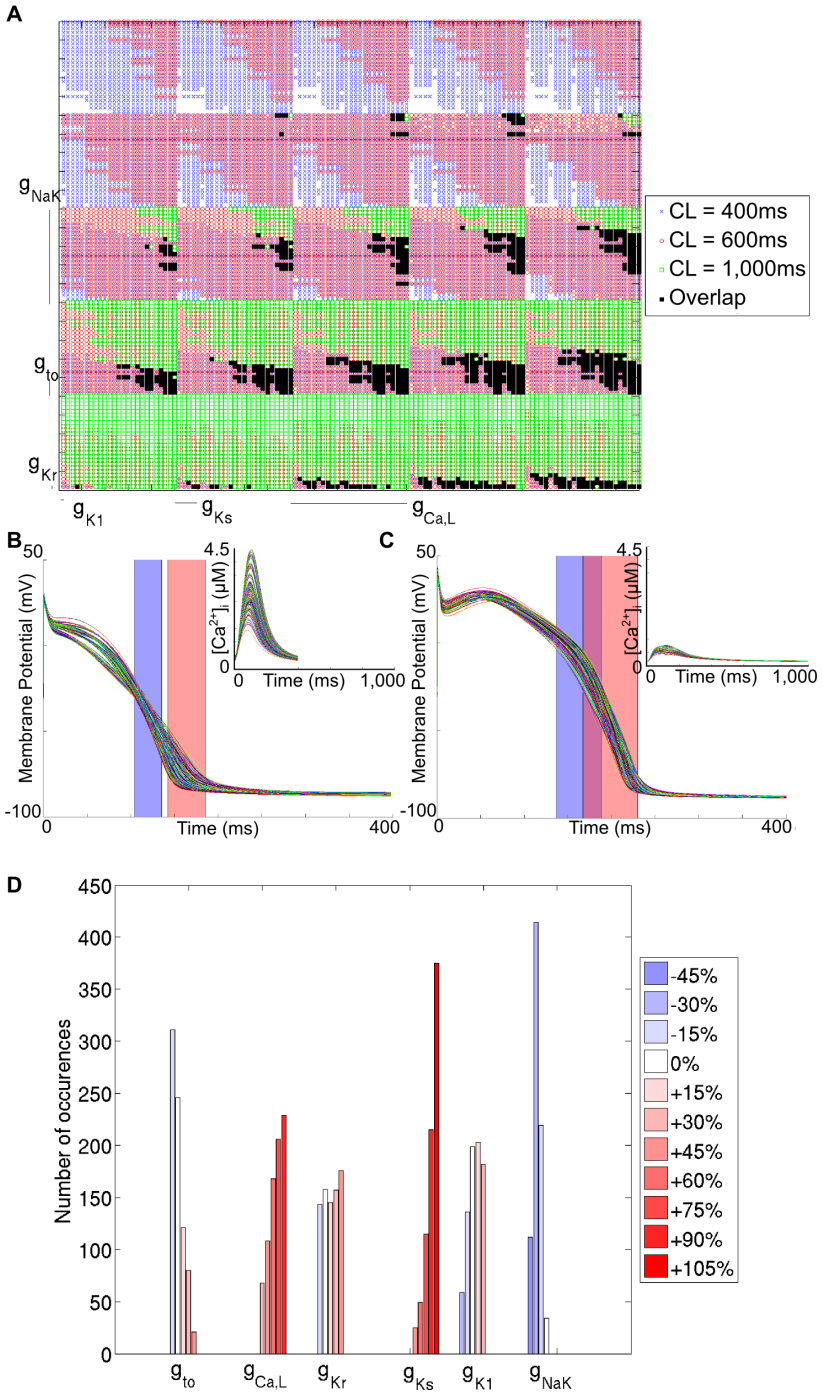


Figure 5.4: *Model population for the expanded Mahajan framework that produces values of both APD_{50} and APD_{90} that fall within the experimentally derived range. (A) Dimensional stack image showing the location of matching parameter sets for each CL and their overlap. (B) V_m and $[Ca^{2+}]_i$ (inset) profiles for the matching parameter sets at a CL of 400 ms. (C) V_m and $[Ca^{2+}]_i$ (inset) profiles for the matching parameter sets at a CL of 1,000 ms. (D) Distribution of conductance values for the valid parameter sets. For both (B) and (C), the physiological ranges of APD_{50} and APD_{90} are represented by the blue and red rectangles, respectively.*

careful of any applications for which the model/framework was not explicitly designed. On a related note, it can be observed that there is little variation observed in V_{rest} in both populations. This is not a failing of the populations, as the populations were not designed in any way to reproduce this variability (which is caused primarily by the changes in K^+ concentration across the cell membrane). Rather, such an observation serves to reinforce the importance of proper consideration of a model's goal, aims and the outcomes by which it can be judged.

While the results presented here suggest that variation in current conductances over a wide range of values may account for normal variability in rabbit ventricular AP repolarisation, other factors may be involved. One of the underlying assumptions of this thesis is that AP variability is primarily a result of differences in the relative magnitude of the currents, rather than underlying current dynamics, which were not varied. Changes in channel properties other than conductance could result in similar changes in AP biomarkers, and also account for some of the experimentally observed variability. Romero *et al.* (2011) presented a one-dimensional sensitivity analysis of the rabbit-specific frameworks used in this thesis with a similar range of parameter variation, and showed that along with repolarisation currents, APD was significantly modified by changes in the activation and inactivation rates of the associated channels. At the same time, further constraints to the model populations (such as matching of rate-adaptation of restitution properties), as well as consideration of additional biomarkers (for instance, relating to intracellular ion concentration), may be necessary to ensure their applicability to additional physiological states. This has been recently demonstrated in Walmsley *et al.* (2013), in which populations of failing and non-failing human ventricular myocytes with variation in current conductances were compared using various biomarkers at numerous CLs to investigate which currents drive variability in the two cell populations. Finally, as the range and resolution of parameter space sampling in the present study was limited by computational tractability, there may be additional influences and interactions of current conductances important for ventricular AP variability that were not appreciated. As mentioned earlier, it is difficult to properly assess the true physiological ranges of the current conductances considered in this study, so that they may be related to the values included in the calibrated populations of models. We initially varied all conductances by $\pm 30\%$, yet it was necessary with the Mahajan framework to expand this range to generate a physiological output. Other computational

studies have used a larger range of conductances than presented here (Sobie, 2009; Davies *et al.*, 2012; Britton *et al.*, 2013), possibly representing the true physiological range of values, and supporting the expanded range used with the Mahajan framework.

5.4.2 Connectivity within the Parameter Space

Of note is the question that has been touched upon earlier, both in this study and others: are the populations generated here 'connected'? By this, it is meant to ask whether or not one can connect all models in the population within a single parameter space, or does the population consist of several separate populations within the population space (Gemmell *et al.*, 2010). The answer to this is irritatingly dependent on how, exactly, one defines 'connected'. If one requries connection only by one step in multiple dimensions, then the populations derived here are connected. However, if one adopts a stricter definition of connection (two models are connected only if they are one step away from each other in a single dimension), then the populations are not connected—this is shown in a dimensional stack in Fig. 5.5.

It is beyond the scope of this thesis to determine whether the two definitions of connectivity can be reconciled—whether by increased resolution, or by inclusion of alternative parameters, those semi-connected regions will become connected. However, if we work on the (somewhat reasonable) assumption that either they can, or that the looser defintion of connectivity is a reasonable approximation, this has significant implications for population construction, in that it implies that, once a 'valid' model has been found, the search for other 'valid' models can be directed, and thus the computational task of searching the entire parameter space is reduced.

5.5 Effects of Parameter Variation

Using the biomarkers thus defined as providing measures of goodness-of-fit, it is now possible to assess the effects of parameter variation on the model populations; it also allows judgement of how these different biomarkers are affected by these different parameters, and how these differences are altered based on CL. The dimensional stack images showing these effects are presented in Fig. 5.6 (for

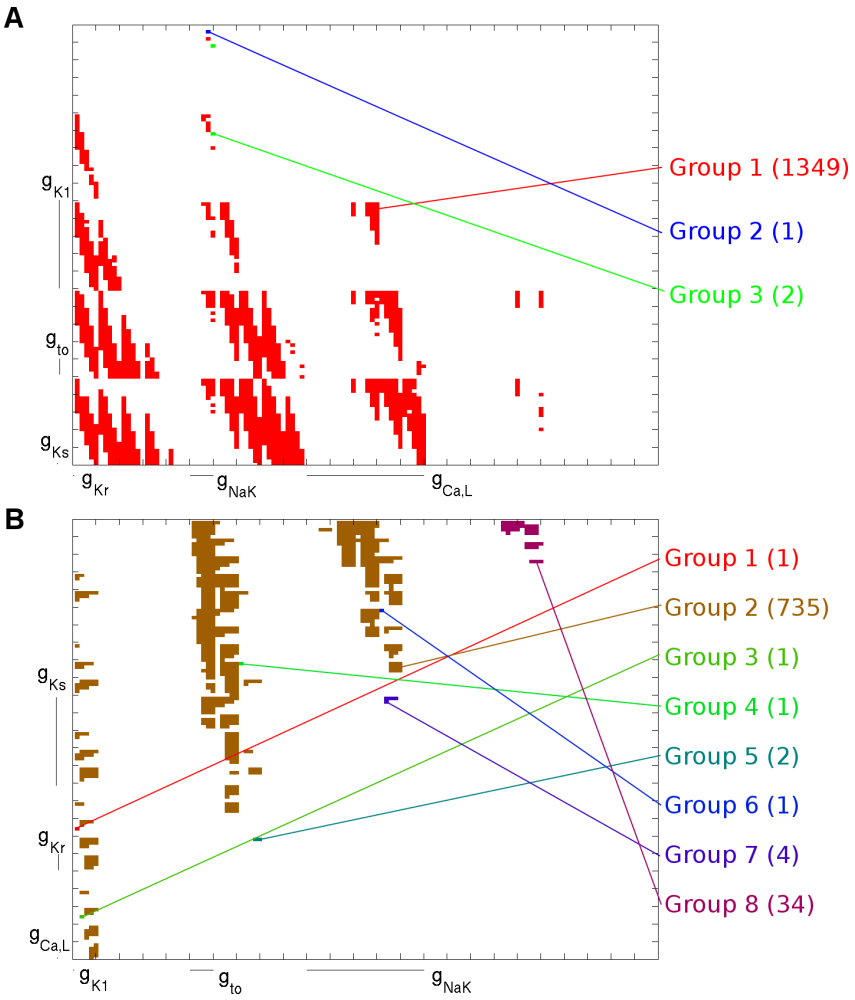


FIGURE 5.5: *Dimensional stack images showing connectivity within model populations for the Shannon (A) and Mahajan (B) frameworks, with a space defined as being connected if two points are connected only if they are one step away from each other in a single dimension. The numbers within the parentheses represent the number of models within each group.*

the Shannon population) and Fig. 5.7 (for the Mahajan population). In addition, the optimum stack orders are shown in Table 5.4.

These results demonstrate how the relative importance of the varied current conductances was dependent on both the CL, and on the biomarker being considered. In considering this, it should be noted that the non-linear interactions between currents and ion concentrations often resulted in different changes in the current magnitudes that might be expected from the change in current conductance. For instance, while conductances were subject to $\pm 30\%$ variation at a CL of 400 ms, the amplitude of I_{Ks} varied from -97% to $+118\%$ compared the the amplitude for the control model for the Mahajan

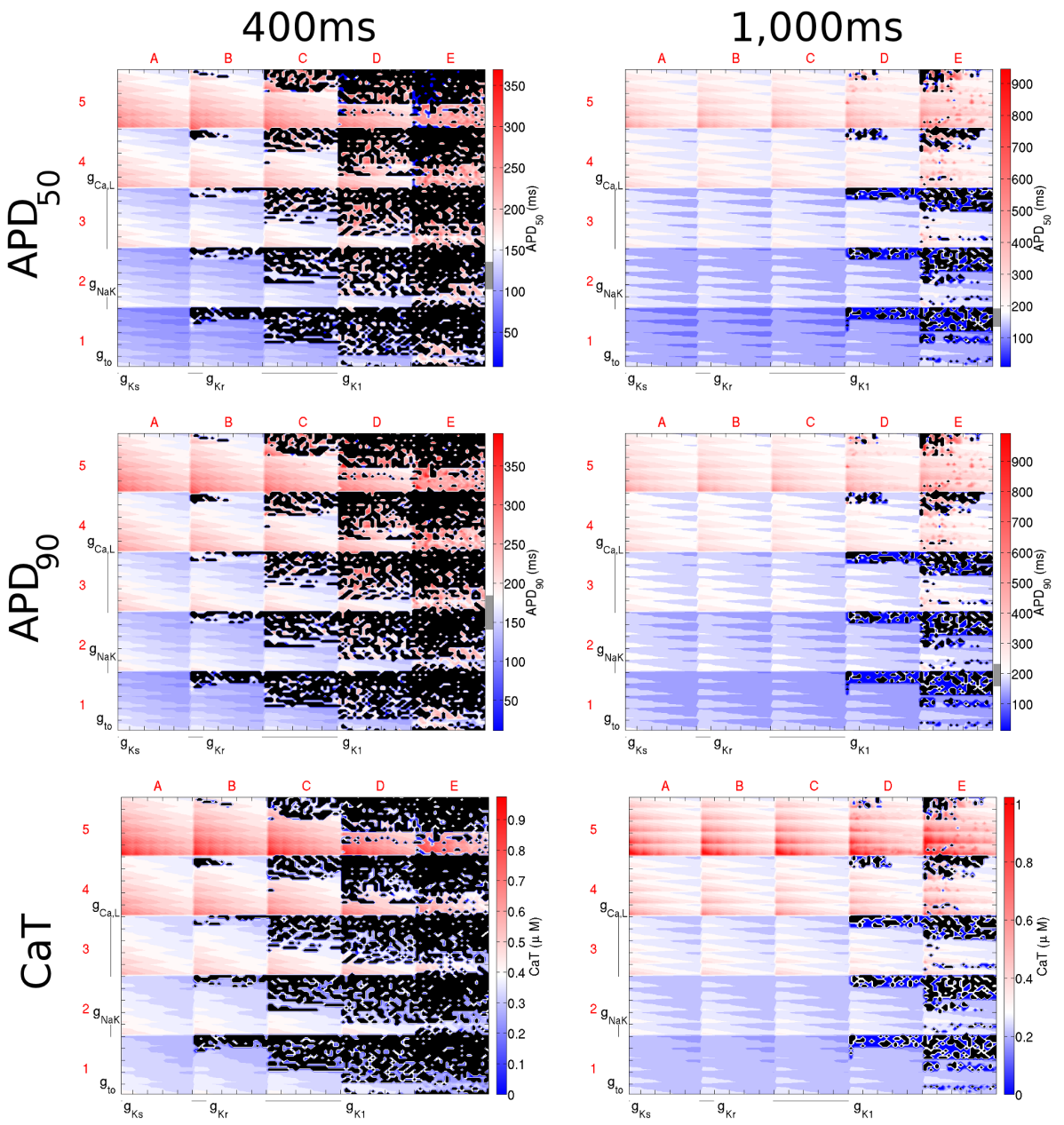


Figure 5.6: *Dimensional stack images demonstrating the effect of simultaneously varying the magnitude of six repolarising current conductances in the Shannon model. The top, middle, and bottom rows show the effects on APD_{50}, APD_{90}, and CaT, respectively. The left column is based on simulations with a CL of* 400 *ms and the right with a CL of* 1,000 *ms. In the contour plots, red represents an increase from the initial parameter value, blue a decrease, and white no change. The physiological range for APD_{50} and APD_{90} determined from the literature (see §5.4 for details) is represented by the grey region next to the colour bars in each panel. Black dots represent parameter sets with which the model did not reach steady state. The optimum stack order for each image is not used; rather, a common stack order has been used that represents the 'overall optimum', which allows direct comparison of the stacks to reveal differences in effects on each biomarker.*

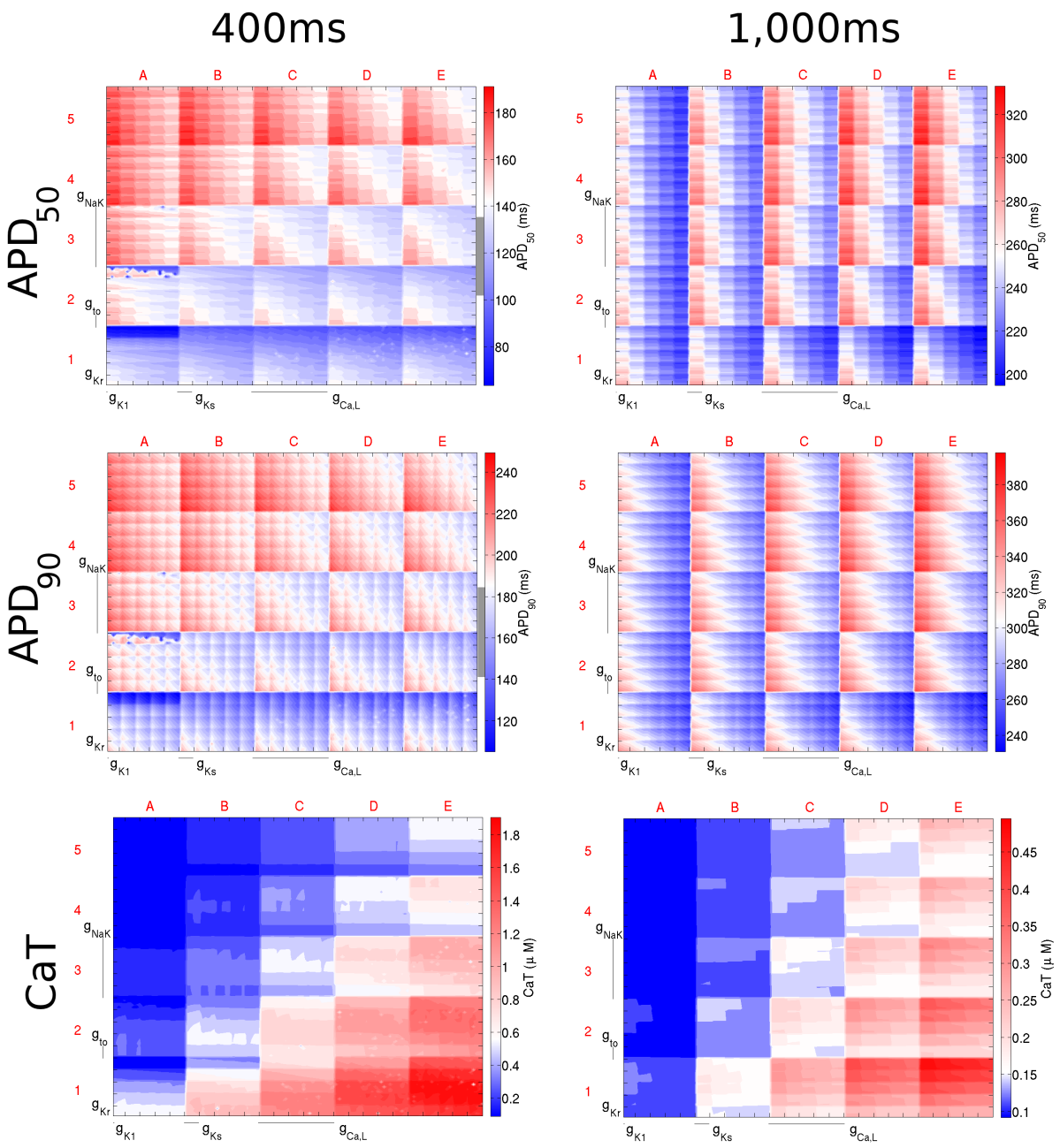


FIGURE 5.7: *Dimensional stack images demonstrating the effect of simultaneously varying the magnitude of six repolarising current conductances in the Mahajan model. The top, middle, and bottom rows show the effects on APD_{50}, APD_{90}, and CaT, respectively. The left column is based on simulations with a CL of* 400 *ms and the right with a CL of* 1,000 *ms. In the contour plots, red represents an increase from the initial parameter value, blue a decrease, and white no change. The physiological range for APD_{50} and APD_{90} determined from the literature for a CL of* 400 *ms is represented by the grey region next to the colour bars in each panel (the grey region is absent for a CL of* 1,000 *ms as the APD values fell outside of the physiological range). The optimum stack order for each image is not used; rather, a common stack order has been used that represents the 'overall optimum', which allows direct comparison of the stacks to reveal differences in effects on each biomarker.*

Framework	Biomarker	CL (ms)	Optimum Stack Order (x, y) Low Order $\longrightarrow$ High Order		
Shannon	APD_{50}	400	(g_{to}, g_{Ks})	(g_{NaK}, g_{Kr})	$(g_{Ca,L}, g_{K1})$
		1,000	(g_{K1}, g_{Ks})	(g_{NaK}, g_{Kr})	$(g_{Ca,L}, g_{to})$
	APD_{90}	400	(g_{to}, g_{Ks})	(g_{NaK}, g_{Kr})	$(g_{Ca,L}, g_{K1})$
		1,000	(g_{K1}, g_{Ks})	(g_{NaK}, g_{Kr})	$(g_{Ca,L}, g_{to})$
	CaT	400	(g_{K1}, g_{Ks})	(g_{NaK}, g_{to})	$(g_{Ca,L}, g_{Kr})$
		1,000	(g_{K1}, g_{Ks})	(g_{NaK}, g_{Kr})	$(g_{Ca,L}, g_{to})$
Mahajan	APD_{50}	400	(g_{Kr}, g_{K1})	$(g_{Ks}, g_{Ca,L})$	(g_{to}, g_{NaK})
		1,000	(g_{Kr}, g_{K1})	$(g_{to}, g_{Ca,L})$	(g_{Ks}, g_{NaK})
	APD_{90}	400	$(g_{Kr}, g_{Ca,L})$	(g_{K1}, g_{Ks})	(g_{to}, g_{NaK})
		1,000	(g_{Kr}, g_{K1})	(g_{Ks}, g_{to})	$(g_{Ca,L}, g_{NaK})$
	CaT	400	(g_{Kr}, g_{K1})	(g_{to}, g_{Ks})	$(g_{NaK}, g_{Ca,L})$
		1,000	(g_{Kr}, g_{K1})	(g_{Ks}, g_{to})	$(g_{NaK}, g_{Ca,L})$

Table 5.4: *Optimum stack order for APD_{50}, APD_{90}, and CaT for the Shannon and Mahajan frameworks, at CLs of* 400 *and* 1,000 *ms. Each pair of parameters represents low, medium, or high order current conductances. For each pair, the first component is plotted on the x-axis and the second component on the y-axis. The (x, y) order can be reversed without affecting the result, though only if* all (x, y) *pairs are reversed.*

population.

The optimum stack order, which is an indication of both the relative importance of the individual conductances on the biomarker and the inter-relation between parameters, changes with CL. The extent of this change is unpredictable, and can be dramatic. This is best demonstrated with the Shannon framework, and the change in influence of g_{to} on APD_{50} and APD_{90}. At a CL of 400 ms, g_{to} was a low-order conductance (reflecting a low importance), while at a CL of 1,000 ms, it became a high-order conductance. The relative importance of g_{K1} decreases at the same time. However, this degree of change does not always occur—$g_{Ca,L}$ was consistently of high-order and g_{Ks} of low-order, while g_{Kr} and g_{NaK} were generally of medium-order. It is worthy of note that the changes in relative importance of conductances is mainly revealed via changes in the optimum stack order rather than by visial inspection of the dimensional stack images themselves. As such, it is possible that there is no 'true' change, but rather that the actual underlying relative importance of conductances is revealed as more models are judged to reach steady state, and thus included in the calculation of the optimum stack order.

For the Mahajan framework, as CL increased, the relative importance of g_{to} decreased. This is opposite to the response seen with the Shannon framework. At the same time, g_{Ks} becomes more influential, despite little change in its position in the optimum stack order. This can be seen by examining the difference between the dimensional stacks with CLs of 400 and 1, 000 ms shown in Fig. 5.7. At a CL of 400 ms, the greatest effect on APD (represented by deep red and blue) is seen at the edges of the dimensional stack image (squares A1, A5, E1 and E5), indicating an extreme increase/decrease in $g_{Ca,L}$ and g_{NaK} is required for such effects. However, with an increase in CL, the maximum effect of the change in seen throughout the dimensional stack image, as a result of the increased importance of g_{Ks}. In contrast, the relative importance of g_{NaK} and g_{Kr} were independent of CL, being consistently one of the highest and lowest order conductances, respectively.

The same optimum stack order is rarely shared between APD_{50}/APD_{90} and CaT; moreover, there are instances where even the APD biomarkers have different optimum stack orders (see the Mahajan framework results). This point becomes more evident with inspection of the dimensional stack images—the distribution of changes is drastically different between AP and $[Ca^{2+}]_i$ biomarkers, and subtly different between the AP biomarkers themselves. This emphasises the folly, already noted elsewhere (Walmsley *et al.*, 2013), of the thinking of 'parameter X' as being very influential. Rather, the conditions under which parameter X is important, and by which metric it is important, must always be added as caveats to such sweeping statements.

These results can be contrasted with the results presented in Heijman *et al.* (2013), which indicated I_{Na} and I_{Kr} as the most influential for affecting BVR. While the obvious differences between these studies, both in terms of methods and in terms of goals, should be remembered, it is instructive to note the common themes, and the implications of these works on the current results. For example, Heijman *et al.* demonstrated little stochastic effects of pumps and exchangers due to their low throughput and high expression rate 'smoothing out' stochastic effects. This is compared to the results presented here, and in the work from Sobie *et al.*, which noted the effect of I_{NaK} and I_{NaCa}—while they may be noted as having little stochastic effect, their interactions with other components reinforces their importance in their own right. Furthermore, it is implied that their effects are mediated via their effect on ion

concentrations rather than direct effect on the AP, as these do not affect BVR directly.

The results presented in this section serve as an illustration of the importance of considering (i) the independence of the relative importance of parameters on the different biomarkers, and (ii) the effect of CL when determining the effects of current conductance variability on biomarkers. It is also worth noting the differences that exist between the two frameworks when subjected to identical degrees of parameter variation, with the consideration that the Mahajan framework is based in large part on the Shannon framework. However, the non-linear nature of the interactions between the components that make up a biophysically detailed cell model mean that, even with these common elements, the response can be drastically different.

5.6 Rate Dependence of Biomarkers

Related to the changes in parameter importance varying with rate is variability of the biomarker distribution itself to changes in CL. Histograms showing the variability of APD_{50}, APD_{90} and CaT across all combinations of current conductances are shown in Fig. 5.8. Both frameworks demonstrated similar distributions for both APD_{50} and APD_{90} (upper and middle panels). They differed, however, in that the Mahajan framework demonstrated more narrow distributions than the Shannon framework, while the Shannon framework generated more APD values that fell within the physiological range (discussed in §5.4.1). For the Shannon framework, the shape of the APD_{50} and APD_{90} distributions were relatively well conserved between a CL of 400 and 1, 000 ms, other than an increase in the number of matching parameter sets. In constrast, the Mahajan framework demonstrated a widening of the APD_{50} and APD_{90} distributions, as well as an increase in their mean. In the case of simulations with a CL of 1, 000 ms, the increase in APD was such that the entire distribution fell outside of the physiological range. The change in CaT distribution with a change in CL was more dramatic (lower panels in Fig. 5.8). For the Shannon framework, the distribution narrowed with an increase in CL. The distribution with the Mahajan framework followed a similar pattern, however with an even larger change. At a CL of 400 ms, the range of CaT was very broad ($\sim 0.1\,\mu M$ to $\sim 1.9\,\mu M$), indicating that CaT was relatively poorly constrained within the parameter space. When CL was increased, however,

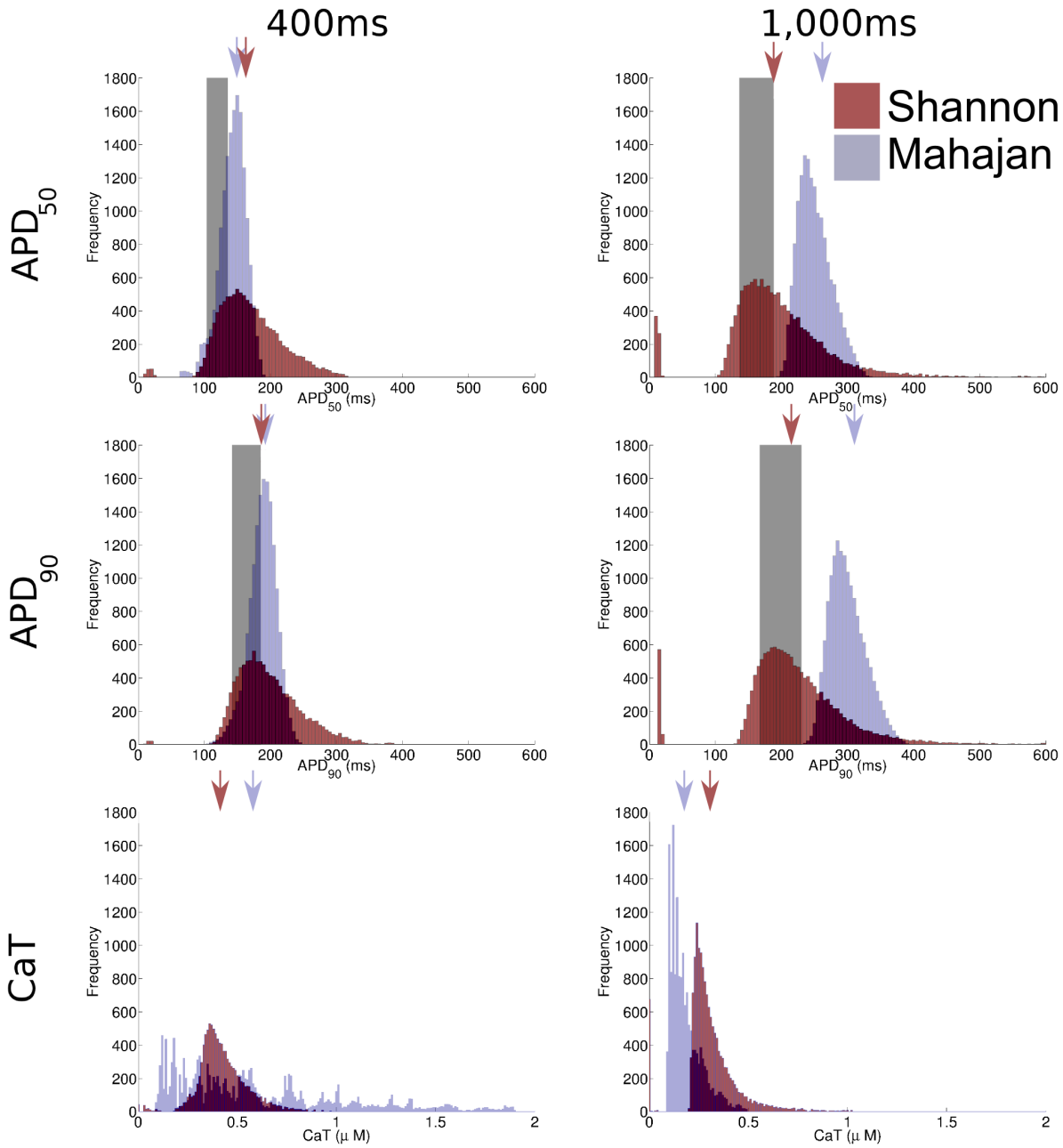


FIGURE 5.8: *Histograms showing the range of APD_{50}, APD_{90}, and CaT in the model populations. The value generated with the initial parameter set for each framework is indicated by the arrow. The physiological ranges of APD_{50} and APD_{90} derived from the literature are represented by the boxed area.*

the range was greatly reduced ($\sim$ 0.1 μM to $\sim$ 0.5 μM).

5.7 Summary

In this chapter, the effects of simultaneous variation in multiple parameters was investigated. Using the wealth of data thus available, it was possible to assess the accuracy of commonly used biomarkers as measures of goodness-of-fit. Using the NRMSD metrics as the 'gold standard', and assuming the most accurate biomarkers would select similar models as matching given training data as these metrics, it was established that the combined use of APD_{50} and APD_{90} provide the best measure of goodness-of-fit to training data; the addition of CaT if Ca^{2+} data were available increases the accuracy of the fit.

The relative importance of individual ion channels on these biomarkers was investigated, not just under conditions of single parameter variation, but under conditions of simultaneous multiple parameter variation. This took advantage of the CBDR method to pair conductances according to their influence on the output space, and allow visualisation of the multi-dimensional space. This method permitted demonstration of the interactions between ion channel conductances that could not be revealed without such a comprehensive examination of the parameter space.

Furthermore, by examining the parameter space at multiple pacing rates, how these interactions varied was also evaluated, demonstrating the importance of considering the original training environment of a framework. This was especially true for the Mahajan model, whose AP, while accurate at short pacing rates, demonstrated unphysiological lengthening for greater values of CL.

Data were collected from the literature to allow defintion of a range of values for APD_{50} and APD_{90} that could be said to reproduce experimentally observed variability, and models within the tested parameter space were selected as part of a population based on the original framework that could thus reproduce experimental variability. Due to the aforementioned AP prolongation demonstrated by the originally tested Mahajan space, the variation applied to the Mahajan conductances was adapted, and a new parameter space was tested. From this new space, it was possible to extract a population of models that matched experimental data. Both the Shannon and Mahajan populations demonstrated a high degree of connectivity in the parameter space across multiple dimensions. The distribution

of conductances within these populations was assessed, with the dimensional stack images allowing fine-grained analysis of inter-relations between currents that would not be possible otherwise.

These populations represent the key link between this chapter and the next—it is these populations that are adapted for simulation of ischæmia, and used to investigate the changes in variability that are caused by ischæmia. However, the work in this chapter is not a mere stepping-stone, representing important work in its own right.

6 Effect of Ischæmia on Model Population Variability

Doch ein gekränktes Herz erholt sich schwer [A wounded heart can with difficulty be cured].
Johann Wolfgang von Goethe, *Torquato Tasso*

This chapter details the results of the investigation of the effects of ischæmia on the variability exhibited by the model populations defined in the previous chapter. The motivation is presented, along with the resulting goals and aims, with the methods used to this end briefly recapitulated. The changes in cellular repolarisation across the populations during ischæmia are discussed, with the effects of each underlying condition and its contribution to the total ischæmic effect being elucidated. The breakdown in relation between APD_{90} and ERP is analysed. The changes in the relative importance of channel conductances during ischæmia are discussed, and the alterations evident in individual model response within the context of the population considered. Finally, ischæmic changes to other biomarkers potentially important for re-entry are noted.

As was detailed in §2.3, ischæmia represents one of the leading causes of SCD, and thus it is of key importance for experimental investigation. The mechanisms by which ischæmia leads to SCD are gradually being revealed, and it is known that changes in the APD and ERP, caused by the hyper-

kalæmia, acidosis and anoxia incident with ischæmia, predispose the ischæmic tissue to re-entry, and consequently arrhythmia and SCD.

It has also been demonstrated that increased heterogeneity in repolarisation and refractoriness in tissue enhance arrhythmic risk. This is not to imply that normal, non-arrhythmic tissue is homogeneous—entirely normal and expected variability was the focus of the previous chapter, with its reproduction using model populations. It is intended here to investigate the claim that the benign variation that exists in normal tissue can be exaggerated to the point of malign variation by the application of ischæmic conditions.

With this motivation in mind, the goal of the work presented in this chapter is thus to investigate the changes in model population variability caused by ischæmic conditions. The hypothesis underlying this goal is that the application of ischæmic conditions causes the underlying variability of the model population to increase. The investigation of the effects of ischæmia on population variability shall be conducted using the two rabbit ventricular myocyte model populations derived in the previous chapter, which were defined to reproduce APD variability under normal conditions.

The methods for simulating ischæmia are as detailed in §4.1.2. Ischæmia will be simulated for the model populations at discrete points during the first 10 minutes of acute Phase 1A ischæmia, and the effects on the populations assessed. Furthermore, the effects of the individual conditions inherent within ischæmia (hyperkalæmia, acidosis and anoxia) will be measured, both individually and simultaneously, to trace the causes of the changes observed in ischæmia itself.

This work represents (i) the first time that the effect of ischæmia on model populations has been examined, and (ii) the most comprehensive examination to date of the interactions between conditions said to underlie ischæmia. This second aspect builds on the efforts previous work to derive the causes and consequences of changes in the ischæmic milieu (Moréna *et al.*, 1980; Ruiz-Ceretti *et al.*, 1983; Kodama *et al.*, 1984; Ferrero *et al.*, 1996; Shaw and Rudy, 1997b,a), but moves to apply these investigations to a population approach in a comprehensive manner. The results also permit investigation of the variation that exists both spatially and temporally (in that the work presents snapshots of the effects of ischæmia at different points in time, rather than a direct assessment of the temporal evolution

of ischæmia).

It should be noted from the outset that the results presented in this chapter cannot be said to indicate increased susceptibility to arrhythmogenesis or not—arrhythmias are a tissue level phenomenon, and thus the results from the cellular models presented here can be said to be indicative of tissue level phenomena at most. With this caveat, the distinction between the chapter's hypothesis and its motivation is clear.

The model populations defined in the previous chapter shall be used in this chapter as the underlying basis to investigate variability. These models shall be adapted to prepare them for simulation of ischæmia in the manner as detailed in §4.1.2—this includes retraining I_{stim} to a value appropriate for the average population model, and including terms to reproduce the effects of hyperkalæmia, acidosis and anoxia. Changes in these so-called *environmental parameters* shall be applied according to the progression detailed in Table 4.2, as well as independently in an investigation of the ischæmic parameter space. Biomarkers relevant to this chapter (principally APD_{90} and ERP) shall be calculated according to the details provided in §4.3, with analysis of changes to variability conducted using metrics defined in §4.4. Use shall also be made of the dimensional stack image technique defined in §4.2.

6.1 Ischæmic Changes in Cellular Repolarisation and Refractoriness

6.1.1 Changes during Phase 1A Ischæmia

The APs for the two model populations at different points during phase 1A ischæmia, and histograms showing the evolution of APD_{90} at these same time points, are shown in Fig. 6.1. The model populations are successful in qualitatively reproducing the notable AP changes associated with ischæmia reviewed in §2.3.1, namely a decrease in APD, AP amplitude and $(\text{d}V_m/\text{d}t)_{\text{max}}$, and an increase in V_{rest}.

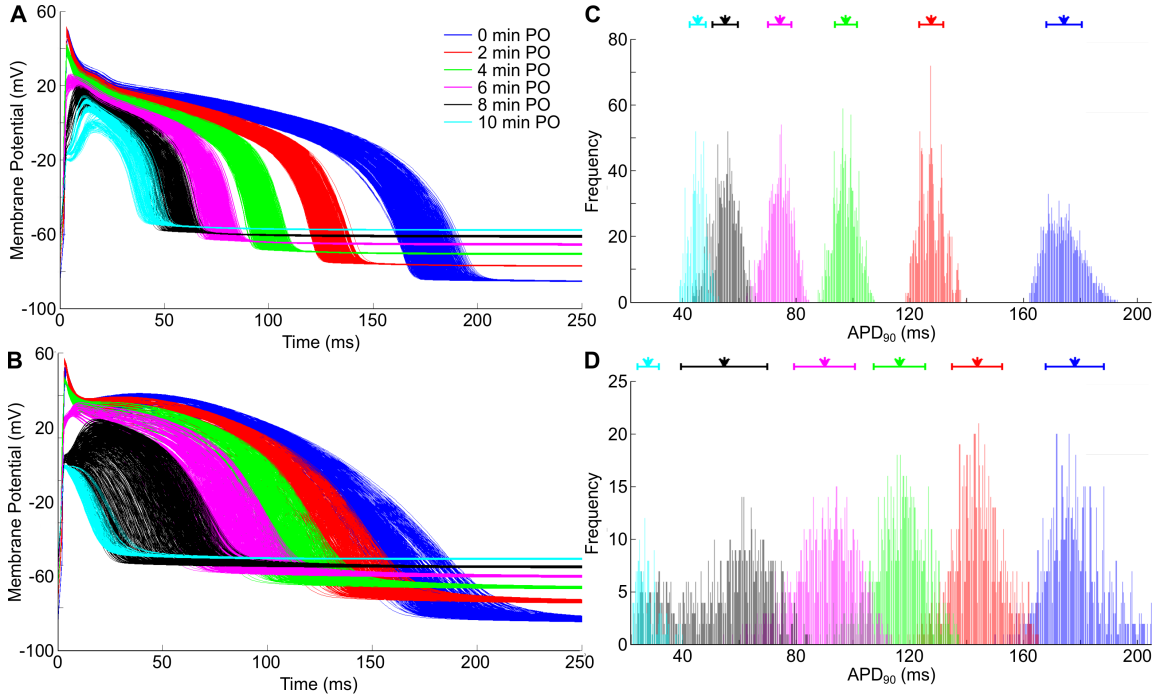


Figure 6.1: *Effect of different degrees of ischæmia on the Shannon and Mahajan model populations, with environmental parameters as defined in Table 4.2. AP traces for non-failing models of the Shannon and Mahajan populations are shown in* (A) *and* (B)*, respectively, with histograms of the APD_{90} values associated with these traces shown in (*C*, Shannon) and (*D*, Mahajan). In* (C) *and* (D)*, the arrows at the top of the figures indicate the mean APD_{90} of the population, with the bars representing plus/minus standard deviation from the mean.*

Mean APD_{90} Response & Comparison with Experimental Data

The rate of mean APD_{90} decline tends to itself decline during the progression of ischæmia, for both model populations. The exception to this declining rate is a spike between 6 and 8 min PO for the Mahajan population—this spike is caused by a phenomenon that is referred to in this dissertation as *dome collapse*. This phenomenon refers to a reduced depolarisation during Phase 2 of the AP, leading to a reduced value for V_{plat}. From this reduced V_{plat}, repolarisation occurs more rapidly, which in turn causes severe reduction in the duration of the Phase 2 section of the AP, and an associated decline in APD. It should be noted that this phenomenon is morphologically different from a simple shortening of the plateau, due to the reduced value for V_{plat}. With some of the models within the Mahajan population exhibiting this phenomenon at 8 min PO, and thus demonstrating a significantly reduced APD_{90}, there is a significant decrease in mean APD_{90}.

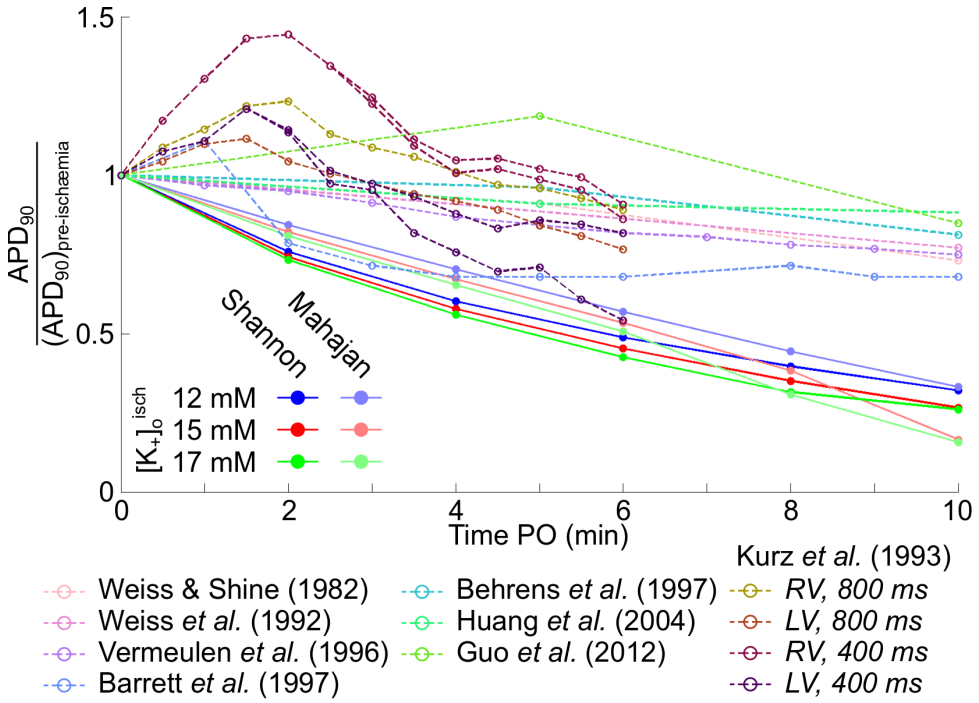


FIGURE 6.2: *Comparison of APD_{90} response between simulation results and literature reported values. The mean values for the Shannon and Mahajan populations are plotted for several different values of $[K^+]_{o,isch}$, and compared against the response reported in the literature for the effects of ischæmia on rabbit hearts. It must be noted that while the experimental data are measured according to time post-occlusion, the simulation data are more accurately composed of parameters detailed in Table 4.2. The data for Kurz* et al. *(1993) include data for alternans—the long/short durations are plotted, diverging at ∼ 2 min PO. Further details regarding the measurements presented in this figure are given in §B.1.*

A comparison of the APD_{90} mean data to experimentally reported changes for rabbit data is shown in Fig. 6.2. To reduce the influence of pacing rate and other experimental considerations on absolute values of APD_{90}, all presented data are normalised against their pre-ischæmic values. The complete data used in the figure are given in §B.1, along with data for non-rabbit species which are not represented in the figure.

The early response of the model populations (measured according to population mean) approximately matches the results of Barrett *et al.* (1997), as well as results presented for dog and human that are not shown in the figure (Russell *et al.*, 1977; Sutton *et al.*, 2000). However, at 4 min PO the normalised experimental range for APD_{90} ranges from 0.68 to 1.15, with the normalised simulation population mean ranging from 0.55 to 0.70—not only is the experimental range very wide, but the

simulation data are restricted to the very low end of these results.

The experimental data for Kurz *et al.* (1993) demonstrate some degree of alternans at a CL of 400 ms in both ventricles—the data representing the short and long APDs in these alternans are plotted. The mid ischæmic response (from $\sim$ 4 min PO to $\sim$ 6 min PO) match the data from Barrett *et al.* (1997) to a lesser degree, and the results corresponding to the short duration alternans APD from the left ventricle of Kurz *et al.* (1993).

The late response of the simulation data (from $\sim$ 8 min PO to $\sim$ 10 min PO) does not match experimental data (save for a comparison to pig data presented in Downar *et al.* (1977b)), demonstrating a fractional shortening of the APD_{90} in excess of that observed in the literature.

Population Variability

The evolution of the population variation for the AP can be traced by reference to Fig. 6.1, especially by using the histograms presented in Fig. 6.1C for the Shannon population and Fig.6.1D for the Mahajan population. For the Shannon population, the variation under 'normal' conditions is relatively high ($s^2(APD_{90}) = 6.23\,(ms)^2$, $\Delta(APD_{90}) = 30.9$ ms)—out of the 124 simulated environments, only 5 environments exist where variance exceeds normal, and 9 where range is greater. From this high starting point of variation, the population variation decreases to a minimum at 4 min PO. From this point of minimum variation, it increases until 8 min PO (where $s^2(APD_{90}) = 4.44\,(ms)^2$ and $\Delta(APD_{90}) = 23.5$ ms). At 10 min PO, the variation decreases significantly.

The Mahajan population shows a similar pattern of variability, but tends to show greater variability than the Shannon population at all points. As with the Shannon population, the population variation initially decreases from 0 to 2 min PO. It is of note that the minimum and maximum values within the population decrease at a greater rate than the mean population, which manifests as the peak of the APD_{90} distribution moving to the left (Fig. 6.1D). However, after this decrease, variation increases from 2 min PO (for the range) and 4 min PO (for the variance), with both variance and range exceeding normal values at 6 min PO.

Variation within the Mahajan population at 8 min PO is significantly greater than at other points, and this is due to the 'dome collapse' mentioned earlier. At 8 min PO, the population spans a continuum of dome collapse—some models within the population demonstrate a relatively unaffected AP morphology (with depolarisation after the initial upstroke leading to a higher V_{plat} from which a noticeable 'dome' phase of the AP extends with subsequent later repolarisation), while others demonstrate complete 'dome collapse' (with negligible depolarisation from the initial upstroke leading to severely reduced V_{plat}, from which rapid repolarisation occurs). It is this *spread* of models within the population, with significant variability in AP morphology, that leads to a high variation in APD_{90}, and a similarly high variation in ERP. At 10 min PO, it appears that all models within the population now experience dome collapse, resulting in minimal (but non-zero) variation.

As was explicitly stated in §4.1.2, prior to detailed analysis, models were assessed to confirm whether or not they remained excitable: if $V_{\text{max}} - V_{\text{rest}} < 44.0$ mV, the model was judged to have not been excitable in response to I_{stim}, and was excluded from further analysis. This criterion was decided upon after preliminary tests using the Shannon framework—there is no immediately apparent way to determine such a criterion *a priori*. The inexcitability rate of both model populations under specified environmental conditions, including various points during the progression of ischæmia, is given in Table 6.1. It can be seen that, during the progression of ischæmia, it is only at conditions of 10 min PO that any models display inexcitability.

Fig. 6.3 shows the APs of the entire Shannon and Mahajan populations at 10 min PO, with those models that are classed as inexcitable (and excluded from all other figures) shown in red. For the Shannon population (Fig. 6.3A), it is immediately apparent that there is a clear distinction between excitable and inexcitable models, and the criterion is successful in distinguishing between the two. The success is not especially surprising, as the criterion was designed using the Shannon model as a base. The binary distinction is also preserved in the Ca^{2+} data (Fig. 6.3A, inset). It is worthwhile to point out that it is not clear whether it is the inexcitability of the AP that drives the reduced Ca^{2+} transient, or *vice versa*, in the same way that it is still unclear whether Ca^{2+} alternans drives AP alternans, as detailed in §2.3.2. However, due to the framework construction, it is more likely that AP failure drives the

$[K^+]_o$ (mM)	$f_{K\text{-}ATP}$ (%)	f_{inhib} (%)	f_{NaK} (%)	Shannon AP Failure	Shannon ERP≥CL	Mahajan AP Failure	Mahajan ERP≥CL
5.4	0.00	0	0	0	0	0	0
7.72	0.16	5	6	0	0	0	0
10.04	0.32	10	12	0	0	0	0
12.36	0.48	15	18	0	0	0	0
14.68	0.64	20	24	0	0	0	0
17.0	0.80	25	30	605 (44.7%)	0	613 (78.7%)	166 (100%)
17.0	0.60	25	30	414 (30.6%)	471 (50.2%)	578 (74.2%)	201 (100%)
17.0	1.00	25	30	847 (62.6%)	0	720 (92.4%)	59 (100%)
12.0	0.80	25	30	0	0	0	0
15.0	0.80	25	30	32 (2.37%)	0	0	0
17.0	0.00	0	0	3 (0.0%)	1349 (100%)	0	779 (100%)
5.4	0.80	0	0	0	0	0	0
5.4	0.00	25	0	0	0	0	0
5.4	0.00	0	30	0	0	0	0
5.4	0.80	25	30	0	0	0	0
17.0	0.00	25	30	72 (5.3%)	1280 (100%)	183 (23.5%)	596 (100%)
17.0	0.80	0	30	150 (11.1%)	192 (16.0%)	432 (55.5%)	347 (100%)
17.0	0.80	25	0	411 (30.4%)	82 (8.7%)	584 (75.0%)	193 (99.0%)

Table 6.1: *Effect of different conditions associated with ischæmia on the number of models within the populations that are inexcitable, and of those that are excitable, those that exhibit ERP≥CL (the percentages for ERP≥CL are for the non-failing models, not the entire population). The first group represents those conditions simulating a linear progression from normal to ischæmic conditions; the second group represents ischæmic conditions with decreased/increased $I_{K\text{-}ATP}$ activation, and increased/decreased $[K^+]_{o,isch}$; the third group represents normal conditions when one condition is 'ischæmic'; the fourth group represents ischæmia when one condition remains 'normal'.*

reduced $[Ca^{2+}]_i$ transient.

The Mahajan population (Fig. 6.3B) presents less of a clear cut distinction between 'excitable' and 'inexcitable' models, both for AP data and Ca^{2+} data. Furthermore, by recalling the dome collapse at 8 min PO, it becomes clear that a clear cut distinction between excitable and inexcitable states would not exist at a different time—the model population from 6 min PO to 10 min PO presents a gradual progression from models that can be obviously be considered as excitable to models which are not so obviously excitable. Consequently, a criterion is unlikely to be established that provides the same clear-cut distinction that is apparent for the Shannon population.

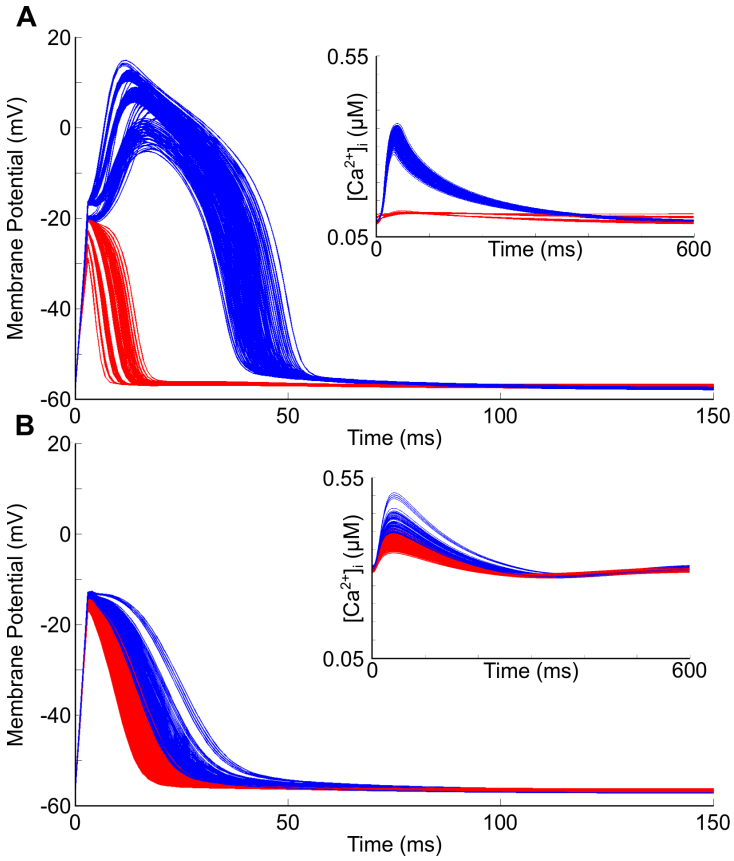


FIGURE 6.3: *Illustration of models that are classed as either succeeding or failing to produce an AP in response to stimulus at* 10 *min PO for the Shannon* (A) *and Mahajan* (B) *populations; successful APs are shown in blue, while those model outputs that are not considered successful APs are shown in red.* Inset: *Data for* $[Ca^{2+}]_i$.

6.1.2 Rôle of $f_{\text{K-ATP}}$

As was noted in §2.3.1, the shortening of APD during ischæmia is often attributed primarily to the activation of $I_{\text{K-ATP}}$. The results of the simulation analysis permit investigation of the influence of different degrees of activation of $I_{\text{K-ATP}}$, and how this influences the variability in repolarisation (and consequently, variability of ERP).

The importance of $I_{\text{K-ATP}}$ in shortening the APD is maintained across all environmental populations tested in the parameter sweep. The percentage decrease in APD_{90} caused by changing a parameter from its normal value to its ischæmic value is shown in Fig. 6.4. It should be noted that the data presented intrinsically involve changes in other parameters, and it is possible a parameter's effect may be due less to its own action, but rather due to its effect and interaction with other variables.

These results indicate that the action of $I_{\text{K-ATP}}$ has a profound effect on cellular repolarisation, with the modal percentage decrease caused by activation of $I_{\text{K-ATP}}$ being greater than that caused by any

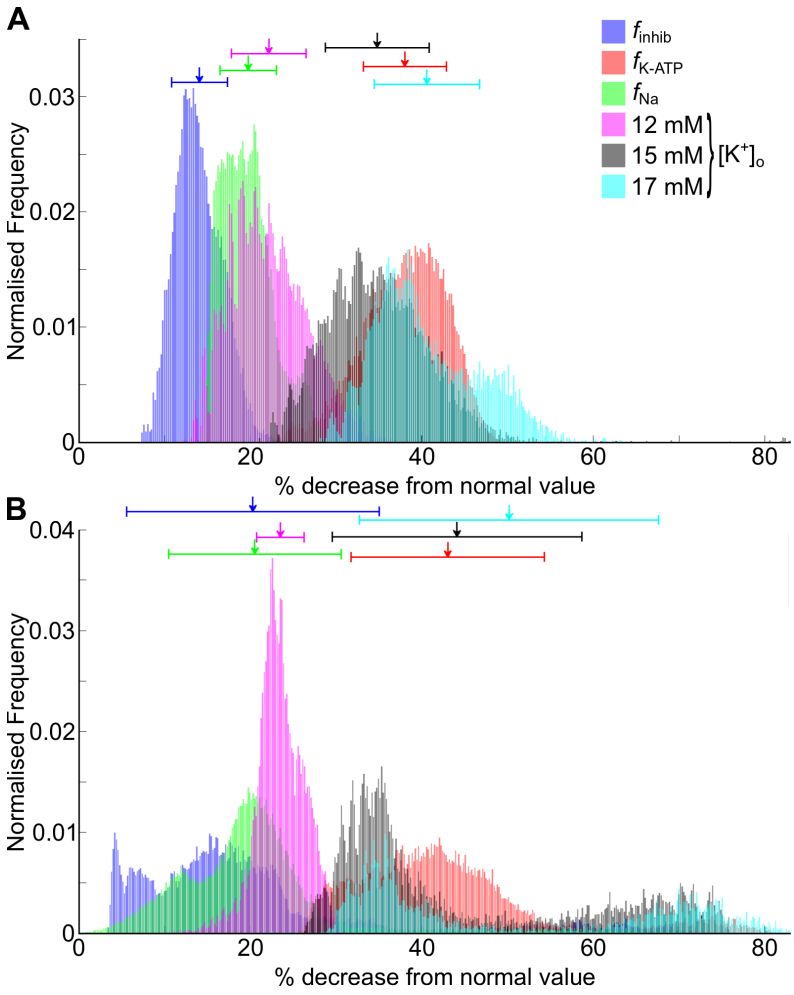


Figure 6.4: *Histograms demonstrating the population distribution (*(A)*: Shannon,* (B)*: Mahajan) for the percentage decrease in APD_{90} caused by changing the specified parameter from its normal to its ischæmic value, with all other parameters held constant; all combinations of parameters are represented in this figure. The histograms are normalised according to the total number of models within each histogram. The arrow represents the mean decrease for the specified variable, with the lines representing plus/minus standard deviation.*

other parameter for both populations (the percentage decreased caused by changes in $[K^+]_o$, and a comparison with the effects of $I_{\text{K-ATP}}$, will be discussed in §6.1.4).

The influence of $I_{\text{K-ATP}}$ on APD shortening remains significant, even when $f_{\text{K-ATP}}$ (and thus total channel conductance) is reduced. Fig. 6.5 shows the effect of $f_{\text{K-ATP}}$ variability for 3 different environments: conditions that are otherwise normal, conditions that are otherwise ischæmic, and conditions that are ischæmic but with no changes to either the initial value of $[Na^+]_i$ or in the conductance of I_{NaK} (*i.e.* $f_{\text{NaK}} = 0\%$). For all three environments, activation and subsequent increase of $f_{\text{K-ATP}}$ results in a significant fractional decrease in APD_{90}. The extent of this decrease is greater than that caused by a change in any other parameter from their normal to ischæmic (or, for $[K^+]_o$ where further data exist, near-ischæmic) value under similar conditions.

It was earlier mentioned that the variation evident for the Shannon population under normal conditions was high, and thus very few of the environments tested produced a greater extent of variability. It is thus implied that changing any parameter from its normal value to its ischæmic value tends to result in a decrease in Shannon population variability. However, this does not necessarily hold true for all environments, and $f_{\text{K-ATP}}$ demonstrates that interactions between parameters can complicate the changes in variability. While increasing $f_{\text{K-ATP}}$ tends to lead to a decrease in APD_{90} variability, there are notable exceptions: under ischæmic conditions with $[K^+]_{o,\text{isch}}$ set to 15 mM, application of any tested value of $f_{\text{K-ATP}}$ results in an increase in range. Despite this increase in range, variance tends to decline upon application of $I_{\text{K-ATP}}$. However, the details of the changes in variance are complicated, with the minimum variance occurring for a $f_{\text{K-ATP}}$ of 0.8%, which is when the greatest range is noted. Furthermore, variance is maximal when $f_{\text{K-ATP}}$ is set to 1.0%, eclipsing the variance for no activation of $I_{\text{K-ATP}}$.

The complicated changes for variance and range amongst the Shannon population may in part be explained by a process of slowed secondary depolarisation/partial dome collapse, which occurs haphazardly within the population. This describes a situation wherein the depolarisation from Phase 1 of the AP (the 'notch') is slowed, which either leads to (or is linked with) a reduced plateau potential. From this reduced V_{plat}, repolarisation occurs more rapidly, thus resulting in a reduced APD. This is

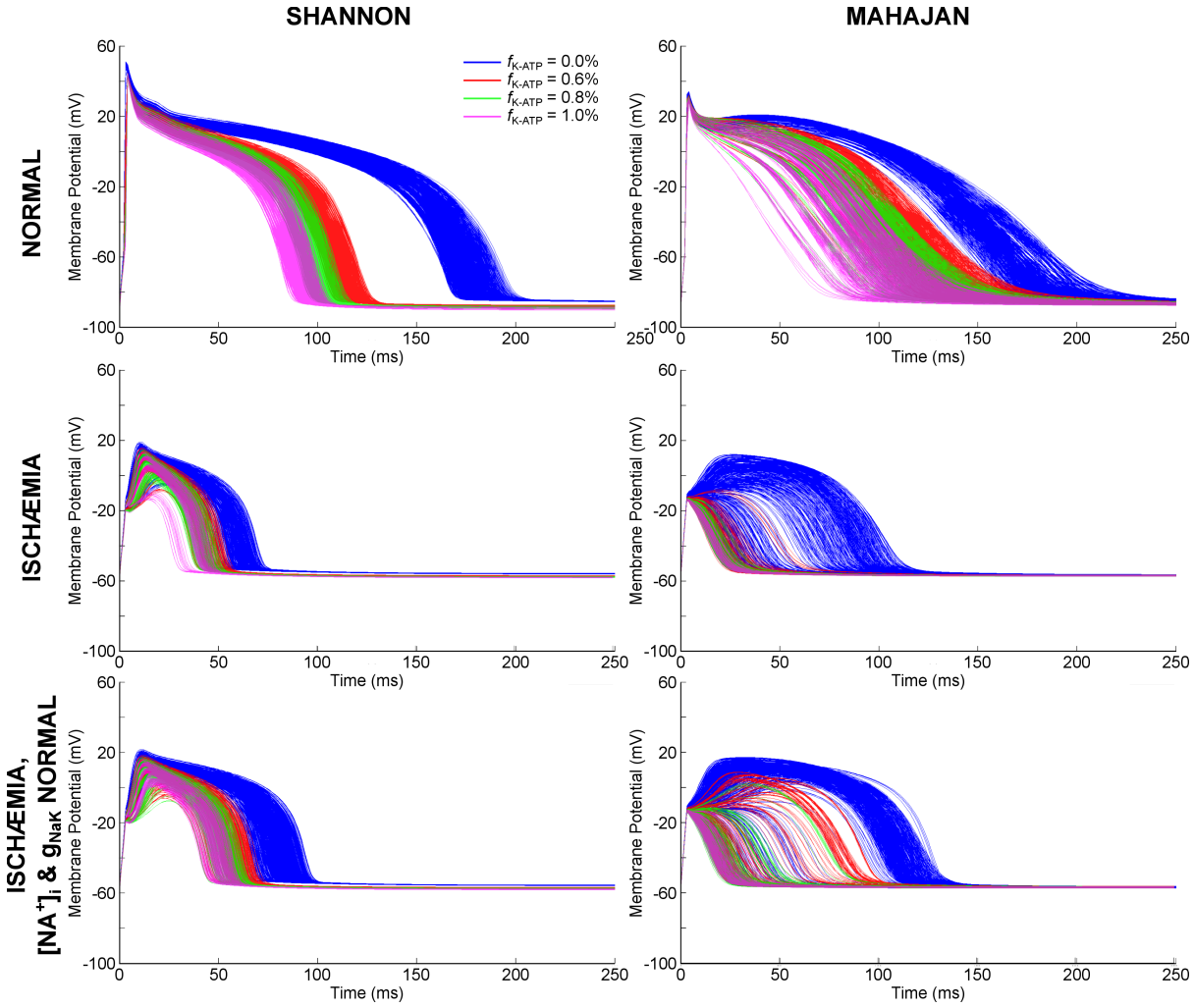


Figure 6.5: *Effect of $f_{\text{K-ATP}}$ variability on the Shannon (left) and Mahajan (right) model populations given normal conditions (*top, *$[K^+]_o$ = 5.4 mM, f_{inhib} = 0%, f_{NaK} = 0%), ischæmic conditions (*middle, *$[K^+]_o$ = 17.0 mM, f_{inhib} = 25%, f_{NaK} = 30%), and ischæmic conditions where changes in $[Na^+]_i$ and I_{NaK} are not modelled (*bottom, *$[K^+]_o$ = 17.0 mM, f_{inhib} = 25%, f_{NaK} = 0%).*

distinct from the dome collapse of the Mahajan population, which is a gradual process—the Shannon population demonstrates a more binary distinction. This occurs at unpredictable points, and only for some of the models within the population, some of which are seen in Fig. 6.5. At 10 min PO, slowed secondary depolarisation occurs for some models for almost all values of $f_{\text{K-ATP}}$, including 0%, with the exception of 0.8%. Due to the reduction in a model's APD_{90} caused by slowed depolarisation, this transient appearance of slowed depolarisation means that while the mean APD_{90} values still decrease with increasing $f_{\text{K-ATP}}$, the *minimum* value of APD_{90} within the population does not decline when $f_{\text{K-ATP}}$ is increased from 0.6% to 0.8%.

If f_{NaK} is set to 0% (*i.e.* changes to the $[\text{Na}^+]_\text{i}$ and I_{NaK} are not modelled), as is often the case when simulating ischæmia, slowed secondary depolarisation is no longer seen when $f_{\text{K-ATP}}= 0\%$, and thus is only seen for $f_{\text{K-ATP}}$ values of 0.6% and 0.8%, with no decline in $(\text{APD}_{90})_{\text{min}}$ evident when $f_{\text{K-ATP}}$ is increased from 0.8% to 1.0%.

The effect of $f_{\text{K-ATP}}$ on the Mahajan population is more clear cut (Fig. 6.5). The population's dome collapse can be at least partly attributable to the action of $I_{\text{K-ATP}}$, with the application of, and subsequent increase in, $f_{\text{K-ATP}}$ working to increase the extent of dome collapse. Under otherwise normal conditions (where there is no dome collapse when $f_{\text{K-ATP}}$ is set to 0%), activation of $I_{\text{K-ATP}}$ acts to reduce the duration of the plateau phase; the initial upstroke under these conditions is great enough that V_{plat} is necessarily relatively high, and thus the dome collapse is mostly via a reduced ability of the model to maintain an extended plateau. By inducing dome collapse for some models within the population, APD_{90} variation is increased. Increasing $f_{\text{K-ATP}}$ increases the proportion of models suffering some form of dome collapse, and thus variation tends to increase with increasing $f_{\text{K-ATP}}$.

However, this does not mean that dome collapse is caused solely by $f_{\text{K-ATP}}$, as can be seen for ischæmic conditions with $f_{\text{K-ATP}}= 0\%$ (Fig. 6.5), where significant dome collapse is evident. Under these conditions, increasing $f_{\text{K-ATP}}$ works to complete the dome collapse of the population that is otherwise partial across the population, and variation is decreased.

As such, $I_{\text{K-ATP}}$ should perhaps be considered to act to increase the *rate* of dome collapse. Consequently, when conditions already favour dome collapse (*e.g.* during ischæmia), activation and increase

of $f_{\text{K-ATP}}$ actually leads to a decrease in variation, hastening the point of full population dome collapse; this process is independent of the value of $[K^+]_{o,isch}$.

The effect of $f_{\text{K-ATP}}$ on the rate at which models are designated as inexcitable is worthy of note: for both populations, increasing $f_{\text{K-ATP}}$ under otherwise ischæmic conditions causes an increase in the inexcitability rate for both populations (Table 6.1). For the Mahajan population, this could be related to the increase in rate of dome collapse 'spilling over' to an increase in the rate of inexcitability ($I_{\text{K-ATP}}$ is active for the duration of the AP, and thus influences the entire course of the AP). However, no such ready explanation presents itself for the Shannon population.

Finally, it may be noted that the over-estimation of APD_{90} decline during late Phase 1A acute ischæmia noted earlier, being independent of the value of $[K^+]_{o,isch}$ used, indicates that $g_{\text{K-ATP}}$ is likely over-estimated, resulting in excessive total conductance through the channel, in turn leading to the excessive shortening of APD. This presents an apparent discrepancy between the total channel conductance used here being smaller than values used in other work (see §4.1.2) and yet at the same time decreasing APD_{90} further than has been experimentally observed. However, this can likely be explained in some part by the fact that the frameworks/models used are subtly different. While $g_{\text{K-ATP}}$ was trained using previous values from rabbit data, the original Shannon and Mahajan models (and thus those most similar to the previous work) are not included in the model populations. Consequently, it may be suggested that the differences in ion channel conductances and other framework properties between the populations used here and the models used in prior work may thus render direct comparison between the experiments invalid.

6.1.3 Rôle of Changes in $I_{\text{Ca,L}}$ & Na^+ Dynamics

The results presented in this thesis indicate that changes in the conductances of $I_{\text{Ca,L}}$, I_{Na} and I_{NaK}, and alterations in $[Na^+]_i$ (represented by changes to the parameters f_{inhib} and f_{NaK}), have comparatively little effect on reducing APD_{90}, and perhaps consequent to that, f_{NaK} appears to have relatively effect on the inexcitability rate (Table 6.1).

A matter that has already been touched upon is the effect of modelling f_{NaK}—in most computational

modelling of ischæmia to reproduce the changes in the AP, changes in f_{NaK} (and thus changes in $[Na^+]_i$ and I_{NaK}) are not included. The overarching effect of including f_{NaK} in the modelling process is to increase the effects of ischæmia on cellular repolarisation. This potentiation is present for both populations, but is more dramatic for the Mahajan population, where the inclusion of f_{NaK} in the modelling process increases the rate of dome collapse amongst the population. This can be seen in Fig. 6.5: when $I_{K\text{-}ATP}$ is not activated, dome collapse does not occur within the population without f_{NaK} also being modelled. Conversely, when $I_{K\text{-}ATP}$ is activated, f_{NaK} hastens the complete dome collapse of the population, and thus reduces variability. Due to the effect of dome collapse on variability, inclusion of f_{NaK} can thus have a great impact on variability. This serves as a timely reminder of the importance of the population modelling process—in cases where a single model is used to investigate ischæmia, the effect of f_{NaK} could be judged to only marginally increase/decrease the effect of ischæmia on APD_{90}, and thus judged to be of marginal importance in the modelling process. When populations are used, however, and variability can be assessed, the possible importance of f_{NaK} becomes clearer.

6.1.4 Rôle of $[K^+]_o$

The APs for different values of $[K^+]_o$, under both normal and ischæmic conditions, are shown in Fig. 6.6, along with histograms showing the APD_{90} distribution.

For the Shannon population, changes in $[K^+]_o$ can result in an increase in variability—variation is higher than normal for both mild hypokalæmic ($[K^+]_o$= 4.0 mM) and hyperkalæmic ($[K^+]_o$= 15 mM and 17 mM) conditions, with minimum variation occurring at 9 mM.

However, this pattern of variability is strongly dependent on the values given to the other ischæmic parameters: under otherwise ischæmic conditions, variation increases from 4.0 mM to 15 mM. The extent of this increase means if $[K^+]_{o,isch}$ is set to 15 mM rather than 17 mM, the variation at 10 min PO actually exceeds normal variation. Across the entire range of simulated conditions, the minimum variability tends to occur when $[K^+]_o$ is at 7 mM rather than 9 mM.

The Mahajan population remains more susceptible to changes in $[K^+]_o$, but demonstrates a different

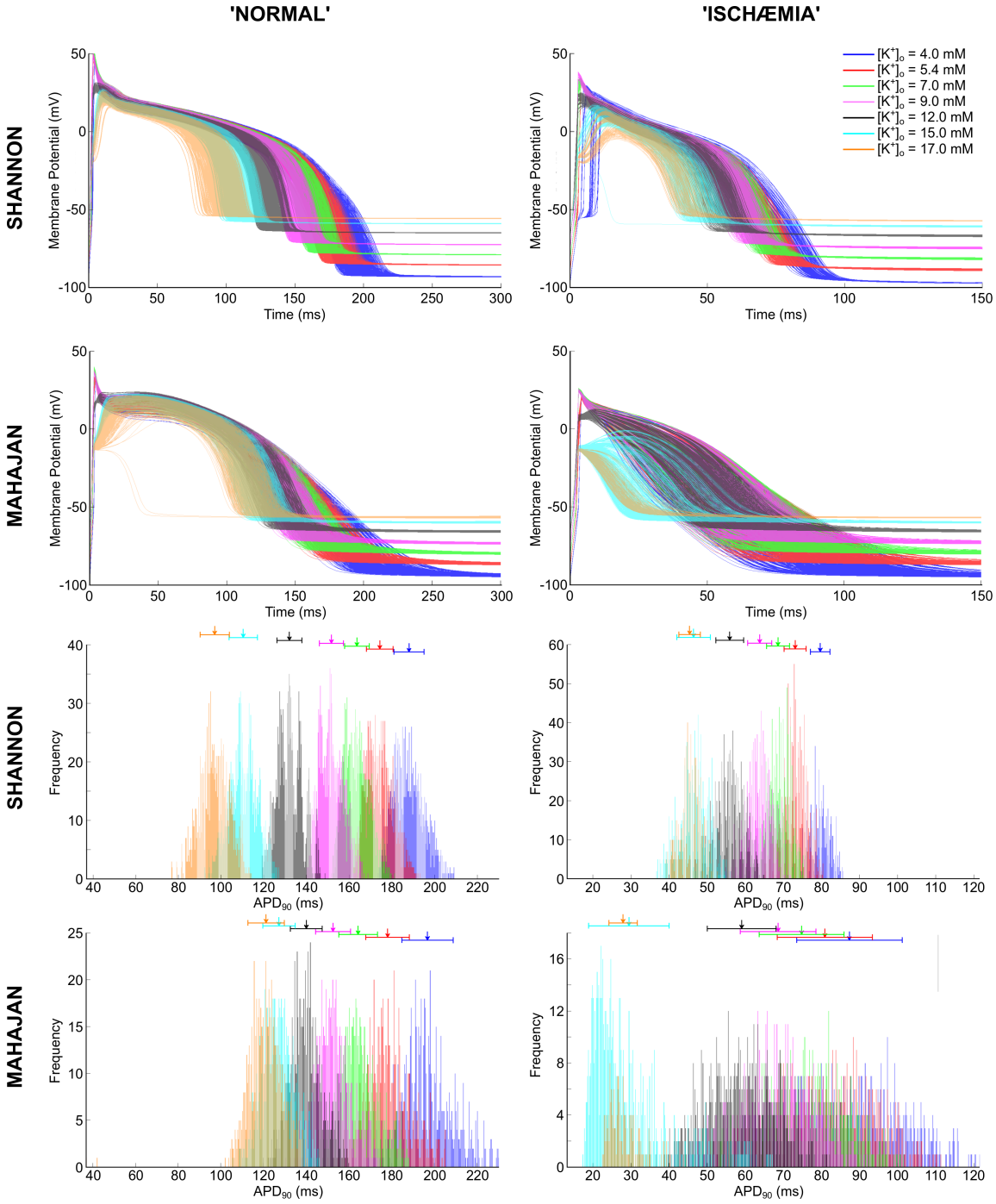


Figure 6.6: *Effect of $[K^+]_o$ variability on the Shannon and Mahajan model populations. Effect of $[K^+]_o$ variation is shown for when other environmental conditions are 'normal' (f_{inhib} = 0%, $f_{\text{K-ATP}}$ = 0.0%, f_{NaK} = 0%) to the left, and 'ischæmic' (f_{inhib} = 25%, $f_{\text{K-ATP}}$ = 0.8%, f_{NaK} = 30%) to the right. The top half of the figure shows the AP traces, with the bottom half of the figure showing the associated histograms of the APD_{90} distributions (arrows indicate the mean value, and the bars represent plus/minus standard deviation from the mean). The text to the left of the figures indicate whether the figures refer to the Shannon or Mahajan population.*

pattern of evolution of variation to the Shannon population. Variation is greatest for hypokalæmic conditions, and decreases from that point to reach a minimum at 12 mM (which is also the average value at which minimum variability occurs across all tested conditions), from which there is a slight increase. It is often the case that variation under ischæmic conditions is greater than under normal conditions.

The Mahajan population's variability also demonstrates the importance of overall environmental conditions, as can be seen by examining the effects of changing the value of $[K^+]_{o,isch}$. Until 6 min PO, variation is highest if $[K^+]_{o,isch} = 12$ mM; however, this does not mean lower $[K^+]_{o,isch}$ leads to greater variability, as at the same time, variation is greater for a $[K^+]_{o,isch}$ of 17 mM than for 15 mM. At 6 min PO, however, the greatest variation is exhibited if $[K^+]_{o,isch}$ is 17 mM, with the pattern being repeated at 8 min PO (recall that it is at this point that dome collapse occurs if $[K^+]_{o,isch}$ is 17 mM). Finally, at 10 min PO, when variability for $[K^+]_{o,isch}$ of 17 mM is minimal due to completed dome collapse, the greatest variability is for 15 mM.

The importance of interactions between parameters can also be seen by comparing the changes in APD_{90} caused by $[K^+]_o$ variability, under both normal conditions, ischæmic conditions and during progression of overall ischæmia (Fig. 6.7A and 6.7B). Of special interest is the change from 15 mM to 17 mM under otherwise ischæmic conditions for both populations, wherein the minimum value for APD_{90} increases despite the maximum and mean values continuing their decline. The same pattern is seen for the Mahajan population during ischæmia, but the interaction with other environmental conditions means it is not seen during ischæmia for the Shannon population.

The reason for this phenomenon can be seen in the APs presented in Fig. 6.6. The Shannon population has a lone model with a shortened AP at 15 mM that is no longer shortened at 17 mM. However, closer examination of the APs, and of the APD histograms, indicate that many models within the population have very similar values of APD at both values of $[K^+]_o$—this can also be seen by the small decrease in the standard deviation bounds between 15 mM and 17 mM in Fig. 6.7A. Such a result implies that the APD_{90} values reached at 15/17 mM represent close to a 'hard limit', *i.e.* the Shannon model is unable to produce an AP shorter than this. However, establishing such a hypoth-

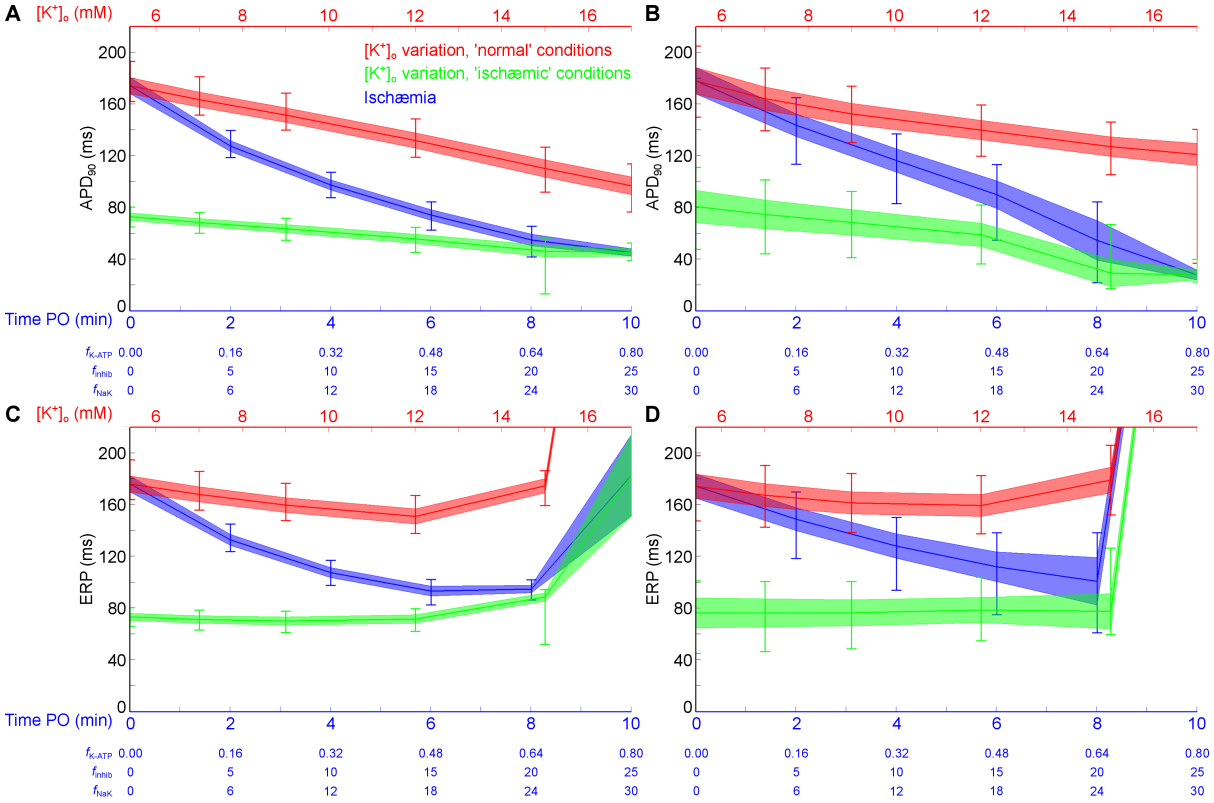


Figure 6.7: *Evolution of APD_{90} and ERP for the Shannon ((A) and (C), respectively) and Mahajan ((B) and (D), respectively) populations due to changes in $[K^+]_o$ under different conditions. In all cases, the central line represents the population mean, the shaded region indicates the mean plus/minus standard deviation, and the errorbars indicate the range exhibited by the population. The data shown in red are for $[K^+]_o$ variation when other environmental conditions are normal ($f_{\text{inhib}} = 0\%$, $f_{\text{K-ATP}} = 0.0\%$, $f_{\text{NaK}} = 0\%$), with the green data for otherwise ischæmic conditions ($f_{\text{inhib}} = 25\%$, $f_{\text{K-ATP}} = 0.8\%$, $f_{\text{NaK}} = 30\%$). The blue data represent evolution during ischæmia when $[K^+]_{o,\text{isch}}$ is 17 mM. The variation of $[K^+]_o$ for all data is indicated on the top abscissa, with the additional conditions for ischæmia noted on the bottom abscissa.*

esis is beyond the scope of this thesis.

The Mahajan population, on the other hand, has a significant number of models at $[K^+]_o$= 15 mM with otherwise ischæmic conditions with APD_{90} shorter than the minimum APD_{90} at 17 mM—231 out of 779 models. Examination of the APs indicate that this is due to a more rapid repolarisation from a V_{plat} that is not significantly different from V_{plat} at 17 mM. However, it is possible that this phenomenon is misleading, as it should be noted that at 17 mM, 613 of the Mahajan models are classed as not being able to elicit an AP. If these 'inexcitable' models are included (as may be considered rea-

sonable considering the lack of distinguishing feature between 'inexcitable' and 'excitable' for the Mahajan population), the minimum APD_{90} at 17 mM is once again lower.

$[K^+]_o$, due to its effect on V_{rest}, is the most significant factor on the basis of the stated criterion for determining whether a model is 'excitable' or 'inexcitable', based on the results presented in Table 6.1—if $[K^+]_o$ is kept at a normal value while all other factors are changed to their ischæmic values, all models remain excitable for both populations. However, this does not mean that increasing $[K^+]_o$ necessarily increases the rate of model inexcitability—while such a correlation can be seen for the Mahajan population, the inexcitability rate for the Shannon population under ischæmic conditions is greatest when $[K^+]_o$ is 4.0 mM.

The variable effect of $[K^+]_o$ depending on other parameters can also be seen by examining the percentage decrease in APD_{90} caused by changes in $[K^+]_o$ across all tested environments (Fig. 6.4). The figure demonstrates that the extent of the percentage decrease in APD_{90} is strongly dependent on the value to which $[K^+]_o$ is changed. If it is changed from 5.4 mM to 12 mM, the effect across all populations tends to be comparable to the effect of f_{inhib}/f_{NaK}. If it is changed to 15 mM, the effect increases, but still remains less potent than the effect of $f_{K\text{-}ATP}$.

However, if $[K^+]_o$ is changed to 17 mM (as is the usual case in this dissertation for considering the change from normal to ischæmic conditions), the effect can be comparable to, or often exceeding that of, $f_{K\text{-}ATP}$. For both populations, while the modal value for the percentage change is less than the modal/mean percentage change for $f_{K\text{-}ATP}$, there are significant tails to greater percentage decreases, resulting in the mean percentage decrease being higher in both cases. This tail is significantly greater for the Mahajan model, and is likely related to the process of dome collapse. However, this should not be taken to imply that hyperkalæmia is the cause of this dome collapse, nor that it represents the primary means of APD_{90} decline—as was seen in Fig. 6.6, dome collapse occurs under circumstances where $[K^+]_o$ does not reach 17 mM. Rather, changing $[K^+]_o$ from 12 mM to 17 mM can be viewed as priming a model for dome collapse, with the actual phenomenon requiring changes in other parameters as well.

With this caveat regarding the precise extent of $[K^+]_o$ involvement in APD_{90} decline, it can be noted

that some research indicates that $[K^+]_o$ can play a prime rôle in APD shortening (Yan *et al.*, 1993), while other research indicates that its effect during ischæmia is not comparable to the effect of $I_{K\text{-}ATP}$ (Ferrero *et al.*, 1996; Shaw and Rudy, 1997b). However, Moréna *et al.* (1980) demonstrated that, while the effect of hyperkalæmia on APD shortening is less than the effect of hypoxia, it does indicate that the combination of the two produces ischæmic results.

6.2 APD_{90}/ERP Relationship During Ischæmia

The discussion in the previous section focussed on the effects of ischæmia and ischæmic parameters on APD_{90}, and changes in the variability of APD_{90}. Many of these conclusions also hold for ERP, with APD_{90} demonstrating a strong correlation with ERP. However, the precise *relation* between the two changes depending on ischæmic conditions, and moreover, the correlation can also be demonstrated to decline, or even break down. As such, it is the focus of this section to determine how the relation between APD_{90} and ERP changes, and under what conditions the conclusions reached for APD_{90} in the previous section can no longer be applied to ERP.

The extent of the correlation between APD_{90} and ERP can be seen by investigating the variability of PRR—if the two are highly correlated, there will be little resulting variability in PRR.[1] The distribution of APD_{90}, ERP and PRR for various conditions are shown in Fig. 6.8. Under most conditions, there is very little variability for PRR, indicating the mapping between APD_{90} and ERP is relatively straight-forward. This mapping only seems to break down, resulting in increasing variability for PRR, when ERP→CL (which limits the data available for the 'actual' values of ERP/PRR, and thus the extent of the conclusions that can be made).

It is thus only under conditions of relatively severe acute ischæmia that the correlation between APD_{90} and ERP can be said to break down, and thus only under those conditions that the conclusions made for APD_{90} may not necessarily hold for ERP. Fig. 6.9 shows the correlation between APD_{90} and ERP for both populations at various points during ischæmia, with variability for $f_{K\text{-}ATP}$ also shown at conditions appropriate for 10 min PO.

[1] It can be noted that technically low variability of PRR actually indicates a consistent mapping between the two.

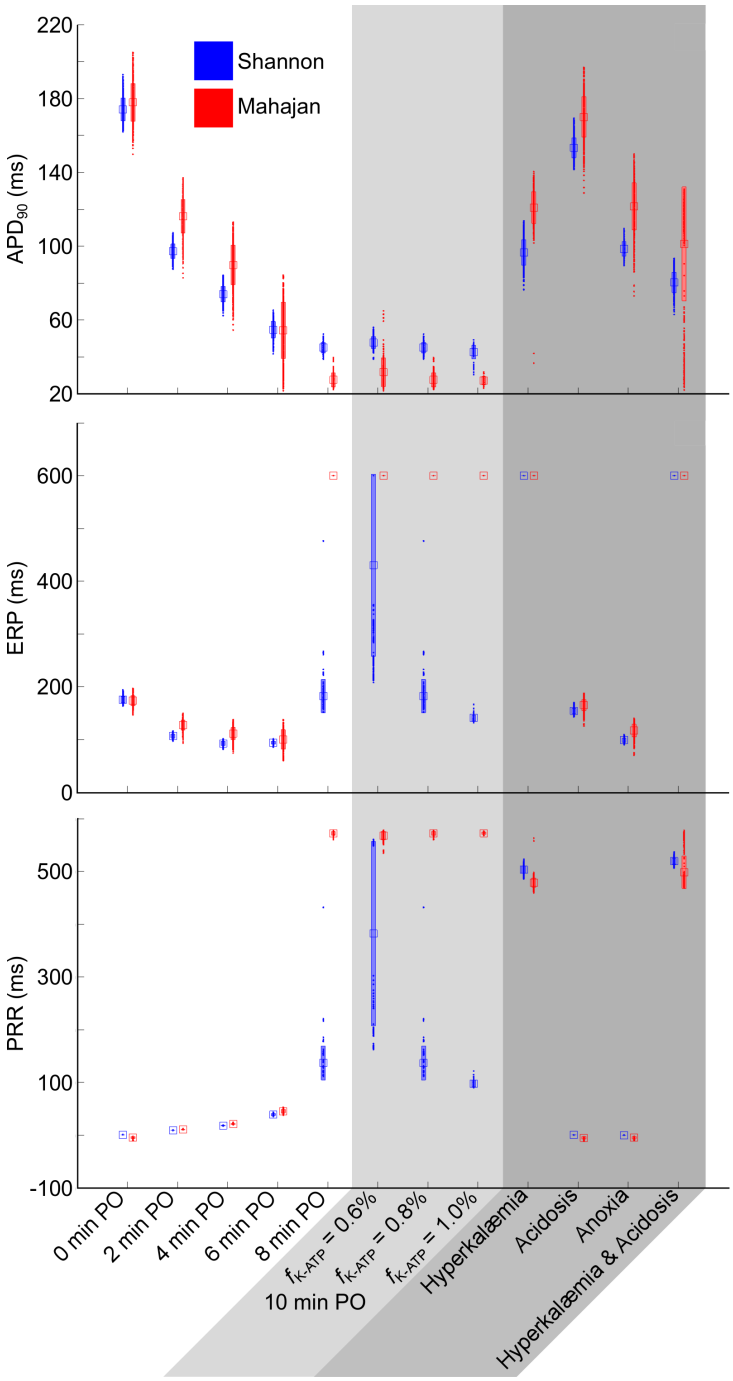


FIGURE 6.8: *Distribution of values for APD_{90} (top), ERP (middle) and PRR (bottom) within the population for non-failing models, under specified conditions. To the left are the population distributions for conditions appropriate to specified points during ischæmia, up to 8 min PO; for specific environmental parameter values, see Table 4.2. In the light gray shaded region are population distributions for conditions appropriate to 10 min PO ischæmia, with variation in $f_{\text{K-ATP}}$. To the right, in the dark grey shaded region, are population distributions for conditions that occur within ischæmia, while other parameters are kept at their 'normal' values: hyperkalæmia ($[K^+]_o = 17.0$ mM), acidosis ($f_{\text{inhib}} = 25\%$), anoxia ($f_{\text{K-ATP}} = 0.8\%$), and hyperkalæmia & acidosis combined ($[K^+]_o = 17$ mM, $f_{\text{inhib}} = 25\%$). In all cases, the value for each model in the population is represented by a single dot, the mean value is represented by a large square marker, and the region defined by mean ± standard deviation is represented by a shaded box. It must be remembered that for ERP, and thus for related PRR values, 600 ms represents a lower limit for the actual possible value.*

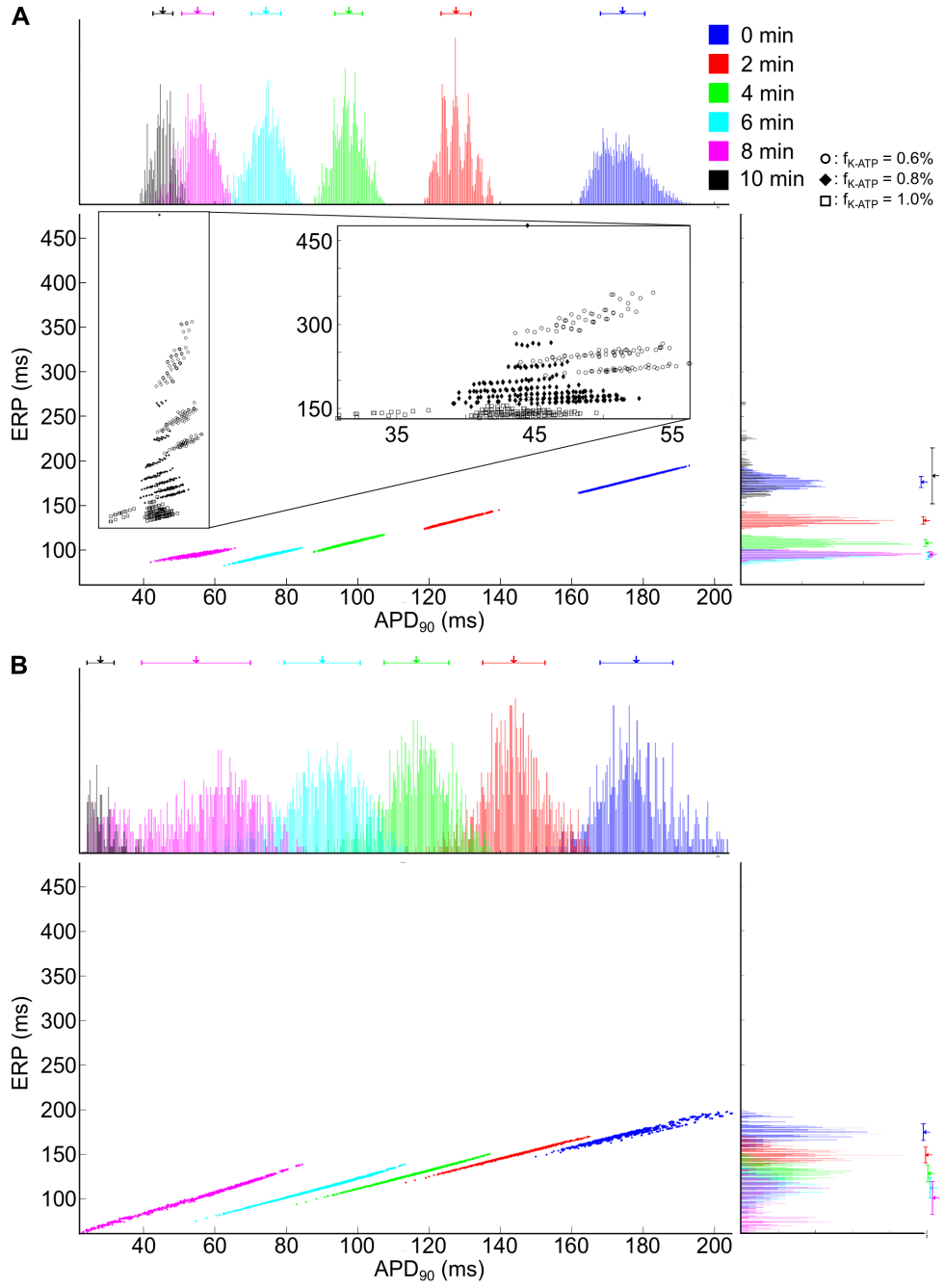


Figure 6.9: *Relation between APD_{90} and ERP at various points during ischæmia for the Shannon* (A) *and Mahajan* (B) *populations. For* 10 *min PO, the APD_{90}/ERP relation is also shown for increased/decreased $f_{\text{K-ATP}}$ ($[K^+]_o$ = 17 mM, f_{inhib} = 25%, $f_{\text{K-ATP}}$ = $\{0.6\%, 0.8\%, 1.0\%\}$, f_{NaK} = 30%) for the Shannon population (data are not available for the Mahajan population). Histograms showing APD_{90}/ERP distribution are shown according to the same scales as the main plot: APD_{90} is above the central plot, ERP to the right. In* (A)*, the inset reproduces the highlighted region, showcasing the variability due to $f_{\text{K-ATP}}$ variation.*

For the Shannon population, the APD_{90}/ERP correlation decreases with ischæmic severity—this decrease in correlation is greater if $[K^+]_{o,isch}$ is higher. A similar decrease in correlation is also evident for variation of $[K^+]_o$ under otherwise normal conditions, though this decrease is not to the same extent as the ischæmic decrease. However, this does not indicate a simple cause and effect relation between increased $[K^+]_o$ and decreased APD_{90}/ERP correlation, as hypokalæmia (under otherwise normal conditions) also causes a decrease in correlation, to an extent greater than the decease caused by increasing $[K^+]_o$ to 12 mM. However, to further demonstrate the interactions between parameters, if $[K^+]_o$ variability is simulated under otherwise ischæmic conditions, the pattern of correlation almost reverses, increasing from 4 mM through to 7 mM, remaining the same until 9 mM, and then declining from there.

At 10 min PO, changes in $f_{\text{K-ATP}}$ have a noticeable effect on the correlation/relationship between APD_{90} and ERP, with increasing $f_{\text{K-ATP}}$ serving to increase the correlation—this is possibly due to $f_{\text{K-ATP}}$ having a greater effect on ERP than on APD_{90} at this stage, and the increases in ERP that would otherwise occur are being curtailed by the action of $I_{\text{K-ATP}}$. However, the relationship is not as simple as this may indicate. If $[K^+]_{o,isch}$ is set to 15 mM, the correlation coefficient σ alters in response to changes in $f_{\text{K-ATP}}$ according to $\sigma(f_{\text{K-ATP}} = 0\%) < \sigma(0.8\%) < \sigma(0.6\%) < \sigma(1.0\%)$, whereas if $[K^+]_{o,isch}$= 12 mM, σ changes as $\sigma(0\%) < \sigma(0.6\%) < \sigma(1.0\%) < \sigma(0.8\%)$.

The Mahajan population demonstrates a different pattern of correlation, with correlation increasing until 4 min PO (or 6 min PO, if $[K^+]_{o,isch}$ is set to 12 mM), before decreasing. This pattern of correlation corresponds to the effects of $[K^+]_o$ variability, wherein the greatest APD_{90}/ERP correlation is found at 9 mM for both normal and ischæmic conditions. As with the Shannon population, $f_{\text{K-ATP}}$ variability has little effect on the APD_{90}/ERP correlation under normal conditions, and a discernible effect to reduce correlation only becomes apparent when $[K^+]_o$ reaches 15 mM or greater.

The results presented in Fig. 6.9 also indicate that, while correlation remains high under most conditions, the exact *relation* between the two depends on the environment. These changes in relation can be subtle—for example, there is little change in relation for the Shannon population between 0 and 4 min PO. Some of the changes in the APD_{90}/ERP relation can be correlated with changes in $[K^+]_o$,

while the APD_{90}/ERP correlation remains strong. This can be seen by comparing the evolution of APD_{90} with $[K^+]_o$ against the evolution of ERP in Fig. 6.7, *i.e.* comparing *(A)* and *(B)* with *(C)* and *(D)*, respectively. Were the relation to remain constant, the evolution of APD_{90} and ERP should be identical—this is not the case, and it can be seen that the differences between the two increase with both increasing ischæmic severity and increasing $[K^+]_o$.

Even under conditions of high correlation, the variance and range of APD_{90} and ERP are not the same, indicating that the mapping is not precise. Furthermore, lower values of $f_{\text{K-ATP}}$ coincide with a tail in the ERP histograms to greater values that is not present in histograms of APD_{90} (data not shown).

It is also worth considering the rate of the models within the populations that exhibit ERP≥CL, and thus those models which cannot be used to investigate the correlation, relation and mapping between APD_{90} and ERP. The number of models in the populations that encounter this upper limit are given in Table 6.1. The significant increase in ERP that is evident by increasing beyond CL is not reflected with similar increase in APD_{90}, and thus indicates a further decline in the correlation between the two metrics.

For hyperkalæmic conditions (with normal conditions otherwise), all models for both populations have ERP≥CL (apart from 3 Shannon models that are inexcitable). The effect of hyperkalæmia in this regard is even more severe for the Mahajan population: where a successful AP is generated when $[K^+]_o$ is set to 17 mM, only 6 out of these 12,464 models have ERP<CL. It can be noted that hyperkalæmia represents the key condition for prolongation of ERP beyond CL, with such an extension not occurring unless $[K^+]_o$ is set to 17 mM.

The reason for this difference in response between the two populations can be found by the population variability of V_{rest}: the relationship between V_{rest} and ERP for both populations is shown in Fig. 6.10. There is a clear tipping point for V_{rest}: when V_{rest} is less than this threshold value ($V_{\text{rest}}^{\text{threshold}}$), ERP remains relatively insensitive to V_{rest}, but once this value is exceeded, ERP almost invariably increases to values at least as great as 600 ms.

The value for $V_{\text{rest}}^{\text{threshold}}$ can be determined with a great degree of accuracy: −57.395 mV for the

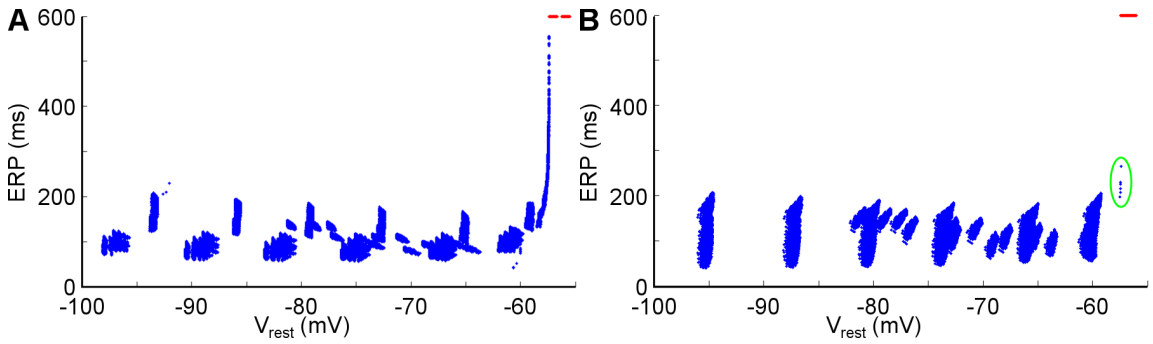


FIGURE 6.10: *Relation between V_{rest} and ERP across the Shannon* (A) *and Mahajan* (B) *populations for all simulated conditions. Those models with ERP≥CL are highlighted in red. For the Mahajan population in* (B)*, those models with V_{rest}>$V_{rest}^{threshold}$ and yet with ERP<CL are highlighted by the green circle.*

Shannon population, and −57.448 mV for the Mahajan population. These values correlate with the observed data for the threshold of inexcitability presented in Moréna *et al.* (1980). It should be noted that 6 Mahajan models have V_{rest}>$V_{rest}^{threshold}$ and yet still maintain ERP<CL, though their ERP is still high compared to the majority of ERP values within the super-population—they are highlighted in Fig. 6.10B. It can be noted that these models are those same 6 models that were noted as having $[K^+]_o$ at 17 mM, and yet do not have ERP≥CL.

There is no simple way of predicting $V_{rest}^{threshold}$ from the framework equations, but it is of note that the Shannon and Mahajan population values, though different, are very similar, and these two frameworks share the equation describing the activity of I_{Na} (along with other ion currents). Due to this threshold, the explanation for ERP<CL would appear to be found in explaining the increase in V_{rest}.

The rise in V_{rest} is mainly caused by increases in $[K^+]_o$—f_{inhib} and f_{NaK} cause negligible changes to V_{rest}, and $f_{K\text{-}ATP}$ only causes noticeable changes for the Shannon population. It is this minor effect of $f_{K\text{-}ATP}$ on V_{rest} for the Shannon population that leads to $f_{K\text{-}ATP}$ also having a demonstrable effect on the rate of models with ERP≥CL—by acting to reduce V_{rest} slightly, $f_{K\text{-}ATP}$ has a noticeable effect on reducing ERP. As $f_{K\text{-}ATP}$ does not have the same effect on V_{rest} for the Mahajan population, it does not have a similar impact on ERP. This effect (and lack thereof) can be noted by the Mahajan population demonstrating a more striking 'banded' grouping of V_{rest} than the Shannon population.

The populations do not reproduce any significant variability in V_{rest}, with the range never exceeding

2 mV, and mostly being restricted to values of less that 1.5 mV. This is due to V_{rest} being determined mainly by the ratios of $[K^+]_o$ and $[K^+]_i$, with variability in these parameters not being a goal of the analysis presented in this dissertation (though the variation in $[K^+]_o$ applied in this work would permit such an investigation using the data available, were this desired).

6.3 Relations Between Channel Conductances During Ischæmia

In much the same way that the relative importances of the conductances tested in the previous chapter changed depending on the pacing rate, they change depending on environmental factors, and thus are affected by the progression of ischæmia. Fig. 6.11 shows the changes in population properties for APD_{90} and ERP, both in terms of a dimensional stack image, and a column plot.

It should be remembered when analysing partial stack images that they represent an incomplete parameter space, and that the populations have been restricted according to APD behaviour. Consequently, if a particular parameter has a strong effect on APD, this effect will be masked within the population that has been defined to only accept those models wherein this effect is reduced. Conclusions made for a subset of the entire parameter space are valid *only for that subset*, and should not be confused with conclusions for the overall space.

The dimensional stack images for the Shannon population are optimised to maximise the connectivity of the space (the same stack order was used in Fig. 5.5). Fig. 6.11A shows that a large range of variability is exhibited at the smallest level (Level 1, using the nomenclature previously defined) in the x-direction, indicating high sensitivity to changes in g_{Kr}. Similarly, there is little difference between the rows/columns on the largest scale, Level 3 (*e.g.* between row 1 and row 2), implying that $g_{\text{Ca,L}}$ and g_{K1} are comparatively unimportant in altering the population's APD_{90}. The distribution for ERP under identical environmental conditions (Fig. 6.11C) is almost identical, with almost identical absolute values, confirming the almost direct coincidence of APD_{90} and ERP under normal conditions.

Under ischæmic conditions, however, the relative importances of the conductances changes for those models that remain excitable. For the distribution of APD_{90} (Fig. 6.11B), $g_{\text{Ca,L}}$ and g_{K1} become more

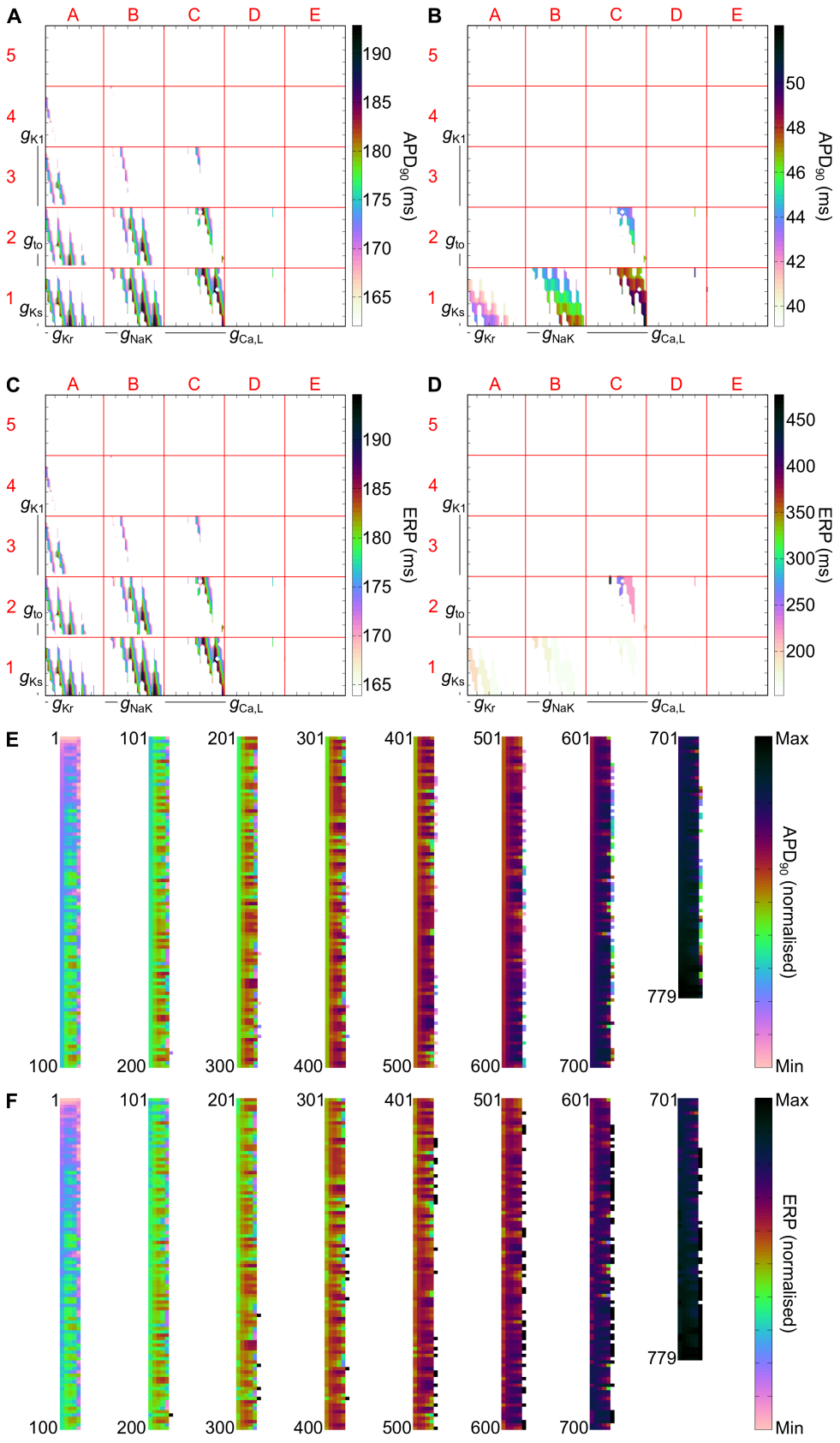

A
B
C
D
E
A B C D E
5
4
3
2
1
g_{K1}
g_{to}
g_{Ks}
g_{Kr}
g_{NaK}
$g_{Ca,L}$
190
185
180
175
170
165
APD_{90} (ms)
50
48
46
44
42
40
ERP (ms)
450
400
350
300
250
200
1
101
201
301
401
501
601
701
779
100
200
300
400
500
600
700
Max
Min
APD_{90} (normalised)
ERP (normalised)

Figure 6.11 *(previous page)*: *Changing distributions of APD_{90}* (A,B,E) *and ERP* (C,D,F) *for the Shannon* (A-D) *and Mahajan* (E-F) *populations under normal conditions* (A,C,E) *and conditions appropriate for* 10 *min PO* (B,D,F). *In all figures, a model is not plotted if it is not excitable for the specified conditions. The dimensional stack images for the Shannon population are optimised for connectivity of the parameter space. The column plots for the Mahajan population are arranged with each row representing a single model (the numbers indicate the model number), and each column representing the value of APD_{90}/ERP for a given level of ischæmic severity, progressing from normal to* 10 *min PO (normalised according to the values in that column). The models are arranged in sequence of APD_{90} value under normal conditions.*

influential (consider the differences between rows and columns at the highest level, *e.g.* columns A and B for $g_{\mathrm{Ca,L}}$ and rows 1 and 2 for g_{K1}). In addition, there are differences between rows at Level 2 of the dimensional stack, indicating increased importance of g_{to}. At the same time, the range of variability is no longer seen at the lowest level, indicating declining relative importance of g_{Kr}. It is evident, however, that the same details do not apply to the ERP distribution, emphasising that the mapping between APD_{90} and ERP is not maintained during severe Phase 1A ischæmia (Fig. 6.11C). The colour distribution of the ERP plot is dominated by high values in the square C2, but it is possible to observe two distinct differences from the APD_{90} distribution. First, there is no noticeable difference between rows at Level 2, indicating the increased importance noted for g_{to} for APD_{90} is not maintained for ERP. Second, while increasing g_{K1} results in a decline in APD_{90}, it results in an increase in ERP (compare the details of C1 and C2).

A dimensional stack image is less useful to show the data for the Mahajan population—the smaller population size results in a greater degree of fragmentation of the image, making it harder to analyse effectively. The proportion of models demonstrating inexcitability at 10 min PO makes this problem more acute. As such, data for the Mahajan population are instead plotted using column plots, wherein each row represents the data for a single model, and each column represents the value of a given metric for a given environment. In Fig. 6.11E and 6.11F, which represent the effect of increasing ischæmic severity, the columns thus progress from 'normal' to 10 min PO, left to right. The models are placed in sequence of increasing APD_{90} under normal conditions, with the results for each column normalised according to the data for that column. These column plots (Fig. 6.11E for APD_{90}

and Fig. 6.11F for ERP) demonstrate that the model distribution does vary, with the model that elicits the shortest APD_{90}/ERP not doing so under all environmental conditions. The data also demonstrate that the mapping between APD_{90} and ERP is not direct. The same model order is used for both plots, and it can be seen that the order representing increasing APD_{90} does not correlate exactly to the order for increasing ERP (for example, see the ERP distribution at 0 min PO for models 301-400). However, the differences between the optimum orders actually decreases during the early stages of acute ischæmia, before increasing significantly beyond ∼6 min PO, with the same being true for the Shannon model. This concurs with the earlier discussion of the correlation between APD_{90} and ERP.

Some conclusions can be drawn regarding the disposition of models toward inexcitability by use of Fig. 6.11B. By examining where in the parameter space the inexcitable models are, those models with increased g_{K1}, especially where paired with reduced $g_{Ca,L}$, are more likely to be inexcitable at 10 min PO: all models in rows 3 and 4 are no longer excitable, along with models in A2 and B2. The inexcitability rate appears to be relatively unaffected by other parameters—there is no discernible change in the remaining squares on scales where other parameters would influence the outcome.

The distribution of inexcitable models in Fig. 6.11E indicates that models with longer APs under normal circumstances are more likely to remain excitable at 10 min PO. However, it is not a simple correlation between $(V_{max} - V_{rest})$ and APD_{90}—during early ischæmia, there is very little variation in $(V_{max} - V_{rest})$, and at 4 min PO, if any relation could be said to exist, it is inverse. It is only at $\sim$ 8 min PO that any correlation between long APD_{90} and greater $(V_{max} - V_{rest})$ could be said to exist, with this implying that the link is correlation rather than causation.

6.4 Ischæmic Effects on other Biomarkers

While repolarisation and recovery of excitability are often regarded as key risk markers of arrhythmogenic behaviour, variability in other biomarkers can also indicate susceptibility. Furthermore, as was commented upon at the outset, the 'key' changes in the AP caused by ischæmia cover more than just changes in APD_{90} and ERP. While changes in V_{rest}, due to their influence on changes in ERP, have

already been discussed, the ischæmic decrease in AP amplitude is also caused in part by a decrease in V_{max}. For both populations, from 0 to 2 min PO V_{max} increases with a concomitant decrease in variation. Subsequent to this, however, V_{max} decreases (which, accompanying an increase in V_{rest}, leads to a more pronounced decrease in AP amplitude), with variation increasing, apart from at 10 min PO for the Mahajan population when $[K^+]_{o,isch}$ is set to either 15 mM or 17 mM.

It is of note that while the Mahajan population has all models' V_{max} increasing from 0 to 2 min PO regardless of what value is used for $[K^+]_{o,isch}$, the Shannon population is not so uniform, with some models' V_{max} decreasing from 0 to 2 min PO, and the population mean decreasing if $[K^+]_{o,isch}$ is set to 12 mM. This can be explained by the fact that changing any parameter apart from $[K^+]_o$ from its normal to ischæmic value causes a decrease in V_{max} for the Shannon population. $[K^+]_o$, on the other hand, increases V_{max} until 7/9 mM (depending on the population and other conditions). As such, the initial increase in V_{max} observed in ischæmia normally, caused by increasing $[K^+]_o$, is offset by the decrease caused by other factors for the Shannon population when $[K^+]_{o,isch}$ is set to 12 mM, resulting in an initial decrease instead. However, this explanation is complicated by the fact that the rate of models with decreasing V_{max} between 0 and 2 min PO within the population actually increases if $[K^+]_{o,isch}$ is increased from 15 mM to 17 mM, from 4% to 8% (though both are significantly less than the 90% rate if $[K^+]_{o,isch}$ is set to 12 mM).

It can be noted that the variability for V_{max} exhibited by the populations is significantly greater than the variability shown in V_{rest}—as a result, variability in AP amplitude is likely caused to a greater degree by variability in V_{max}. Furthermore, the population distribution of V_{max} for both populations changes significantly during the progression of ischæmia. Both populations have an approximately normal distribution of V_{max} value, with a slight left skew to smaller values, at 0 and 2 min PO. For the Mahajan population, this skew is reversed at 4 min PO, before reversing again at 6 min PO. However, for both populations at some point during ischæmia (Shannon at 4 min PO, Mahajan at 6 min PO), the population distribution demonstrates a 'sub-group' phenomenon—the overall distribution remains as described, but is broken up into smaller distributions, mirroring the overall shape. The overall effect is similar to a super-position of two self-similar waves, one of a higher frequency than the others.

This phenomenon, however, is only observed at the single specified time point—after this point, the distribution appears to lose this sub-group phenomenon, though the spread increases and thus may mask it (the increase in spread is especially noticeable for the Mahajan population).

The time at which V_{max} is reached ($t(V_{\text{max}})$) is not a biomarker that is commonly recorded, but the data presented here indicate that it changes significantly during ischæmia. Under normal conditions, V_{max} occurs during the initial upstroke of the AP (Phase 0). However, at $\sim$ 6 min PO, both populations instead tend to achieve V_{max} during the dome of the AP (Phase 2), with this progression toward later $t(V_{\text{max}})$ continuing with increasing ischæmic severity (Fig. 6.1). Furthermore, this increase in $t(V_{\text{max}})$ is enhanced by $f_{\text{K-ATP}}$ (recall the already mentioned slowed depolarisation phenomenon—see Fig. 6.5). In addition to this sensitivity to $f_{\text{K-ATP}}$, changes in $[\text{K}^+]_o$ also influence the progression of $t(V_{\text{max}})$—under otherwise normal conditions, both populations have delayed $t(V_{\text{max}})$ at $\sim$ 15 mM, though the delay amongst the Shannon population is far smaller than for the Mahajan population (Fig. 6.6). If other conditions are set to their ischæmic values, the delay to $t(V_{\text{max}})$ is increased further for both populations, but this is accompanied by the dome collapse for models in the Mahajan population—without a dome present in the AP, there is no possibility for delayed V_{max}. When some models in the Mahajan population experience dome collapse, while others do not (at $\sim$ 15 mM), the conditions allow for a wide variation in $t(V_{\text{max}})$.

In tissue, variability of $t(V_{\text{max}})$ has the potential to be arrhythmogenic, especially when coupled with reduced conduction velocity—consider a region of tissue with reduced ischæmic severity adjoining a region of tissue with increased ischæmic severity (and consequently, decreased conduction velocity and delayed $t(V_{\text{max}})$). This could lead to heterogeneity in the source-sink relationship that leads to AP activation in ventricular tissue. With differences in activation time, the likelihood of an AP wavefront becoming fragmented, leading to re-entry or other sources of arrhythmia, is increased.

With changes in conduction velocity in mind, the variability in $(\text{d}V_m/\text{dt})_{\text{max}}$ can be considered—recall from §2.3.1 that the conduction velocity in tissue is proportional to the square root of $(\text{d}V_m/\text{dt})_{\text{max}}$, and thus $(\text{d}V_m/\text{dt})_{\text{max}}$ can be used as a cellular proxy for conduction velocity. Indeed, the evolution of mean $(\text{d}V_m/\text{dt})_{\text{max}}$ during ischæmia matches qualitatively the evolution of conduction velocity (initial

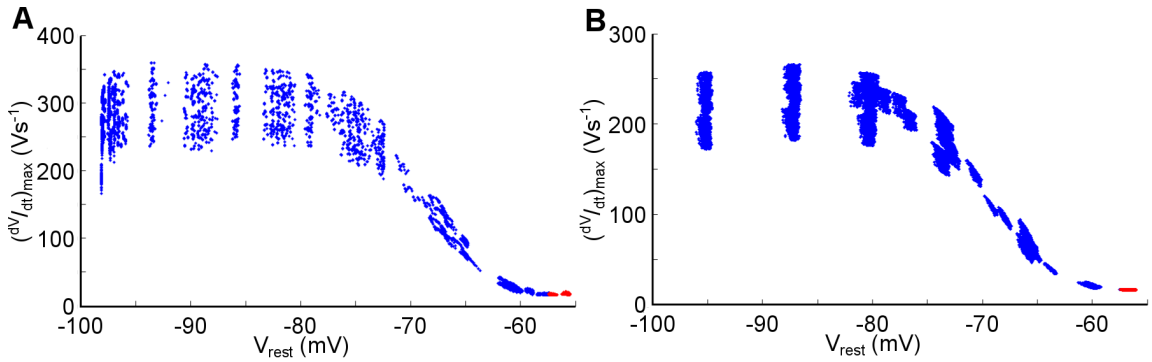


Figure 6.12: *Relation between V_{rest} and $(dV_m/dt)_{max}$ across the Shannon* (A) *and Mahajan* (B) *populations for all simulated conditions. Those models that also have ERP≥CL are highlighted in red.*

increase as V_{rest} increases to a value closer to the activation threshold, followed by a decrease as the rise in V_{rest} affects the recovery of excitability). This mooted dependence on V_{rest} is maintained for $(dV_m/dt)_{max}$—the relation between the two variables is shown in Fig. 6.12.

As the increase of V_{rest} correlates with the progression of ischæmia, the analysis of the progression of ischæmia may be performed using the increase in V_{rest} in Fig. 6.12 as a proxy for increase in ischæmic progression. As V_{rest} increases (and during the progression of ischæmia), the variability of $(dV_m/dt)_{max}$ decreases. For lesser values of V_{rest}, an increase in V_{rest} correlates with an increase in $(dV_m/dt)_{max}$, though with minimum values within the population increasing at a faster rate (resulting in the aforementioned decrease in variability). Once $V_{rest} \gtrsim -85$ mV, this increase in $(dV_m/dt)_{max}$ is halted. However, this does not result in a uniform decrease in $(dV_m/dt)_{max}$—rather, the minimum values within the population remain relatively steady, while the maximum values decrease, again resulting in a decrease in variability. Once V_{rest} exceeds -80 mV, all measured values of $(dV_m/dt)_{max}$ in the population fall, though with maximum values falling faster, resulting in further decrease in variability. It should be noted that for high values of V_{rest} (which here correspond to severe ischæmia/high $[K^+]_o$), the results for $(dV_m/dt)_{max}$ likely reflect a lower bound provided by the application of I_{stim}.

6.5 Summary

This chapter shows the results of investigation into variability in the ischæmic milieu. This was in two forms: firstly, the effect of applying conditions that represent ischæmia on the variability shown by the model populations derived in the previous chapter. Secondly, the ischæmic parameter space itself was investigated, and the effects of these ischæmic parameters, both individually and in concert, was investigated.

The initially stated hypothesis for the work presented in this chapter was that the effects of ischæmia would work to increase variability within a population of models, indicating increased heterogeneity in tissue that could prove to be arrhythmogenic. The results, which agree qualitatively with the experimental data regarding the evolution of key biomarkers, provide no clear answer to this hypothesis, with changes in variability depending on several different factors, including: (i) the model framework being used, (ii) the severity of the ischæmic conditions being simulated, (iii) the biomarker being assessed. The results do, however, indicate significant changes in the relation between APD_{90} and ERP, caused principally by changes in V_{rest}.

The effect of simulated ischæmia on cellular repolarisation of the model populations was compared to experimental values from the literature, and indicated that the value of $g_{K\text{-}ATP}$ was miscalibrated, leading to excessive shortening of the AP by $I_{K\text{-}ATP}$. This is despite the peak conductance of $I_{K\text{-}ATP}$ during ischæmia being trained to match previous studies, thus demonstrating the importance of ensuring a model's parameters are entirely suited to the question being posed. While the results indicated that changing $[K^+]_o$ from its 'normal' value to a value of 17 mM could produce significant decreases in APD_{90}, it is concluded that the action of $I_{K\text{-}ATP}$ is the principal cause. Population variability of APD_{90} did not consistently increase with ischæmic severity, but rather showed a decline during early Phase 1A ischæmia, before increasing again. The extent of repolarisation variability was population dependent, with the Mahajan population demonstrating significantly greater variability. The interaction of the parameters used to simulate ischæmia resulted in unpredictable patterns of repolarisation within the population, which could not easily be predicted by any other means.

Under normal conditions, cellular excitability was recovered at approximately the same moment as repolarisation was completed (as was expected). As ischæmia progressed, the correlation between repolarisation and excitability remained strong, even if the precise nature of the relation between the two changed (demonstrating a steady increase in post-repolarisation refractoriness). The changes in variability for the ERP thus closely mirror the changes in variability for APD_{90}, with very little variability evident in PRR. However, as ischæmic severity increased beyond ∼6 min PO, the correlation between the two decreases for both populations, with a consequent increase in variability in PRR. The results are unable to describe fully the extent of the breakdown in correlation under conditions of late Phase 1A ischæmia due to the method of calculating ERP, with results indicating that ERP increases rapidly once V_{rest} passes a threshold value. This threshold value, which is difficult to predict from the framework equations, is similar between the two populations.

This chapter also investigated the effect of ischæmia on other commonly used biomarkers, and confirmed the population responses qualitatively matched experimental literature. Changes in the relative importance of ion channel conductances within the populations were also calculated, and compared to the results from the previous chapter—much as changes in CL lead to changes in relative importances, ischæmia precipitates changes in the population distribution of APD_{90}. Similarly, the distribution of models, *i.e.* which models produce the minimum/maximum values of particular biomarkers, does not remain constant.

The potential implications of model inexcitability were also examined—while the Shannon population demonstrated a clear, binary distinction between 'excitable' and 'inexcitable', the Mahajan population demonstrated a graded 'collapse' of the AP that meant distinguishing between the two was difficult. This graded collapse (also present to a smaller degree in the Shannon population) further emphasised the importance of population modelling in understanding pathological response.

7 Conclusions

Now this is not the end. It is not even the beginning of the end. But it is, perhaps, the end of the beginning.

Winston Churchill

This dissertation concludes with a summary of the results presented within. The thesis originally posed is addressed, with brief synopses of the preceding chapters and how the results presented there are relevant to the thesis. The key contributions of this dissertation to the corpus of knowledge are outlined, and placed in context regarding the existing literature. Possible avenues for future work are outlined, before concluding remarks are given.

7.1 Summary

Due to its severity, high incidence, and high physical and economic cost, it is unsurprising that such effort is expended to elucidate the mechanisms behind sudden cardiac death. This thesis continues in this tradition, and looks to shed some light on the interactions between variability and ischæmia, two properties which are known for their arrhythmogenic properties. More specifically, this thesis looked to focus on the computational modelling of variability and its application to ischæmia. The thesis originally posed was thus:

> The variability in cellular repolarisation exhibited in the experimental literature for rabbit ventricle data can be reproduced by use of a population of computational models.

The variability reproduced therein will then increase when the population is subjected to conditions simulating acute phase 1A ischæmia.

This thesis was then investigated by specifying 3 separate goals, with each one building on the advances offered by the previous goal. These goals were:

1. Investigate the effects of variability in ion channel conductance on the repolarisation of computational models of rabbit ventricular cardiomyocytes.
2. Derive model populations that reproduce experimentally observed variation.
3. Determine the effects of ischæmic conditions on the variability exhibited by these populations.

The background necessary for this thesis was provided in Chapters 2 and 3. The physiological background provided details covering the basic electrophysiology of the heart, with further detail given on cardiomyocytes and ion channels that are the focus of this investigation. How these ion channels interact in producing the cellular action potential was discussed, both in terms of membrane potential and Ca^{2+} dynamics. A brief summary was given on cardiac dysfunction, with the main focus being on ischæmia: the causes of changes in the AP are described, and some of the effects of the changes caused by ischæmia are explained. Finally, some of the mechanisms by which arrhythmias are generated, whose incidence is increased by acute ischæmia, are mentioned.

Chapter 3 provided the background necessary for the computational modelling used in this thesis. A summary of the development of computational models of cardiac electrophysiology was given, with outlines of some of the key concepts involved in computational modelling of the heart. Various methods for reproducing variability in a computational environment were summarised, which in turn lead to the adoption of parameter sweeps and population modelling as the cornerstone for this thesis. A review of some of the current methods employed to simulate the effects of ischæmia was given.

With this background in place, Chapter 4 outlined how the simulations in this dissertation were conducted. The details regarding the parameter sweep method were outlined, and how the model frame-

works were adapted to permit investigation of the effects of ischæmia. The Nimrod/G distributed computing grid was described. Analysis techniques were outlined, including how multi-dimensional data was to be represented in order to permit effective analysis, and how, in particular, the biomarkers were calculated.

All simulations in this thesis are conducted based on the model frameworks originally presented in Shannon *et al.* (2004) and Mahajan *et al.* (2008), which are designed to reproduce the action potential for rabbit ventricular myocytes. Rabbit models, and rabbit data, are used in this thesis due to (i) the wealth of available experimental data for comparison, and (ii) the ability of rabbit hearts to reproduce many of the salient features of human hearts, especially in electrophysiological response to ischæmia. These models in particular are used due to their biophysically detailed nature, permitting convincing analysis of the effects of specific changes to specific ion channel conductances.

Chapter 5 demonstrated results appropriate to the first half of the thesis, and covered Goals 1 and 2. The main focus of this chapter was on the effects of variation on cell models, and how variability in six different ion channel conductances (listed in §5.2) interact to produce changes on the higher-level phenomenon of the action potential. The first result presented in this chapter was an assessment of the relative accuracy of commonly used biomarkers in determining goodness-of-fit to given training data. By determining which models fit a specified output using the 'gold standard' of the NRMSD metrics, and comparing how closely these same models were predicted using combinations of other common biomarkers (defined in §4.3), APD_{50} and APD_{90} were determined to be the most accurate combination of commonly available biomarkers; in situations where Ca^{2+} data were also available, CaT increased the degree of overlap between those models judged as matching as determined by the biomarkers and those determined by the NRMSD metrics, and thus was judged to increase the accuracy of the fit to training data.

The effect of simultaneous variation in multiple parameters describing peak conductance through several ion channels important for cellular repolarisation was then investigated for the Shannon and Mahajan model frameworks. By using the parameter sweep method to comprehensively investigate the parameter space, themes and relations were determined. These themes included details regard-

ing the importance of individual ion channel conductances to particular biomarkers, and how these conductances demonstrated relations to each other to produce a particular outcome to a particular biomarker. These relative importances and inter-connections differed between the two model populations, despite the Mahajan framework sharing a large part of its equations with the Shannon framework. This served to emphasise the non-linear nature of cell models, wherein small changes in a single equation can have profound impacts on the eventual outcome due to the interactions between components leading to emergent phenomena. This is further demonstrated by the extent of changes observed in the currents exceeding the changes made to the conductances. The results also demonstrated the importance of pacing rate to the parameter space, with the relative importance of conductances and relations between conductances changing based on the pacing rate.

Using the results from the parameter sweep, models that produced APD_{50} and APD_{90} within an experimentally derived range to reproduce variability in these biomarkers were isolated, and thus two model populations (one for the Shannon framework, one for the Mahajan framework) were defined. The patterns of conductances within these populations was examined, with the changes in conductances required to maintain a physiological output noted. As such, the first part of the originally posed thesis, which mainted that experimental variability could be reproduced computationally using a population approach, was confirmed.

These model populations were then used to investigate the consequences of acute Phase 1A ischæmia in Chapter 6, after being adapted as detailed in §4.1.2. The results demonstrated the changes in variability of cellular repolarisation due to ischæmia, and allowed elucidation of the driving mechanisms behind these changes. Unexpected transient phenomena were noted for some models within the population under certain conditions. These included slowed secondary depolarisation, leading to a reduced plateau of the AP and more rapid repolarisation, which was noted for unpredictable values of $f_{\text{K-ATP}}$. The influence of $[K^+]_o$ on APD_{90} was also chaotic. In the midst of these results, the second part of the posed thesis can only be answered ambiguously, in that any increase in variability caused by ischæmia is dependent on (i) the precise conditions being simulated, (ii) the model framework being used, and (iii) the biomarker being assessed. However, the total combination of these considerations

does indicate a potentially significant rôle for underlying variability is assessing arrhythmogenic risk.

Under most circumstances, ERP and APD_{90} demonstrated a high degree of correlation—the extent of this correlation, and the conditions under which it breaks down, were investigated. Furthermore, the precise *relationship* that exists between APD_{90}, and how it changes in response to ischæmia, was elucidated; this includes consideration not just of how effectively APD_{90} can be used to predict ERP under several different conditions, but also how a model's APD_{90} value relative to other values within the population can be used to predict its relative value under different conditions.

Changes in the relative importance of ion channel conductances caused by ischæmic conditions were investigated. Finally, changes due to ischæmia in the population level response of biomarkers other than APD_{90} and ERP, and yet still implicated for their importance in determining risk for re-entry, are considered.

The population response to ischæmia, and particularly the changes in population variability, are not easily predictable—increasing ischæmic severity does not necessarily lead to an increase in population variability, and nor does it necessarily lead to a decrease. Changes in the population response could not be reliably predicted solely by knowledge of the changes that underlie ischæmia, *i.e.* knowledge of the effect of hyperkalæmia, acidosis and anoxia as separate conditions does not provide knowledge of the overall ischæmic response. This can be demonstrated by consideration of the dome collapse phenomenon of the Mahajan population, with the results indicating that application of any individual condition underlying ischæmia only *primes* the population for dome collapse, and the phenomenon occurs in response to multiple conditions working in unison.

The several transient phenomenon noted in the dissertation also served to demonstrate the potential significance of population modelling. Transient phenomena, or those that occur gradually across the entire population, are evident only in the context of the entire population—examination of a single model in isolation does not reveal the full extent of these phenomena.

The data presented also indicated the profound effects ischæmia (and potentially, the cellular environment generally) can have on the input/output mapping of parameters, with the relation for biomarker distribution amongst the population subject to significant change. The effect of the cellular environ-

ment can be especially significant, causing a complete failure of a particular model to produce an AP in response to stimulation. Such inexcitability could, in tissue, prove to be significantly arrhythmogenic.

7.2 Key Contributions & Findings

As with almost all scientific advances, this work cannot stand in isolation—it both builds on, and complements, existing work. The work presented here may be considered a natural extension of the work and results initially presented in Romero *et al.* (2009a) and Romero *et al.* (2011), wherein the effect of single parameter variation in ventricular cell models was investigated. The results in this work are achieved by applying the parameter sweep methodology used in prior neuroscience work to the cardiac electrophysiology domain (Taylor *et al.*, 2009; Marder and Taylor, 2011). Notable work has already been done to investigate the variability of populations, with perhaps the most significant to date, apart from the work presented within this dissertation, by Britton *et al.* (2013). However, this work sampled from the parameter space, rather than exhaustively sweeping it, and is thus likely to give an incomplete picture. Similarly, the complementary results obtained through multi-variable regression analysis (Sobie, 2009; Sarkar and Sobie, 2010, 2011) also sample from the parameter space to determine the effects of different parameters on different biomarkers. We presented results in Gemmell *et al.* (2010) that indicated that 'islands' of particular behaviour can exist within a population, which could be missed by either of these approaches.

Furthermore, by use of the parameter sweep, coupled with clutter-based dimension reordering to provide a visual representation of these results, it is possible to provide in-depth investigation of the interactions between parameters for each tested biomarker. Significantly, this provided evidence for complicated interactions between ion channels that are difficult to predict, and can vary depending on the environmental conditions such as pacing rate—similar results were demonstrated in the stochastic study in Heijman *et al.* (2013), indicating that the importance of these interactions is not a coincidence of the modelling choice, but rather an important physiological reality. The results of this thesis further indicated the importance of considering multiple data sets in deriving model response, with changes in environment having significant influences on model response.

By detailed investigation of the multi-dimensional parameter space, comprehensive model populations could be defined that successfully reproduce ranges for APD that are derived to represent experimentally observed reality. These model populations were then successfully used to investigate the effects of ischæmia on population, and not just model, response. By this process, insights into the interactions of the individual conditions, that considered together are regarded as sufficient to constitute ischæmia, were gained. This served to highlight once more the non-linearity of models and model repsonses at all scales, from individual ion channels to environmental factors. These non-linear population effects result in responses to ischæmia and its related conditions that are impossible to predict from single model simulations—processes such as dome collapse, or slowed repolarisation, or the potential effect of f_{NaK} on the ischæmic response, would be impossible to place in full context without full population results. Furthermore, the model properties within the population are not constant, with the model that produces the minimum value for a given biomarker under certain conditions not necessarily doing so under alternative conditions.

7.3 Future Work

One of the key aspects of this work is to prove the validity of the parameter sweep and population modelling approaches to problems in cardiac electrophysiology. This work has demonstrated that the population methodology has great power to comprehensively investigate the effect of variability of input parameters, and reproduce the effects of population variability. Furthermore, these benefits come with the potential to be easily scalable and parallelisable, thus bringing modelling of variability to a far more computationally tractable level.

Future avenues can work to extend these approaches, either by means of increasing the range or resolution of the parameters being varied, the number of parameters being varied, or the problem to which the approach is applied. It is to be noted that the potential future applications of the population modelling methodology are vast, with any given pathological condition being amenable to examination with this technique. With suitable computational resources at the investigator's disposal, the possible breadth and depth of any given population is significant, and with it the potential ability to

resolve the causes and consequences of variability. Arguably, the greatest limitation is the ability to interpret the generated data, but the judicious application of the visualisation techniques used in this dissertation provide a means to overcome this obstacle.

The computational load in defining further populations is potentially reduced by the indicative results presented in this thesis regarding population connectivity. The extension of the work would thus look to explore the 'boundaries' of the population in the parameter space, and determining whether any apparent 'island' populations are connected to the main population via variations in other parameters.

Another natural extension of the work in this thesis is to investigate the effects of tissue modelling on the variability exhibited in population modelling—it has already been mentioned that the electrotonic coupling between cells works to reduce variability. With this coupling reduced the *measured* variability, it is possible that uncoupled cells would demonstrate far greater variability than that mooted here, with the differences being 'smoothed out' across the tissue. Similarly, some of the phenomena noted in this study may, in tissue, prove to be red herrings—electrotonic interactions may work to eliminate gradual dome collapse and other such phenomena. However, such theories would need to be tested. Tissue modelling would also permit a diffferent (and perhaps more accurate) assessment of ERP.

A topic of growing importance within cardiac computational biology is that of drug effects—a significant portion of the costs of drug development come from research into compounds that fail safety testing. Computational biology offers an efficient means of testing possible interactions, and significant work has already been performed, demonstrating the utility of computational modelling (Mirams *et al.*, 2011; Davies *et al.*, 2012; Beattie *et al.*, 2013; Britton *et al.*, 2013; Elkins *et al.*, 2013; Zemzemi *et al.*, 2013). The model population approach used in this thesis provides a computationally efficient means of reproducing variability, and thus is ideally suited to high-throughput simulations to determine the possible side-effects of drug block.

Diffusion

This appendix gives greater detail about the ionic movement theories, and electric theory properties generally, of the modelling of electrically active cells—note that this applies equally well to both cardiac cells and to neurons.

A.1 Simple Diffusion

Simple diffusion refers to the net movement of particles from a region of high concentration to a region of low concentration with simple thermal movement. This movement can be described according to Fick's Law, which relates the diffusive flux to the concentration gradient under the assumption of steady state. It should be noted that this represents *net* diffusion: there will be movement of particles in both directions.

In one spatial dimension, this can be represented as

$$F_X = -D\frac{\partial C_X}{\partial x}, \tag{A.1}$$

where F_X and C_X represent the flux and concentration of particle X respectively, and D represents the diffusion coefficient (also called the diffusivity). D is proportional to the squared velocity of the diffusing particles, and is thus dependent on the temperature of the system, viscosity of the fluid and the size of the particles. In two or more dimensions, Fick's Law can be generalised as

$$\mathbf{F}_X = -D\nabla C_X. \tag{A.2}$$

In the above equations, D is assumed to be a constant for all values of $\mathbf{x}$. However, this does not necessarily have to be the case, and in instances where diffusion is being considered through an anisotropic medium (*i.e.* with different diffusivity in different directions), D represents a symmetric tensor.

For circumstances where D is constant, Eq. (A.1) can be solved to produce

$$F_X = P(C_{X,o} - C_{X,i}), \tag{A.3}$$

where P represents the permeability of the medium, and is equivalent to D/d, where d represents the thickness of the medium; this can be extended to solve for Eq. (A.2). $C_{X,o}$ and $C_{x,i}$ represent the extracellular and intracellular concentrations of X, respectively; thus F_X in this form describes flux from the extra- to the intracellular space. It can be noted that for substances that diffuse through the lipid phase of the membrane, the permeability also depends on the oil/water partition coefficient β, according to $P = \beta\mathrm{D}/\mathrm{d}$.

The above solution is true only momentarily—it makes no account for changes with time. Conservation of mass implies that the rate of change in concentration within a given region is equal to the flux of X from that region. Application of this principle to Eq. (A.1) allows derivation of the *diffusion equation* for one dimension:

$$\frac{\partial C_X}{\partial t} = -\frac{\partial F_X}{\partial x}, \tag{A.4}$$

$$= D\frac{\partial^2 C_X}{\partial x^2}. \tag{A.5}$$

This is easily extensible to multiple dimensions, where the diffusion equation is given according to

$$\frac{\partial C_X}{\partial t} = \nabla \cdot (D\nabla C_X), \tag{A.6}$$

and is valid for cases when D is a symmetric tensor (as mentioned earlier). If D does not vary according to position or concentration, the right-hand side of the equation simplifies to $D\nabla^2 C_X$.

A.2 Facilitated Diffusion, Michaelis-Menten Kinetics

Fick's Law and the diffusion equation are entirely suitable and appropriate in cases where the movement of the substance is driven purely by the concentration gradient. However, a problem is presented by larger molecules that are too large to diffuse across the membrane. A simple pore would

not permit selectivity of substance movement across the membrane, and thus specific channels are designed to facilitate the movement of specific substances across the membrane, while still permitting selectivity of transport. This mediated transfer of substances across the membrane is referred to as *carrier-mediated diffusion* (or facilitated diffusion), and represents a situation where the movement of the substance from the extracellular space to the intracellular space is via an intermediate state. This intermediate state is often where a channel binds the the substance being translocated, and a conformational change moves the substance across the membrane. This mechanism can be described using *Michaelis-Menten kinetics*, with the reaction being a translation of substance across the membrane rather than a chemical reaction.

The process of moving a substance X from the extracellular environment to the intracellular environment via a carrier/channel C can be thought of as a two step reaction. The first step is a binding of the substance to the carrier for translocation, and the second step is the release after translocation. By analogy to a chemical reaction, this may be represented as

$$\mathrm{C} + \mathrm{X_o} \rightleftharpoons \mathrm{CX} \rightleftharpoons \mathrm{C} + \mathrm{X_i}, \tag{A.7}$$

where $\mathrm{X_o}$ and $\mathrm{X_i}$ represent the extracellular and intracellular substance respectively, and C the carrier; CX represents the translocation process. Eq. (A.7) is a reversible reaction—it is as able to move the substance from the intracellular to the extracellular environment as *vice versa*. However, it is assumed that the rate of binding between the intracellular substance and the carrier is negligible, providing the working situation of

$$\mathrm{C} + \mathrm{X_o} \underset{k_{-1}}{\overset{k_1}{\rightleftharpoons}} \mathrm{CX} \xrightarrow{k_2} \mathrm{C} + \mathrm{X_i}, \tag{A.8}$$

where k_1, k_{-1}, k_2 represent the rate constants for the transitions between these states. The rate of 'concentration' change of the bound form CX can be calculated according to

$$\frac{\mathrm{d}[\mathrm{CX}]}{dt} = -k_{-1}[\mathrm{CX}] - k_2[\mathrm{CX}] + k_1[C][\mathrm{X_o}] \tag{A.9}$$

If we assume a quasi-steady state, wherein $\mathrm{d}[\mathrm{CX}]/\mathrm{d}t = 0$, and perform a partial substitution of ($[\mathrm{C_T}]$ = [CX] + [C]) where $[\mathrm{C_T}]$ represents the *total* concentration of channels, we can represent [CX] as

$$[\mathrm{CX}] = \frac{k_1[\mathrm{C_T}][\mathrm{X_o}]}{(k_{-1} + k_2) + k_1[\mathrm{X_o}]} \tag{A.10}$$

$$= \frac{[\mathrm{C_T}][\mathrm{X_o}]}{K_m + [\mathrm{X_o}]} \tag{A.11}$$

where $K_m = (k_{-1} + k_2)/k_1$, and is referred to as the Michaelis-Menten constant. From this, the velocity v of the reaction (*i.e.*the rate at which X is translocated across the membrane) can be represented by

$$v = k_2[\mathrm{CX}] = k_2 \frac{[\mathrm{C_T}][\mathrm{X_o}]}{K_m + [\mathrm{X_o}]}, \tag{A.12}$$

$$= v_{\max} \frac{[\mathrm{X_o}]}{K_m + [\mathrm{X_o}]}, \tag{A.13}$$

where $v_{\max}$ represents the maximum velocity at which the translocation can take place. From this expression, it can be seen that K_m represents the concentration at which the half-maximum speed occurs.

This derivation demonstrates that facilitated diffusion suffers from saturation (the point at which increasing the extracellular concentration further does not lead to an increase in flux). However, it should be noted that the above derivation makes no account of competitive and non-competitive inhibition or stereo-specificity. Furthermore, in comparison to pores directly through the membrane, facilitated diffusion suffers from a relatively slow turnover.

A.3 Electrodiffusion

This section deals with the form of transportation that is of most interest for this thesis: the passive movement of charged substances (ions) in the presences of an electrochemical gradient. It should be noted that the content in this section, while being in the appendix, is nonetheless vital for almost all mathematical models of electrically active cellular activity.

A.3.1 The Nernst Equation

A key concept is that of the *Nernst Potential* (also called the reversal potential), derived using the Nernst Equation, which describes the potential difference across the cell membrane that is required to oppose the net flow of an ionic species against a specified concentration gradient. Thus it must be remembered that this is not a phenomenological equation, with parameters fitted to match data: the results here are entirely, completely accurate (within the approximations made). The equation shall here be derived in full using statistical mechanics.

Initially, recall that the probability of a system being in a particular state α is given by

$$P(\alpha) = \frac{1}{Z} e^{-\beta E_\alpha}; \qquad Z = \sum_i e^{\beta E_i}, \tag{A.14}$$

where E_i is the energy of state i, and $\beta = k_\mathrm{B} T$, with T being the absolute temperature of the system.

For a large number of molecules, $[A] \propto P(A)$. Furthermore, if we consider the diffusion of ions from one location to another to be a reversible reaction according to A $\underset{k_2}{\overset{k_1}{\rightleftharpoons}}$ B, by applying the law of mass action ($F_{A \to B} \propto [A]$), at steady state we achieve the following equation, which can be manipulated accordingly:

$$k_1[A] = k_2[B] \tag{A.15}$$

$$\frac{[A]}{[B]} = \frac{k_2}{k_1} \tag{A.16}$$

$$= \frac{\frac{1}{Z} e^{-\beta E_A}}{\frac{1}{Z} e^{-\beta E_B}} \tag{A.17}$$

$$= e^{-\beta (E_A - E_B)} \tag{A.18}$$

$$\Delta E = k_\mathrm{B} T \ln \frac{[B]}{[A]}. \tag{A.19}$$

At this stage, the electric gradient is introduced to the equation as the reason for the energy difference that maintains the steady state, with $\Delta E = zqV$, where z is the valence of the ionic species being considered, q_e is the charge (in this case equal to the charge of an electron, *i.e.* the charge of a singly ionised ion), and V is the potential difference.

$$zq_e V = k_\mathrm{B} T \ln \frac{[B]}{[A]} \tag{A.20}$$

$$V = \frac{k_\mathrm{B} T}{z q_e} \ln \frac{[B]}{[A]} \tag{A.21}$$

$$= \frac{RT}{zF} \ln \frac{[B]}{[A]}. \tag{A.22}$$

Equations A.21 and A.22 are equivalent, the only difference being the constants used in the expression. Eq. A.22 is the more common formulation, using the gas constant R and the Faraday constant F in place of the Boltzmann constant k_B and the electron charge q_e respectively. The Nernst potential is, therefore, the potential difference that must be applied to maintain a specified concentration gradient, and is given by either equation.

When a channel is entirely selective, the reversal potential is given by the Nernst equation for the specific ion. However, some ion channels are permeable to more than one type of ion, in which case their reversal potential for channel α is given by the *Goldman-Hodgkin-Katz equation*:

$$E_\alpha = \frac{RT}{F} \ln \frac{\Sigma_i^N P_{A_i^+}[A_i^+]_\text{o} + \Sigma_j^M P_{B_j^-}[B_j^-]_\text{i}}{\Sigma_i^N P_{A_i^+}[A_i^+]_\text{i} + \Sigma_j^M P_{B_j^-}[B_j^-]_\text{o}}. \tag{A.23}$$

The above equation describes the situation for N different monovalent positive ionic species and M monovalent negative ionic species; different valencies complicate matters further. Here, E_α represents the reversal potential for the channel, *i.e.* the potential at which, with the given ion concentrations, no net electric flow will occur. The permeability of the membrane to a given ionic species X is given by P_X; as with the concentrations, the terms have been split into positive (A_i^+) and negative (B_i^-) ionic terms.

B Changes in APD During Ischæmia

B.1 Literature Data for Ischæmic APD_{90}

The data referenced in Fig. 6.2, regarding data for changes in APD during ischæmia under various experimental conditions, are given in full here. These include further details regarding the experimental protocol for each paper.

Study	Type	Metric	Cycle Length (ms)	Time PO (min)	Value (ms)	% decrease from control
Weiss and Shine (1982)	Septum tissue, global ischæmia	APD	$830 \rightarrow 1,000$	5		9 ± 11
				10		27 ± 10
Weiss *et al.* (1992)	Septum tissue, global ischæmia	APD	800	0	209 ± 13	
				10	161 ± 6	23
Vermeulen *et al.* (1996)	Healthy papillary tissue, global ischæmia	APD_{80}	450	0	159 ± 7.5	
				2	151	5
				4	138	13
				6	130	18
				8	124	22
				10	119	25
Barrett *et al.* (1997)	Whole heart *in vivo*, local ischæmia	APD_{90}	~ 250	0	140	
				1	155	−11
				2	110	21
				3	100	29
				$4 \rightarrow 10$	95	32
Behrens *et al.* (1997)	Langendorff perfused rabbit hearts, local ischæmia	APD_{90}	500	0	154	
				5	148	4
				10	125	19
Huang *et al.* (2004)	Whole heart *in vivo*, local ischæmia	APD_{90}	300	0	232 ± 15	
				5	211 ± 22	9
				15	198 ± 19	15
Guo *et al.* (2012)	Whole heart *in vivo*, local ischæmia	APD_{90}	~ 630	0	118	
				5	140	−19
				10	100 ± 19	15

Table B.1: *Changes in APD values observed in the experimental literature for rabbit, under specified experimental conditions, at specified durations of ischæmia. In cases where the original paper does not specify the extent of repolarisation used to calculate APD, or where the method used does not permit such specificity, it is referred to as 'APD'. Where possible, data are given as mean±standard deviation; in many cases, the data are estimated from figures provided in the paper. Weiss and Shine (1982) does not give actual APD values, but instead gives the values for* $APD/APD_{control}$*, which are given here.*

Cycle Length (ms)	Time PO (min)	Right Ventricle APD	Right Ventricle % decrease from control	Left Ventricle APD	Left Ventricle % decrease from control
800	0.0	193		183	
	0.5	210	−9	191	−4
	1.0	221	−15	201	−10
	1.5	235	−22	204	−11
	2.0	238	−23	191	−4
	2.5	218	−13	184	−1
	3.0	210	−9	178	3
	3.5	204	−6	172	6
	4.0	195	−1	168	8
	4.5	187	3	163	11
	5.0	185	4	154	16
	5.5	179	7	148	19
	6.0	172	11	140	23
400 (Short)	0.0	151		148	
	0.5	177	−17	159	−7
	1.0	197	−30	164	−11
	1.5	216	−42	179	−21
	2.0	218	−43	168	−14
	2.5	203	−34	144	3
	3.0	185	−22	141	5
	3.5	165	−9	121	18
	4.0	152	−1	112	24
	4.5	154	−2	103	30
	5.0	149	1	105	29
	5.5	144	5	90	39
	6.0	130	14	80	46
400 (Long)	0.0	151		148	
	0.5	177	−17	159	−7
	1.0	197	−30	164	−11
	1.5	216	−42	179	−21
	2.0	218	−43	169	−14
	2.5	203	−34	150	−1
	3.0	188	−25	144	3
	3.5	168	−11	138	7
	4.0	158	−5	130	12
	4.5	159	−5	123	17
	5.0	154	−2	127	14
	5.5	150	1	125	16
	6.0	137	9	121	18

TABLE B.2: *Changes in APD values during ischæmia reported in Kurz* et al. *(1993)—these figures are derived from Figure 2 of that paper. This study used Lagendorff-perfused rabbit hearts undergoing global ischæmia, with measurements for the AP for both left and right ventricles at different cycle lengths. At short cycle lengths, alternans develops, especially in the left ventricle recordings—data are given as 'short' and 'long'.*

Study	Species	Type	Metric	Cycle Length (ms)	Time PO (min)	Value (ms)	% decrease from control
Downar *et al.* (1977b)	Pig	Whole heart perfused with ischæmia blood	APD_{90}	700	0	231	
					2	218	6
					4	175	24
					8	100	57
					9	100	57
Russell *et al.* (1977)	Dog	Whole heart, local ischæmia	APD	Unknown	0	220	
					2	171	22
					4	141	36
Sutton *et al.* (2000)	Human	Local ischæmia during surgery	APD_{90}	500	0	256 ± 5	
					1	231 ± 6	10
					2	209 ± 8	18
					3	189 ± 9	26

Table B.3: *Changes in APD values observed in the experimental literature for species other than rabbit, under specified experimental conditions, at specified durations of ischæmia. In cases where the original paper does not specify the extent of repolarisation used to calculate APD, or where the method used does not permit such specificity, it is referred to as 'APD'. Where possible, data are given as mean±standard deviation; in many cases, the data are estimated from figures provided in the paper.*

Bibliography

Abramson, D., Bernabeu, M. O., Bethwaite, B., Burrage, K., Corrias, A., Enticott, C., Garic, S., Gavaghan, D. J., Peachey, T., Pitt-Francis, J., Pueyo, E., Rodríguez, B., Sher, A., and Tan, J. (2010). High-throughput cardiac science on the Grid. *Philosophical Transactions of the Royal Society A: Mathematical, Physical and Engineering Sciences*, 368(1925):3907–23.

Abramson, D., Bethwaite, B., Enticott, C., Garic, S., and Peachey, T. (2009). Parameter Space Exploration Using Scientific Workflows. In Allen, G., Nabrzyski, J., Seidel, E., Albada, G. D., Dongarra, J., and Sloot, P. M. A., editors, *Computational Science - ICCS 2009*, volume 5544 of *Lecture Notes in Computer Science*, pages 104–113. Springer Berlin Heidelberg, Berlin, Heidelberg.

Abramson, D., Bethwaite, B., Enticott, C., Garic, S., and Peachey, T. (2011). Parameter Exploration in Science and Engineering Using Many-Task Computing. *IEEE Transactions on Parallel and Distributed Systems*, 22(6):960–973.

Abramson, D., Foster, I., Giddy, J., Lewis, A., Sosic, R., Sutherst, R., and White, N. (1997). The Nimrod Computational Workbench: A Case Study in Desktop Metacomputing. In *20th Australasian Computer Science Conference*.

Abramson, D., Giddy, J., and Kotler, L. (2000). High performance parametric modeling with Nimrod/G: killer application for the global grid? In *14th International Parallel and Distributed Processing Symposium*, pages 520–528, Cancun, Mexico. IEEE Comput. Soc.

Achard, P. and de Schutter, E. (2006). Complex parameter landscape for a complex neuron model. *PLoS Computational Biology*, 2(7):e94.

Adeniran, I., McPate, M. J., Witchel, H. J., Hancox, J. C., and Zhang, H. (2011). Increased Vulnerability of Human Ventricle to Re-entrant Excitation in hERG-linked Variant 1 Short QT Syndrome. *PLoS Computational Biology*, 7(12):e1002313.

Adler, C.-P., Friedburg, H., Herget, G. W., Neuburger, M., and Schwalb, H. (1996). Variability of cardiomyocyte DNA content, ploidy level and nuclear number in mammalian hearts. *Virchows Archiv: An International Journal of Pathology*, 429(2-3):159–64.

Ainseba, B., Bendahmane, M., and Ruiz-Baier, R. (2012). Analysis of an optimal control problem for the tridomain model in cardiac electrophysiology. *Journal of Mathematical Analysis and Applications*, 388(1):231–247.

Aistrup, G. L., Kelly, J. E., Kapur, S., Kowalczyk, M., Sysman-Wolpin, I., Kadish, A. H., and Wasserstrom, J. A. (2006). Pacing-induced heterogeneities in intracellular Ca^{2+} signaling, cardiac alternans, and ventricular arrhythmias in intact rat heart. *Circulation Research*, 99(7):e65–73.

Allen, D. G. and Orchard, C. H. (1983). Intracellular calcium concentration during hypoxia and metabolic inhibition in mammalian ventricular muscle. *Journal of Physiology*, 339(1983):107–22.

Allessie, M. A., Bonke, F. I. M., and Schopman, F. J. G. (1976). Circus movement in rabbit atrial muscle as a mechanism of tachycardia. II. The role of nonuniform recovery of excitability in the occurrence of unidirectional block, as studied with multiple microelectrodes. *Circulation Research*, 39(2):168–77.

Allessie, M. A., Bonke, F. I. M., and Schopman, F. J. G. (1977). Circus movement in rabbit atrial muscle as a mechanism of tachycardia. III. The "leading circle" concept: a new model of circus movement in cardiac tissue without the involvement of an anatomical obstacle. *Circulation Research*, 41(1):9–18.

Alvarez-Lacalle, E., Cantalapiedra, I. R., Peñaranda, A., Cinca, J., Hove-Madsen, L., and Echebarria, B. (2013). Dependency of calcium alternans on ryanodine receptor refractoriness. *PloS One*, 8(2):e55042.

Alwan, A., Armstrong, T., Bettcher, D., Branca, F., Chisholm, D., Ezzati, M., Garfield, R., MacLean, D., Mathers, C., Mendis, S., Poznyak, V., Riley, L., Tang, K. C., and Wild, C. (2010). World Health Organisation Global status report on noncommunicable diseases 2010. Technical report, World Health Organization.

Antzelevitch, C., Sicouri, S., Litovsky, S. H., Lukas, A., Krishnan, S. C., Di Diego, J. M., Gintant, G. A., and Liu, D.-W. (1991). Heterogeneity within the ventricular wall. Electrophysiology and pharmacology of epicardial, endocardial, and M cells. *Circulation Research*, 69(6):1427–1449.

Applegate, R. J., Walsh, R. A., and O'Rourke, R. A. (1987). Effects of nifedipine on diastolic function during brief periods of flow-limiting ischemia in the conscious dog. *Circulation*, 76(6):1409–21.

Arevalo, H., Rodríguez, B., and Trayanova, N. A. (2007). Arrhythmogenesis in the heart: Multiscale modeling of the effects of defibrillation shocks and the role of electrophysiological heterogeneity. *Chaos*, 17(1):015103.

Armstrong, C. M. and Bezanilla, F. (1977). Inactivation of the sodium channel. II. Gating current experiments. *Journal of General Physiology*, 70(5):567–90.

Auerbach, D. S., Grzęda, K. R., Furspan, P. B., Sato, P. Y., Mironov, S. F., and Jalife, J. (2011). Structural heterogeneity promotes triggered activity, reflection and arrhythmogenesis in cardiomyocyte monolayers. *Journal of Physiology*, 589(Pt 9):2363–81.

Avitall, B. (1979). Computer simulation of ventricular tachyarrhythmias during coronary artery ligation and release. *Journal of Electrocardiology*, 12(1):17–22.

Barrett, T. D., MacLeod, B. A., and Walker, M. J. A. (1997). A model of myocardial ischemia for the simultaneous assessment of electrophysiological changes and arrhythmias in intact rabbits. *Journal of Pharmacological and Toxicological Methods*, 37(1):27–36.

Bassani, J. W. M., Bassani, R. A., and Bers, D. M. (1994). Relaxation in rabbit and rat cardiac cells: species-dependent differences in cellular mechanisms. *Journal of Physiology*, 476(2):279–93.

Bassani, R. A., Altamirano, J., Puglisi, J. L., and Bers, D. M. (2004). Action potential duration determines sarcoplasmic reticulum Ca^{2+} reloading in mammalian ventricular myocytes. *Journal of Physiology*, 559(Pt 2):593–609.

Beattie, K. A., Luscombe, C., Williams, G., Munoz-Muriedas, J., Gavaghan, D. J., Cui, Y., and Mirams, G. R. (2013). Evaluation of an in silico cardiac safety assay: using ion channel screening data to predict QT interval changes in the rabbit ventricular wedge. *Journal of Pharmacological and Toxicological Methods*, 68(1):88–96.

Beeler, G. W. and Reuter, H. (1977). Reconstruction of the Action Potential of Ventricular Myocardial Fibres. *Journal of Physiology*, 268:177–210.

Behrens, S., Li, C., and Franz, M. R. (1997). Effects of myocardial ischemia on ventricular fibrillation inducibility and defibrillation efficacy. *Journal of the American College of Cardiology*, 29(4):817–24.

Bers, D. M. (1991). *Excitation-Contraction Coupling and Cardiac Contractile Force*. Kluwer.

Bers, D. M. and Berlin, J. R. (1995). Kinetics of $[Ca]_i$ decline in cardiac myocytes depend on peak $[Ca]_i$. *American Journal of Physiology*, 268(1 Pt 1):C271–7.

Bers, D. M. and Ellis, D. (1982). Intracellular calcium and sodium activity in sheep heart Purkinje fibres. Effect of changes of external sodium and intracellular pH. *Pflügers Archiv: European Journal of Physiology*, 393(2):171–8.

Bezanilla, F. (2000). The voltage sensor in voltage-dependent ion channels. *Physiological Reviews*, 80(2):555–92.

Bezanilla, F. and Armstrong, C. M. (1977). Inactivation of the sodium channel. I. Sodium Current Experiments. *Journal of General Physiology*, 70(5):549–66.

Bhalla, U. S. and Bower, J. M. (1993). Exploring parameter space in detailed single neuron models: simulations of the mitral and granule cells of the olfactory bulb. *Journal of Neurophysiology*, 69(6):1948–65.

Bhargava, A., Lin, X., Novak, P., Mehta, K., Khorchev, Y., Delmar, M., and Gorelik, J. (2013). Super-Resolution Scanning Patch-Clamp Reveals Clustering of Functional Ion Channels in the Adult Ventricular Myocyte. *Circulation Research*, pages 1112–1120.

Biagetti, M. O. and Quinteiro, R. A. (2006). Gender differences in electrical remodeling and susceptibility to ventricular arrhythmias in rabbits with left ventricular hypertrophy. *Heart Rhythm: The Official Journal of the Heart Rhythm Society*, 3(7):832–9.

Blanchard, E. M. and Solaro, R. J. (1984). Inhibition of the activation and troponin calcium binding of dog cardiac myofibrils by acidic pH. *Circulation Research*, 55:382–91.

Bourdillon, P. D. and Poole-Wilson, P. A. (1982). The effects of verapamil, quiescence, and cardioplegia on calcium exchange and mechanical function in ischemic rabbit myocardium. *Circulation Research*, 50:360–8.

Britton, O. J., Bueno-Orovio, A., van Ammel, K., Lu, H. R., Towart, R., Gallacher, D. J., and Rodríguez, B. (2013). Experimentally calibrated population of models predicts and explains intersubject variability in cardiac cellular electrophysiology. *Proceedings of the National Academy of Sciences of the United States of America*.

Brown, K. S. and Sethna, J. P. (2003). Statistical mechanical approaches to models with many poorly known parameters. *Physical Review E, Statistical, Nonlinear, and Soft Matter Physics*, 68(2):021904.

Bueno-Orovio, A., Cherry, E. M., and Fenton, F. H. (2008). Minimal model for human ventricular action potentials in tissue. *Journal of Theoretical Biology*, 253:544–60.

Cabo, C., Pertsov, A. M., Davidenko, J. M., Baxter, W. T., Gray, R. A., and Jalife, J. (1996). Vortex shedding as a precursor of turbulent electrical activity in cardiac muscle. *Biophysical journal*, 70:1105–11.

Caldwell, B. J., Trew, M. L., Sands, G. B., Hooks, D. A., LeGrice, I. J., and Smaill, B. H. (2009). Three distinct directions of intramural activation reveal nonuniform side-to-side electrical coupling of ventricular myocytes. *Circulation: Arrhythmia and Electrophysiology*, 2(4):433–40.

Caldwell, J., Burton, F. L., Smith, G. L., and Cobbe, S. M. (2007). Heterogeneity of ventricular fibrillation dominant frequency during global ischemia in isolated rabbit hearts. *Journal of Cardiovascular Electrophysiology*, 18(8):854–61.

Camacho, S. A., Brandes, R., Figueredo, V. M., and Weiner, M. W. (1994). Ca^{2+} transient decline and myocardial relaxation are slowed during low flow ischemia in rat hearts. *Journal of Clinical Investigation*, 93:951–7.

Camacho, S. A., Figueredo, V. M., Brandes, R., and Weiner, M. W. (1993). Ca^{2+}-dependent fluorescence transients and phosphate metabolism during low-flow ischemia in rat hearts. *American Journal of Physiology*, 265(1 Pt 2):H114–22.

Carmeliet, E. (1961). Chloride ions and the membrane potential of Purkinje fibres. *Journal of Physiology*, 156:375–388.

Carmeliet, E. (1999). Cardiac ionic currents and acute ischemia: from channels to arrhythmias. *Physiological Reviews*, 79:917–1017.

Carmeliet, E. (2006). Repolarization Reserve in Cardiac Cells. *Journal of Medical and Biological Engineering*, 26:97–105.

Carmeliet, E. and Vereecke, J. (2002). *Cardiac Cellular Electrophysiology*. Springer.

Carusi, A., Burrage, K., and Rodríguez, B. (2012). Bridging experiments, models and simulations: an integrative approach to validation in computational cardiac electrophysiology. *American Journal of Physiology - Heart and Circulatory Physiology*, 303(2):H144–55.

Cascio, W. E. (2001). Myocardial ischemia: what factors determine arrhythmogenesis? *Journal of cardiovascular electrophysiology*, 12(6):726–9.

Ch'en, F. F.-T., Vaughan-Jones, R. D., Clarke, K., and Noble, D. (1998). Modelling myocardial ischaemia and reperfusion. *Progress in Biophysics and Molecular Biology*, 69(2-3):515–38.

Chen, W., Wasserstrom, J. A., and Shiferaw, Y. (2009). Role of coupled gating between cardiac ryanodine receptors in the genesis of triggered arrhythmias. *American Journal of Physiology - Heart and Circulatory Physiology*, 297(1):H171–80.

Chen, X., Cordes, J. S., Bradley, J. A., Sun, Z., and Zhou, J. (2006). Use of arterially perfused rabbit ventricular wedge in predicting arrhythmogenic potentials of drugs. *Journal of Pharmacological and Toxicological Methods*, 54:261–72.

Cherry, E. M. and Fenton, F. H. (2007). A tale of two dogs: analyzing two models of canine ventricular electrophysiology. *American Journal of Physiology - Heart and Circulatory Physiology*, 292(1):H43–55.

Cherry, E. M., Fenton, F. H., and Gilmour, R. F. (2012). Mechanisms of ventricular arrhythmias: a dynamical systems-based perspective. *American Journal of Physiology - Heart and Circulatory Physiology*, 302(12):H2451–63.

Chou, C.-C., Zhou, S., Hayashi, H., Nihei, M., Liu, Y.-B., Wen, M.-S., Yeh, S.-J., Fishbein, M. C., Weiss, J. N., Lin, S.-F., Wu, D., and Chen, P.-S. (2007). Remodelling of action potential and intracellular calcium cycling dynamics during subacute myocardial infarction promotes ventricular arrhythmias in Langendorff-perfused rabbit hearts. *Journal of Physiology*, 580(Pt.3):895–906.

Chudin, E., Goldhaber, J. I., Garfinkel, A., Weiss, J. N., and Kogan, B. (1999). Intracellular Ca^{2+} dynamics and the stability of ventricular tachycardia. *Biophysical Journal*, 77(6):2930–41.

Clancy, C. E. and Kass, R. S. (2005). Inherited and acquired vulnerability to ventricular arrhythmias: cardiac Na^+ and K^+ channels. *Physiological Reviews*, 85(1):33–47.

Clancy, C. E. and Rudy, Y. (1999). Linking a genetic defect to its cellular phenotype in a cardiac arrhythmia. *Nature*, 400(6744):566–9.

Cleemann, L., Wang, W., and Morad, M. (1998). Two-dimensional confocal images of organization, density, and gating of focal Ca^{2+} release sites in rat cardiac myocytes. *Proceedings of the National Academy of Sciences of the United States of America*, 95(18):10984–9.

Clusin, W. T. (1983). Caffeine induces a transient inward current in cultured cardiac cells. *Nature*, 301(5897):248–50.

Clusin, W. T. (2003). Calcium and cardiac arrhythmias: DADs, EADs, and alternans. *Critical Reviews in Clinical Laboratory Sciences*, 40:337–75.

Coetzee, W. A. and Opie, L. H. (1987). Effects of components of ischemia and metabolic inhibition on delayed afterdepolarizations in guinea pig papillary muscle. *Circulation Research*, 61(2):157–65.

Colquhoun, D., Neher, E., Reuter, H., and Stevens, C. F. (1981). Inward current channels activated by intracellular Ca in cultured cardiac cells. *Nature*, 294(5843):752–754.

Connolly, S. J., Camm, A. J., Halperin, J. L., Joyner, C., Alings, M., Amerena, J., Atar, D., Avezum, A., Blomström, P., Borggrefe, M., Budaj, A., Chen, S.-A., Ching, C. K., Commerford, P., Dans, A., Davy, J.-M., Delacrétaz, E., Di Pasquale, G., Diaz, R., Dorian, P., Flaker, G., Golitsyn, S., Gonzalez-Hermosillo, A., Granger, C. B., Heidbüchel, H., Kautzner, J., Kim, J. S., Lanas, F., Lewis, B. S., Merino, J. L., Morillo, C., Murin, J., Narasimhan, C., Paolasso, E., Parkhomenko, A., Peters, N. S., Sim, K.-H., Stiles, M. K., Tanomsup, S., Toivonen, L., Tomcsányi, J., Torp-Pedersen, C., Tse, H.-F., Vardas, P., Vinereanu, D., Xavier, D., Zhu, J., Zhu, J.-R., Baret-Cormel, L., Weinling, E., Staiger, C., Yusuf, S., Chrolavicius, S., Afzal, R., and Hohnloser, S. H. (2011). Dronedarone in high-risk permanent atrial fibrillation. *New England Journal of Medicine*, 365(24):2268–76.

Cook, C., Cole, G., Asaria, P., Jabbour, R., and Francis, D. P. (2014). The annual global economic burden of heart failure. *International Journal of Cardiology*, 171:368–76.

Cook, D. L., Satin, L. S., Ashford, M. L. J., and Hales, C. N. (1988). ATP-sensitive K^+ channels in pancreatic beta-cells. Spare-channel hypothesis. *Diabetes*, 37(5):495–8.

Cooper, J., Mirams, G. R., and Niederer, S. A. (2011). High-throughput functional curation of cellular electrophysiology models. *Progress in Biophysics and Molecular Biology*, 107(1):11–20.

Coronel, R., Janse, M. J., Opthof, T., Wilde, A. A. M., and Taggart, P. (2012). Postrepolarization refractoriness in acute ischemia and after antiarrhythmic drug administration: action potential duration is not always an index of the refractory period. *Heart Rhythm: The Official Journal of the Heart Rhythm Society*, 9(6):977–82.

Coronel, R., Wilms-Schopman, F. J. G., Opthof, T., and Janse, M. J. (2009). Dispersion of repolarization and arrhythmogenesis. *Heart Rhythm: The Official Journal of the Heart Rhythm Society*, 6(4):537–43.

Corrias, A., Giles, W. R., and Rodríguez, B. (2011). Ionic mechanisms of electrophysiological properties and repolarization abnormalities in rabbit Purkinje fibers. *American Journal of Physiology - Heart and Circulatory Physiology*, 300(5):H1806–13.

Cross, H. R., Lu, L., Steenbergen, C., Philipson, K. D., and Murphy, E. (1998). Overexpression of the cardiac Na^+/Ca^{2+} exchanger increases susceptibility to ischemia/reperfusion injury in male, but not female, transgenic mice. *Circulation Research*, 83(12):1215–23.

Dangerfield, C. E., Kay, D., and Burrage, K. (2012). Modeling ion channel dynamics through reflected stochastic differential equations. *Physical Review E, Statistical, Nonlinear, and Soft Matter Physics*, 85(5 Pt 1):051907.

Davies, M. R., Mistry, H. B., Hussein, L., Pollard, C. E., Valentin, J.-P., Swinton, J., and Abi-Gerges, N. (2012). An in silico canine cardiac midmyocardial action potential duration model as a tool for early drug safety assessment. *American Journal of Physiology - Heart and Circulatory Physiology*, 302(7):H1466–80.

Dhalla, N. S., Panagia, V., Singal, P. K., Makino, N., Dixon, I. M. C., and Eyolfson, D. A. (1988). Alterations in heart membrane calcium transport during the development of ischemia-reperfusion injury. *Journal of Molecular and Cellular Cardiology*, 20 Suppl 2(Supplement II):3–13.

DiFrancesco, D. and Noble, D. (1985). A Model of Cardiac Electrical Activity Incorporating Ionic Pumps and Concentration Changes. *Philosophical Transactions of the Royal Society B: Biological Sciences*, 307(1133):353–398.

Downar, E., Janse, M. J., and Durrer, D. (1977a). The effect of acute coronary artery occlusion on subepicardial transmembrane potentials in the intact porcine heart. *Circulation*, 56(2):217–224.

Downar, E., Janse, M. J., and Durrer, D. (1977b). The effect of "ischemic" blood on transmembrane potentials of normal porcine ventricular myocardium. *Circulation*, 55:455–62.

Dumaine, R., Wang, Q., Keating, M. T., Hartmann, H. A., Schwartz, P. J., Brown, A. M., and Kirsch, G. E. (1996). Multiple mechanisms of Na^+ channel-linked long-QT syndrome. *Circulation Research*, 78(5):916–24.

Dutta, S., Bishop, M. J., Pathmanathan, P., Lee, P., Kohl, P., Quinn, T. A., and Rodríguez, B. (2011). Interpreting Optical Mapping Recordings in the Ischemic Heart: A Combined Experimental and Computational Investigation. In *Functional Imaging and Modeling of the Heart*, pages 20–27.

Eckardt, L., Haverkamp, W., Göttker, U., Madeja, M., Johna, R., Borggrefe, M., and Breithardt, G. (1998). Divergent effect of acute ventricular dilatation on the electrophysiologic characteristics of d,l-sotalol and flecainide in the isolated rabbit heart. *Journal of Cardiovascular Electrophysiology*, 9(4):366–83.

Edelman, G. M. and Gally, J. A. (2001). Degeneracy and complexity in biological systems. *Proceedings of the National Academy of Sciences of the United States of America*, 98(24):13763–8.

Eisner, D. A., Choi, H. S., Díaz, M. E., O'Neill, S. C. O., and Trafford, A. W. (2000). Integrative analysis of calcium cycling in cardiac muscle. *Circulation Research*, 87(12):1087–94.

Eisner, D. A. and Sipido, K. R. (2004). Sodium calcium exchange in the heart: necessity or luxury? *Circulation Research*, 95(6):549–51.

Elkins, R. C., Davies, M. R., Brough, S. J., Gavaghan, D. J., Cui, Y., Abi-Gerges, N., and Mirams, G. R. (2013). Variability in high-throughput ion-channel screening data and consequences for cardiac safety assessment. *Journal of Pharmacological and Toxicological Methods*, 68(1):112–22.

Elliott, A. C., Smith, G. L., and Allen, D. G. (1989). Simultaneous measurements of action potential duration and intracellular ATP in isolated ferret hearts exposed to cyanide. *Circulation Research*, 64:583–91.

Esumi, K., Nishida, M., Shaw, D., Smith, T. W., and Marsh, J. D. (1991). NADH measurements in adult rat myocytes during simulated ischemia. *American Journal of Physiology*, 260(6 Pt 2):H1743–52.

Fabiato, A. (1992). Two kinds of calcium-induced release of calcium from the sarcoplasmic reticulum of skinned cardiac cells. *Advances in Experimental Medicine and Biology*, 311:245–62.

Fauconnier, J., Meli, A. C., Thireau, J., Roberge, S., Shan, J., Sassi, Y., Reiken, S. R., Rauzier, J.-M., Marchand, A., Chauvier, D., Cassan, C., Crozier, C., Bideaux, P., Lompré, A.-M., Jacotot, E., Marks, A. R., and Lacampagne, A. (2011). Ryanodine receptor leak mediated by caspase-8 activation leads to left ventricular injury after myocardial ischemia-reperfusion. *Proceedings of the National Academy of Sciences of the United States of America*, 108(32):13258–63.

Fauconnier, J., Roberge, S., Saint, N., and Lacampagne, A. (2013). Type 2 ryanodine receptor: a novel therapeutic target in myocardial ischemia/reperfusion. *Pharmacology & Therapeutics*, 138:323–32.

Fedorov, V. V., Glukhov, A. V., and Chang, R. (2012). Conduction barriers and pathways of the sinoatrial pacemaker complex: their role in normal rhythm and atrial arrhythmias. *American Journal of Physiology - Heart and Circulatory Physiology*, 302(9):H1773–83.

Feher, J. J., LeBolt, W. R., and Manson, N. H. (1989). Differential effect of global ischemia on the ryanodine-sensitive and ryanodine-insensitive calcium uptake of cardiac sarcoplasmic reticulum. *Circulation Research*, 65(5):1400–8.

Ferrero, J. M., Sáiz, J., and Thakor, N. V. (1996). Simulation of Action Potentials From Metabolically Impaired Cardiac Myocytes. *Circulation Research*, 79(2):208–221.

Ferrero, J. M., Trénor, B., Rodríguez, B., and Sáiz, J. (2003a). Electrical Activity and Reentry During Regional Myocardial Ischemia: Insights From Simulations. *International Journal of Bifurcation and Chaos*, 13(12):3703–3715.

Ferrero, J. M., Trénor, B., and Romero, L. (2014). Multiscale computational analysis of the bioelectric consequences of myocardial ischaemia and infarction. *Europace: European Pacing, Arrhythmias, and Cardiac Electrophysiology: Journal of the Working Groups on Cardiac Pacing, Arrhythmias, and Cardiac Cellular Electrophysiology of the European Society of Cardiology*, 16:405–15.

Ferrero, J. M., Trénor, B., Sáiz, J., Montilla, F., and Hernandez, V. (2003b). Electrical activity and reentry in acute regional ischemia: insights from simulations. In *Annual International Conference of the IEEE Engineering in Medicine and Biology Society*, pages 17–20. IEEE.

Ferrier, G. R., Moffat, M. P., and Lukas, A. (1985). Possible mechanisms of ventricular arrhythmias elicited by ischemia followed by reperfusion. Studies on isolated canine ventricular tissues. *Circulation Research*, 56(2):184–94.

Fink, M., Noble, D., Virág, L., Varró, A., and Giles, W. R. (2008). Contributions of HERG K^+ current to repolarization of the human ventricular action potential. *Progress in Biophysics and Molecular Biology*, 96(1-3):357–76.

Fitzhugh, R. (1960). Thresholds and plateaus in the Hodgkin-Huxley nerve equations. *Journal of General Physiology*, 43:867–96.

Fitzhugh, R. (1961). Impulses and Physiological States in Theoretical Models of Nerve Membrane. *Biophysical Journal*, 1(6):445–66.

Forbush, B. (1987). Rapid release of ^{42}K and ^{86}Rb from an occluded state of the Na,K-pump in the presence of ATP or ADP*. *Journal of Biological Chemistry*, 262(23):11104–15.

Franzini-Armstrong, C., Protasi, F., and Tijskens, P. (2005). The assembly of calcium release units in cardiac muscle. *Annals of the New York Academy of Sciences*, 1047:76–85.

Fülöp, L., Bányász, T., Magyar, J., Szentandrássy, N., Varró, A., and Nánási, P. P. (2004). Reopening of L-type calcium channels in human ventricular myocytes during applied epicardial action potentials. *Acta Physiologica Scandinavica*, 180(1):39–47.

Furukawa, T., Kimura, S., Furukawa, N., Bassett, A. L., and Myerburg, R. J. (1991). Role of cardiac ATP-regulated potassium channels in differential responses of endocardial and epicardial cells to ischemia. *Circulation Research*, 68(6):1693–702.

Gaborit, N., Le Bouter, S., Szuts, V., Varró, A., Escande, D., Nattel, S., and Demolombe, S. (2007). Regional and tissue specific transcript signatures of ion channel genes in the non-diseased human heart. *Journal of Physiology*, 582(Pt 2):675–93.

Garfinkel, A., Kim, Y.-H., Voroshilovsky, O., Qu, Z., Kil, J. R., Lee, M.-H., Karagueuzian, H. S., Weiss, J. N., and Chen, P.-S. (2000). Preventing ventricular fibrillation by flattening cardiac restitution. *Proceedings of the National Academy of Sciences of the United States of America*, 97(11):6061–6.

Garny, A., Kohl, P., and Noble, D. (2003). Cellular Open Resource (COR): A Public CellML Based Environment For Modeling Biological Function. *International Journal of Bifurcation and Chaos*, 13(12):3579–3590.

Garny, A., Noble, D., Hunter, P. J., and Kohl, P. (2009). CELLULAR OPEN RESOURCE (COR): current status and future directions. *Philosophical Transactions of the Royal Society A: Mathematical, Physical and Engineering Sciences*, 367(1895):1885–905.

Gasser, R. N. A. and Vaughan-Jones, R. D. (1990). Mechanism of potassium efflux and action potential shortening during ischaemia in isolated mammalian cardiac muscle. *Journal of Physiology*, 431:713–41.

Gemmell, P. M., Burrage, K., Rodríguez, B., and Quinn, T. A. (2010). Exploring the parameter space of a rabbit ventricular action potential model to investigate the effect of variation on action potential and calcium transients. *Annual International Conference of the IEEE Engineering in Medicine and Biology Society*, 2010:2662–5.

Gemmell, P. M., Burrage, K., Rodríguez, B., and Quinn, T. A. (2012). Quantifying Importance of Repolarization Currents Underlying Physiological Variability in Rabbit Cellular Electrophysiology. *Biophysical Journal*, 102:540a.

Gemmell, P. M., Burrage, K., Rodríguez, B., and Quinn, T. A. (2014). Population of computational rabbit-specific ventricular action potential models for investigating sources of variability in cellular repolarisation. *PloS ONE*, 9(2):e90112.

Gemmell, P. M., Burrage, K., Rodríguez, B., and Quinn, T. A. (2015). Effects of ischæmia on variability in model populations of rabbit ventricular myocytes. *In Preparation*.

Giles, W. R. and Imaizumi, Y. (1988). Comparison of potassium currents in rabbit atrial and ventricular cells. *Journal of Physiology*, 405:123–45.

Girod, S. and Becker, A. (2006). Cardiac muscle.

Glynn, P., Unudurthi, S. D., and Hund, T. J. (2014). Mathematical modeling of physiological systems: An essential tool for discovery. *Life Sciences*, 111(1-2):1–5.

Goaillard, J.-M., Taylor, A. L., Schulz, D. J., and Marder, E. (2009). Functional consequences of animal-to-animal variation in circuit parameters. *Nature Neuroscience*, 12(11):1424–30.

Goldhaber, J. I., Xie, L.-H., Duong, T., Motter, C., Khuu, K., and Weiss, J. N. (2005). Action potential duration restitution and alternans in rabbit ventricular myocytes: the key role of intracellular calcium cycling. *Circulation Research*, 96(4):459–66.

Goldman, M. S., Golowasch, J., Marder, E., and Abbott, L. F. (2001). Global structure, robustness, and modulation of neuronal models. *Journal of Neuroscience*, 21(14):5229–38.

Golowasch, J., Goldman, M. S., Abbott, L. F., and Marder, E. (2002). Failure of averaging in the construction of a conductance-based neuron model. *Journal of Neurophysiology*, 87(2):1129–31.

Gough, W. B., Mehra, R., Restivo, M., Zeiler, R. H., and El-Sherif, N. (1985). Reentrant ventricular arrhythmias in the late myocardial infarction period in the dog. 13. Correlation of activation and refractory maps. *Circulation Research*, 57:432–42.

Gray, R. A., Pertsov, A. M., and Jalife, J. (1998). Spatial and temporal organization during cardiac fibrillation. *Nature*, 392(6671):75–8.

Greenstein, J. L. and Winslow, R. L. (2002). An integrative model of the cardiac ventricular myocyte incorporating local control of Ca^{2+} release. *Biophysical Journal*, 83(6):2918–45.

Guo, X., Gao, X., Wang, Y., Peng, L., Zhu, Y., and Wang, S. (2012). I_{Ks} protects from ventricular arrhythmia during cardiac ischemia and reperfusion in rabbits by preserving the repolarization reserve. *PloS One*, 7(2):e31545.

Gutenkunst, R. N., Waterfall, J. J., Casey, F. P., Brown, K. S., Myers, C. R., and Sethna, J. P. (2007). Universally sloppy parameter sensitivities in systems biology models. *PLoS Computational Biology*, 3(10):1871–78.

Haïssaguerre, M., Jaïs, P., Shah, D. C., Takahashi, A., Hocini, M., Quiniou, G., Garrigue, S., Le Mouroux, A., Le Métayer, P., and Clémenty, J. (1998). Spontaneous initiation of atrial fibrillation by ectopic beats originating in the pulmonary veins. *New England Journal of Medicine*, 339(10):659–66.

Hall, A. E., Hutter, O. F., and Noble, D. (1963). Current-Voltage Relations of Purkinje Fibres in Sodium Deficient Solutions. *Journal of Physiology*, 166:225–240.

Harris, A. S., Bisteni, A., Russell, R. A., Brigham, J. C., and Firestone, J. E. (1954). Excitatory factors in ventricular tachycardia resulting from myocardial ischemia. Potassium a major excitant. *Science*, 119(3085):200–3.

Hashambhoy, Y. L., Winslow, R. L., and Greenstein, J. L. (2011). CaMKII-dependent activation of late I_{Na} contributes to cellular arrhythmia in a model of the cardiac myocyte. *Annual International Conference of the IEEE Engineering in Medicine and Biology Society*, pages 4665–8.

Haverkamp, W., Breithardt, G., Camm, A. J., Janse, M. J., Rosen, M. R., Antzelevitch, C., Escande, D., Franz, M. R., Malik, M., Moss, A. J., and Shah, R. (2000). The potential for QT prolongation and pro-arrhythmia by non-anti-arrhythmic drugs: clinical and regulatory implications. Report on a Policy Conference of the European Society of Cardiology. *Cardiovascular Research*, 47(2):219–33.

Heijman, J., Zaza, A., Johnson, D. M., Rudy, Y., Peeters, R. L. M., Volders, P. G. A., and Westra, R. L. (2013). Determinants of Beat-to-Beat Variability of Repolarization Duration in the Canine Ventricular Myocyte: A Computational Analysis. *PLoS Computational Biology*, 9(8):e1003202.

Henderson, S. A., Goldhaber, J. I., So, J. M., Han, T., Motter, C., Ngo, A., Chantawansri, C., Ritter, M. R., Friedlander, M., Nicoll, D. A., Frank, J. S., Jordan, M. C., Roos, K. P., Ross, R. S., and Philipson, K. D. (2004). Functional adult myocardium in the absence of Na^{+}-Ca^{2+} exchange: cardiac-specific knockout of NCX1. *Circulation Research*, 95(6):604–11.

Hindmarsh, A. C., Brown, P. N., Grant, K. E., Lee, S. L., Serban, R., Shumaker, D. E., and Woodward, C. S. (2005). SUNDIALS: Suite of nonlinear and differential/algebraic equation solvers. *ACM Trans. Math. Softw.*, 31:363–396.

Hiraoka, M., Sunami, A., Fan, Z., and Sawanobori, T. (1992). Multiple ionic mechanisms of early afterdepolarizations in isolated ventricular myocytes from guinea-pig hearts. *Annals of the New York Academy of Sciences*, 644:33–47.

Hodgkin, A. L. (1954). A note on conduction velocity. *Journal of Physiology*, 125(1):221–4.

Hodgkin, A. L. and Huxley, A. F. (1952). A quantative description of membrane current and its application to conduction and excitation in nerve. *Journal of Physiology*, 117:500–544.

Hoyt, R. H., Cohen, M. L., and Saffitz, J. E. (1989). Distribution and three-dimensional structure of intercellular junctions in canine myocardium. *Circulation Research*, 64:563–74.

Huang, C., Bao, M., Jiang, H., Liu, J., Yang, B., and Wang, T. (2004). Differences in the changing trends of monophasic action potential duration and effective refractory period of the ventricular myocardium after myocardial infarction in vivo. *Circulation Journal: Official Journal of the Japanese Circulation Society*, 68(12):1205–9.

Hund, T. J., Kucera, J. P., Otani, N. F., and Rudy, Y. (2001). Ionic charge conservation and long-term steady state in the Luo-Rudy dynamic cell model. *Biophysical Journal*, 81(6):3324–31.

Hunter, P. J., Robbins, P., and Noble, D. (2002). The IUPS human Physiome Project. *Pflügers Archiv: European Journal of Physiology*, 445(1):1–9.

Hurst, J. W., Schlant, R. C., Rackley, C. E., Sonnenblick, E. H., and Wenger, N. K. (1990). *The Heart*. McGraw-Hill, 7th edition.

Hutter, O. F. and Noble, D. (1960). Rectifying properties of heart muscle. *Nature*, 188:495.

Ichihara, K., Haga, N., and Abiko, Y. (1984). Is ischemia-induced pH decrease of dog myocardium respiratory or metabolic acidosis? *American Journal of Physiology*, 246(5 Pt 2):H652–7.

Inoue, R., Jensen, L. J., Shi, J., Morita, H., Nishida, M., Honda, A., and I_{to}, Y. (2006). Transient receptor potential channels in cardiovascular function and disease. *Circulation Research*, 99(2):119–31.

Iost, N., Virág, L., Opincariu, M., Szécsi, J., Varró, A., and Papp, J. G. (1998). Delayed rectifier potassium current in undiseased human ventricular myocytes. *Cardiovascular Research*, 40:508–15.

Ishihara, K., Yan, D.-H., Yamamoto, S., and Ehara, T. (2002). Inward rectifier K^+ current under physiological cytoplasmic conditions in guinea-pig cardiac ventricular cells. *Journal of Physiology*, 540(Pt 3):831–41.

Isoyama, S., Apstein, C. S., Wexler, L. F., Grice, W. N., and Lorell, B. H. (1987). Acute decrease in left ventricular diastolic chamber distensibility during simulated angina in isolated hearts. *Circulation Research*, 61(6):925–33.

Jalife, J. (2003). Rotors and spiral waves in atrial fibrillation. *Journal of Cardiovascular Electrophysiology*, 14(7):776–80.

Jalife, J. (2009). Inward rectifier potassium channels control rotor frequency in ventricular fibrillation. *Heart Rhythm: The Official Journal of the Heart Rhythm Society*, 6(11 Suppl):S44–8.

Jalife, J. (2013). Introduction to the Series on Computational Approaches to Cardiac Arrhythmias: Translation Into Diagnostics and Therapy. *Circulation Research*, 112(5):831–833.

Janse, M. J. and Kléber, A. G. (1981). Electrophysiological changes and ventricular arrhythmias in the early phase of regional myocardial ischemia. *Circulation Research*, 49(5):1069–81.

Janse, M. J., Vermeulen, J. T., Opthof, T., Coronel, R., Wilms-Schopman, F. J. G., Rademaker, H. M. E., Baartscheer, A., and Dekker, L. R. C. (2001). Arrhythmogenesis in heart failure. *Journal of Cardiovascular Electrophysiology*, 12(4):496–9.

John, R. M., Tedrow, U. B., Koplan, B. A., Albert, C. M., Epstein, L. M., Sweeney, M. O., Miller, A. L., Michaud, G. F., and Stevenson, W. G. (2012). Ventricular arrhythmias and sudden cardiac death. *Lancet*, 380(9852):1520–9.

Johnson, D. M., Heijman, J., Pollard, C. E., Valentin, J.-P., Crijns, H. J. G. M., Abi-Gerges, N., and Volders, P. G. A. (2010). I_{Ks} restricts excessive beat-to-beat variability of repolarization during beta-adrenergic receptor stimulation. *Journal of Molecular and Cellular Cardiology*, 48(1):122–30.

Jost, N., Papp, J. G., and Varró, A. (2007). Slow delayed rectifier potassium current (I_{Ks}) and the repolarization reserve. *Annals of Noninvasive Electrocardiology : The Official Journal of the International Society for Holter and Noninvasive Electrocardiology, Inc*, 12(1):64–78.

Jost, N., Virág, L., Bitay, M., Takács, J., Lengyel, C., Biliczki, P., Nagy, Z., Bogáts, G., Lathrop, D. A., Papp, J. G., and Varró, A. (2005). Restricting excessive cardiac action potential and QT prolongation: a vital role for I_{Ks} in human ventricular muscle. *Circulation*, 112(10):1392–9.

Jung, B.-C., Lee, S.-H., Cho, Y.-K., Park, H.-S., Kim, Y.-N., Lee, Y.-S., and Shin, D.-G. (2011). Role of the alternans of action potential duration and aconitine-induced arrhythmias in isolated rabbit hearts. *Journal of Korean Medical Science*, 26(12):1576–81.

Jurkat-Rott, K. and Lehmann-Horn, F. (2005). Muscle channelopathies and critical points in functional and genetic studies. *Journal of Clinical Investigation*, 115(8):2000–9.

Kagiyama, Y., Hill, J. L., and Gettes, L. S. (1982). Interaction of acidosis and increased extracellular potassium on action potential characteristics and conduction in guinea pig ventricular muscle. *Circulation Research*, 51(5):614–23.

Kamisago, M., Sharma, S. D., DePalma, S. R., Solomon, S., Sharma, P., McDonough, B., Smoot, L., Mullen, M. P., Woolf, P. K., Wigle, E. D., Seidman, J. G., and Seidman, C. E. (2000). Mutations in sarcomere protein genes as a cause of dilated cardiomyopathy. *New England Journal of Medicine*, 343(23):1688–96.

Kannankeril, P., Roden, D. M., and Darbar, D. (2010). Drug-induced long QT syndrome. *Pharmacological Reviews*, 62(4):760–81.

Kaplan, P., Hendrikx, M., Mattheussen, M., Mubagwa, K., and Flameng, W. (1992). Effect of ischemia and reperfusion on sarcoplasmic reticulum calcium uptake. *Circulation Research*, 71(5):1123–1130.

Kaplinsky, E., Ogawa, S., Balke, C. W., and Dreifus, L. S. (1979). Two periods of early ventricular arrhythmia in the canine acute myocardial infarction model. *Circulation*, 60(2):397–403.

Keener, J. P. and Sneyd, J. (2009). *Mathematical Physiology*, volume 8/2 of *Interdisciplinary Applied Mathematics*. Springer New York, New York, NY, 2nd edition.

Keller, E. F. (2000). Models Of and Models For: Theory and Practice in Contemporary Biology. *Philosophy of Science*, 67:S72–S86.

Kherlopian, A. R., Ortega, F. A., and Christini, D. J. (2011). Cardiac myocyte model parameter sensitivity analysis and model transformation using a genetic algorithm. In *13th Annual Conference Companion on Genetic and Evolutionary Computation*, page 755, New York, New York, USA. ACM Press.

Kihara, Y., Grossman, W., and Morgan, J. P. (1989). Direct measurement of changes in intracellular calcium transients during hypoxia, ischemia, and reperfusion of the intact mammalian heart. *Circulation Research*, 65(4):1029–1044.

Kirchhof, P. F., Degen, H., Franz, M. R., Eckardt, L., Fabritz, C. L., Milberg, P., Läer, S., Neumann, J., Breithardt, G., and Haverkamp, W. (2003). Amiodarone-induced postrepolarization refractoriness suppresses induction of ventricular fibrillation. *Journal of Pharmacology and Experimental Therapeutics*, 305(1):257–263.

Klabunde, R. E. (2005). *Cardiovascular Physiology Concepts*. Lippincott Williams & Wilkins.

Kléber, A. G. (1987). Conduction of the impulse in the ischemic myocardium—implications for malignant ventricular arrhythmias. *Experientia*, 43(10):1056–61.

Kléber, A. G., Janse, M. J., van Capelle, F. J. L., and Durrer, D. (1978). Mechanism and time course of S-T and T-Q segment changes during acute regional myocardial ischemia in the pig heart determined by extracellular and intracellular recordings. *Circulation Research*, 42(5):603–13.

Kléber, A. G., Riegger, C. B., and Janse, M. J. (1987a). Electrical uncoupling and increase of extracellular resistance after induction of ischemia in isolated, arterially perfused rabbit papillary muscle. *Circulation Research*, 61(2):271–279.

Kléber, A. G., Riegger, C. B., and Janse, M. J. (1987b). Extracellular K^+ and H^+ shifts in early ischemia: mechanisms and relation to changes in impulse propagation. *Journal of Molecular and Cellular Cardiology*, 19 Suppl 5(Supplement V):35–44.

Kléber, A. G. and Rudy, Y. (2004). Basic mechanisms of cardiac impulse propagation and associated arrhythmias. *Physiological Reviews*, 84(2):431–88.

Kodama, I., Wilde, A. A. M., Janse, M. J., Durrer, D., and Yamada, K. (1984). Combined effects of hypoxia, hyperkalemia and acidosis on membrane action potential and excitability of guinea-pig ventricular muscle. *Journal of Molecular and Cellular Cardiology*, 16:247–59.

Kohl, P., Crampin, E. J., Quinn, T. A., and Noble, D. (2010). Systems biology: an approach. *Clinical Pharmacology and Therapeutics*, 88(1):25–33.

Krause, H., Antoni, H., and Fleckenstein, A. (1966). [An electronic model for the formation of local and transmitted stimuli on the myocardium fibers based upon variable current-voltage characteristics for potassium and sodium ions]. *Pflügers Archiv für die gesamte Physiologie des Menschen und der Tiere*, 289(1):12–36.

Krause, S. and Hess, M. L. (1984). Characterization of cardiac sarcoplasmic reticulum dysfunction during short-term, normothermic, global ischemia. *Circulation Research*, 55(2):176–84.

Kuo, C.-S., Munakata, K., Reddy, C. P., and Surawicz, B. (1983). Characteristics and possible mechanism of ventricular arrhythmia dependent on the dispersion of action potential durations. *Circulation*, 67(6):1356–1367.

Kurokawa, J., Kodama, M., Furukawa, T., and Clancy, C. E. (2012). Sex and gender aspects in antiarrhythmic therapy. *Handbook of Experimental Pharmacology*, 214:237–63.

Kurz, R. W., Mohabir, R., Ren, X. L., and Franz, M. R. (1993). Ischaemia induced alternans of action potential duration in the intact-heart: dependence on coronary flow, preload and cycle length. *European Heart Journal*, 14(10):1410–20.

Laurita, K. R. and Rosenbaum, D. S. (2008). Cellular mechanisms of arrhythmogenic cardiac alternans. *Progress in Biophysics and Molecular Biology*, 97(2-3):332–47.

LeBlanc, J., Ward, M. O., and Wittels, N. (1990). Exploring N-Dimensional Databases. In *Proceedings of the 1st Conference on Visualization*, pages 230–237.

Lee, H.-C., Mohabir, R., Smith, N., Franz, M. R., and Clusin, W. T. (1988). Effect of ischemia on calcium-dependent fluorescence transients in rabbit hearts containing indo 1. Correlation with monophasic action potentials and contraction. *Circulation*, 78(4):1047–59.

Lee, K. S., Ladinsky, H., and Stuckey, J. H. (1967). Decreased Ca^{2+} Uptake by Sarcoplasmic Reticulum after Coronary Artery Occlusion for 60 and 90 Minutes. *Circulation Research*, 21(4):439–444.

Lemay, M., de Lange, E., and Kucera, J. P. (2011). Effects of stochastic channel gating and distribution on the cardiac action potential. *Journal of Theoretical Biology*, 281(1):84–96.

Lengyel, C., Iost, N., Virág, L., Varró, A., Lathrop, D. A., and Papp, J. G. (2001). Pharmacological block of the slow component of the outward delayed rectifier current (I_{Ks}) fails to lengthen rabbit ventricular muscle QT_c and action potential duration. *British Journal Of Pharmacology*, 132(1):101–10.

Levick, J. R. (1995). *An Introduction to Cardiovascular Physiology*. Butterworth Heinemann, 2nd edition.

Levitsky, D. O., Benevolensky, D. S., Ikemoto, N., Syrbu, S. I., and Watras, J. (1989). Monoclonal antibodies to dog heart sarcoplasmic reticulum as markers of endoplasmic reticulum. *Journal of Molecular and Cellular Cardiology*, 21(Supplement I):55–8.

Levkau, B., Schäfers, M., Wohlschlaeger, J., von Wnuck Lipinski, K., Keul, P., Hermann, S., Kawaguchi, N., Kirchhof, P., Fabritz, L., Stypmann, J., Stegger, L., Flögel, U., Schrader, J., Fischer, J. W., Fischer, J., Hsieh, P., Ou, Y.-L., Mehrhof, F., Tiemann, K., Ghanem, A., Matus, M., Neumann, J., Heusch, G., Schmid, K. W., Conway, E. M., and Baba, H. A. (2008). Survivin determines cardiac function by controlling total cardiomyocyte number. *Circulation*, 117(12):1583–93.

Li, G.-R., Yang, B., Feng, J., Bosch, R. F., Carrier, M., and Nattel, S. (1999). Transmembrane I_{Ca} contributes to rate-dependent changes of action potentials in human ventricular myocytes. *American Journal of Physiology*, 276(1 Pt 2):H98–H106.

Liu, D.-W., Gintant, G. A., and Antzelevitch, C. (1993). Ionic bases for electrophysiological distinctions among epicardial, midmyocardial, and endocardial myocytes from the free wall of the canine left ventricle. *Circulation Research*, 72:671–687.

Lloyd, C. M., Lawson, J. R., Hunter, P. J., and Nielsen, P. F. (2008). The CellML Model Repository. *Bioinformatics*, 24(18):2122–3.

Lukas, A. and Antzelevitch, C. (1996). Phase 2 reentry as a mechanism of initiation of circus movement reentry in canine epicardium exposed to simulated ischemia. *Cardiovascular Research*, 32:593–603.

Luke, R. A. and Saffitz, J. E. (1991). Remodeling of ventricular conduction pathways in healed canine infarct border zones. *Journal of Clinical Investigation*, 87(5):1594–602.

Luo, C.-H. and Rudy, Y. (1991). A Model of the Ventricular Cardiac Action Potential: Depolarization, Repolarization and Their Interaction. *Circulation Research*, 68:1501–1526.

Luo, C.-H. and Rudy, Y. (1994a). A dynamic model of the cardiac ventricular action potential. I. Simulations of ionic currents and concentration changes. *Circulation Research*, 74(6):1071–96.

Luo, C.-H. and Rudy, Y. (1994b). A dynamic model of the cardiac ventricular action potential. II. Afterdepolarizations, triggered activity, and potentiation. *Circulation Research*, 74(6):1097–113.

Mahajan, A., Shiferaw, Y., Sato, D., Baher, A., Olcese, R., Xie, L.-H., Yang, M.-J., Chen, P.-S., Restrepo, J. G., Karma, A., Garfinkel, A., Qu, Z., and Weiss, J. N. (2008). A rabbit ventricular action potential model replicating cardiac dynamics at rapid heart rates. *Biophysical Journal*, 94(2):392–410.

Malloy, C. R., Buster, D. C., Castro, M. M. C. A., Geraldes, C. F. G. C., Jeffrey, F. M. H., and Sherry, A. D. (1990). Influence of global ischemia on intracellular sodium in the perfused rat heart. *Magnetic Resonance in Medicine : Official Journal of the Society of Magnetic Resonance in Medicine / Society of Magnetic Resonance in Medicine*, 15(1):33–44.

Mandapati, R., Skanes, A., Chen, J., Berenfeld, O., and Jalife, J. (2000). Stable microreentrant sources as a mechanism of atrial fibrillation in the isolated sheep heart. *Circulation*, 101(2):194–9.

Marder, E. and Taylor, A. L. (2011). Multiple models to capture the variability in biological neurons and networks. *Nature Neuroscience*, 14(2):133–8.

McAllister, R. E., Noble, D., and Tsien, R. W. (1975). Reconstruction of the electrical activity of cardiac Purkinje fibres. *Journal of Physiology*, 251(1):1–59.

McIntosh, M. A., Cobbe, S. M., and Smith, G. L. (2000). Heterogeneous changes in action potential and intracellular Ca^{2+} in left ventricular myocyte sub-types from rabbits with heart failure. *Cardiovascular Research*, 45(2):397–409.

McKay, M. D., Beckman, R. J., and Conover, W. J. (1979). Comparison of Three Methods for Selecting Values of Input Variables in the Analysis of Output from a Computer Code. *Technometrics*, 21(2):239–245.

Meech, R. W. and Standen, N. B. (1975). Potassium activation in Helix aspersa neurones under voltage clamp: a component mediated by calcium influx. *Journal of Physiology*, 249(2):211–39.

Michailova, A., Lorentz, W., and McCulloch, A. D. (2007). Modeling transmural heterogeneity of K_{ATP} current in rabbit ventricular myocytes. *American Journal of Physiology - Cell Physiology*, 293(2):C542–57.

Michailova, A., Saucerman, J., Belik, M. E., and McCulloch, A. D. (2005). Modeling regulation of cardiac K_{ATP} and L-type Ca^{2+} currents by ATP, ADP, and Mg^{2+}. *Biophysical Journal*, 88:2234–49.

Mino, H., Rubinstein, J. T., and White, J. A. (2002). Comparison of algorithms for the simulation of action potentials with stochastic sodium channels. *Annals of Biomedical Engineering*, 30(4):578–87.

Mirams, G. R., Arthurs, C. J., Bernabeu, M. O., Bordas, R., Cooper, J., Corrias, A., Davit, Y., Dunn, S.-J., Fletcher, A. G., Harvey, D. G., Marsh, M. E., Osborne, J. M., Pathmanathan, P., Pitt-Francis, J., Southern, J., Zemzemi, N., and Gavaghan, D. J. (2013). Chaste: an open source C++ library for computational physiology and biology. *PLoS Computational Biology*, 9:e1002970.

Mirams, G. R., Cui, Y., Sher, A., Fink, M., Cooper, J., Heath, B. M., McMahon, N. C., Gavaghan, D. J., and Noble, D. (2011). Simulation of multiple ion channel block provides improved early prediction of compounds' clinical torsadogenic risk. *Cardiovascular Research*, 91(1):53–61.

Miura, M., Boyden, P. A., and ter Keurs, H. E. (1998). Ca^{2+} waves during triggered propagated contractions in intact trabeculae. *American Journal of Physiology*, 274(1 Pt 2):H266–76.

Mohabir, R., Lee, H.-C., Kurz, R. W., and Clusin, W. T. (1991). Effects of ischemia and hypercarbic acidosis on myocyte calcium transients, contraction, and pH_i in perfused rabbit hearts. *Circulation Research*, 69(6):1525–1537.

Moréna, H., Janse, M. J., Fiolet, J. W. T., Krieger, W. J. G., Crijns, H. J. G. M., and Durrer, D. (1980). Comparison of the effects of regional ischemia, hypoxia, hyperkalemia, and acidosis on intracellular and extracellular potentials and metabolism in the isolated porcine heart. *Circulation Research*, 46(5):634–46.

Moyé, L. (2014). DAMASCENE and Meta-Ecological Research: A Bridge Too Far. *Circulation Research*.

Mubagwa, K. (1995). Sarcoplasmic reticulum function during myocardial ischaemia and reperfusion. *Cardiovascular Research*, 30(2):166–75.

Nattel, S., Frelin, Y., Gaborit, N., Louault, C., and Demolombe, S. (2010). Ion-channel mRNA-expression profiling: Insights into cardiac remodeling and arrhythmic substrates. *Journal of Molecular and Cellular Cardiology*, 48(1):96–105.

Neely, J. R., Whitmer, J. T., and Rovetto, M. J. (1975). Effect of coronary blood flow on glycolytic flux and intracellular pH in isolated rat hearts. *Circulation Research*, 37(6):733–41.

Negretti, N., O'Neill, S. C. O., and Eisner, D. A. (1993). The effects of inhibitors of sarcoplasmic reticulum function on the systolic Ca^{2+} transient in rat ventricular myocytes. *Journal of Physiology*, 468:35–52.

Nekouzadeh, A. and Rudy, Y. (2011). Continuum molecular simulation of large conformational changes during ion-channel gating. *PloS One*, 6(5):e20186.

Niederer, S. A. (2013). Regulation of ion gradients across myocardial ischemic border zones: a biophysical modelling analysis. *PloS One*, 8(4):e60323.

Niederer, S. A., Fink, M., Noble, D., and Smith, N. P. (2009). A meta-analysis of cardiac electrophysiology computational models. *Experimental Physiology*, 94(5):486–95.

Noble, D. (1960). Cardiac Action and Pacemaker Potentials based on the Hodgkin-Huxley Equations. *Nature*, 4749:495–497.

Noble, D. (1962). A modification of the Hodgkin-Huxley equations applicable to Purkinje fibre action and pace-maker potentials. *Journal of Physiology*, 160:317–52.

Noble, D. (2002). Simulation of Na/Ca exchange activity during ischemia. *Annals of the New York Academy of Sciences*, 976:431–7.

Noble, D. (2011). Successes and failures in modeling heart cell electrophysiology. *Heart Rhythm: The Official Journal of the Heart Rhythm Society*, 8(11):1798–803.

Noble, D., Garny, A., and Noble, P. J. (2012). How the Hodgkin-Huxley equations inspired the Cardiac Physiome Project. *Journal of Physiology*, 590(Pt 11):2613–28.

Noble, D. and Rudy, Y. (2001). Models of cardiac ventricular action potentials: iterative interaction between experiment and simulation. *Philosophical Transactions of the Royal Society A: Mathematical, Physical and Engineering Sciences*, 359(1783):1127–1142.

Nolasco, J. B. and Dahlen, R. W. (1968). A graphic method for the study of alternation in cardiac action potentials. *Journal of Applied Physiology*, 25(2):191–6.

Noma, A. (1983). ATP-regulated K^+ channels in cardiac muscle. *Nature*, 305(5930):147–8.

Noujaim, S. F., Berenfeld, O., Kalifa, J., Cerrone, M., Nanthakumar, K., Atienza, F., Moreno, J., Mironov, S. F., and Jalife, J. (2007). Universal scaling law of electrical turbulence in the mammalian heart. *Proceedings of the National Academy of Sciences of the United States of America*, 104(52):20985–9.

Nygren, A., Fiset, C., Firek, L., Clark, J. W., Lindblad, D. S., Clark, R. B., and Giles, W. R. (1998). Mathematical model of an adult human atrial cell: the role of K^+ currents in repolarization. *Circulation Research*, 82(1):63–81.

Page, E., McCallister, L. P., and Power, B. (1971). Stereological measurements of cardiac ultrastructures implicated in excitation-contraction coupling. *Proceedings of the National Academy of Sciences of the United States of America*, 68(7):1465–6.

Pakdaman, K., Thieullen, M., and Wainrib, G. (2010). Fluid limit theorems for stochastic hybrid systems with application to neuron models. *Advances in Applied Probability*, 42:761–794.

Pandit, S. V. and Jalife, J. (2013). Rotors and the Dynamics of Cardiac Fibrillation. *Circulation Research*, 112(5):849–862.

Panfilov, A. V. (2006). Is heart size a factor in ventricular fibrillation? Or how close are rabbit and human hearts? *Heart Rhythm: The Official Journal of the Heart Rhythm Society*, 3(7):862–4.

Peng, W. (2005). *Clutter-Based Dimension Reordering in Multi-Dimensional Data Visualization*. MSc (computer science), Worcester Polytechnic Institute.

Peng, W., Ward, M. O., and Rundensteiner, E. A. (2004). Clutter Reduction in Multi-Dimensional Data Visualization Using Dimension Reordering. In Ward, M. and Munzner, T., editors, *IEEE Symposium on Information Visualization*, pages 89–96. IEEE.

Pike, M. M., Luo, C. S., Clark, M. D., Kirk, K. A., Kitakaze, M., Madden, M. C., Cragoe, E. J., and Pohost, G. M. (1993). NMR measurements of Na^+ and cellular energy in ischemic rat heart: role of Na^+-H^+ exchange. *American Journal of Physiology*, 265(6 Pt 2):H2017–26.

Pitt-Francis, J., Pathmanathan, P., Bernabeu, M. O., Bordas, R., Cooper, J., Fletcher, A. G., Mirams, G. R., Murray, P., Osborne, J. M., Walter, A., Chapman, S. J., Garny, A., van Leeuwen, I. M. M., Maini, P. K., Rodríguez, B., Waters, S. L., Whiteley, J. P., Byrne, H. M., and Gavaghan, D. J. (2009). Chaste: A test-driven approach to software development for biological modelling. *Computer Physics Communications*, 180(12):2452–2471.

Ponard, J. G. C., Kondratyev, A. A., and Kucera, J. P. (2007). Mechanisms of intrinsic beating variability in cardiac cell cultures and model pacemaker networks. *Biophysical Journal*, 92(10):3734–52.

Pozzan, T., Rizzuto, R., Volpe, P., and Meldolesi, J. (1994). Molecular and cellular physiology of intracellular calcium stores. *Physiological Reviews*, 74:595–636.

Prinz, A. A., Billimoria, C. P., and Marder, E. (2003). Alternative to hand-tuning conductance-based models: construction and analysis of databases of model neurons. *Journal of Neurophysiology*, 90(6):3998–4015.

Pruvot, E. J., Katra, R. P., Rosenbaum, D. S., and Laurita, K. R. (2004). Role of calcium cycling versus restitution in the mechanism of repolarization alternans. *Circulation Research*, 94(8):1083–90.

Pueyo, E., Corrias, A., Virág, L., Jost, N., Szél, T., Varró, A., Szentandrássy, N., Nánási, P. P., Burrage, K., and Rodríguez, B. (2011). A multiscale investigation of repolarization variability and its role in cardiac arrhythmogenesis. *Biophysical Journal*, 101(12):2892–902.

Puglisi, J. L. and Bers, D. M. (2001). LabHEART: an interactive computer model of rabbit ventricular myocyte ion channels and Ca transport. *American Journal of Physiology - Cell Physiology*, 281(6):C2049–60.

Puglisi, J. L., Wang, F., and Bers, D. M. (2004). Modeling the isolated cardiac myocyte. *Progress in Biophysics and Molecular Biology*, 85(2-3):163–78.

Qian, Y.-W., Clusin, W. T., Lin, S.-F., Han, J., and Sung, R. J. (2001). Spatial Heterogeneity of Calcium Transient Alternans During the Early Phase of Myocardial Ischemia in the Blood-Perfused Rabbit Heart. *Circulation*, 104(17):2082–2087.

Qu, Z., Garfinkel, A., Chen, P.-S., and Weiss, J. N. (2000). Mechanisms of Discordant Alternans and Induction of Reentry in Simulated Cardiac Tissue. *Circulation*, 102(14):1664–1670.

Quinn, T. A., Granite, S., Allessie, M. A., Antzelevitch, C., Bollensdorff, C., Bub, G., Burton, R. A. B., Cerbai, E., Chen, P.-S., Delmar, M., DiFrancesco, D., Earm, Y. E., Efimov, I. R., Egger, M., Entcheva, E., Fink, M., Fischmeister, R., Franz, M. R., Garny, A., Giles, W. R., Hannes, T., Harding, S. E., Hunter, P. J., Iribe, G., Jalife, J., Johnson, C. R., Kass, R. S., Kodama, I., Koren, G., Lord, P., Markhasin, V. S., Matsuoka, S., McCulloch, A. D., Mirams, G. R., Morley, G. E., Nattel, S., Noble, D., Olesen, S. P., Panfilov, A. V., Trayanova, N. A., Ravens, U., Richard, S., Rosenbaum, D. S., Rudy, Y., Sachs, F., Sachse, F. B., Saint, D. A., Schotten, U., Solovyova, O., Taggart, P., Tung, L., Varró, A., Volders, P. G. A., Wang, K., Weiss, J. N., Wettwer, E., White, E., Wilders, R., Winslow, R. L., and Kohl, P. (2011). Minimum Information about a Cardiac Electrophysiology Experiment (MICEE): standardised reporting for model reproducibility, interoperability, and data sharing. *Progress in Biophysics and Molecular Biology*, 107(1):4–10.

Quinn, T. A. and Kohl, P. (2013). Combining wet and dry research: experience with model development for cardiac mechano-electric structure-function studies. *Cardiovascular Research*, 97(4):601–11.

Restrepo, J. G., Weiss, J. N., and Karma, A. (2008). Calsequestrin-mediated mechanism for cellular calcium transient alternans. *Biophysical Journal*, 95(8):3767–89.

Riccio, M. L., Koller, M. L., and Gilmour, R. F. (1999). Electrical restitution and spatiotemporal organization during ventricular fibrillation. *Circulation Research*, 84(8):955–63.

Roden, D. M. (1998). Taking the "idio" out of "idiosyncratic": predicting torsades de pointes. *Pacing and Clinical Electrophysiology : PACE*, 21(5):1029–34.

Roden, D. M., Balser, J. R., George Jr., A. L., and Anderson, M. E. (2002). Cardiac ion channels. *Annual Review of Physiology*, 64:431–75.

Rodríguez, B. and Ferrero, J. M. (2001a). Integrated mechanisms of K^+ loss in myocardial ischemia: a simulation study. In *2001 Conference Proceedings of the 23rd Annual International Conference of the IEEE Engineering in Medicine and Biology Society*, volume 1, pages 48–51. IEEE.

Rodríguez, B. and Ferrero, J. M. (2001b). Mechanistic investigation of the causes of cellular K^+ loss during acute myocardial ischemia: a simulation study. In *Computers in Cardiology*, pages 361–364. IEEE.

Rodríguez, B., Ferrero, J. M., and Trénor, B. (2002). Mechanistic investigation of extracellular K^+ accumulation during acute myocardial ischemia: a simulation study. *American Journal of Physiology - Heart and Circulatory Physiology*, 283(2):H490–500.

Rodríguez, B., Tice, B. M., Eason, J. C., Aguel, F., and Trayanova, N. A. (2004). Cardiac vulnerability to electric shocks during phase 1A of acute global ischemia. *Heart Rhythm: The Official Journal of the Heart Rhythm Society*, 1(6):695–703.

Rodríguez, B., Trayanova, N. A., and Noble, D. (2006). Modeling cardiac ischemia. *Annals of the New York Academy of Sciences*, 1080:395–414.

Romero, L., Carbonell, B., Trénor, B., Rodríguez, B., Sáiz, J., and Ferrero, J. M. (2010). Human and rabbit inter-species comparison of ionic mechanisms of arrhythmic risk: A simulation study. In *Annual International Conference of the IEEE Engineering in Medicine and Biology Society*, volume 2010, pages 3253–6.

Romero, L., Carbonell, B., Trénor, B., Rodríguez, B., Sáiz, J., and Ferrero, J. M. (2011). Systematic characterization of the ionic basis of rabbit cellular electrophysiology using two ventricular models. *Progress in Biophysics and Molecular Biology*, 107(1):60–73.

Romero, L., Pueyo, E., Fink, M., and Rodríguez, B. (2009a). Impact of ionic current variability on human ventricular cellular electrophysiology. *American Journal of Physiology - Heart and Circulatory Physiology*, 297(4):H1436–45.

Romero, L., Trénor, B., Alonso, J. M., Tobón, C., Sáiz, J., and Ferrero, J. M. (2009b). The relative role of refractoriness and source-sink relationship in reentry generation during simulated acute ischemia. *Annals of Biomedical Engineering*, 37(8):1560–71.

Rosati, B. and McKinnon, D. (2004). Regulation of ion channel expression. *Circulation Research*, 94(7):874–83.

Rosati, B., Pan, Z., Lypen, S., Wang, H.-S., Cohen, I., Dixon, J. E., and McKinnon, D. (2001). Regulation of KChIP2 potassium channel beta subunit gene expression underlies the gradient of transient outward current in canine and human ventricle. *Journal of Physiology*, 533(1):119–25.

Rudy, Y. and Silva, J. R. (2006). Computational biology in the study of cardiac ion channels and cell electrophysiology. *Quarterly Reviews of Biophysics*, 39(1):57–116.

Ruiz-Ceretti, E., Ragault, P., Leblanc, N., and Ponce Zumino, A. Z. (1983). Effects of hypoxia and altered K_0 on the membrane potential of rabbit ventricle. *Journal of Molecular and Cellular Cardiology*, 15(12):845–54.

Russell, D. C., Oliver, M. F., and Wojtczak, J. (1977). Combined electrophysiological technique for assessment of the cellular basis of early ventricular arrhythmias. *Lancet*, 2(8040):684–6.

Saffitz, J. E., Kanter, H. L., Green, K. G., Tolley, T. K., and Beyer, E. C. (1994). Tissue-specific determinants of anisotropic conduction velocity in canine atrial and ventricular myocardium. *Circulation Research*, 74(6):1065–1070.

Sanguinetti, M. C. and Jurkiewicz, N. K. (1990). Two components of cardiac delayed rectifier K^+ current. Differential sensitivity to block by class III antiarrhythmic agents. *Journal of General Physiology*, 96(1):195–215.

Sanguinetti, M. C. and Jurkiewicz, N. K. (1992). Role of external Ca^{2+} and K^+ in gating of cardiac delayed rectifier K^+ currents. *Pflügers Archiv: European Journal of Physiology*, 420(2):180–6.

Sarkar, A. X., Christini, D. J., and Sobie, E. A. (2012). Exploiting mathematical models to illuminate electrophysiological variability between individuals. *Journal of Physiology*, 590(11):2555–2567.

Sarkar, A. X. and Sobie, E. A. (2010). Regression analysis for constraining free parameters in electrophysiological models of cardiac cells. *PLoS Computational Biology*, 6(9):e1000914.

Sarkar, A. X. and Sobie, E. A. (2011). Quantification of repolarization reserve to understand interpatient variability in the response to proarrhythmic drugs: a computational analysis. *Heart Rhythm: The Official Journal of the Heart Rhythm Society*, 8(11):1749–55.

Sato, D., Shiferaw, Y., Garfinkel, A., Weiss, J. N., Qu, Z., and Karma, A. (2006). Spatially discordant alternans in cardiac tissue: role of calcium cycling. *Circulation Research*, 99(5):520–7.

Sato, D., Xie, L.-H., Nguyen, T. P., Weiss, J. N., and Qu, Z. (2010). Irregularly appearing early afterdepolarizations in cardiac myocytes: random fluctuations or dynamical chaos? *Biophysical Journal*, 99:765–73.

Sato, D., Xie, L.-H., Sovari, A. A., Tran, D. X., Morita, N., Xie, F., Karagueuzian, H. S., Garfinkel, A., Weiss, J. N., and Qu, Z. (2009). Synchronization of chaotic early afterdepolarizations in the genesis of cardiac arrhythmias. *Proceedings of the National Academy of Sciences of the United States of America*, 106(9):2983–8.

Scherlag, B. J., El-Sherif, N., Hope, R., and Lazzara, R. (1974). Characterization and Localization of Ventricular Arrhythmias Resulting from Myocardial Ischemia and Infarction. *Circulation Research*, 35:372–383.

Schulz, D. J., Goaillard, J.-M., and Marder, E. (2006). Variable channel expression in identified single and electrically coupled neurons in different animals. *Nature Neuroscience*, 9:356–62.

Serizawa, T., Momomura, S.-i., Kohmoto, O., Ohya, T., Sato, H., Takahashi, T., Mochizuki, T., Iizuka, M., and Sugimoto, T. (1987). Mechanisms of abnormal myocardial relaxation induced by ischemia: comparison of low flow ischemia and hypoxia in isolated rabbit heart. *Japanese Circulation Journal*, 51(1):90–7.

Serizawa, T., Vogel, W. M., Apstein, C. S., and Grossman, W. (1981). Comparison of acute alterations in left ventricular relaxation and diastolic chamber stiffness induced by hypoxia and ischemia. Role of myocardial oxygen supply-demand imbalance. *Journal of Clinical Investigation*, 68(1):91–102.

Severi, S., Cavalcanti, S., Mancini, E., and Santoro, A. (2002). Effect of electrolyte and pH changes on the sinus node pacemaking in humans. *Journal of Electrocardiology*, 35(2):115–24.

Shannon, T. R., Ginsburg, K. S., and Bers, D. M. (2000). Potentiation of fractional sarcoplasmic reticulum calcium release by total and free intra-sarcoplasmic reticulum calcium concentration. *Biophysical Journal*, 78(1):334–43.

Shannon, T. R., Wang, F., Puglisi, J. L., Weber, C. R., and Bers, D. M. (2004). A mathematical treatment of integrated Ca dynamics within the ventricular myocyte. *Biophysical Journal*, 87(5):3351–71.

Shannon, T. R., Wang, F., Puglisi, J. L., Weber, C. R., and Bers, D. M. (2012). Correction. *Biophysical Journal*, 102(8):1996–2001.

Shaw, R. M. and Rudy, Y. (1994). Electrophysiological changes of ventricular tissue under ischemic conditions: a simulation study. In *Computers in Cardiology*, pages 641–644. IEEE Comput. Soc. Press.

Shaw, R. M. and Rudy, Y. (1997a). Electrophysiologic effects of acute myocardial ischemia. A mechanistic investigation of action potential conduction and conduction failure. *Circulation Research*, 80(1):124–38.

Shaw, R. M. and Rudy, Y. (1997b). Electrophysiologic effects of acute myocardial ischemia: a theoretical study of altered cell excitability and action potential duration. *Cardiovascular Research*, 35(2):256–72.

Shaw, R. M. and Rudy, Y. (1997c). Ionic mechanisms of propagation in cardiac tissue. Roles of the sodium and L-type calcium currents during reduced excitability and decreased gap junction coupling. *Circulation Research*, 81(5):727–41.

Shiferaw, Y., Sato, D., and Karma, A. (2005). Coupled dynamics of voltage and calcium in paced cardiac cells. *Physical Review E, Statistical, Nonlinear, and Soft Matter Physics*, 71(2):021903.

Shiferaw, Y., Watanabe, M. A., Garfinkel, A., Weiss, J. N., and Karma, A. (2003). Model of intracellular calcium cycling in ventricular myocytes. *Biophysical Journal*, 85(6):3666–86.

Silva, J. R. and Rudy, Y. (2005). Subunit interaction determines I_{Ks} participation in cardiac repolarization and repolarization reserve. *Circulation*, 112(10):1384–91.

Silverman, H. S., Ninomiya, M., Blank, P. S., Hano, O., Miyata, H., Spurgeon, H. A., Lakatta, E. G., and Stern, M. D. (1991). A cellular mechanism for impaired posthypoxic relaxation in isolated cardiac myocytes. Altered myofilament relaxation kinetics at reoxygenation. *Circulation Research*, 69(1):196–208.

Sims, C., Reisenweber, S., Viswanathan, P. C., Choi, B.-R., Walker, W. H., and Salama, G. (2008). Sex, age, and regional differences in L-type calcium current are important determinants of arrhythmia phenotype in rabbit hearts with drug-induced long QT type 2. *Circulation Research*, 102(9):e86–100.

Smaill, B. H., Zhao, J., and Trew, M. L. (2013). Three-Dimensional Impulse Propagation in Myocardium: Arrhythmogenic Mechanisms at the Tissue Level. *Circulation Research*, 112(5):834–848.

Sobie, E. A. (2009). Parameter sensitivity analysis in electrophysiological models using multivariable regression. *Biophysical Journal*, 96(4):1264–74.

Sobie, E. A. and Ramay, H. R. (2009). Excitation-contraction coupling gain in ventricular myocytes: insights from a parsimonious model. *Journal of Physiology*, 587(Pt 6):1293–9.

Sobie, E. A. and Sarkar, A. X. (2011). Regression methods for parameter sensitivity analysis: applications to cardiac arrhythmia mechanisms. In *Annual International Conference of the IEEE Engineering in Medicine and Biology Society*, pages 4657–60.

Soeller, C. and Cannell, M. B. (1997). Numerical simulation of local calcium movements during L-type calcium channel gating in the cardiac diad. *Biophysical Journal*, 73(1):97–111.

Song, S. O., Chakrabarti, A., and Varner, J. D. (2010). Ensembles of signal transduction models using Pareto Optimal Ensemble Techniques (POETs). *Biotechnology Journal*, 5(7):768–80.

Spach, M. S., Dolber, P. C., and Heidlage, J. F. (1988). Influence of the passive anisotropic properties on directional differences in propagation following modification of the sodium conductance in human atrial muscle. A model of reentry based on anisotropic discontinuous propagation. *Circulation Research*, 62(4):811–32.

Spector, P. S., Curran, M. E., Zou, A., Keating, M. T., and Sanguinetti, M. C. (1996). Fast inactivation causes rectification of the I_{Kr} channel. *Journal of General Physiology*, 107(5):611–9.

Sperelakis, N. and McConnell, K. (2002). Electric field interactions between closely abutting excitable cells. *IEEE Engineering in Medicine and Biology Magazine : The Quarterly Magazine of the Engineering in Medicine & Biology Society*, 21(1):77–89.

Stern, M. D. (1992). Theory of excitation-contraction coupling in cardiac muscle. *Biophysical Journal*, 63(2):497–517.

Stern, M. D., Song, L.-S., Cheng, H., Sham, J. S. K., Yang, H. T., Boheler, K. R., and Ríos, E. (1999). Local control models of cardiac excitation-contraction coupling. A possible role for allosteric interactions between ryanodine receptors. *Journal of General Physiology*, 113:469–89.

Sun, Y.-L., Hu, S.-J., Wang, L.-H., Hu, Y., and Zhou, J.-Y. (2005). Effect of beta-blockers on cardiac function and calcium handling protein in postinfarction heart failure rats. *Chest*, 128:1812–21.

Sutton, P. M. I., Taggart, P., Opthof, T., Coronel, R., Trimlett, R., Pugsley, W., and Kallis, P. (2000). Repolarisation and refractoriness during early ischaemia in humans. *Heart (British Cardiac Society)*, 84(4):365–9.

Syed, Z., Vigmond, E., Nattel, S., and Leon, L. J. (2005). Atrial cell action potential parameter fitting using genetic algorithms. *Medical & Biological Engineering & Computing*, 43(5):561–71.

Szentandrássy, N., Bányász, T., Biro, T., Szabo, G., Toth, B. I., Magyar, J., Lazar, J., Varró, A., Kovacs, L., and Nánási, P. P. (2005). Apico-basal inhomogeneity in distribution of ion channels in canine and human ventricular myocardium. *Cardiovascular Research*, 65(4):851–60.

Szigligeti, P., Pankucsi, C., Bányász, T., Varró, A., and Nánási, P. P. (1996). Action potential duration and force-frequency relationship in isolated rabbit, guinea pig and rat cardiac muscle. *Journal of Comparative Physiology. B, Biochemical, Systemic, and Environmental Physiology*, 166(2):150–5.

Taggart, P., Sutton, P. M. I., Boyett, M. R., Lab, M., and Swanton, H. (1996). Human ventricular action potential duration during short and long cycles. Rapid modulation by ischemia. *Circulation*, 94(10):2526–34.

Talukder, M. A. H., Zweier, J. L., and Periasamy, M. (2009). Targeting calcium transport in ischaemic heart disease. *Cardiovascular Research*, 84:345–52.

Tani, M. and Neely, J. R. (1989). Role of intracellular Na^+ in Ca^{2+} overload and depressed recovery of ventricular function of reperfused ischemic rat hearts. Possible involvement of H^+-Na^+ and Na^+-Ca^{2+} exchange. *Circulation Research*, 65(4):1045–1056.

Tanskanen, A. J., Greenstein, J. L., O'Rourke, B., and Winslow, R. L. (2005). The role of stochastic and modal gating of cardiac L-type Ca^{2+} channels on early after-depolarizations. *Biophysical Journal*, 88(1):85–95.

Tasaki, I. and Hagiwara, S. (1957). Capacity of muscle fiber membrane. *American Journal of Physiology*, 188:423–9.

Taylor, A. L., Goaillard, J.-M., and Marder, E. (2009). How multiple conductances determine electrophysiological properties in a multicompartment model. *Journal of Neuroscience*, 29(17):5573–86.

Taylor, A. L., Hickey, T. J., Prinz, A. A., and Marder, E. (2006). Structure and visualization of high-dimensional conductance spaces. *Journal of Neurophysiology*, 96(2):891–905.

Taylor, J. A. and Lipsitz, L. A. (1997). Heart rate variability standards. *Circulation*, 95(1):280–1.

Temsah, R. M., Netticadan, T., Chapman, D., Takeda, S., Mochizuki, S., and Dhalla, N. S. (1999). Alterations in sarcoplasmic reticulum function and gene expression in ischemic-reperfused rat heart. *American Journal of Physiology*, 277(2 Pt 2):H584–94.

Terkildsen, J. R., Crampin, E. J., and Smith, N. P. (2007). The balance between inactivation and activation of the Na^+-K^+ pump underlies the triphasic accumulation of extracellular K^+ during myocardial ischemia. *American Journal of Physiology - Heart and Circulatory Physiology*, 293(5):H3036–45.

Terkildsen, J. R., Niederer, S. A., Crampin, E. J., Hunter, P. J., and Smith, N. P. (2008). Using Physiome standards to couple cellular functions for rat cardiac excitation-contraction. *Experimental Physiology*, 93(7):919–29.

Tice, B. M., Rodríguez, B., Eason, J. C., and Trayanova, N. A. (2007). Mechanistic investigation into the arrhythmogenic role of transmural heterogeneities in regional ischaemia phase 1A. *Europace: European Pacing, Arrhythmias, and Cardiac Electrophysiology: Journal of the Working Groups on Cardiac Pacing, Arrhythmias, and Cardiac Cellular Electrophysiology of the European Society of Cardiology*, 9 Suppl 6:vi46–58.

Toba, K., Katagiri, T., and Takeyama, Y. (1978). Studies of the cardiac sarcoplasmic reticulum in myocardial infarction. *Japanese Circulation Journal*, 42(4):447–53.

Tobón, C., Ruiz, C., Rodríguez, J. F., Hornero, F., Ferrero, J. M., and Sáiz, J. (2010). Vulnerability for reentry in a three dimensional model of human atria: a simulation study. In *Annual International Conference of the IEEE Engineering in Medicine and Biology Society*, volume 2010, pages 224–7.

Tohse, N. (1990). Calcium-sensitive delayed rectifier potassium current in guinea pig ventricular cells. *American Journal of Physiology - Heart and Circulatory Physiology*, 258(4):H1200–H1207.

Townsend, N., Wickramasinghe, K., Bhatnagar, P., Smolina, K., Nichols, M., Leal, J., Luengo-Fernandez, R., and Rayner, M. (2012). *Coronary Heart Disease Statistics 2012 Edition*. British Heart Foundation: London.

Trayanova, N. A., Constantino, J., and Gurev, V. (2011). Electromechanical models of the ventricles. *American Journal of Physiology - Heart and Circulatory Physiology*, 301(2):H279–86.

Trénor, B., Ferrero, J. M., Rodríguez, B., and Montilla, F. (2005). Effects of pinacidil on reentrant arrhythmias generated during acute regional ischemia: a simulation study. *Annals of Biomedical Engineering*, 33(7):897–906.

Trénor, B., Romero, L., Ferrero, J. M., Sáiz, J., Moltó, G., and Alonso, J. M. (2007). Vulnerability to reentry in a regionally ischemic tissue: a simulation study. *Annals of Biomedical Engineering*, 35(10):1756–70.

van Echteld, C. J. A., Kirkels, J. H., Eijgelshoven, M. H. J., van der Meer, P., and Ruigrok, T. J. C. (1991). Intracellular sodium during ischemia and calcium-free perfusion: a ^{23}Na NMR study. *Journal of Molecular and Cellular Cardiology*, 23:297–307.

Vandenberg, J. I., Walker, B. D., and Campbell, T. J. (2001). HERG K^+ channels: friend and foe. *Trends in Pharmacological Sciences*, 22(5):240–6.

Varró, A. and Baczkó, I. (2011). Cardiac ventricular repolarization reserve: a principle for understanding drug-related proarrhythmic risk. *British Journal Of Pharmacology*, 164(1):14–36.

Varró, A., Baláti, B., Iost, N., Takács, J., Virág, L., Lathrop, D. A., Csaba, L., Tálosi, L., and Papp, J. G. (2000). The role of the delayed rectifier component I_{Ks} in dog ventricular muscle and Purkinje fibre repolarization. *Journal of Physiology*, 523 Pt 1(2000):67–81.

Verkerk, A. O., Wilders, R., Veldkamp, M. W., de Geringel, W., Kirkels, J. H., and Tan, H. L. (2005). Gender disparities in cardiac cellular electrophysiology and arrhythmia susceptibility in human failing ventricular myocytes. *International Heart Journal*, 46(6):1105–18.

Vermeulen, J. T., Tan, H. L., Rademaker, H. M. E., Schumacher, C. A., Loh, P., Opthof, T., Coronel, R., and Janse, M. J. (1996). Electrophysiologic and extracellular ionic changes during acute ischemia in failing and normal rabbit myocardium. *Journal of Molecular and Cellular Cardiology*, 28(1):123–31.

Virág, L., Acsai, K., Hála, O., Zaza, A., Bitay, M., Bogáts, G., Papp, J. G., and Varró, A. (2009). Self-augmentation of the lengthening of repolarization is related to the shape of the cardiac action potential: implications for reverse rate dependency. *British Journal Of Pharmacology*, 156(7):1076–84.

Viswanathan, P. C. and Rudy, Y. (1999). Pause induced early afterdepolarizations in the long QT syndrome: a simulation study. *Cardiovascular Research*, 42(2):530–42.

Viswanathan, P. C. and Rudy, Y. (2000). Cellular Arrhythmogenic Effects of Congenital and Acquired Long-QT Syndrome in the Heterogeneous Myocardium. *Circulation*, 101(10):1192–1198.

Vogel, W. M., Apstein, C. S., Briggs, L. L., Gaasch, W. H., and Ahn, J. (1982). Acute alterations in left ventricular diastolic chamber stiffness. Role of the "erectile" effect of coronary arterial pressure and flow in normal and damaged hearts. *Circulation Research*, 51(4):465–78.

Volders, P. G. A., Kulcśar, A., Vos, M. A., Sipido, K. R., Wellens, H. J. J., Lazzara, R., and Szabo, B. (1997). Similarities between early and delayed afterdepolarizations induced by isoproterenol in canine ventricular myocytes. *Cardiovascular research*, 34(2):348–59.

Wagner, M. B., Namiki, T., Wilders, R., Joyner, R. W., Jongsma, H. J., Verheijck, E. E., Kumar, R., Golod, D. A., Goolsby, W. N., and van Ginneken, A. C. G. (1999). Electrical interactions among real cardiac cells and cell models in a linear strand. *American Journal of Physiology - Heart and Circulatory Physiology*, 276:H391–H400.

Walmsley, J., Mirams, G. R., Bahoshy, M., Bollensdorff, C., Rodríguez, B., and Burrage, K. (2010). Phenomenological modeling of cell-to-cell and beat-to-beat variability in isolated guinea pig ventricular myocytes. In *Annual International Conference of the IEEE Engineering in Medicine and Biology Society*, volume 2010, pages 1457–60.

Walmsley, J., Rodríguez, J. F., Mirams, G. R., Burrage, K., Efimov, I. R., and Rodríguez, B. (2013). mRNA Expression Levels in Failing Human Hearts Predict Cellular Electrophysiological Remodeling: A Population-Based Simulation Study. *PloS One*, 8(2):e56359.

Walton, M. K. and Fozzard, H. A. (1983). The conducted action potential. Models and comparison to experiments. *Biophysical Journal*, 44(1):9–26.

Wang, C., Liu, N., Luan, R., Li, Y., Wang, D., Zou, W., Xing, Y., Tao, L., Cao, F., and Wang, H. (2013). Apelin protects sarcoplasmic reticulum function and cardiac performance in ischaemia-reperfusion by attenuating oxidation of sarcoplasmic reticulum Ca^{2+}-ATPase and ryanodine receptor. *Cardiovascular Research*.

Watanabe, M. A., Fenton, F. H., Evans, S. J., Hastings, H. M., and Karma, A. (2001). Mechanisms for discordant alternans. *Journal of Cardiovascular Electrophysiology*, 12(2):196–206.

Weber, C. R., Ginsburg, K. S., Philipson, K. D., Shannon, T. R., and Bers, D. M. (2001). Allosteric regulation of Na/Ca exchange current by cytosolic Ca in intact cardiac myocytes. *Journal of General Physiology*, 117(2):119–31.

Weiss, J. N., Garfinkel, A., Karagueuzian, H. S., Chen, P.-S., and Qu, Z. (2010). Early afterdepolarizations and cardiac arrhythmias. *Heart Rhythm: The Official Journal of the Heart Rhythm Society*, 7(12):1891–9.

Weiss, J. N., Karma, A., Shiferaw, Y., Chen, P.-S., Garfinkel, A., and Qu, Z. (2006). From pulsus to pulseless: the saga of cardiac alternans. *Circulation Research*, 98(10):1244–53.

Weiss, J. N. and Shine, K. I. (1982). $[K^+]_o$ accumulation and electrophysiological alterations during early myocardial ischemia. *American Journal of Physiology*, 243(2):H318–27.

Weiss, J. N., Venkatesh, N., and Lamp, S. T. (1992). ATP-sensitive K^+ channels and cellular K^+ loss in hypoxic and ischaemic mammalian ventricle. *Journal of Physiology*, 447:649–673.

Wilde, A. A. M., Peters, R. J. G., and Janse, M. J. (1988). Catecholamine release and potassium accumulation in the isolated globally ischemic rabbit heart. *Journal of Molecular and Cellular Cardiology*, 20(10):887–96.

Wilson, L. D., Wan, X., and Rosenbaum, D. S. (2006). Cellular alternans: a mechanism linking calcium cycling proteins to cardiac arrhythmogenesis. *Annals of the New York Academy of Sciences*, 1080:216–34.

Wilson, M. and Bower, J. M. (1992). Cortical oscillations and temporal interactions in a computer simulation of piriform cortex. *Journal of Neurophysiology*, 67(4):981–95.

Wu, L., Ma, J., Li, H., Wang, C., Grandi, E., Zhang, P., Luo, A., Bers, D. M., Shryock, J. C., and Belardinelli, L. (2011). Late sodium current contributes to the reverse rate-dependent effect of I_{Kr} inhibition on ventricular repolarization. *Circulation*, 123(16):1713–20.

Wu, L., Shryock, J. C., Song, Y., and Belardinelli, L. (2006). An increase in late sodium current potentiates the proarrhythmic activities of low-risk QT-prolonging drugs in female rabbit hearts. *Journal of Pharmacology and Experimental Therapeutics*, 316(2):718–26.

Xiao, L., Xiao, J., Luo, X., Lin, H., Wang, Z., and Nattel, S. (2008). Feedback remodeling of cardiac potassium current expression: a novel potential mechanism for control of repolarization reserve. *Circulation*, 118(10):983–92.

Xie, Y., Hu, G., Sato, D., Weiss, J. N., Garfinkel, A., and Qu, Z. (2007). Dispersion of refractoriness and induction of reentry due to chaos synchronization in a model of cardiac tissue. *Physical Review Letters*, 99(11):118101.

Xu, A., Hawkins, C., and Narayanan, N. (1993). Phosphorylation and activation of the Ca^{2+}-pumping ATPase of cardiac sarcoplasmic reticulum by Ca^{2+}/calmodulin-dependent protein kinase. *Journal of Biological Chemistry*, 268(12):8394–7.

Xu, K. Y., Zweier, J. L., and Becker, L. C. (1997). Hydroxyl radical inhibits sarcoplasmic reticulum Ca^{2+}-ATPase function by direct attack on the ATP binding site. *Circulation Research*, 80(1):76–81.

Yamazaki, M., Honjo, H., Ashihara, T., Harada, M., Sakuma, I., Nakazawa, K., Trayanova, N. A., Horie, M., Kalifa, J., Jalife, J., Kamiya, K., and Kodama, I. (2012). Regional cooling facilitates termination of spiral-wave reentry through unpinning of rotors in rabbit hearts. *Heart Rhythm: The Official Journal of the Heart Rhythm Society*, 9(1):107–14.

Yan, G.-X., Rials, S. J., Wu, Y., Liu, T., Xu, X., Marinchak, R. A., and Kowey, P. R. (2001). Ventricular hypertrophy amplifies transmural repolarization dispersion and induces early afterdepolarization. *American Journal of Physiology - Heart and Circulatory Physiology*, 281:H1968–H1975.

Yan, G.-X., Yamada, K. A., Kléber, A. G., McHowat, J., and Corr, P. B. (1993). Dissociation between cellular K^+ loss, reduction in repolarization time, and tissue ATP levels during myocardial hypoxia and ischemia. *Circulation Research*, 72:560–570.

Yang, P.-C. and Clancy, C. E. (2012). In silico Prediction of Sex-Based Differences in Human Susceptibility to Cardiac Ventricular Tachyarrhythmias. *Frontiers in Physiology*, 3(September):360.

Yang, T., Chun, Y. W., Stroud, D. M., Mosley, J. D., Knollmann, B. C., Hong, C. C., and Roden, D. M. (2014). Screening for Acute I_{Kr} Block is Insufficient to Detect Torsades de Pointes Liability: Role of Late Sodium Current. *Circulation*, pages 224–234.

Yang, T., Snyders, D. J., and Roden, D. M. (1997). Rapid inactivation determines the rectification and $[K^+]_o$ dependence of the rapid component of the delayed rectifier K^+ current in cardiac cells. *Circulation Research*, 80(6):782–9.

Yu, Z., Holst, M. J., Hayashi, T., Bajaj, C. L., Ellisman, M. H., McCammon, J. A., and Hoshijima, M. (2008). Three-dimensional geometric modeling of membrane-bound organelles in ventricular myocytes: bridging the gap between microscopic imaging and mathematical simulation. *Journal of Structural Biology*, 164:304–13.

Yue, L., Feng, J., Li, G.-R., and Nattel, S. (1996). Transient outward and delayed rectifier currents in canine atrium: properties and role of isolation methods. *American Journal of Physiology*, 270(6 Pt 2):H2157–68.

Zaniboni, M., Pollard, A. E., Yang, L., and Spitzer, K. W. (2000). Beat-to-beat repolarization variability in ventricular myocytes and its suppression by electrical coupling. *American Journal of Physiology - Heart and Circulatory Physiology*, 278:H677–87.

Zemzemi, N., Bernabeu, M. O., Sáiz, J., Cooper, J., Pathmanathan, P., Mirams, G. R., Pitt-Francis, J., and Rodríguez, B. (2013). Computational assessment of drug-induced effects on the electrocardiogram: from ion channel to body surface potentials. *British Journal of Pharmacology*, 168:718–33.

Zeng, J., Laurita, K. R., Rosenbaum, D. S., and Rudy, Y. (1995). Two Components of the Delayed Rectifier K^+ Current in Ventricular Myocytes of the Guinea Pig Type: Theoretical Formulation and Their Role in Repolarization. *Circulation Research*, 77(1):140–152.

Zhang, H., Wang, J., Yang, L., Wu, R.-J., Mei, X., and Zhao, W. (2011). Vulnerability in simulated ischemic ventricular transmural tissues. *Chinese Journal of Physiology*, 54(6):427–34.

Zhao, M., Franzen, D., and Eng, C. (1988). The effect of coronary arterial pressure on myocardial distensibility. Absence of a "garden hose" effect during in-vivo conditions. *Basic Research in Cardiology*, 83(6):626–33.

Zweier, J. L. (1988). Measurement of superoxide-derived free radicals in the reperfused heart. Evidence for a free radical mechanism of reperfusion injury. *Journal of Biological Chemistry*, 263:1353–7.